NASA CONTRACTOR REPORT

NASA CR-2547

NASA CR-2547

THE NATA CODE - THEORY AND ANALYSIS

W. L. Bade and J. M. Yos

Prepared by
AVCO SYSTEMS DIVISION
Wilmington, Mass. 01887
for Lyndon B. Johnson Space Center

NATIONAL AERONAUTICS AND SPACE ADMINISTRATION • WASHINGTON, D. C. • JUNE 1975

1. Report No.	2. Government Accession No.	3. Recipient's Catalog No.
NASA CR-2547		

4. Title and Subtitle	5. Report Date
THE NATA CODE — THEORY AND ANALYSIS, VOLUME I	June 1975
	6. Performing Organization Code

7. Author(s)	8. Performing Organization Report No.
W. L. Bade and J. M. Yos	AVSD-0288-74-RR
	10. Work Unit No.

9. Performing Organization Name and Address	11. Contract or Grant No.
Avco Systems Division 201 Lowell Street Wilmington, Massachusetts 01887	NAS9-9744
	13. Type of Report and Period Covered Contractor Report, Final Report
12. Sponsoring Agency Name and Address National Aeronautics and Space Administration Washington, D. C. 20546	14. Sponsoring Agency Code

15. Supplementary Notes

Volume II of this report is NASA CR-141743.
Volume III of this report is NASA CR-141744.

16. Abstract

The NATA code is a computer program for calculating quasi-one-dimensional gas flow in axisymmetric and two-dimensional nozzles and rectangular channels. The flow is assumed to start from a state of thermochemical equilibrium at a high temperature in an upstream reservoir. The program provides solutions based on frozen chemistry, chemical equilibrium, and nonequilibrium flow with finite reaction rates. Electronic nonequilibrium effects can be included using a two-temperature model. An approximate laminar boundary layer calculation gives the shear and heat flux on the nozzle wall. Boundary layer displacement effects on the inviscid flow are taken into account. Chemical equilibrium and transport property calculations are provided by subroutines. NATA contains precoded thermochemical, chemical kinetic, and transport cross section data for high-temperature air, CO_2-N_2-Ar mixtures, helium, and argon. It provides calculations of the stagnation conditions on axisymmetric or two-dimensional models, and of the conditions on the flat surface of a blunt wedge. The code's primary purpose is to describe the flow conditions and test conditions in electric arc heated wind tunnels.

17. Key Words (Suggested by Author(s))		18. Distribution Statement
Nonequilibrium flow	Nozzle flow	STAR Subject Category: 34 (Fluid Mechanics and Heat Transfer)
Arc-heated wind tunnels	Thermal nonequilibrium	
Stagnation-point heat transfer		
Wedge heat transfer		
Laminar boundary layer		

19. Security Classif. (of this report)	20. Security Classif. (of this page)	21. No. of Pages	22. Price*
Unclassified	Unclassified	230	$7.50

*For sale by the National Technical Information Service, Springfield, Virginia 22151

PREFACE

This report (Volume I of three volumes, with Volume II to be NASA CR-141743 and Volume III to be NASA CR-141744) partially documents the development of a computer program (NATA) for calculating the flow in arc-heated wind tunnels and the conditions on models tested in such reentry simulation facilities. The objective was to provide a means for predicting and interpreting test conditions used in the experimental evaluation of thermal protection materials for reentry vehicles such as the Space Shuttle Orbiter. Much effort was expended to make the program reliable and easily usable by engineers without great expertise in gas phase chemical kinetics, gas transport properties, thermochemistry, and computer programming. The capabilities of NATA are summarized concisely in the abstract, and in somewhat more detail in the Introduction (Section 1). Comparisons with available experimental data indicate that the results produced by the program have a useful level of accuracy.

TABLE OF CONTENTS

TABLE OF CONTENTS (Concl'd)

LIST OF ILLUSTRATIONS

LIST OF ILLUSTRATIONS (Cont'd)

LIST OF ILLUSTRATIONS (Concl'd)

LIST OF TABLES

MATHEMATICAL SYMBOLS

All mathematical symbols used in this report are defined in the text where they are first used. In addition, the definitions of symbols used in several different sections of the report are summarized below for convenience of reference.

Latin Symbols

A_e	Effective area ratio, A'_e/A'_{e*}
A'_e	Effective cross sectional area of the inviscid flow at a given axial position
A'_{e*}	Effective cross sectional area of the inviscid flow at the sonic point
$\tilde{A}_e$	Effective area ratio in the non-equilibrium solution by the inverse method
A_g	Geometric area ratio, A'_g/A'_{g0}
A'_g	Geometric cross sectional area of a nozzle or channel at a given axial position
A'_{g0}	Geometric cross sectional area at the throat
A_i	Constant coefficient in formula for forward reaction rate constant for the i^{th} reaction
A_{ki}	Inverse matrix of the matrix $\bar{\alpha}_{ij}$
c	Number of chemical elements present in the gas mixture
c_p	Specific heat of the gas at constant pressure
c_{pj}	Specific heat for the j^{th} species at constant pressure
C_p	Molar heat capacity of the gas at constant pressure
C_{pe}	Molar heat capacity for the electrons
C_{pj}	Molar heat capacity for the j^{th} species at constant pressure
D_{am}	Atom-molecule binary diffusion coefficient
E	Molar internal energy
E_{ai}	Activation energy in formula for forward reaction rate constant for the i^{th} reaction
E_k	Energy of electronic excitation for the k^{th} state in a molecule

g_k	Degeneracy of the k^{th} electronic state in a molecule
h	Specific enthalpy
h^*	Reference enthalpy
h_r	Recovery enthalpy
h_0	Specific stagnation enthalpy
H	Molar enthalpy
H_j	Molar enthalpy for the j^{th} species
H_{j0}°	Heat of formation at standard pressure (1 atm) for the j^{th} species
k_{fi}	Forward rate constant for the i^{th} reaction
k_{ri}	Reverse rate constant for the i^{th} reaction
K_e	Equilibrium thermal conductivity
K_f	Chemically frozen thermal conductivity
K_i	Equilibrium constant for the i^{th} reaction
m	Mass flux, ρu
m_e	Electron mass
m_j	Mass of a molecule of the j^{th} species
M_j	Symbol for a chemical species
$[M_j]$	Concentration of the j^{th} species in moles/cm^3
n	Number of chemical species
n_e	Number of free electrons per unit volume
N_{fi}	Number of occurrences of the i^{th} reaction per unit volume per unit time in the forward direction
N_{Le}	Lewis number, $D_{am}\rho\, c_p / K$
N_{Nu}	Nusselt number, $q_s \times c_p / K(h_e - h_w)$
N_{Pr}	Prandtl number, $c_p\, \mu / K$
N_{Re}	Reynolds number, $\rho u x/\mu$

N_{ri}	Number of occurrences of the i^{th} reaction per unit volume per unit time in the reverse direction
N_0	Avogadro's number, 6.023×10^{23} mole^{-1}
p	Pressure
p_j	Partial pressure of the j^{th} species
p_0	Reservoir pressure
P_i	Rate factor in equation for rate of change of the concentration of a species due to the i^{th} reaction, $(\rho^{\nu_i - 1}/u)\, k_{fi} \prod_k \gamma_k^{\nu_{ik}}$
$\dot{q}_e$	Rate of energy addition to the electron gas per unit volume
q_{fi}	Mean radiative energy loss from the gas in N_0 occurrences of the i^{th} reaction in the forward direction
$\dot{q}_r$	Radiative power loss from the gas per unit volume
q_{ri}	Negative of the mean radiative energy loss from the gas in N_0 occurrences of the i^{th} reaction in the reverse direction
q_s	Stagnation point heat flux
q_w	Heat flux to the wall
Q_k	Number of gram-atoms of the k^{th} element per mole of the cold gas mixture
r	Number of reactions in the reaction system
R_a	Area rescaling factor in non-equilibrium solution
R_A	Reynolds analogy factor
R_0	Universal gas constant
s	Specific entropy
s_0	Specific entropy in the reservoir
S	Molar entropy
S_j	Molar entropy of the j^{th} species
S_j^o	Molar entropy of the j^{th} species at the standard pressure (1 atm)
T	Absolute temperature

T_e	Absolute electron temperature
T_0	Reservoir temperature
u	Flow velocity
V	Molar volume
W	Mean molecular weight of gas
W_j	Molecular weight of the j^{th} species
x	Axial coordinate in the nozzle or channel
x_0	Axial coordinate at the start of the boundary layer
X_j	Mole fraction of the j^{th} species

Greek Symbols

α_{ij}	Number of atoms of the j^{th} chemical element in a molecule of the i^{th} species
$\bar{\alpha}_{ij}$	Square submatrix of α_{ij} for i = 1 to c, j = 1 to c
β_i	$\sum_j \beta_{ij}$
β_{ij}	$\nu'_{ij} - \nu_{ij}$
γ	Specific heat ratio, c_p / c_v
γ_e	Electron concentration (moles/gm)
γ_h	Heavy particle concentration, $\sum_{j=2}^{n} \gamma_j$
γ_j	Concentration of j^{th} species (moles/gm)
δ	Followed by another symbol, represents the perturbation of the quantity represented by that symbol
δ^*	Boundary layer displacement thickness
δ_{kj}	Kronecker symbol, 1 for k = j , 0 otherwise
Δ	Followed by another symbol, represents the change in the quantity represented by that symbol over a step in the flow solution
ϵ	Specific internal energy
ϵ_ρ	Shock density ratio, ρ_1 / ρ_2

ϵ_{fi}	Mean energy gained by the electron gas in N_0 occurrences of the i^{th} reaction in the forward direction
ϵ_{ri}	Negative of the mean energy gained by the electron gas in N_0 occurrences of the i^{th} reaction in the reverse direction
η_i	Temperature exponent in formula for forward reaction rate constant for the i^{th} reaction
θ	Boundary layer momentum thickness
μ	Viscosity
μ_j	Chemical potential for the j^{th} species
μ_j^o	Chemical potential of the j^{th} species at the standard pressure (1 atm)
ν_i	$\sum_{j=1}^{n} \nu_{ij}$
ν_i'	$\sum_{j=1}^{n} \nu'_{ij}$
ν^*_{i-c}	$\sum_{k=1}^{c} \bar{\nu}_{i-c,k}$
$\bar{\nu}_{i-c,k}$	Matrix of coefficients for expressing the dependent species in terms of the c independent species
ν_{ij}	Number of molecules of the j^{th} species on the reactant side of the i^{th} reaction
ν'_{ij}	Number of molecules of the j^{th} species on the pr side of the i^{th} reaction
ρ	Density
$\tilde{\rho}$	Effective density in treatment of gas imperfections
ρ_0	Density in reservoir
τ_w	Shear stress on wall
χ_i	Departure-from-equilibrium factor in formula for rate of change of a species concentration due to the i^{th} reaction, $1-(\rho^{\beta_i}/K_i)\prod_k \gamma_k^{\beta_{ik}}$

Subscripts

e	Conditions in the flow external to the boundary layer
s	Stagnation conditions on a model
w	Wall conditions
0	Reservoir or stagnation conditions
*	Sonic conditions

THE NATA CODE - THEORY AND ANALYSIS

By W. L. Bade and J. M. Yos
Avco Systems Division
Wilmington, Massachusetts

1. INTRODUCTION

The NATA* code was developed by Avco Systems Division from 1968 through 1974, under the sponsorship of the NASA Johnson Space Center, to meet a need for predicting and interpreting the flow conditions in electric-arc heated wind tunnels. Test facilities of this type are used at the Johnson Space Center, and elsewhere, for evaluating thermal protection materials for reentry systems. The present report documents the theory and analysis upon which the current version of NATA is based. A user's manual and a programmer's manual for the code are to be issued separately.

The earliest version of NATA was based upon a computer program developed at Cornell Aeronautical Laboratory (CAL) (ref. 1). This CAL program performed calculations of quasi-one-dimensional flow through a nozzle of specified geometry. The flow was assumed to start from a state of thermochemical equilibrium at specified temperature and pressure in an upstream reservoir. The program included options for flow solutions based on chemical equilibrium, frozen chemistry, and chemical non-equilibrium with specified reaction rate constants. Boundary layer effects were neglected. There was no provision for calculating conditions on models immersed in the flow. The program used fixed-format input; i.e., the numerical data were punched, without alphanumeric identifiers, in prescribed fields of the input cards. The input was voluminous (100 to 200 cards per case), as all of the gas species properties and reaction rate data had to be read in. The output was in the form of non-dimensional ratios of the gas flow properties to standard values.

During the development of NATA, the basic calculations of frozen, equilibrium, and non-equilibrium flow as coded in the CAL program have been retained with only minor changes. Many new features have been added, including a laminar boundary layer calculation, internal gas transport property calculations, options for specifying the reservoir conditions by input of the total mass flow together with the reservoir pressure or the stagnation enthalpy, and computations of the heating and stresses on models immersed in the flow. In addition, a radical revision of the input and output arrangements has been carried out to make the code easier to use. The fixed-format input of the CAL program has been replaced by namelist input, in which only the variables whose values are to be changed have to be read in. The control inputs are all preset to standard values which are generally satisfactory. All species and reaction data for several standard gas models, including argon-free air, are compiled into the program and can be invoked by specifying a single input variable. Curvefits to the geometries of several of the nozzles and channels used at NASA Johnson Space Center are also included in the program. As a result of these changes, the number of input cards required per case has been reduced to 4 to 8 (typically). The output has been

*Acronym for Non-equilibrium Arc Tunnel Analysis.

expanded to include additional quantities, such as the boundary layer properties, and is now presented in dimensional form to allow direct comparison of the code results with experimental data. Each output variable is labeled with an alphanumeric identifier. In addition, much effort has been expended to ensure that NATA will almost always generate a successful solution when run with the standard values of the control inputs. A major objective of these revisions was to make the code usable by gas dynamicists who are not necessarily expert in thermochemistry, transport property theory, chemical kinetics, or computer programming.

The remaining parts of this introduction outline the capabilities of NATA, discuss its limitations, and describe the subsequent sections of the present report.

1.1 Programming

NATA is a Fortran IV program consisting of a main program and 68 subroutines. The source deck contains approximately 8500 cards. The program exists in two versions, one for use on the IBM 360 system, the other for the Univac 1108. The IBM 360 version is entirely in double precision, whereas the Univac version is a single precision program with some double precision arrays and subroutines. One version can be converted into the other by inserting or removing the cards which type all floating-point variables as double precision in the IBM 360 version.

The IBM 360 version requires about 410K bytes of core storage, including buffers. The Univac version is run on the 1108 using overlay, and fits into the two-bank processors at NASA/JSC with about 2000 words of storage to spare.

1.2 Gas Models

NATA provides four options for specifying the species properties and reactions defining the gas model.

1.2.1 Standard Gas Models

Six compiled-in standard gas models are available in the code. One of these is a model for argon-free air at low and moderate temperatures where NO^+ is the only important ion species. Another is a high-temperature air model including five atomic and molecular ions. There are two planetary atmosphere models for mixtures of 75 mole percent CO_2, 20 mole percent Ar, and 5 mole percent N_2. Finally, there is an electronic non-equilibrium (two-temperature) model for argon and one for helium. These rare-gas models include a non-equilibrium treatment of electronic excited states. Any of these standard models can be selected by input of a single index value.

1.2.2 Standard Gas Models with Input Mole Fractions

The elemental composition of the gas mixture is specified in terms of the mole fractions of "cold species" which are stable at low temperature. For example, the weight fractions of C, O, N, and Ar in the planetary atmosphere models

are determined from the assumed mole fractions of CO_2, N_2, and Ar in the gas before it is heated. Optionally, these cold species mole fractions can be set in the input without disturbing the standard species properties or the reaction system. Thus, the standard models for air and the planetary atmosphere can easily be applied to mixtures of the same cold species in different proportions.

1.2.3 User-Generated Gas Models with Standard Species and Reactions

A gas model based upon the available, compiled-in species and reactions, but with a non-standard selection of species and reactions, can be set up in the input. For example, some of the reactions can be deleted from a standard model to assess their effect upon the solution of a particular case. Input of such a non-standard gas model requires about 4 to 8 input cards, depending upon the numbers of species and reactions included.

1.2.4 Input of Species and Reaction Data

Finally, the basic data for species and reactions can be set in the input. The data for standard species and reactions can be changed in part or in whole, and new species and reactions can be introduced. About two input cards are required per new reaction, and about 3 to 4 cards per species.

1.3 Transport Properties

NATA includes a self-contained capability for computing the transport properties of gas mixtures, based upon the temperature, pressure, and mole fractions given by the equilibrium or non-equilibrium calculations of the flow solution. The transport collision cross sections for the standard species are provided by compiled-in data. Collision cross section data can also be specified in the input. The transport properties calculated are the viscosity, the chemically frozen Prandtl number, the atom-molecule Lewis number, and the electrical conductivity. The viscosity and Prandtl number are used in the calculations of the boundary layer on the nozzle wall and in calculations of stagnation-point heating on models and of the heat transfer to wedge models. The Lewis number is used in stagnation-point heat transfer calculations. The electrical conductivity is not used in NATA, but is printed out.

1.4 Flow Geometry

The geometries of nozzles and channels are specified, in NATA, by means of curvefits to their profiles. A profile is the curve of intersection of the inner surface of a nozzle or channel with a symmetry plane. For an axisymmetric nozzle, there is one such profile. For a rectangular channel, there are two profiles. Each profile is represented as a sequence of straight lines and circular arcs, joined end-to-end with value and slope continuity. A separate computer program (NOZFIT) is available for generating such curvefits from nozzle design data.

If boundary layer displacement effects are neglected, the inviscid flow depends only upon the ratio of the nozzle cross sectional area to the area at the throat, not upon the shape of the cross section. However, the convergence or divergence of streamlines in the boundary layer does depend upon the type of nozzle geometry, and affects the rate of boundary layer growth. To take such boundary layer effects into account, NATA contains explicit treatments of three types of nozzle geometry: axisymmetric nozzles, two-dimensional nozzles, and rectangular channels.

1.5 Reservoir Conditions

The flow is always assumed to start from a state of thermochemical equilibrium in an upstream reservoir. For a gas of given elemental composition, the thermochemical state is a function of two variables, and its specification therefore requires two inputs. NATA provides three options for the input specification of reservoir conditions.

1.5.1 Temperature and Pressure

The basic method is the one used in the original CAL program (ref. 1), namely, direct input of the reservoir temperature and reservoir pressure. NATA contains a subroutine for determining the equilibrium species mole fractions from these data and the species thermochemical properties.

1.5.2 Pressure and Mass Flow

The upstream stagnation pressure can be measured easily in arc heated wind tunnels in which the flow stagnates in a plenum chamber downstream of the arc heater and upstream of the throat. However, the reservoir temperature is difficult to determine. For this reason, an option is provided to calculate the reservoir conditions from data on the reservoir pressure and the total mass flow (which is easily measured). When this option is used, the reservoir temperature is estimated and the resulting total mass flow is calculated based on an equilibrium flow solution from the reservoir to the throat. An iteration is then carried out to determine the reservoir temperature corresponding to the input mass flow. If the boundary layer is to be included in the main flow solution, a correction is made for the effect of the displacement thickness at the throat.

1.5.3 Mass Flow and Stagnation Enthalpy

Many arc heated wind tunnels lack an upstream stagnation region. In such facilities upstream pressure measurements do not give the effective reservoir pressure. To deal with such cases, NATA provides a third option in which the reservoir conditions are determined from input data on the total mass flow and the stagnation enthalpy. The mean stagnation enthalpy of the gas stream can be calculated from measurements of the electrical power input, thermal losses to the facility cooling system, and mass flow. In this option, the reservoir temperature and pressure are calculated by a double iteration to match the input mass flow and enthalpy values, assuming equilibrium flow from the reservoir to

the throat. If the boundary layer is included, a correction is made for the effect of the displacement thickness on the effective throat area.

1.6 Boundary Layer

The boundary layer in an arc heated wind tunnel can be either laminar or turbulent. According to a correlation of available boundary layer transition data, the layer is expected to remain laminar throughout the nozzle for most operating conditions of the existing NASA/JSC arc heaters. NATA contains an approximate laminar boundary layer calculation based upon an integral method devised by Cohen and Reshotko. The calculation includes the effects of the streamwise pressure gradient in the nozzle. The Cohen-Reshotko method utilizes analytical curvefits to relations among non-dimensional boundary layer parameters, based on similar boundary layer solutions. The curvefits employed in NATA include the dependence of the parameters upon the Prandtl number, the viscosity-temperature index, and the hypersonic parameter. The boundary layer is assumed to start at a specified position upstream of the nozzle throat, and is computed step by step along with the inviscid flow solution. Beyond the throat, the inviscid flow is coupled with the boundary layer through the effect of the displacement thickness on the effective area ratio. The coupled flow is stabilized with the aid of a computational artifice. In the case of flow in a rectangular channel, two separate boundary layer solutions are computed, one for each pair of channel faces. Besides determining the displacement effects on the inviscid flow, the boundary layer solution yields predictions of the heat flux and shear stress on the nozzle or channel wall.

1.7 Flow Solutions

NATA provides frozen, equilibrium, and non-equilibrium flow solutions. These are the same flow options offered by the original CAL program (ref. 1) and the methods used in generating the solutions are largely identical with those used in the CAL program. In the frozen solution, the species mole fractions are held constant at their reservoir values. This type of solution approximates the actual non-equilibrium flow fairly well in cases with low reservoir pressure. In the equilibrium solution, the gas is assumed to be in a state of local thermochemical equilibrium at each point in the nozzle. The actual flow always departs radically from equilibrium in the supersonic region downstream of the throat. However, equilibrium flow is often a good approximation in the region upstream of the throat and in the throat region.

The non-equilibrium solution is intended to model the actual flow as closely as possible within the basic approximation of quasi-one-dimensionality. The species concentrations are assumed to be governed by chemical rate equations. The basic method of solution is numerical integration of these rate equations together with the differential equations formulating conservation of mass, momentum and energy. However, it is found that the system of difference equations is stable only for extremely small step sizes when the flow is close to equilibrium. Because the flow starts from a state of equilibrium in the reservoir, the numerical integration technique therefore cannot be used initially. Instead, the solution is started by treating the non-equilibrium flow as a perturbed equilibrium flow. The perturbation method is used until the departure from equilibrium

has become large enough to allow use of the numerical integration. Another difficulty is that the sonic mass flux for the non-equilibrium solution is not known until the solution has reached the sonic point. This problem is circumvented by using an inverse method upstream of the throat and for a short distance beyond the throat.

When a two-temperature electronic non-equilibrium model is used, the electron temperature is one of the integration variables. In such cases, radiative energy losses and energy transfer between the electrons and the heavy particles in the gas are taken into account, and some of the electronic excited states may be treated as separate species governed by rate equations and not necessarily in equilibrium with the ground state.

1.8 Model Conditions

A major objective of NATA is to provide calculations of test conditions on models for comparison with experimental heat flux and pressure measurements. The code provides model calculations of two types: stagnation point conditions and conditions on blunt wedges.

1.8.1 Stagnation Point

The calculations of stagnation point model conditions begin with a normal shock solution. The gas immediately behind the shock can be assumed to be frozen (with mole fractions equal to those in the free stream ahead of the shock) or in chemical equilibrium. Either or both of these types of solution can be obtained in a given NATA run, regardless of whether the free stream solution is frozen, equilibrium, or non-equilibrium. The conditions at a point on the stagnation streamline just outside the boundary layer on the model are then calculated. The pressure at this point is the stagnation pressure, which can be compared with Pitot measurements. The stagnation point heat flux is then calculated using a modification of the Fay-Riddell formula. Heat flux calculations are done for both hemispherical and flat-faced models, and for both an equilibrium and a frozen boundary layer. Effects of surface catalytic efficiency can be included. The shock standoff distance is also calculated approximately. These calculations of stagnation conditions on models are done independently for the frozen shock and the equilibrium shock.

Calculations of stagnation point conditions are normally done for axisymmetric models. However, the calculations can be done, instead, for two-dimensional models such as a cylinder with its axis normal to the direction of flow.

1.8.2 Wedge Models

The pressure and heat flux distributions on the flat surface of a blunt wedge are calculated using a modification of the results of the Cheng-Kemp theory. Effects of bluntness and the boundary layer displacement thickness are taken into account. For a given model location in a particular NATA solution, wedge conditions can be calculated for a series of input-specified leading edge radii and wedge angles of attack.

1.9 Supplementary Program Functions

NATA contains several features designed to aid the user during the development of new gas models and under other abnormal circumstances. These features are not normally exercised during runs to produce flow solutions based on standard gas models.

1.9.1 Equilibrium Gas Properties

The code contains an option to compute only the reservoir conditions, i.e., the equilibrium thermodynamic properties and mole fractions. This features allows the user to determine the equilibrium equation of state of a gas mixture of specified composition, based on a particular set of assumed species properties. Normally, the transport properties in the reservoir are also computed. However, the transport property calculations can be suppressed, if desired, to avoid input of the required collision cross sections.

1.9.2 Species Thermal Properties

Another option produces tables of the free energy, enthalpy, specific heat, and entropy as functions of temperature for each of the species in a gas model. This feature provides, for example, a convenient means for testing proposed thermo fits for the species, and allows direct comparison of the properties, as computed by NATA, with other tabulations such as the JANAF tables.

1.9.3 Transport Cross Section Edits

A third option produces an edit of the steps in the transport cross section calculation for all of the species in the gas model. This edit is a useful aid to setting up or modifying cross section inputs for a gas model. In addition, NATA can be made to produce a deck of punched cards containing the averaged collision cross sections for all pairs of species in a gas model. In this form, the data can be read and used by other computer programs.

1.9.4 Tape Output

NATA contains provisions for writing selected results of the flow, boundary layer, and model calculations on a binary tape for subsequent processing by other programs. An auxiliary program (NATA/PLOT) is available for producing certain types of plots of such data using SD-4060 or similar equipment.

1.9.5 Error Processing

When a large, multicase NATA job is run, one or more of the cases may fail because of input errors, inadequacy of standard values for the control parameters, or possible previously undetected coding errors. NATA contains numerous provisions to aid the user in identifying the cause of trouble in case of code failure, and to facilitate the running of large jobs in spite of the failure of some of

the cases. First, the program contains many validity checks designed to detect errors before they cause the program to execute an operation which is not allowed by the computer system, such as dividing by zero or calling a Fortran function with an illegal argument. Such an operation would lead to immediate termination of the entire run. Second, when an error condition is detected, in most cases NATA prints a diagnostic message to identify its nature. Third, execution of the current case in the job is terminated. Fourth, a special subroutine is called to print out most of the data stored in common, together with alphanumeric identifiers. The name of the subroutine in which the error was detected is also printed. Finally, the program proceeds to read the input data for the next case, and execution of the job continues.

1.10 Limitations

The calculations performed by NATA involve many approximations which limit the code's accuracy and applicability. The basic approximation in the inviscid flow solutions is that of quasi-one-dimensionality. Each flow variable is assumed to vary with the axial coordinate of the nozzle, but to be constant over any nozzle cross section. Actual flows in arc heated wind tunnels always show some radial non-uniformity. In some facilities, the non-uniformity is sufficiently moderate that the quasi-one-dimensional description can be considered to be a roughly valid and useful idealization. In others, the non-uniformity is so severe that the usefulness of an analysis based on radially uniform flow appears doubtful.

The boundary layer calculations involve many approximations related to the boundary layer starting condition, the method of solution, and the stabilization of the coupled boundary layer/inviscid flow problem beyond the throat. Also of course, the laminar boundary layer calculation is applicable only when the actual boundary layer has not undergone transition.

It would be extremely difficult to carry through an error analysis for the code by evaluating and combining the effects of all of the approximations used. Such a calculation has not been attempted. Instead, results from the code have been compared with experimental data from arc heater facilities in which the radial non-uniformity is not very severe. It has been found that NATA predictions of static pressure and stagnation pressure generally agree with the measurements to within about 20 percent. Based on a limited number of comparisons, it appears that NATA predictions of heat flux to a channel wall or a wedge model are too low by about 20 to 30 percent. NATA results for stagnation point heat transfer are roughly in agreement with experimental data for hemispherical models, when allowance is made for surface catalytic efficiency and for low-density effects which are not treated by the code.

1.11 Organization of Report

The remaining sections of this report document the theoretical relations and mathematical analyses upon which the NATA code is based. Section 2 treats the description of chemical species and chemical reactions. Section 3 deals with the calculation of gas transport properties. Section 4 explains how the

geometry of the nozzle or channel is described, and how the boundary layer displacement effect on the inviscid flow is formulated. Section 5 gives the analytical basis of the boundary layer calculation. Section 6 discusses the equilibrium and frozen inviscid flow calculations, and Section 7 the non-equilibrium flow. Finally, Section 8 treats the calculations of conditions on models.

2. THERMODYNAMIC AND KINETIC MODELS

The treatment of chemical equilibrium and reaction kinetics in NATA is still essentially the same as that in the Cornell Aeronautical Laboratory program (ref. 1). Section 2.1 explains how the code describes chemical species and formulates the conservation of chemical elements and electric charge. Section 2.2 discusses the calculation of thermal properties of species and Section 2.3 the specification of chemical reaction rates. Simple models for vibrational non-equilibrium and for imperfections in the gas equation of state are described in Sections 2.4 and 2.5.

2.1 Elements and Chemical Species

The gas stream whose flow is computed by the NATA code can consist of up to 20 chemical species. The types of species normally treated are atoms (including, in some instances, atoms in specific electronic excited states), atomic ions, diatomic molecules and molecular ions, linear triatomic molecules or ions (such as CO_2), and the electron. The number of species included in a particular problem will be denoted by n. The gas composition is expressed, in different parts of the calculation, in terms of either the mole fractions X_j or the molar concentrations γ_j in units of moles of species j per gram of mixture. These quantities are related by

$$X_j = W \gamma_j \tag{1}$$

in which W denotes the local mean molecular weight of the gas mixture in grams per mole.

The number of chemical elements present in the gas is denoted by c. The chemical formulas of the species are represented by a matrix α, whose general element α_{ij} is the number of atoms of the j^{th} element per molecule of the i^{th} species. Thus, if the i^{th} species is denoted by M_i and the j^{th} element by E_j, the chemical formula of the species may be represented by the equation

$$M_i = \sum_{j=1}^{c} \alpha_{ij} E_j \tag{2}$$

If ion species are present, the electron is included among the elements. In that case, positive ions are represented as compounds containing a negative number of electrons; for example, N_2^+ is considered to be a compound N_2e_{-1}. With this convention, conservation of electric charge during reactions becomes a special case of conservation of the chemical elements.

NATA calculations of thermochemical equilibrium* are carried out using a technique in which the concentrations of the "dependent species" are expressed in terms of those of the "independent species" (or "components"), where the

*See Section 6.

number of independent species is equal to the number of elements. The advantage of this technique is that it reduces the number of equations, which must be solved simultaneously to determine the equilibrium species mole fractions, from n to c. For example, the high temperature model for air used in NATA contains 11 species but only 3 elements (N, O, and e), so that the number of equations is reduced from 11 to 3.

The independent species or components must be chosen such that they are linearly independent combinations of the chemical elements, and must be placed at the beginning of the list of species for each gas model. To avoid computational problems, they should be species which are stable at low temperatures (i.e., at large expansion ratios downstream of the nozzle throat). However, if ion species are included in the model, the electron should be one of the components, and should be listed as species number 1. The ion species should all be placed at the end of the list of species. This arrangement allows the code to drop the charged particles from the model for equilibrium flow when the equilibrium electron mole fraction becomes negligible ($<10^{-20}$). As an illustration of an arrangement satisfying these requirements, in the NATA models for air the components are e, N_2, and O_2, in that order.

Because the components head the list of species, the relation between them and the elements is specified by the square submatrix $\bar{\alpha}_{ij}$ of α_{ij} with i = 1 to c. Since the components are chosen to be linearly independent combinations of the elements, this submatrix is non-singular and has a unique inverse which will be denoted by A_{ki}. The inverse is defined by

$$\sum_{i=1}^{c} A_{ki}\, \bar{\alpha}_{ij} = \delta_{kj} \tag{3}$$

where the Kronecker symbol δ_{kj} is 1 for k = j and 0 otherwise. With the aid of the inverse matrix A_{ki}, the system of equations (2) for i = 1 to c can be solved to obtain the elements as linear combinations of the components:

$$\sum_{i=1}^{c} A_{ki}\, M_i = \sum_{i=1}^{c} \sum_{j=1}^{c} A_{ki}\, \alpha_{ij}\, E_j = \sum_{j=1}^{c} \delta_{kj}\, E_j = E_k \tag{4}$$

Equation (4) can now be substituted into the remaining equations (2) for i = c + 1, c + 2, . . ., n, to obtain expressions for the dependent species in terms of the components:

$$M_i = \sum_{k=1}^{c} \bar{\nu}_{i-c,k}\, M_k \quad (i = c+1, \ldots, n) \tag{5}$$

where

$$\bar{\nu}_{i-c,k} = \sum_{j=1}^{c} \alpha_{ij} A_{jk} \quad (i = c + 1, \ldots, n) \tag{6}$$

The matrix $\bar{\nu}$ gives the composition of the dependent species in terms of the components.

The overall elemental composition of the gas mixture is invariant through all reactions, equilibrium or non-equilibrium. It is specified on input in terms of the mole fractions X_j^c of the species making up the cold gas which is injected into the arc heater. These mole fractions and the chemical formulas for the cold species are used to calculate the number of gram-atoms of each element k per mole of the cold gas, denoted by Q_k:

$$Q_k = \sum_{j=1}^{n_c} X_j^c \alpha_{jk}^c \tag{7}$$

where α_{jk}^c is the number of atoms of the k^{th} element in a molecule of the j^{th} cold species, and n_c is the number of cold species.

For use in the thermochemical equilibrium calculations, the elemental composition of the gas must be re-expressed in terms of the independent species. Because the elements can be expressed as linear combinations of the independent species by equation (4), the elemental composition of the gas is equivalent to a composition in terms of the components. Let q_j^c denote the number of molecules of the j^{th} component per molecule of the cold gas when the gas is considered to consist of the independent species. These quantities q_j^c are related to the Q_k by

$$Q_k = \sum_{j=1}^{c} q_j^c \alpha_{jk} \qquad (k = 1, \ldots, c) \tag{8}$$

Multiplication of this equation by A_{ki} and summation over k gives

$$q_i^c = \sum_{k=1}^{c} A_{ki} Q_k \qquad (i = 1, \ldots, c) \tag{9}$$

NATA computes the q_i^c from equation (9), and then normalizes them,

$$q_i = \frac{q_i^c}{\sum_{j=1}^{c} q_j^c} \qquad (i = 1, \ldots, c) \tag{10}$$

to obtain a set of composition coefficients whose sum is unity. If the gas actually consisted of the components and no other species, the q_i would be the mole fractions of the components.

The above definitions and relations can be used to derive a formula for the mole fractions of the independent species in terms of the q_i and the mole fractions of the $(n-c)$ dependent species. This formula is used in the equilibrium calculations. Let N_j represent the number of molecules of species j in a gas sample containing $N = \sum_{j=1}^{n} N_j$ molecules altogether. Also, let N_j^* denote the number of molecules of the j^{th} independent species that the sample would contain if all of the atoms making up molecules of the dependent species were rearranged to form molecules of the independent species. From the definition (5) of the $\bar{\nu}_{i-c,k}$ matrix,

$$N_j^* = N_j + \sum_{i=c+1}^{n} N_i \bar{\nu}_{i-c,j} \qquad (j = 1, \ldots, c) \tag{11}$$

where the first term is the number of molecules of species j actually present and the sum represents the extra species j molecules that could be formed from the dependent species. From the definition of q_j,

$$q_j = \frac{N_j^*}{\sum_{k=1}^{c} N_k^*} \tag{12}$$

From (11) and (12),

$$q_j \sum_{k=1}^{c} \left[N_k + \sum_{i=c+1}^{n} N_i \bar{\nu}_{i-c,k} \right] = N_j + \sum_{i=c+1}^{n} N_i \bar{\nu}_{i-c,j} \tag{13}$$

This equation may now be divided through by N to convert the subscripted N's to mole fractions, X. It is noted that

$$\sum_{k=1}^{c} X_k = 1 - \sum_{i=c+1}^{n} X_i \tag{14}$$

Also, the singly subscripted array ν^*_{i-c} is defined by

$$\nu^*_{i-c} \equiv \sum_{k=1}^{c} \bar{\nu}_{i-c,k} \tag{15}$$

Equation (13) then becomes

$$X_j = q_j - \sum_{i=c+1}^{n} X_i \left[\bar{\nu}_{i-c,j} - q_j (\nu^*_{i-c} - 1)\right] \tag{16}$$

which gives the mole fractions X_j of the independent species ($j = 1$ to c) in terms of the q_j and the mole fractions X_i ($i = c + 1, \ldots, n$) for the dependent species.

2.2 Thermodynamic Properties of Species

The thermochemical equilibrium calculations for the reservoir and the nozzle flow calculations require data on the following properties for each chemical species (j) in the gas: the molar enthalpy H_j, the chemical potential μ^o_j and molar entropy S^o_j at a standard pressure p^o, and the molar heat capacity C_{pj}. For a mixture of ideal gases, these thermal properties are functions only of temperature.

The chemical potential may be defined (ref. 2, p. 283) as the partial derivative of the free energy of a gas mixture with respect to the quantity of one of its constituents:

$$\mu_j = (\partial F / \partial N_j)_{S, V, N_k} \tag{17}$$

where the subscripts indicate that the entropy S, volume V, and quantities of the other constituents are held constant. The units of μ_j depend upon those for F and N_j. The quantity measure N_j can be molecules, moles, grams, etc. On a molar basis, μ_j can be calculated using the relation (ref. 2, p. 953)

$$\mu_j = - R_0 T \ln\left(\frac{f_j}{e}\right) + H^o_{j0} \tag{18}$$

in which R_0 is the universal gas constant, f_j is the molecular partition function for species j, defined as a sum over all energy states E_i

$$f_j = \sum_i e^{-E_i/kT} \tag{19}$$

and H^o_{j0} is the enthalpy of formation of the species at standard conditions (usually zero temperature). For an ideal gas

$$f_j = \frac{(2\pi m_j kT)^{3/2} e}{h^3 n_j} f_{int}(T) \tag{20}$$

where f_{int} is the partition function for the internal degrees of freedom. In the first factor on the right, which is the translational partition function, n_j denotes the number of particles of species j per unit volume and m_j the particle mass; k is Boltzmann's constant, h Planck's constant, and e the base of natural logarithms. The partition function depends upon the pressure through n_j. For convenience in calculations, equation (18) is rewritten in the form

$$\mu_j = \mu_j^o + R_0 T \ln p_j \tag{21}$$

where p_j denotes the partial pressure in atmospheres and μ_j^o is the chemical potential at a partial pressure of 1 atmosphere (a function only of temperature). From equations (18), (20), (21) and the ideal gas law

$$p_j = n_j kT$$

it is possible to show that

$$\mu_j^o = -R_0 T \ln \left(\frac{r_j kT}{p^o} \right) + H^o_{j0} \tag{22}$$

where $p^o = 1.01326 \times 10^6$ dyne/cm^2 (a pressure of 1 atmosphere expressed in absolute cgs units) and r_j is a function only of the temperature:

$$r_j \equiv n_j f_j / e \tag{23}$$

Because the molar internal energy of a species is given by (ref. 2, p. 335)

$$E_j = R_0 T^2 \left(\frac{\partial \ln f_j}{\partial T} \right)_{V, N_j} \tag{24}$$

one can show, by differentiating (22), that the molar enthalpy $H_j = E_j + R_0 T$ is given by

$$\frac{H_j - \overset{o}{H}_{j0}}{R_0 T} = - T \frac{d}{dT} \left(\frac{\overset{o}{\mu}_j - \overset{o}{H}_{j0}}{R_0 T} \right) \tag{25}$$

in which $\overset{o}{H}_{j0}$ is the enthalpy of formation of the species. The molar enthalpy of the gas mixture is simply the sum of the species enthalpies weighed by the mole fractions:

$$H = \sum_{j=1}^{n} X_j H_j \tag{26}$$

The other required species thermodynamic properties can be calculated from H_j and $\overset{o}{\mu}_j$. The entropy S_j of the j^{th} species is given by (ref. 2, p. 261 and 287)

$$S_j = \frac{H_j - \mu_j}{T} \tag{27}$$

With (21), this can be rewritten

$$S_j = \overset{o}{S}_j - R_0 \ell n \, p_j \tag{28}$$

where p_j is the species partial pressure in atmospheres, and

$$\overset{o}{S}_j = \frac{H_j - \overset{o}{\mu}_j}{T} \tag{29}$$

is the species entropy at the standard pressure (1 atm), a function only of temperature. The molar entropy of the gas mixture is given in terms of the species entropies by (ref. 2, p. 618)

$$S = \sum_{j=1}^{n} X_j S_j \tag{30a}$$

If p denotes the total pressure in atmospheres, (30a) can be rewritten, with the aid of the relation $p_j = X_j p$ between the partial pressures and mole fractions, in the form

$$S = \sum_{j=1}^{n} X_j S_j^{\circ} - R_0 \ln p - R_0 \sum_{j=1}^{n} X_j \ln X_j \tag{30b}$$

in which the last term is the entropy of mixing.

The molar heat capacity of the j^{th} species is defined by

$$C_{pj} = \frac{dH_j}{dT} \tag{31}$$

The heat capacity of the gas mixture is then

$$C_p = \sum_{j=1}^{n} X_j C_{pj} \tag{32}$$

Equations (25), (29) and (31) show that H_j, S_j° and C_{pj} can all be calculated from the chemical potentials μ_j° at the standard pressure. Two methods are available in the NATA code for calculating the chemical potentials themselves. Both are based fundamentally upon the statistical mechanical expression (18) for μ_j in terms of the molecular partition function f_j. One method, called the thermo-fit technique, relies upon accurate calculations of μ_j° by other computer programs. The data on μ_j° as a function of temperature are curvefitted in the form

$$\frac{\mu_j^{\circ} - H_{j0}^{\circ}}{R_0 T} = a_j(1 - \ln T) - b_j T - \frac{1}{2} c_j T^2 - \frac{1}{3} d_j T^3 - \frac{1}{4} e_j T^4 - k_j \tag{33}$$

Then from (25),

$$\frac{H_j - H_{j0}^{\circ}}{R_0 T} = a_j + b_j T + c_j T^2 + d_j T^3 + e_j T^4 \tag{34}$$

Thus, the parameters a_j, b_j, etc., are simply the coefficients of a fourth-degree polynomial curvefit to $(H_j - H_{j0}^{\circ})/R_0 T$. The thermo-fit method has the following advantages:

1. The thermal property data generated by a specialized thermal-property computer program can be highly accurate, because the program can perform elaborate calculations, taking account of effects such as vibrational anharmonicity and vibration-rotation coupling in molecules.

2. The computer time required for evaluation of the curvefit formulas (33) and (34) is small.

3. The method is applicable to molecules which are too complicated to be treated by the other technique available in NATA, e.g., non-linear triatomic molecules and molecules containing four or more atoms.

The curvefit coefficients a_j , b_j , etc., are determined by least-squares fitting of equation (34) to computed enthalpy values over a certain temperature range. Within the range of the data, the fit has good accuracy, but above and below this range the accuracy can become very poor. If the range of the data is simply extended, the overall accuracy deteriorates because the polynomial form (34) is not sufficiently flexible.

This limitation of the thermo-fit method can be circumvented by using the second NATA technique for calculating species thermal properties to obtain the properties at relatively low temperatures. The second technique, called the "physical model"*, is based upon approximate evaluation of the internal partition function f_{int} in (20) for each species. For a monatomic species, the only internal energy states are those of electronic excitation, and

$$f_{int} = f_{elec} = \sum_{i=1}^{L} g_i \, e^{-E_i/kT} \tag{35}$$

In this equation, E_i is the energy of the i^{th} electronic state relative to the ground state ($i = 1$), and g_i is the state degeneracy. In principle, the upper limit of summation L should be at the highest bound state below the effective ionization potential. In practice, results of good accuracy can be obtained by including only a few states of the lowest energy. High-lying states of nearly equal energy can be lumped together by using an average E_i and summing the degeneracies. Array dimensions in NATA allow use of up to 10 states, including the ground state.

For species containing more than one atom, the internal partition function sum includes states with various values of the vibrational-rotational energy. In the NATA physical model, the partition function for molecules is approximated as a product

$$f_{int} = f_{rot} \cdot f_{vibr} \cdot f_{elec} \tag{36}$$

of rotational, vibrational, and electronic factors. This approximation neglects the variation of the molecular moment of inertia with the vibrational quantum number as well as the difference in vibrational frequencies between different electronic states of the molecule. As a further approximation, the vibrational energy states for each normal mode are approximated by those of a harmonic oscillator. These approximations to the partition function for molecules become inaccurate at high temperatures, but are expected to give good results at moderate temperatures where most of the molecules are in their electronic ground state and the degree of vibrational excitation is not too high.

*It is called the "harmonic-oscillator model" in reference 1.

For linear molecules (including all diatomic species), the rotational partition function, f_{rot} , neglecting quantum effects as is appropriate for the temperatures of interest in NATA, is given by (ref. 2, p. 345 and 454)

$$f_{rot} = \frac{8\pi^2 I k T}{\sigma h^2} = \frac{k T}{\sigma h c B_0} \tag{37}$$

where I denotes the molecular moment of inertia about an axis, passing through the center of mass, perpendicular to the line joining the constituent atoms. The symmetry factor σ is unity for asymmetric molecules and equal to 2 for symmetric molecules (with identical nuclei at opposite ends of the molecule). The quantity B_0 in the final expression of (37) is the rotational constant of the molecule in the ground vibrational state. For diatomic molecules, it is given in terms of tabulated spectroscopic constants by

$$B_0 = B_e - \frac{1}{2} a_e \tag{38}$$

where B_e denotes the rotational constant for the equilibrium internuclear separation and a_e is the coefficient giving the dependence of the rotational constant upon the vibrational quantum number. The term $\frac{1}{2} a_e$ is normally quite small and can be neglected without serious error within the context of the approximations being used. In terms of B_0, the moment of inertia is given by

$$I = \frac{h}{8\pi^2 c B_0} \tag{39}$$

Thus, (37) can be written

$$f_{rot} = \frac{T}{\theta_r} \tag{40a}$$

where the characteristic rotational temperature θ_r is defined as

$$\theta_r = \frac{h c \sigma}{k} B_0 = 1.43879\ \sigma B_0 \tag{40b}$$

with B_0 given in cm^{-1}.

For non-linear triatomic molecules* (ref. 2, p. 454),

$$f_{rot} = \frac{\pi^{1/2} (8\pi^2 k T)^{3/2} (I_A I_B I_C)^{1/2}}{\sigma h^3} \tag{41}$$

where I_A , I_B , and I_C are the three principal moments of inertia.

*The non-linear case is not treated in the present version of NATA. The formulas for this case are given with a view toward possible future development of the code.

For diatomic molecules, the vibrational partition function in the harmonic-oscillator approximation is (ref. 2, p. 345)

$$f_{vibr} = \left(1 - e^{-h\nu_1/kT}\right)^{-1} \equiv \left(1 - e^{-\theta_v/T}\right)^{-1} \tag{42}$$

where $h\nu_1$ is the energy difference between the ground state and the first vibrationally excited state, and θ_v the characteristic vibrational temperature

$$\theta_v = h\nu_1/k \tag{43}$$

The vibrational term of a diatomic molecule is represented in the form (ref. 3, p. 92)

$$G(v) = \omega_e \left(v + \frac{1}{2}\right) - \omega_e x_e \left(v + \frac{1}{2}\right)^2 + \omega_e y_e \left(v + \frac{1}{2}\right)^3 \tag{44}$$

The vibrational constants ω_e, $\omega_e x_e$, and $\omega_e y_e$ have been determined from spectroscopic studies for many diatomic molecules (ref. 3, p. 501-581). The vibrational excitation energy $h\nu_1$ is given by $h\nu_1 = hc\,[G(1) - G(0)]$. Thus, from (43) and (44)

$$\theta_v = \frac{hc}{k}\left(\omega_e - 2\omega_e x_e + \frac{13}{4}\,\omega_e y_e\right) \tag{45}$$

It is clear from (44) that $G(v) - G(v-1)$ varies with the vibrational quantum number v. For this reason, the present harmonic oscillator approximation (which neglects this variation) becomes inaccurate at high temperatures where several vibrational levels are populated to a significant degree.

A triatomic molecule has three vibrational normal modes. The vibrational partition function for a non-linear triatomic species is

$$f_{vibr} = \prod_{k=1}^{3} \left(1 - e^{-\theta_{vk}/T}\right)^{-1} \tag{46}$$

In a linear triatomic molecule, there are only two rotational degrees of freedom and the "bending" vibrational mode is degenerate. In this case, the vibrational partition function is given by

$$f_{vibr} = \prod_{k=1}^{4} \left(1 - e^{-\theta_{vk}/T}\right)^{-1} \tag{47}$$

in which two of the θ_{vk}, say $\theta_{v2} = \theta_{v3}$, are equal to the vibrational temperature for the bending mode.

The chemical potential μ_j^o at standard pressure can now be evaluated by substituting the expressions for the internal partition function, based on the physical model, into the general relations (20), (22) and (23). For monatomic species, f_{int} is given by (35), so that

$$\frac{\mu_j^o - H_{j0}^o}{R_0 T} = -\left\{ \frac{3}{2} \ln\left(\frac{2\pi m_j k}{h^2}\right) + \ln\left(\frac{k}{p^o}\right) + \frac{5}{2} \ln T + \ln (f_{elec}) \right\} \tag{48}$$

For molecular species, from (36),

$$\frac{\mu_j^o - H_{j0}^o}{R_0 T} = -\left\{ \frac{3}{2} \ln\left(\frac{2\pi m_j k}{h^2}\right) + \ln\left(\frac{k}{p^o}\right) + \frac{5}{2} \ln T + \ln (f_{rot}) + \ln (f_{vibr}) + \ln (f_{elec}) \right\} \tag{49}$$

The chemical potential formulas for monatomic and diatomic species can be combined into a single equation involving the number n_j of atoms in a molecule of the species:

$$\frac{\mu_j^o - H_{j0}^o}{R_0 T} = -\left\{ b_j + \frac{5 + 2(n_j - 1)}{2} \ln T - (n_j - 1) \ln (1 - e^{-\theta_{vj}/T}) + \ln \left(\sum_{i=1}^{L_j} g_{ij} \, e^{-E_{ij}/kT} \right) \right\} \tag{50}$$

where

$$b_j = \frac{3}{2} \ln\left(\frac{2\pi m_j k}{h^2}\right) + \ln\left(\frac{k}{p^o}\right) - (n_j - 1) \ln \theta_{rj} \tag{51a}$$

In these formulas, equations (35), (39) and (42) have been used to evaluate the electronic, rotational, and vibrational factors in the partition function. If numerical values are substituted for the physical constants, (51) becomes

$$b_j = -3.66505 + \frac{3}{2} \ln W_j - (n_j - 1) \ln \theta_{rj} \tag{51b}$$

in which W_j is the species molecular weight in grams per mole.

In the case of a linear triatomic species, from (49), (35), (39), and (47)

$$\frac{\mu_j^o - H_{j0}^o}{R_0 T} = -\left\{ B_j + \frac{7}{2} \ln T - \sum_{i=1}^{4} \ln\left(1 - e^{-\theta_{vji}/T}\right) + \ln\left(\sum_{i=1}^{L_j} g_{ij}\, e^{-E_{ij}/kT} \right) \right\} \tag{52}$$

where

$$B_j = \frac{3}{2} \ln\left(\frac{2\pi m_j k}{h^2}\right) + \ln\left(\frac{k}{p^o}\right) - \ln \theta_{rj} \tag{53}$$

The enthalpy can be calculated for monatomic and diatomic species by applying equation (25) to (50):

$$\frac{H_j - H_{j0}^o}{R_0 T} = \frac{5 + 2(n_j - 1)}{2} + (n_j - 1)\,\frac{\theta_{vj}}{T} \cdot \frac{1}{e^{\theta_{vj}/T} - 1} + \frac{1}{kT} \cdot \frac{\sum_{i=1}^{L_j} g_{ij}\, E_{ij}\, e^{-E_{ij}/kT}}{\sum_{i=1}^{L_j} g_{ij}\, e^{-E_{ij}/kT}} \tag{54}$$

In the case of linear triatomic species, application of (25) to (52) gives

$$\frac{H_j - H_{j0}^o}{R_0 T} = \frac{7}{2} + \sum_{i=1}^{4} \frac{\theta_{vji}}{T} \cdot \frac{1}{e^{\theta_{vji}/T} - 1} + \frac{1}{kT} \cdot \frac{\sum_{i=1}^{L_j} g_{ij}\, E_{ij}\, e^{-E_{ij}/kT}}{\sum_{i=1}^{L_j} g_{ij}\, e^{-E_{ij}/kT}} \tag{55}$$

The molar heat capacity for monatomic and diatomic species is, from (31) and (54),

$$\frac{C_{pj}}{R_0} = \frac{5 + 2(n_j - 1)}{2} + (n_j - 1)\left(\frac{\theta_{vj}}{T}\right)^2 \cdot \frac{e^{\theta_{vj}/T}}{(e^{\theta_{vj}/T} - 1)^2} + \frac{S_1 S_3 - S_2^2}{S_1^2} \tag{56a}$$

where

$$S_1 \equiv \sum_{i=1}^{L_j} g_{ij}\, e^{-E_{ij}/kT} \tag{56b}$$

$$S_2 \equiv \sum_{i=1}^{L_j} g_{ij}\, \frac{E_{ij}}{kT}\, e^{-E_{ij}/kT} \tag{56c}$$

$$S_3 \equiv \sum_{i=1}^{L_j} g_{ij}\, \left(\frac{E_{ij}}{kT}\right)^2 e^{-E_{ij}/kT} \tag{56d}$$

For linear triatomic species, from (31) and (55),

$$\frac{C_{pj}}{R_0} = \frac{7}{2} + \sum_{i=1}^{4} \left[\left(\frac{\theta_{vji}}{T}\right)^2 \cdot \frac{e^{\theta_{vji}/T}}{\left(e^{\theta_{vji}/T} - 1\right)^2}\right] + \frac{S_1 S_3 - S_2^2}{S_1^2} \tag{57}$$

The thermal properties of a species can be specified using the thermo-fit, the physical model, or both techniques. In the case of a non-linear triatomic species or a species whose molecules contain four or more atoms, the programming of NATA does not provide a treatment based on the physical model. The properties of such species must be described using the thermo-fit at all temperatures. On the other hand, for monatomic species, the physical model is accurate at all temperatures. Accordingly, only this model is used for the atoms and atomic ions whose properties are compiled into NATA. For most molecular species, both thermo-fit data and physical model properties are provided in the code. The physical model is used for temperatures up to a "switching" temperature T_{sw} which is preset to 5000° K; and the thermo-fit is used for temperatures above T_{sw}. To avoid disturbance of the flow solution by a small discontinuity in thermal properties

at the switching temperature, the transition between the two models is spread out over a temperature range 1000° K wide, between T_{sw} - 500° K and T_{sw} + 500° K. Within this range, the species thermal properties are calculated by mixing the results from the thermo-fit and the physical model; e.g., for the enthalpy,

$$H_j = w_{TF} \cdot (H_j)_{TF} + w_{PM} \cdot (H_j)_{PM} \tag{58a}$$

where

$$w_{TF} = \frac{500 + (T - T_{sw})}{1000} \tag{58b}$$

$$w_{PM} = \frac{500 - (T - T_{sw})}{1000} \tag{58c}$$

and where the subscript TF denotes the thermo-fit and PM the physical model.

2.3 Reaction Rates

A chemical reaction* involving some of the species present in the gas mixture can be denoted

$$\sum_{j=1}^{n} \nu_{ij} M_j \underset{k_{ri}}{\overset{k_{fi}}{\rightleftharpoons}} \sum_{j=1}^{n} \nu'_{ij} M_j \tag{59}$$

in which M_j represents a molecule of the j^{th} species and the ν_{ij} , ν'_{ij} are stoichiometric coefficients. For the molecules which do not participate in the reaction as reactants, $\nu_{ij} = 0$; for those which do not appear among the products, $\nu'_{ij} = 0$. The subscript i serves to distinguish the different reactions. The total number of reactions is denoted by r .

The molar concentration of species j will be denoted by $[M_j]$. If (59) represents an actual reaction mechanism, then the number of moles of forward reactions occurring per unit volume is given by

$$N_{fi} = k_{fi} \prod_{k=1}^{n} [M_k]^{\nu_{ik}} \tag{60a}$$

*See reference 4, Chapter XVII, for a background discussion of classical chemical kinetics.

in which the reaction rate constant k_{fi} is independent of the species concentrations but is, in general, a function of temperature. Correspondingly, for the reverse reaction

$$N_{ri} = k_{ri} \prod_{k=1}^{n} [M_k]^{\nu_{ik}} \tag{60b}$$

If (59) represents the net result of two or more steps in the actual reaction mechanism, then equations (60) are inapplicable. In such a case, if (60) were forced to fit experimental rate data, it would be found that the apparent rate constants k_{fi} and k_{ri} would vary with the species concentrations.

From equations (59) and (60), the net rate of change of the concentration $[M_j]$ of species j due to the i^{th} reaction is

$$\left\{\frac{d[M_j]}{dt}\right\}_i = (\nu'_{ij} - \nu_{ij})\, k_{fi} \prod_{k=1}^{n} [M_k]^{\nu_{ik}} - (\nu'_{ij} - \nu_{ij})\, k_{ri} \prod_{k=1}^{n} [M_k]^{\nu_{ik}} \tag{61}$$

In equilibrium, the net rate of production is zero, so that, from (61),

$$k_{ri} = k_{fi} \prod_{k=1}^{n} [M_k]^{(\nu_{ik} - \nu'_{ik})} = \frac{k_{fi}}{K_i} \tag{62}$$

where K_i denotes the equilibrium constant:

$$K_i = \prod_{k=1}^{n} [M_k]^{(\nu'_{ik} - \nu_{ik})} \tag{63}$$

The equilibrium constant for the reaction can be determined from the condition (ref. 2, p. 953):

$$\sum_{j=1}^{n} \nu_{ij} \mu_j = \sum_{j=1}^{n} \nu'_{ij} \mu_j \tag{64}$$

in which μ_j denotes the chemical potential (21) for the j^{th} species. Substitution of (21) into (64) gives

$$\prod_{j=1}^{n} (p_j)^{\beta_{ij}} = \exp\left\{ - \frac{1}{R_0 T} \sum_{j=1}^{n} \beta_{ij} \mu_j^{o} \right\} \tag{65}$$

where

$$\beta_{ij} \equiv \nu'_{ij} - \nu_{ij} \tag{66}$$

For ideal gases, the partial pressures p_j are related to the molar concentrations $[M_j]$ by

$$p_j = [M_j] R_0 T \tag{67}$$

Hence, combination of (63) and (67) gives

$$K_i = \frac{1}{(R_0 T)^{\beta_i}} \exp\left\{ - \frac{1}{R_0 T} \sum_{j=1}^{n} \beta_{ij} \mu_j^{o} \right\} \tag{68}$$

where

$$\beta_i \equiv \sum_j \beta_{ij} .$$

Because the chemical potentials at standard pressure (μ_j^{o}) depend only on the temperature, the equilibrium constant K_i is a function only of temperature.

The relation (62) between the forward and reverse rate constants for a reaction is termed "detailed balancing". Since k_{ri}, k_{fi}, and K_i depend only on the temperature, not the concentrations, this relation is valid even when the concentrations are out of equilibrium, as they normally are throughout a non-equilibrium flow solution.

Only one of the two rate constants for each reaction need be specified, as the other can be determined from the first using the detailed balancing relation (62) and the thermochemical expression (68) for the equilibrium constant. Conventionally, the forward rate is specified. In NATA, it is represented as a function of temperature by a curvefit of the form*

$$K_{fi} = A_i \left(\frac{T}{10000^\circ K} \right)^{\eta_i} e^{-E_{ai}/R_0 T} \tag{69}$$

in which E_{ai} is the activation energy for the reaction. Experimental data on rate constants are usually fitted using a form similar to this, but with T^{η_i} in place of $(T/10000)^{\eta_i}$. The specific form (69) has been adopted for use in NATA because, in reactions with large negative exponents η_i, it permits fitting the experimental data with coefficients A_i of smaller magnitude. When the conventional formula with T^{η_i} is used, some such reactions require A_i values larger than the limit ($\sim 10^{38}$) on floating point numbers in computers such as the UNIVAC 1108.

Many dissociation-recombination reactions involve a "third body", a particle which catalyzes the reaction by supplying part of the dissociation energy or carrying off part of the recombination energy. If the rate constants are the same for several reactions which differ only in the third-body species involved, the kinetic model can be simplified by combining all of these reactions into one. The third-body concentration in the combined reaction is equal to the sum of the concentrations of the actual third bodies. The coding of NATA allows this simplification. The third bodies are omitted from the ν_{ij} and ν'_{ij} matrices for the combined reaction but are listed separately. The rate-constant curvefit (69) for the actual three-body reactions is used. The effect of the combined concentration of all the third bodies for the reaction is taken into account by special coding.

2.4 Vibrational Non-equilibrium

The calculations of species thermal properties performed by NATA (Section 2.2) normally assume that the vibrational degrees of freedom of molecules are in thermal equilibrium with the other degrees of freedom. However, the code also contains an option to calculate these properties on the assumption that the vibrational degrees of freedom are "frozen" at the reservoir temperature. This option, together with the normal, equilibrium property calculations, makes it possible to bracket the possible effects of vibrational non-equilibrium. When this option is used, the code calculates the species properties from the physical model at all temperatures. The thermo-fit cannot be used in this case because it is based on a curvefit to property calculations assuming complete equilibrium.

The formulas for the species thermal properties in the case of frozen vibration can be derived from the equations in Section 2.2 by assuming that the vibrational excitation temperature is constant and equal to the reservoir temperature, T_0. For diatomic molecules, the chemical potential (50) becomes

*Other forms are used for some of the reactions in the electronic non-equilibrium model for argon.

$$\frac{\mu_j^\circ - H_{j0}^\circ}{R_0 T} = -\left\{ b_j + \frac{5 + 2(n_j - 1)}{2} \ln T - (n_j - 1) \ln \left(1 - e^{-\theta_{vj}/T_0}\right) + \ln \left(\sum_{i=1}^{L_j} g_{ij} \, e^{-E_{ij}/kT} \right) \right\} \tag{70}$$

The enthalpy (54) becomes

$$\frac{H_j - H_{j0}^\circ}{R_0 T} = \frac{5+2(n_j-1)}{2} + (n_j - 1) \frac{\theta_{vj}}{T} \cdot \frac{1}{e^{\theta_{vj}/T_0} - 1} + \frac{1}{kT} \cdot \frac{\sum_{i=1}^{L_j} g_{ij} \, E_{ij} \, e^{-E_{ij}/kT}}{\sum_{i=1}^{L_j} g_{ij} \, e^{-E_{ij}/kT}} \tag{71}$$

Because the vibrational contribution to the enthalpy H_j is constant, the heat capacity C_{pj} (31) does not contain a vibrational term. The species entropy at standard pressure is given by

$$\frac{S_j^\circ}{R_0} = b_j + \frac{5+2(n_j-1)}{2} (1 + \ln T) + (n_j - 1) \left[\frac{\theta_{vj}/T_0}{e^{\theta_{vj}/T_0} - 1} - \ln (1 - e^{-\theta_{vj}/T_0}) \right] + \frac{1}{kT} \cdot \frac{\sum_{i=1}^{L_j} g_{ij} \, E_{ij} \, e^{-E_{ij}/kT}}{\sum_{i=1}^{L_j} g_{ij} \, e^{-E_{ij}/kT}} + \ln \left(\sum_{i=1}^{L_j} g_{ij} \, e^{-E_{ij}/kT} \right) \tag{72}$$

For a linear triatomic species, the thermal properties in the case of frozen vibration are given by

$$\frac{\mu_j^o - H_j^o}{R_0 T} = -\left\{ B_j + \frac{7}{2} \ell n\, T - \sum_{i=1}^{4} \ell n\, (1 - e^{-\theta_{vji}/T_0}) + \ell n \left(\sum_{i=1}^{L_j} g_{ij}\, e^{E_{ij}/kT} \right) \right\} \tag{73}$$

$$\frac{H_j - H_{j0}^o}{R_0 T} = \frac{7}{2} + \sum_{i=1}^{4} \frac{\theta_{vji}/T}{e^{\theta_{vji}/T_0} - 1} + \frac{1}{kT} \cdot \frac{\sum_{i=1}^{L_j} g_{ij}\, E_{ij}\, e^{-E_{ij}/kT}}{\sum_{i=1}^{L_j} g_{ij}\, e^{-E_{ij}/kT}} \tag{74}$$

$$\frac{S_j^o}{R_0} = B_j + \frac{7}{2} (1 + \ell n\, T) + \sum_{i=1}^{4} \frac{\theta_{vji}/T_0}{e^{\theta_{vji}/T_0} - 1} - \sum_{i=1}^{4} \ell n \left(1 - e^{-\theta_{vji}/T_0}\right) + \ell n \left(\sum_{i=1}^{L_j} g_{ij}\, e^{-E_{ij}/kT} \right) + \frac{1}{kT} \cdot \frac{\sum_{i=1}^{L_j} g_{ij}\, E_{ij}\, e^{-E_{ij}/kT}}{\sum_{i=1}^{L_j} g_{ij}\, e^{-E_{ij}/kT}} \tag{75}$$

The specific heat again lacks a vibrational contribution.

2.5 Gas Imperfections

The CAL program upon which NATA is based (ref. 1) contained an option to include the effects of gas imperfections due to the finite volume of the molecules. Such effects are negligible under the conditions to which NATA is normally applied.

However, to provide for possible, presently unforeseen, future applications of NATA to nozzle flows with extremely high reservoir pressures*, this option has been retained.

The CAL treatment of gas imperfections is based upon the van der Waals equation of state (ref. 2, p. 581)

$$p = \frac{R_0 T}{V - b_0} - \frac{a}{V^2} \tag{76}$$

in which V represents the molar volume

$$V = \frac{W}{\rho} \tag{77}$$

The quantity b_0 is the molar volume from which the centers of the molecules are excluded because of the finite size of the molecules. If the molecules are assumed to be spherical, then

$$b_0 = \frac{2\pi}{3} N_0 \sigma^3 \tag{78}$$

where N_0 is Avogadro's number and σ denotes the molecular diameter. The second term in (76) represents the effects of attraction between the molecules. In NATA, the coefficient a in this term is assumed to be zero, because the attractive forces have negligible effects in the high temperature flows to which NATA is applied. The remaining term is written

$$p = \frac{\tilde{\rho} R_0 T}{W} \tag{79a}$$

where the effective density $\tilde{\rho}$ is defined as

$$\tilde{\rho} = \frac{\rho}{1 - \frac{b_0 \rho}{W^o}} \tag{79b}$$

The molecular weight W^o in (79b) is written with a superscript o to signify that the coefficient b_0/W^o is read as an input, and is assumed to be constant throughout the solution. The molecular weight W in (79a), however, is the local value, which varies in equilibrium and non-equilibrium solutions.

The van der Waals equation (76) is inaccurate at high densities where V becomes comparable with b_0. Thus, equations (79) provide a valid approximation to the effect of finite molecular volume only so long as the term $b_0 \rho / W^o$ is small compared with unity, say, less than about 0.1.

*In air, these effects are of the order of 3 percent when the pressure in atmospheres is about 0.1 times the reservoir temperature in degrees K.

Because molecular attractive forces are neglected in (79), there is no correction to the ideal-gas internal energy. However, the enthalpy is given by

$$H = E + \frac{P}{\rho} = E + \frac{\tilde{\rho}}{\rho}\,\frac{R_0 T}{W} \tag{80}$$

In terms of the enthalpy H_{ideal} for an ideal gas,

$$H = H_{ideal} + \left(\frac{\tilde{\rho}}{\rho} - 1\right)\frac{R_0 T}{W} \tag{81}$$

In NATA, the computation of reservoir conditions is carried out for specified temperature and pressure. The composition is assumed to be the same as for an ideal gas mixture, but the enthalpy and density are calculated from (81) and (79). These relations are also used throughout the frozen and equilibrium flow solutions, and in the initial portion of the non-equilibrium solution which is calculated by perturbing the equilibrium solution. The correction for gas imperfection is not used during the non-equilibrium integration because, in practice, the flow remains near equilibrium (and thus is calculated by the perturbation method) until the density has dropped to values at which the correction is negligible.

Section 5.3 of reference 1 can be consulted for further discussion of this option. For air, this reference recommends a value of $\sigma = 2.6\ \text{Å} = 2.6 \times 10^{-8}$ cm for use in equation (78).

3. TRANSPORT PROPERTIES

NATA requires transport property values for use in the laminar boundary layer calculations and in calculations of heat transfer to models. Some transport properties and related quantities are also printed out. All of the transport coefficients required in NATA are computed internally by a subroutine package which was adapted from a separate, previously developed transport property program. The basic data required by the calculations are compiled into the code for the standard gas species. Such data can also be set in the input.

To facilitate the use of the code in computing inviscid flow solutions for gas models involving non-standard species whose transport cross sections may be unknown, all transport property calculations can be suppressed by input of a single control variable (NØTRAN). This procedure also suppresses the boundary layer calculation and calculations of stagnation point heat transfer and of conditions on wedge models.

According to kinetic theory (ref. 5) the transport coefficients in a mixture of gases depend upon the scattering cross sections $\bar{\Omega}_{ij}$ (defined below) for collisions between pairs of molecules. The Chapman-Enskog theory provides explicit, but extremely complicated, formulas for the viscosity, thermal conductivity, binary diffusion coefficients, and other transport properties in terms of the collision cross sections, the particle masses, the species mole fractions, and the temperature. Thus, in principle, the problem of calculating the transport coefficients for a given mixture consists of two parts: first, the determination of the collision cross sections $\bar{\Omega}_{ij}$ for all possible pairs of species (i, j); and second, the evaluation of the Chapman-Enskog formulas.

The collision cross sections can be determined or estimated in many different ways. They can be measured directly in molecular-beam scattering experiments or can be determined indirectly from the analysis of data on various gas properties. For simple systems they can also be obtained from *ab initio* or semi-empirical quantum mechanical calculations.

For collisions between heavy particles, it is generally advantageous to express the collision cross sections $\bar{\Omega}_{ij}$ in terms of the interaction potential ϕ_{ij} between the particles. The interaction potential can then often be approximated by a simple empirical form containing one or more adjustable parameters which may be chosen to fit the experimental data. For example, one type of model frequently used in this way is the Lennard-Jones (6-12) potential

$$\phi = 4\epsilon\left[\left(\frac{\sigma}{r}\right)^{12} - \left(\frac{\sigma}{r}\right)^{6}\right] \tag{82}$$

Here, r denotes the center-to-center separation of the two molecules, ϵ and σ are the adjustable parameters, and ϕ is the energy of interaction. The parameters can be evaluated by fitting theoretical predictions based on the models to experimental data on some material property, for example, the viscosity, thermal conductivity, binary diffusion coefficient, or second virial coefficient.

Once the interaction potential ϕ_{ij} between a pair of atoms or molecules has been determined, the averaged collision cross sections $\bar{\Omega}_{ij}^{(\ell, s)}$ required in the transport calculations can be computed by classical mechanics. In general this step requires a lengthy numerical computation; however, this computation has already been carried out for a number of commonly used forms for the interaction potential, and tabulated values of the averaged cross sections as functions of temperature are available in the literature.

In the case of a pair of atoms with unpaired valence electrons, quantum mechanical calculations show that there can be several different interaction potentials which occur with different probabilities. In this case the total cross section may be obtained simply by calculating the cross sections independently for each potential and then averaging the resulting cross sections with the appropriate probabilities to obtain the total cross section.

For collisions involving electrons, classical mechanics is not applicable and quantum calculations are required to relate the collision cross sections $\bar{\Omega}_{ij}$ to the interaction potentials. In this case it is often simpler to analyze the data directly in terms of the collision cross sections, without going through the intermediate step of determining the interaction potentials ϕ_{ij}.

After the cross sections $\bar{\Omega}_{ij}^{(\ell, s)}$ have been determined for all pairs of species in the gas, the transport properties may be computed by evaluating several large determinants. This step is straightforward, but can require a considerable amount of computer time in the case of a gas mixture containing a large number of species.

In NATA, the compiled-in transport property data consist of parameter values and tables for direct calculation of the averaged cross sections $\bar{\Omega}_{ij}^{(\ell, s)}$. The interaction potentials themselves are not used. Thus, the step of calculating the cross sections from the interaction potentials is bypassed. In addition, the amount of computation required to evaluate the mixture transport properties is greatly reduced by using approximate formulas, developed by Yos (ref. 7), in place of the full formulas of the first Chapman-Enskog approximation.

3.1 Basic Equations

The properties generated by the transport property calculations in NATA are the mixture viscosity μ, the electrical conductivity σ, the frozen Prandtl number

$$N_{Pr\,f} = c_{pf}\,\mu/K_f \tag{83}$$

and the atom-molecule Lewis number

$$N_{Le} = \frac{\rho\, c_{pf}\, D_{am}}{K_f} \tag{84}$$

where c_{pf} is the frozen specific heat of the mixture at constant pressure, K_f is the frozen thermal conductivity, ρ is the mixture density, and D_{am} is the binary atom-molecule diffusion coefficient for the mixture. The calculations of these

properties are based on the mixture composition as given by the equilibrium or non-equilibrium flow solution, or by the equilibrium normal shock solution, as appropriate.

The viscosity μ and the translational component K_{tr} of the thermal conductivity are computed from an approximation to the first Chapman-Enskog formulas (ref. 5), developed by Yos (ref. 7):

$$\alpha = \frac{\sum_{i=1}^{n} X_i/(A_i^{(\alpha)} + \bar{a}^{(\alpha)})}{1 - \bar{a}^{(\alpha)} \sum_{i=1}^{n} X_i/(A_i^{(\alpha)} + \bar{a}^{(\alpha)})} \tag{85}$$

Here α may represent either the viscosity μ or the translational thermal conductivity K_{tr} ; n is the number of species in the gas; and X_i is the mole fraction of the i^{th} species. Also,

$$\bar{a}^{(\alpha)} \equiv \frac{\sum_{i,j=1}^{n} X_i X_j \left(\frac{1}{A_i^{(\alpha)}} - \frac{1}{A_j^{(\alpha)}}\right)^2 a_{ij}^{(\alpha)}}{\sum_{i,j=1}^{n} X_i X_j \left(\frac{1}{A_i^{(\alpha)}} - \frac{1}{A_j^{(\alpha)}}\right)^2} \tag{86}$$

and

$$A_i^{(\alpha)} \equiv \sum_{j=1}^{n} X_j A_{ij}^{(\alpha)} \tag{87}$$

For the viscosity, the quantities $a_{ij}^{(\alpha)}$ and $A_{ij}^{(\alpha)}$ appearing in equations (86) and (87) are defined by

$$\begin{aligned} a_{ij}^{(\mu)} &\equiv \frac{N_0}{W_i + W_j}\left[2\,\Delta_{ij}^{(1)} - \Delta_{ij}^{(2)}\right] \\ A_{ij}^{(\mu)} &\equiv \frac{N_0}{W_i}\,\Delta_{ij}^{(2)} \end{aligned} \tag{88}$$

while for the translational thermal conductivity they are defined by

$$\begin{aligned} a_{ij}^{(K)} &\equiv \frac{2}{15k}\,\frac{W_i W_j}{(W_i + W_j)^2}\left[\left(\frac{33}{2} - \frac{18}{5}\,B_{ij}^{*}\right)\Delta_{ij}^{(1)} - 4\,\Delta_{ij}^{(2)}\right] \\ A_{ij}^{(K)} &\equiv \frac{2}{15k(W_i + W_j)^2}\left[8 W_i W_j\,\Delta_{ij}^{(2)} + (W_i - W_j)\left(9 W_i - \frac{15}{2}\,W_j + \frac{18}{5}\,B_{ij}^{*}\,W_j\right)\Delta_{ij}^{(1)}\right] \end{aligned} \tag{89}$$

In these equations, W_i is the molecular weight of the i^{th} species, $N_0 = 6.0225 \times 10^{23}$ molecules/mole and $k = 1.3805 \times 10^{-16}$ ergs/^oK are the usual unit conversion factors,

$$\Delta_{ij}^{(1)} \equiv \frac{8}{3}\sqrt{\frac{2\,W_i\,W_j}{\pi N_0\,kT(W_i+W_j)}}\;\bar{\Omega}_{ij}^{(1,1)}$$

$$\Delta_{ij}^{(2)} \equiv \frac{16}{5}\sqrt{\frac{2\,W_i\,W_j}{\pi N_0\,kT(W_i+W_j)}}\;\bar{\Omega}_{ij}^{(2,2)} \qquad (90)$$

$$B_{ij}^{*} \equiv \frac{5\,\bar{\Omega}_{ij}^{(1,2)} - 4\,\bar{\Omega}_{ij}^{(1,3)}}{\bar{\Omega}_{ij}^{(1,1)}} \qquad (91)$$

and the $\bar{\Omega}_{ij}^{(\ell,s)}$ are averaged collision cross sections for the collisions between species i and j, which are supplied as input to the transport property calculations. Several different definitions of the $\bar{\Omega}_{ij}^{(\ell,s)}$ symbols have appeared in the literature.* The one used here is

$$\bar{\Omega}_{ij}^{(\ell,s)} = \frac{\int_0^\infty \gamma^{2s+3}\exp(-\gamma^2)\,\bar{Q}_{ij}^{(\ell)}\,d\gamma}{\int_0^\infty \gamma^{2s+3}\exp(-\gamma^2)\,d\gamma} = [2/(s+1)!]\int_0^\infty \gamma^{2s+3}\exp(-\gamma^2)\,\bar{Q}_{ij}^{(\ell)}\,d\gamma \qquad (92)$$

where

$$\bar{Q}_{ij}^{(\ell)} = \frac{\int_0^\pi (1-\cos^\ell\chi)\,4\pi\,\sigma_{ij}\sin\chi\,d\chi}{\int_0^\pi (1-\cos^\ell\chi)\sin\chi\,d\chi} \qquad (93)$$

$$= [(1+\ell)/(1+2\ell-(-1)^\ell)]\int_0^\pi (1-\cos^\ell\chi)\,4\pi\,\sigma_{ij}\sin\chi\,d\chi$$

Here $\sigma_{ij} = \sigma_{ij}(\chi, g)$ is the differential scattering cross section for the pair $i-j$, χ is the scattering angle in the center of mass system, g is the relative velocity of the colliding particles, and $\gamma = [m_i m_j/2(m_i+m_j)kT]^{1/2} g$ is the reduced velocity. In NATA, the cross sections $\bar{\Omega}_{ij}^{(\ell,s)}$ are calculated as functions of temperature and gas composition for each pair of species in the mixture from basic cross section data, which are either in tabular form or are given as simple analytical functions of temperature and composition.

*The quantity designated here as $\bar{\Omega}_{ij}^{(\ell,s)}$ is called $\pi\,o^2\,\Omega_{ij}^{(\ell,s)*}$ in ref. 5 and $\pi\,\bar{\Omega}_{ij}^{(\ell,s)}$ in ref. 6.

The frozen thermal conductivity K_f appearing in (83) is calculated from the modified Eucken approximation (ref. 8):

$$K_f = K_{tr} + K_{int} \tag{94}$$

where K_{tr} is the translational component of the thermal conductivity given by equations (85) to (91),

$$K_{int} = k \sum_{i=1}^{n} \left[\left(\frac{W_i c_{pi}}{N_0 k} - \frac{5}{2} \right) X_i \Bigg/ \left(\sum_{j=1}^{n} X_j \Delta_{ij}^{(1)} \right) \right] \tag{95}$$

is the component of the thermal conductivity resulting from the internal excitation energy of the molecules, and c_{pi} is the specific heat at constant pressure for the i^{th} species. The frozen specific heat c_{pf} for the mixture is then given by

$$c_{pf} = \frac{1}{W} \sum_{i=1}^{n} X_i W_i c_{pi} \tag{96}$$

where

$$W = \sum_{i=1}^{n} X_i W_i \tag{97}$$

is the average molecular weight, and $X_i W_i / W$ is the mass fraction of species i in the mixture.

For the electrical conductivity, the NATA code uses an expansion of the first Chapman-Enskog approximation (ref. 5) to lowest order in the ratio (m_e/m_i) between the electron and atom masses,

$$\sigma = \frac{e^2}{kT} \frac{X_e}{\sum_{j=1}^{n}{}' X_j \Delta_{ej}^{(1)}} \tag{98}$$

where e is the electronic charge and the prime on the summation sign indicates that the term $X_e \Delta_{ee}^{(1)}$ is to be omitted from the sum. The complete first Chapman-Enskog approximation,

$$D_{ij} = \frac{W}{\rho N_0 \Delta_{ij}^{(1)}} \tag{99}$$

is used for the atom-molecule diffusion coefficient required in the Lewis number calculations.

3.2 Accuracy of the Calculations

The accuracy of equations (85) to (91), which are used for the calculation of the viscosity and translational thermal conductivity in NATA, has been discussed in reference 7, and it is shown that these equations generally give results within a percent or less of the first Chapman-Enskog approximation, with considerable savings in computation time. The accuracy of the first Chapman-Enskog approximation itself depends primarily on the temperature dependence of the collision cross sections $\bar{\Omega}_{ij}^{(\ell, s)}$ for the various species in the gas. The approximation is exact for cross sections which vary inversely as $\sqrt{T}$ (i.e., constant collision frequency, or force proportional to the inverse fifth power of the internuclear separation), and becomes progressively poorer as the temperature dependence of the cross sections deviates further from this law. For neutral-neutral and neutral-ion collisions, where the cross section dependence is close to $1\sqrt{T}$, the first Chapman-Enskog approximation generally gives transport properties within a few percent of the exact solution (ref. 5). Because the collision cross sections $\bar{\Omega}_{ij}^{(\ell, s)}$ are known only within about 10 to 20 percent at best, for the species considered in the NATA code, the additional error introduced into the calculated transport properties by the use of the first Chapman-Enskog approximation for neutral-neutral and neutral-ion collisions is negligible.

The effects of Coulomb collisions, for which the cross sections are proportional to $1/T^2$, are not given very accurately by the first Chapman-Enskog approximation; for example, in the limiting case of a fully ionized gas, the transport properties calculated from this approximation differ by about a factor of two from those obtained from an exact solution of the Boltzmann equation (ref. 9). Coulomb collisions are treated in NATA using effective cross sections which are chosen to make the transport properties calculated from equations (85) to (99) agree with the exact solutions for a fully ionized gas at low pressures (ref. 9). The transport properties calculated from equations (85) to (99) for partially ionized gases using these effective Coulomb cross sections are then found to agree with accurate calculations for partially ionized gases (refs. 10 to 12) within about 10 to 20 percent at all degrees of ionization, which is again within the accuracy of the available cross section data.

The effective cross sections used for Coulomb collisions in the NATA code are given by the following equations:

$$\bar{\Omega}_{ee}^{(1,1)} = 0.795\, Q_c \qquad \bar{\Omega}_{ee}^{(2,2)} = 1.29\, Q_c$$

$$\bar{\Omega}_{e1}^{(1,1)} = 0.795\, Q_c \qquad \bar{\Omega}_{e1}^{(2,2)} = 1.29\, Q_c$$

$$\bar{\Omega}_{e2}^{(1,1)} = 2.71\, Q_c \qquad \bar{\Omega}_{e2}^{(2,2)} = 5.16\, Q_c$$

$$\bar{\Omega}_{11}^{(1,1)} = 0.795\, Q_c \qquad \bar{\Omega}_{11}^{(2,2)} = 1.36\, Q_c$$

$$\bar{\Omega}_{12}^{(1,1)} = 2.71\, Q_c \qquad \bar{\Omega}_{12}^{(2,2)} = 5.44\, Q_c$$

$$\bar{\Omega}_{22}^{(1,1)} = 12.7\, Q_c \qquad \bar{\Omega}_{22}^{(2,2)} = 21.76\, Q_c$$

$$B_{ij}^{*} = 1.5625 \tag{100a}$$

where the subscripts e , 1 and 2 represent respectively electrons and singly and doubly charged ions,

$$Q_c = \left(\frac{e^2}{kT}\right)^2 \ell n\ (f\,\Lambda) \tag{100b}$$

e is the electronic charge,

$$\Lambda = \frac{3}{2}\,\frac{(kT)^{3/2}}{e^3\,(\pi n_e)^{1/2}} \tag{100c}$$

is the Debye shielding parameter introduced by Spitzer (ref. 9), n_e is the number of free electrons per unit volume, and f is a correction factor to take account of the reduced effectiveness of the shielding at high electron densities. The correct form for the factor f is not known at the present time and a number of different approximations have been suggested for it (refs. 13 to 16). For electron number densities below about 10^{17} to $10^{18}/cm^3$ f is $\sim$1 and all approximations for the transport properties (refs. 13 to 16) agree within about 10 to 20 percent; at higher electron densities, however, substantial differences between the different approximations begin to appear, and the correct treatment of the problem has not yet been established. The NATA code uses the approximation suggested by Yos (ref. 7):

$$f = \sqrt{1 + \frac{64\pi}{9}\,\frac{e^2}{kT}\,n_e^{1/3}} \tag{100d}$$

However, as noted above, the errors in this approximation may be large at the higher electron densities.

Errors in the first Chapman-Enskog approximation may also be large for electron-neutral collisions, ranging up to about a factor of three in the case of electron-argon atom collisions (ref. 10), because of the strong temperature dependence of the cross sections which results from the Ramsauer effect in argon. For this case also, the NATA code makes use of effective collision cross sections in equations (83) to (99) to calculate the transport properties, with the cross sections being chosen to match the experimental electrical conductivity data as well as possible.* For those cases in which comparisons have been made, this approach yields transport properties which agree with the available experimental data within experimental error, which is generally of the order of 20 to 30 percent; however, larger errors than this are of course possible in other cases.

*Note that electrical conductivity is the only transport property which is significantly dependent on the electron-neutral cross sections.

The accuracy of the modified Eucken approximation used in the thermal conductivity calculations for the NATA code has been examined in detail by Mason and Monchick (ref. 17). Errors in this approximation may approach 10 to 20 percent in cases where there is a rapid exchange of energy between excitation and translational states through inelastic collisions, as is normally the case for rotational excitation in low temperature gases; however, the errors become smaller when the exchange is less rapid, and are negligible in cases where 20 or more collisions are required for the exchange of energy between internal excitation and translation. Because the latter situation is normally the case for high temperature gases, errors resulting from the use of the modified Eucken approximation should generally be a few percent or less in the NATA code, though errors of as much as 10 to 20 percent may arise from this source in exceptional cases, where the inelastic collision cross sections for some of the important internal states of a species are large. For atomic gases, of course, internal excitation does not ordinarily contribute very significantly to the thermal conductivity (ref. 18), so that in such cases the modified Eucken approximation is necessarily valid, regardless of the behavior of the inelastic cross sections.

In summary, the accuracy of the transport property calculations in the NATA code appears to be governed in almost all cases by the accuracy of the data on atomic and molecular collision cross sections used in the calculations. For the cross section data compiled into the code, this accuracy should generally be in the range from about 20 to 40 percent, except in the case of carbon containing mixtures, where only rough cross section estimates are available for some species and errors may consequently range up to as much as a factor of two or more on occasion.

The discussion of the accuracy of the transport property calculations in NATA has not included any errors in the calculated transport property values which may arise from errors in the gas composition data used as input to these calculations. When such errors are important, they will of course decrease the absolute accuracy of the calculated transport properties and may need to be considered in evaluating the overall accuracy of the code results.

3.3 Method of Calculation

The formulas in Section 3.1 give the desired transport properties in terms of the temperature T, the species mole fractions X_i, molecular weights W_i, specific heats c_{pi}, and the average collision cross sections $\bar{\Omega}_{ij}^{(\ell, s)}(T)$. All of these data, except the cross sections, are provided by the gas dynamic calculations in NATA.

The cross sections for all of the pairs of species are computed in a series of steps. First, the cross sections for all pairs are set to zero. Then, in each step, the values of $\bar{\Omega}^{(1, 1)}$, $\bar{\Omega}^{(2, 2)}$, and $B^* \bar{\Omega}^{(1, 1)}$ are computed by a particular method (or option) with a particular set of parameter values, and these values are added to the corresponding cross sections $\bar{\Omega}_{ij}^{(1, 1)}$, $\bar{\Omega}_{ij}^{(2, 2)}$, and $B_{ij}^* \bar{\Omega}_{ij}^{(1, 1)}$ for each pair of species (i, j) to which the step is applicable. The information concerning the applicability of steps to species pairs is stored in index arrays. If only one step of the cross section calculation is applicable to a particular species pair, then the cross sections for that pair are the values computed during that step. If more than one step is applicable to the pair, the cross sections for the pair are built up by adding contributions from

the different steps. This procedure provides considerable flexibility in the representation of the cross sections. If the cross sections are poorly known for several minor pairs of species, but are considered likely to be roughly the same for all pairs, then the cross sections for all of these pairs can be set in a single step.

The code contains default provisions for estimating some cross sections if they are not specified explicitly in the compiled-in data or the input. If none of the specified steps is applicable to a particular pair, and if both of the species are ions, then the effective Coulomb cross sections (100) are used. If one species is neutral and the other ionized, the formula

$$\bar{\Omega}_{ij}^{(\ell, s)} = A^{(\ell, s)} \, T^{-0.4} \tag{101}$$

is the default option. The constants $A^{(\ell, s)}$ are compiled into the code. If both species are neutral and are unlike (not the same species), the cross sections are estimated using the simple mixing rule

$$\bar{\Omega}_{ij}^{(\ell, s)} = \frac{1}{4} \left(\sqrt{\bar{\Omega}_{ii}^{(\ell, s)}} + \sqrt{\bar{\Omega}_{jj}^{(\ell, s)}} \right)^2 \tag{102}$$

However, if cross section data are not specified for like-like collisions of a neutral species, the code does not attempt to provide estimates of the cross sections, but returns an error message and terminates the case.

The compiled-in data specify steps for calculating the cross sections for the like-like interactions of all of the standard species, and for those unlike interactions for which experimental or theoretical cross sections are available in the literature. None of the standard gas models requires all of these steps. For example, the air models do not need the steps specified for calculating the cross sections in helium. At the beginning of each NATA case, the code edits the steps of the cross section calculation to eliminate those which are not needed in the current gas model, and to insert required but unspecified steps in accordance with the previously described default options. A printed summary of the steps in the unedited and edited cross section calculations can be obtained by setting a control input.

3.4 Cross Section Models

NATA contains 12 methods or options for calculating $\bar{\Omega}^{(1, 1)}$, $\bar{\Omega}^{(2, 2)}$, and B^* in a particular step. Each of these options is briefly described below.

3.4.1 Coulomb Cross Sections

In this option, the cross sections are

$$\bar{\Omega}^{(1,1)} = 0.8\, C_1\, Q_c$$

$$\bar{\Omega}^{(2,2)} = C_2\, Q_c \tag{103}$$

$$B^* = 1.5625$$

where C_1 and C_2 are specified constants, and Q_c is given by equations (100b) and (100c).

3.4.2 Exponential Potential

Here, the cross sections are obtained from Monchick's (ref. 19) collision integrals for the exponential potential, $\phi = Ae^{-r/\rho}$, which are compiled into the code. The input parameters are A/k and ρ.

3.4.3 Charge Exchange Cross Section

In this option, $\bar{\Omega}^{(1,1)}$ and B^* are calculated for a resonant charge exchange cross section of the form

$$Q_{ex} = (A - B \log_{10} v)^2 \tag{104}$$

where v is the relative velocity. $\bar{\Omega}^{(2,2)}$ is not calculated in this case. The input parameters are A, B, and the atomic weight. The $\bar{\Omega}_{ij}^{(1,1)}$ and B_{ij}^* computed can either replace the value computed in earlier steps of the cross section calculation or be added to them.

3.4.4 Tabulated Cross Section

Here the cross sections are given in tabular form as functions of temperature.

3.4.5 Power Law Potential

This option calculates collision cross sections for an inverse power law potential, $\phi = Ar^{-\eta}$, based on the analysis of Kihara, Taylor, and Hirschfelder (ref. 20). The required inputs are η and the quantities

$$\Omega_1 = \pi \Gamma \left(3 - \frac{2}{\eta}\right) \eta^{2/3}\, A^{(1)}(\eta) \left|\frac{A}{k}\right|^{2/\eta}$$

$$A_1 = \left(\frac{3}{2} - \frac{1}{\eta}\right) A^{(2)}(\eta) \Big/ A^{(1)}(\eta) \tag{105}$$

$$B_1 = \left(1 - \frac{2}{3\eta}\right)\left(1 + \frac{2}{\eta}\right)$$

where $A^{(1)}(\eta)$ and $A^{(2)}(\eta)$ are tabulated functions which are given for both attractive and repulsive potentials in reference 20.

3.4.6 Lennard-Jones (6-12) Potential

This option calculates the cross sections for the Lennard-Jones (6-12) potential, equation (82). The input parameters are ϵ/k and σ. The tabulated collision integrals are compiled into the code.

3.4.7 Transferred Cross Sections

This option allows cross sections calculated for one pair of species to be used also for other pairs, possibly with a constant multiplying factor. The cross sections are calculated from the formulas

$$\begin{aligned} \bar{\Omega}^{(1,1)} &= C_1 \, \bar{\Omega}_{ij}^{(1,1)} \\ \bar{\Omega}^{(2,2)} &= C_1 C_2 \, \bar{\Omega}_{ij}^{(2,2)} \\ B^* &= C_3 \, B^*_{ij} \end{aligned} \tag{106}$$

where the C_k are constant factors and the subscript ij indicates the pair for which the cross sections were previously calculated.

3.4.8 Empirical Mixing Rule

Here the cross sections for a pair of unlike species (i, j) are calculated from the empirical mixing rule (102). These calculated cross sections are then added to the previous values for the pair.

3.4.9 Fairing Option

This option modifies the previously calculated cross section values for a species pair according to the formula

$$\bar{\Omega}^{(\ell,s)}_{new} = f(T) \, \bar{\Omega}^{(\ell,s)}_{old} \tag{107}$$

where $f(T)$ is a linear fairing factor given by

$$f(T) = \max \left[0, \min \left(1, \frac{T - T_0}{T_2 - T_0} \right) \right] \tag{108}$$

This option allows the use of different forms for the cross section in different parts of the temperature range, with a smooth transition between them.

3.4.10 Generalized Mixing Rule

This option is a generalization of the empirical mixing rule (102) in which the cross sections are calculated from the formula

$$\bar{\Omega}^{(\ell, s)} = \frac{1}{4}\left(\sqrt{\bar{\Omega}_{ij}^{(\ell, s)}} + \sqrt{\bar{\Omega}_{mn}^{(\ell, s)}}\right) \tag{109}$$

where (i, j) and (m, n) are any specified species pairs.

3.4.11 Same-pair Transfer

This option calculates one of the averaged collision cross sections $\bar{\Omega}^{(\ell, s)}$ for a pair of species from the previously calculated value of a different $\bar{\Omega}^{(\ell, s)}$ for the pair. In terms of the notation

$$\begin{aligned} \bar{\Omega}_{ij}^{(1)} &= \bar{\Omega}_{ij}^{(1, 1)} \\ \bar{\Omega}_{ij}^{(2)} &= \bar{\Omega}_{ij}^{(2, 2)} \\ \bar{\Omega}_{ij}^{(3)} &= B_{ij}^{*}\ \bar{\Omega}_{ij}^{(1, 1)} \end{aligned} \tag{110}$$

the new cross section is calculated from the formula

$$\bar{\Omega}_{ij}^{(m)} = C\ \bar{\Omega}_{ij}^{(n)} \tag{111}$$

where m and n are two specified integers in the range from 1 to 3, and C is a constant.

3.4.12 Multiplication by a Constant

This option multiplies previously calculated values of the collision cross sections for a pair of species by a constant factor, according to the formulas

$$\begin{aligned} \bar{\Omega}_{ij}^{(1, 1)} &= C_1 \left[\bar{\Omega}_{ij}^{(1, 1)}\right]_{old} \\ \bar{\Omega}_{ij}^{(2, 2)} &= C_1 C_2 \left[\bar{\Omega}_{ij}^{(2, 2)}\right]_{old} \\ B_{ij}^{*} &= C_3 [B_{ij}^{*}]_{old} \end{aligned} \tag{112}$$

This is the same as the option described in Section 3.4.7, except that here the cross sections for a species pair are obtained from previously calculated values for the same pair instead of those for a different pair.

4. NOZZLE AND CHANNEL GEOMETRIES

4.1 Uses of Geometric Information in NATA

The NATA code uses information about nozzle and channel geometries for the following three distinct purposes.

4.1.1 Area Ratio Calculations

In the equilibrium and frozen flow solutions, the gas temperature is taken as the independent variable. The code decrements the temperature repeatedly, starting at the reservoir value, and at each point calculates all the other flow variables, including the effective area ratio:

$$A_e = A_e'/A_{e_*}' \tag{113}$$

Here, A_e' is the effective cross sectional area of the inviscid flow, while A_{e_*}' is the cross sectional area of the flow at the sonic point. The nozzle geometry is then used to determine the position in the nozzle, as specified by the axial coordinate x, corresponding to this effective area ratio. If the boundary layer on the nozzle wall is neglected, this solution for x is straightforward. If the boundary layer is included, the solution must be based on a relation between the effective area ratio A_e, the boundary layer displacement thickness δ^*, and the geometric area ratio.

$$A_g = A_g'(x)/A_{g0}' \tag{114}$$

In (114), A_g' is the geometric cross sectional area at position x, and A_{g0}' is the cross sectional area at the throat.

The non-equilibrium flow solution is started just downstream of the reservoir as a perturbed equilibrium solution. The gas temperature is again the independent variable, and the geometric description of the nozzle is used to determine the axial coordinate corresponding to each computed flow condition. When the perturbations exceed a certain limit, the solution is continued by integration of the non-equilibrium rate equations, using x as the independent variable. In the region of the non-equilibrium integration, the geometric description is used to calculate the geometric area ratio for given values of x. If the boundary layer is included in the solution, it is also necessary to calculate the effective area ratio from the geometric area ratio and the displacement thickness.

4.1.2 Boundary Layer Calculations

The overall geometry of the nozzle or channel wall determines the convergence or divergence of streamlines in the boundary layer, and thus affects the rate of buildup of boundary layer thickness. For example, if the streamlines diverge, the gas flowing in the boundary layer expands laterally, and as a result the thickness increases more slowly than it would if the streamlines were parallel.

4.1.3 Specification of Model Points and Channel Points

NATA can provide calculations of stagnation-point conditions on axisymmetric or two-dimensional models, and of the conditions along the surface of a blunted wedge model. One way of specifying the locations in the flow at which the leading edges of such models will be placed is to input a list of test section diameters. Similarly, points at which flow calculations are desired in a rectangular channel can be specified by inputting a list of values of the channel width. In each such case, the nozzle or channel geometry must be used to determine the values of x corresponding to the input diameters or widths.

4.2 Basic Geometric Options

NATA has been programmed to provide flow calculations for three types of nozzle geometry:

(1) axisymmetric nozzle

(2) two-dimensional nozzle

(3) rectangular channel.

In all three cases, the nozzle shape is specified by means of curvefits to nozzle wall profiles. Each such profile may be described by a function $y(x)$, where y is the perpendicular distance from the nozzle axis to the wall, and x is an axial coordinate, zero at the geometric throat and increasing in the downstream direction.

In the case of an axisymmetric nozzle, the geometric cross sectional area of the nozzle at a station x is given by

$$A_g' = \pi [y(x)]^2 \tag{115}$$

Thus, the geometric area ratio is

$$A_g = \left[\frac{y(x)}{y_0}\right]^2 \tag{116}$$

where $y_0 = y(0)$. For a two-dimensional nozzle, the cross-sectional area per unit length in the z-direction is

$$A_g' = 2\, y(x) \tag{117}$$

and the geometric area ratio is

$$A_g = \frac{y(x)}{y_0} \tag{118}$$

Description of a rectangular channel requires two profiles, $y(x)$ and $z(x)$. The cross sectional area at axial position x is

$$A_g' = 4\, y(x)\ z(x) \tag{119}$$

and thus the geometric area ratio is

$$A_g = \frac{y(x)\, z(x)}{y_0\, z_0} \tag{120}$$

It is assumed in equation (120), and in the code, that both the profiles for a channel have their minima at the same axial location, $x = 0$.

4.3 Profile Description

Each profile used in NATA is represented by an analytical curvefit containing up to 12 sections. The profile must be continuous and must have a continuous first derivative. At least two sections must lie upstream of the throat, and at least two must lie downstream. The throat must be a section boundary. A NATA case involves either one or two profiles, depending upon whether the flow is in a nozzle or a channel.

Each section in a profile fit can have one of three available forms:

(1) Straight Line

$$y(x) = P_1 + P_2\, x \tag{121}$$

(2) Circular Arc Convex Downward

$$y(x) = P_1 - \sqrt{P_3^2 - (x - P_2)^2} \tag{122}$$

(3) Circular Arc Concave Downward

$$y(x) = P_1 + \sqrt{P_3^2 - (x - P_2)^2} \tag{123}$$

In the second and third forms, P_3 is the radius of the circular arc and P_2, P_1 are the x and y coordinates, respectively, of the circle center.

The parameter values P_1, P_2, P_3 for each section must be chosen so that the entire profile fit represents the given nozzle or channel profile with adequate accuracy, subject to the following conditions:

$y(0) = R_0$

dy/dx continuous everywhere

$dy/dx < 0$ for $x < 0$

$dy/dx > 0$ for $x > 0$

where R_0 is the throat radius in centimeters. The last three conditions imply that $dy/dx = 0$ at $x = 0$. A separate computer program called NOZFIT has been developed for computing the parameters of NATA nozzle profile curvefits from the kinds of data available on engineering drawings, i.e., lengths, angles, and radii of curvature.

An additional constraint on the profile fits has been established by experience: There must not be any region of non-zero length in which the geometric area ratio is constant, or nearly constant, and approximately equal to 1. If such a region is present in the nozzle fit, the non-equilibrium solution usually becomes unstable in that region. Thus, if the actual nozzle being represented has a finite region of constant area (i.e., a straight tube) at the throat, it is necessary to modify the curvefit slightly in order to obtain reliable operation of the non-equilibrium solution. In practice, representing such a region as a converging section with a convergence angle of 3 degrees has given satisfactory results in most cases.

4.4 Relations Between the Geometric and Effective Area Ratios

The laminar boundary layer on the nozzle wall displaces the streamlines in the inviscid flow, thus changing the effective nozzle geometry. The amount by which the effective boundary of the inviscid flow is shifted is called the boundary layer displacement thickness, and is denoted by δ^*. The displacement thickness can be either positive or negative, depending on the boundary layer velocity and temperature profiles. In typical NATA solutions, δ^* is negative in the upstream and throat regions, and becomes positive at some point downstream of the throat. In channel flow problems, there are two displacement thicknesses, δ_1^* and δ_2^*, one for each pair of channel walls. These displacement thicknesses are generally unequal because of the different amounts of streamline convergence or divergence in the boundary layers on the two pairs of walls.

In many parts of the code, it is necessary to calculate the geometric area ratio A_g from the effective area ratio A_e, or conversely. The relation between the two area ratios, upon which both of these subroutines are based, depends upon the type of nozzle geometry. For a two-dimensional nozzle, the effective flow area per unit length in the z-direction is

$$A_e' = 2[y(x) - \delta^*] \tag{124}$$

At the sonic point, the effective area is

$$A_{e_*}' = 2[y_* - \delta_*^*] \tag{125}$$

where the subscript * denotes sonic conditions. Hence, the effective area ratio is equal to

$$A_e = \frac{A_e'}{A_{e_*}'} = \frac{y - \delta^*}{y_* - \delta_*^*} = \frac{\dfrac{y}{y_*} - \dfrac{\delta^*}{y_*}}{1 - \dfrac{\delta_*^*}{y_*}} \tag{126}$$

Because the sonic point is near the geometric throat, and because $dy/dx = 0$ at the throat, the profile ordinate y_* at the sonic point is approximately equal to the ordinate y_0 at the throat. In NATA, the difference between these two quantities is neglected. Hence, from (118) and (126),

$$A_g = \frac{\delta^*}{y_0} + \left(1 - \frac{\delta^*_*}{y_0}\right) A_e \tag{127}$$

For an axisymmetric nozzle, the effective flow area is

$$A'_e = \pi (y - \delta^*)^2 \tag{128}$$

and at the sonic point

$$A'_{e_*} = \pi (y_* - \delta^*_*)^2 \tag{129}$$

Hence, with the approximation $y_* \simeq y_0$,

$$A_e = \frac{A'_e}{A'_{e_*}} = \frac{\left(\frac{y}{y_0} - \frac{\delta^*}{y_0}\right)^2}{\left(1 - \frac{\delta^*_*}{y_0}\right)^2} \tag{130}$$

Equations (116) and (130) give

$$A_g = \left[\frac{\delta^*}{y_0} + \left(1 - \frac{\delta^*_*}{y_0}\right)\sqrt{A_e}\right]^2 \tag{131}$$

In the case of a rectangular channel, the effective flow area is

$$A'_e = 4(y - \delta^*_1)(z - \delta^*_2) \tag{132}$$

while at the sonic point

$$A'_{e_*} = 4(y_* - \delta^*_{1*})(z_* - \delta^*_{2*}) \tag{133}$$

Hence, with the approximations $y_* \simeq y_0$, $z_* \simeq z_0$,

$$A_e = \frac{A'_e}{A'_{e_*}} = \frac{\left(\frac{y}{y_0} - \frac{\delta^*_1}{y_0}\right)\left(\frac{z}{z_0} - \frac{\delta^*_2}{z_0}\right)}{\left(1 - \frac{\delta^*_{1*}}{y_0}\right)\left(1 - \frac{\delta^*_{2*}}{z_0}\right)} \tag{134}$$

Combination of (120) and (134) gives

$$A_g = \left(1 - \frac{\delta_1^*}{y_0}\right)\left(1 - \frac{\delta_2^*}{z_0}\right) A_e + \frac{y\,\delta_2^* + z\,\delta_1^*}{y_0\,z_0} - \frac{\delta_1^*\,\delta_2^*}{y_0\,z_0} \qquad (135)$$

This is not an explicit solution for A_g as a function of A_e and δ_1^* , δ_2^* , because the right hand side still contains the profile ordinates, y and z . These are known as functions of x , but x is not known until A_g has been determined. It is therefore necessary to carry out the solution for A_g using an iterative method, in the case of channel geometry.

5. LAMINAR BOUNDARY LAYER

The NATA code contains an optional calculation of the buildup of a laminar boundary layer on the nozzle or channel wall. The results of this calculation are used in two distinct ways:

(1) The boundary layer displacement thickness δ^* is used to relate the effective inviscid area ratio A_e to the geometric area ratio A_g, as explained in Section 4. In this way, the inviscid flow solution is coupled with the boundary layer solution.

(2) The heat flux and shear stress at the wall are printed as code outputs. These data can be used to test the overall flow model by comparison with experimental measurements. In the case of a rectangular channel containing a test panel, these outputs provide predictions of the test conditions on the panel.

5.1 Boundary Layer Transition Criterion

The laminar boundary layer calculation in NATA is applicable, of course, only if the boundary layer in the case being investigated is actually laminar and not turbulent. Schlichting (ref. 21, pp. 457-463) has reviewed the available data on boundary-layer transition in incompressible flows. A stability analysis shows that a laminar boundary layer is unconditionally stable as long as the Reynolds number based on momentum thickness,

$$N_{Re\theta} = \rho_e u_e \theta/\mu_e \tag{136}$$

is less than 162. In (136), ρ_e , u_e , and μ_e are the free-stream density, velocity, and viscosity, respectively, and θ is the momentum thickness,

$$\theta = \int_0^\infty \frac{\rho u}{\rho_e u_e} \left(1 - \frac{u}{u_e}\right) dy \tag{137}$$

In (137), y is a coordinate locally normal to the surface. For values of $N_{Re\theta}$ higher than the critical value of 162, the boundary layer is unstable, but the occurrence of transition depends upon the level of turbulence in the free stream. Transition occurs near $N_{Re\theta} = 162$ only for extremely high turbulence levels. For exceptionally smooth free-stream flows transition does not occur until an $N_{Re\theta}$ of about 900 is reached.

The transition Reynolds number also varies with other flow parameters. It increases with increasing Mach number and with increasing favorable pressure gradient, and decreases with mass injection at the wall. In a recent study (ref. 22), extensive data on boundary layer transition have been compiled and correlated with free-stream Mach number M_e and $N_{Re\theta}$. The data can be fitted by the relation

$$N_{Re\theta, T} = 200\, e^{0.224\, M_{e,T}} \tag{138}$$

where the subscript T refers to conditions at transition. The data contain considerable scatter, so that they do not determine the numerical coefficients in (138) with high precision. The choice of the value 200 for the critical Reynolds number at zero Mach number, in place of 162 or other possible values, takes account of the fairly high level of turbulence present in arc-heated air streams, of the strong favorable pressure gradient accelerating the flow in a converging-diverging wind tunnel nozzle, and of the absence of mass injection through the nozzle wall. At Mach numbers below 6, equation (138) gives a lower transition Reynolds number than the correlation recommended in reference 22 for flight conditions.

The Reynolds number $N_{Re\theta}$ (136) and the transition Reynolds number $N_{Re\theta,T}$ (138) are computed and printed out by NATA. In most cases lying within the operating envelopes of existing NASA/JSC arc-heated wind tunnels, $N_{Re\theta}$ remains smaller than $N_{Re\theta,T}$ throughout the solution.* Thus, the assumption that the boundary layer is laminar is probably valid in most cases of current interest to NASA/JSC. However, a proposed upgraded pumping capability allowing mass flows up to 1.5 lb/sec would make accessible a range of operating conditions in which the boundary layer would often become turbulent.

5.2 Basic Equations and Transformations

The basic non-equilibrium inviscid flow solution carried out by NATA requires, typically, a few minutes of computer time. The equilibrium and frozen inviscid solutions are much faster. The choice of a method for performing the laminar boundary layer calculation was guided, in part, by the requirement that solutions including the boundary layer should not consume a great deal more computer time than the basic inviscid solutions. This criterion ruled out the use of exact solutions of the partial differential equations for the laminar boundary layer, and narrowed the choice to one of several available approximate methods. The technique chosen is an integral method developed by Cohen and Reshotko (ref. 23). This technique is an extension of Thwaites' correlation method for incompressible boundary layers (ref. 24) to the compressible case with heat transfer. It treats the effects of arbitrary variable pressure gradients. According to Hayes and Probstein (ref. 25, pp. 318-320) the Cohen-Reshotko integral method is probably superior in accuracy to the method of local similarity.

The Cohen-Reshotko method uses curvefits to certain boundary layer properties based on similar solutions. In their original report (ref. 23), Cohen and Reshotko based these curvefits on similar solutions for Prandtl number unity and viscosity proportional to the absolute temperature. The corresponding curvefits used in NATA are based on similar solutions carried out by Dewey and Gross (ref. 26), and include the dependence upon Prandtl number, the viscosity-temperature index ω appearing in $\mu \propto T^{\omega}$, and the hypersonic parameter $\sigma = u_e^2/2h_0$. Thus, there is reason to hope that the boundary layer calculations in NATA may be somewhat more accurate than those given by the Cohen-Reshotko method in its original published form.

*An exception is the boundary layer on the non-expanding face of a rectangular channel, which often becomes turbulent a short distance beyond the throat.

The relations used in the Cohen-Reshotko method will be derived starting from the equations for an axisymmetric boundary layer in a compressible fluid. (See ref. 27, pp. 384-385.)

$$\rho u \frac{\partial u}{\partial x} + \rho v \frac{\partial u}{\partial y} = - \frac{\partial p}{\partial x} + \frac{\partial}{\partial y}\left(\mu \frac{\partial u}{\partial y}\right) \tag{139a}$$

$$\frac{\partial}{\partial x}(\rho u r) + \frac{\partial}{\partial y}(\rho v r) = 0 \tag{139b}$$

$$\rho u \frac{\partial h}{\partial x} + \rho v \frac{\partial h}{\partial y} = u \frac{\partial p}{\partial x} + \frac{\partial}{\partial y}\left(\frac{\mu}{N_{Pr}} \frac{\partial h}{\partial y}\right) + \mu\left(\frac{\partial u}{\partial y}\right)^2 \tag{139c}$$

In these equations, ρ denotes the density, p the pressure, μ the viscosity, h the static enthalpy, and N_{Pr} the Prandtl number. The independent variables, x and y, are a pair of locally orthogonal coordinates, with x parallel to the surface along the streamwise direction and y lying along the normal to the surface. The local radius of the surface from the axis of symmetry is denoted by $r(x)$.

The equations (139) for an axisymmetric boundary layer can be converted into those for a two-dimensional boundary layer using the Mangler transformation (refs. 21 and 27):

$$\bar{x} = \frac{1}{L^2} \int_{x_0}^{x} r^2(x)\, dx \tag{140a}$$

$$\bar{y} = \frac{r(x)}{L} y \tag{140b}$$

$$\bar{u} = u \tag{140c}$$

$$\bar{v} = \frac{L}{r}\left(v + \frac{yu}{r}\frac{dr}{dx}\right) \tag{140d}$$

where L is an arbitrary non-zero scale length. The equations for a two-dimensional boundary layer are

$$\rho \bar{u} \frac{\partial \bar{u}}{\partial \bar{x}} + \rho \bar{v} \frac{\partial \bar{u}}{\partial \bar{y}} = - \frac{\partial p}{\partial \bar{x}} + \frac{\partial}{\partial \bar{y}}\left(\mu \frac{\partial \bar{u}}{\partial \bar{y}}\right) \tag{141a}$$

$$\frac{\partial}{\partial \bar{x}}(\rho \bar{u}) + \frac{\partial}{\partial \bar{y}}(\rho \bar{v}) = 0 \tag{141b}$$

$$\rho \bar{u} \frac{\partial h}{\partial \bar{x}} + \rho \bar{v} \frac{\partial h}{\partial \bar{y}} = \bar{u} \frac{\partial p}{\partial \bar{x}} + \frac{\partial}{\partial \bar{y}}\left(\frac{\mu}{N_{Pr}} \frac{\partial h}{\partial \bar{y}}\right) + \mu\left(\frac{\partial \bar{u}}{\partial \bar{y}}\right)^2 \tag{141c}$$

Cohen and Reshotko (ref. 23) base their analysis on equations (141). They first convert these equations into the equations for an incompressible boundary layer using the Stewartson-Illingworth transformation (refs. 21, 28, 29):

$$X = \int_{\bar{x}_0}^{\bar{x}} \lambda(\bar{x}') \frac{a_e(\bar{x}')}{a_0} \frac{p_e(\bar{x}')}{p_0} \, d\bar{x}' \tag{142a}$$

$$Y = \frac{a_e(\bar{x})}{a_0} \int_0^{\bar{y}} \frac{\rho(\bar{x}, \bar{y}')}{\rho_0} \, d\bar{y}' \tag{142b}$$

Here,

$$\lambda(\bar{x}) = \frac{\mu_w / T_w}{\mu_0 / T_0} \tag{143}$$

where T represents the absolute temperature and the subscripts w and 0 denote conditions at the surface (wall) and free-stream stagnation conditions, respectively. The symbol a represents the sound speed, and subscript e indicates local free-stream (external) conditions. The transformation of the velocity components is found by defining a stream function ψ such that

$$\frac{\partial \psi}{\partial \bar{y}} = \frac{\rho \bar{u}}{\rho_0} \tag{144a}$$

$$\frac{\partial \psi}{\partial \bar{x}} = -\frac{\rho \bar{v}}{\rho_0} \tag{144b}$$

Then

$$U = \frac{\partial \psi}{\partial Y} = \frac{a_0}{a_e} \bar{u} \tag{145a}$$

$$V = -\frac{\partial \psi}{\partial X} = \frac{\bar{v} - (\partial Y / \partial \bar{x})_{\bar{y}} \, (a_0 / a_e) \, \bar{u}}{\lambda (\rho_0 / \rho) (a_e / a_0) (p_e / p_0)} \tag{145b}$$

To obtain the desired results it is necessary to assume that

$$\frac{\mu}{\mu_w} = \frac{T}{T_w} \tag{146}$$

which is equivalent to

$$\frac{\mu}{\mu_0} = \lambda \frac{T}{T_0} \tag{147}$$

in which λ is given by (143). It is also necessary to assume that the inviscid flow obeys the equations for a perfect gas, in particular

$$a_e^2 + \frac{\gamma - 1}{2} \bar{u}_e^2 = a_0^2 \tag{148a}$$

and

$$\frac{T}{T_e} = \frac{h}{h_e} \tag{148b}$$

The transformed momentum and continuity equations for the boundary layer are then

$$U \frac{\partial U}{\partial X} + V \frac{\partial U}{\partial Y} = \nu_0 \frac{\partial^2 U}{\partial Y^2} + (1 + S) U_e \frac{dU_e}{dX} \tag{149a}$$

$$\frac{\partial U}{\partial X} + \frac{\partial V}{\partial Y} = 0 \tag{149b}$$

Cohen and Reshotko also give the transformed energy equation, but this is not required in the subsequent analysis. In equation (149a)

$$S = \frac{h_s}{h_0} - 1 \tag{150}$$

where h_s is the local stagnation enthalpy and h_0 is the stagnation enthalpy in the free stream, and

$$\nu_0 = \mu_0 / \rho_0 \tag{151}$$

The transformed boundary conditions are

$$U(X, 0) = 0 \tag{152a}$$

$$V(X, 0) = 0 \tag{152b}$$

$$S(X, 0) = S_w(X) \tag{152c}$$

$$\lim_{Y \to \infty} S = 0 \tag{152d}$$

$$\lim_{Y \to \infty} U = U_e(X) \tag{152e}$$

5.3 Momentum Integral

The incompressible momentum integral equation is now obtained by multiplying the continuity equation (149b) by $(U_e - U)$, and subtracting the resulting relation from the momentum equation (149a). This gives

$$\frac{\partial}{\partial X}\left[U(U_e - U)\right] + \frac{\partial}{\partial Y}\left[V(U_e - U)\right] + (U_e - U)\frac{dU_e}{dX}$$

$$+ SU_e \frac{dU_e}{dX} + \nu_0 \frac{\partial^2 U}{\partial Y^2} = 0 \tag{153}$$

This equation is now integrated with respect to Y from $Y = 0$ to Δ, where Δ is a fixed distance encompassing the entire boundary layer. The result is

$$\frac{d}{dX}(U_e^2 \theta_i) + U_e \frac{dU_e}{dX}(\delta_i^* + \mathfrak{E}) = \nu_0 \left(\frac{dU}{dY}\right)_w \tag{154}$$

where

$$\theta_i \equiv \int_0^\Delta \frac{U}{U_e}\left(1 - \frac{U}{U_e}\right) dY \tag{155a}$$

$$\delta_i^* \equiv \int_0^\Delta \left(1 - \frac{U}{U_e}\right) dY \tag{155b}$$

$$\mathfrak{E} \equiv \int_0^\Delta S\, dY \tag{155c}$$

are the incompressible momentum, displacement, and enthalpy thicknesses for the boundary layer, respectively. Equation (154) is equivalent to

$$\frac{d\theta_i}{dX} + \frac{1}{U_e}(2\theta_i + \delta_i^* + \mathfrak{E})\frac{dU_e}{dX} = \frac{\nu_0}{U_e^2}\left(\frac{\partial U}{\partial Y}\right)_w \tag{156}$$

Cohen and Reshotko define the following non-dimensional boundary layer parameters:

Shear parameter:
$$\ell \equiv \frac{\theta_i}{U_e}\left(\frac{\partial U}{\partial Y}\right)_w \tag{157}$$

Correlation parameter:
$$n \equiv -\frac{\theta_i^2}{\nu_0}\frac{dU_e}{dX} \tag{158}$$

In terms of these parameters, the equation (156) can be expressed (after multiplication with $2\theta_i U_e/\nu_0$) in the form

$$-U_e \frac{d}{dX}\left(\frac{n}{dU_e/dX}\right) = 2\left[n\,(H_{inc} + 2) + \ell\right] \tag{159}$$

where

$$H_{inc} = \frac{\delta_i^* + \mathfrak{G}}{\theta_i} \tag{160}$$

is termed the incompressible form factor.

5.4 Correlation Method

Cohen and Reshotko now assume that the non-dimensional boundary layer parameters ℓ and H_{inc}, and also the Reynolds analogy factor (to be defined later), can be approximated as functions of the correlation parameter n and the value S_w of S at the wall, irrespective of the previous history of the boundary layer. This is their generalization of Thwaites' correlation concept. On this assumption, the right-hand side of equation (159) is a function of n and S_w:

$$N(n, S_w) = 2\left[n\,(H_{inc} + 2) + \ell\right] \tag{161}$$

so that (159) becomes

$$-U_e \frac{d}{dX}\left(\frac{n}{dU_e/dX}\right) = N(n, S_w) \tag{162}$$

Figure 1 shows the form of the function $N(n, S_w)$ for favorable pressure gradients ($n<0$), based on similar boundary layer solutions for Prandtl number unity and the viscosity law (146). The points in this figure represent results tabulated by Dewey and Gross (ref. 26). The parameters n, ℓ, H_{inc}, and N appearing in Cohen and Reshotko's analysis are related to the quantities $f''(0)$, I_1, I_2, and β tabulated by Dewey and Gross as follows:

$$n = -\beta I_2^2 \tag{163a}$$

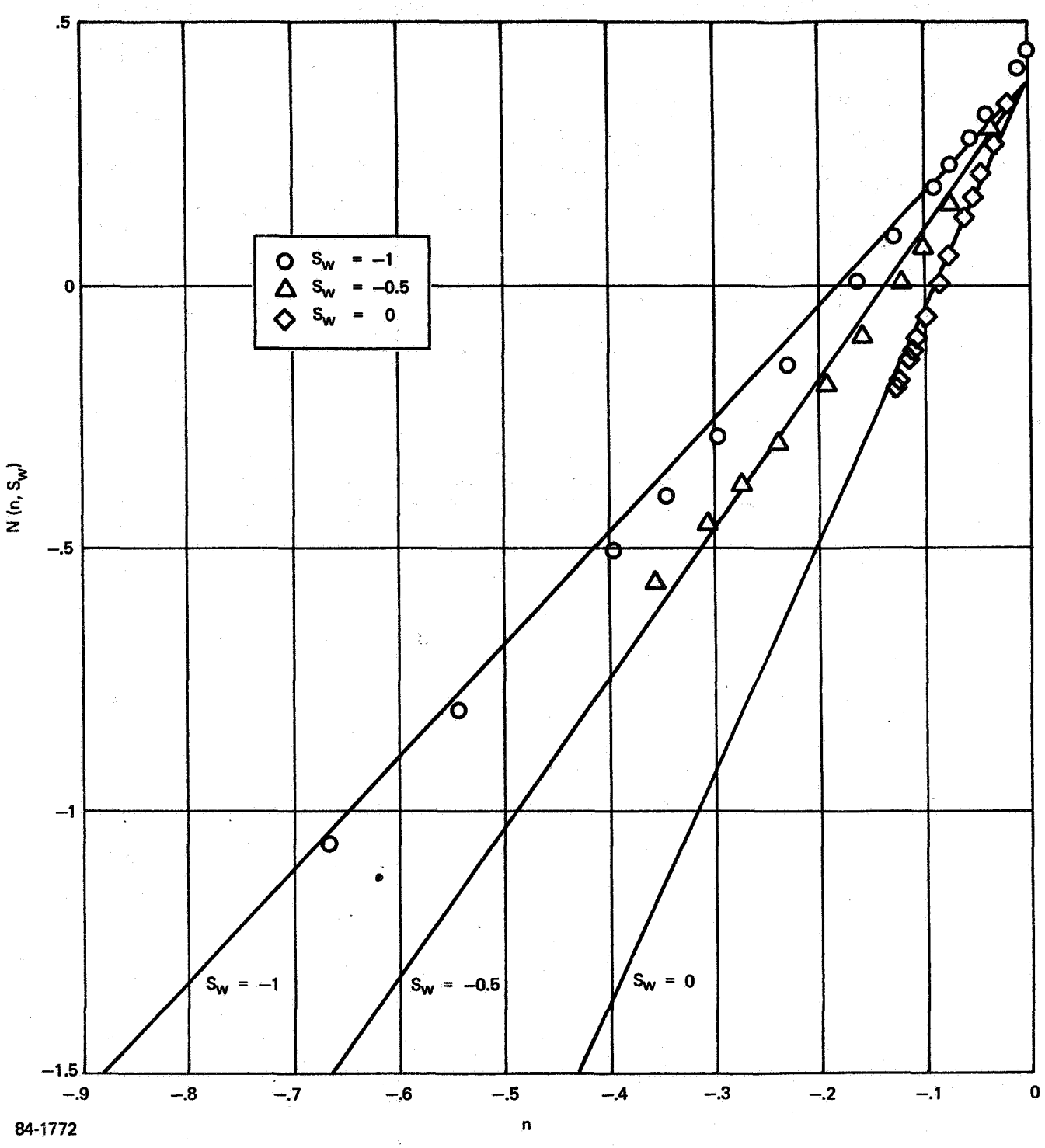

Figure 1 THE FUNCTION N (n, S_w) BASED ON SIMILAR SOLUTIONS FOR $N_{Pr} = 1$, $\omega = 1$

$$\ell = I_2 f''(0) \tag{163b}$$

$$H_{inc} = \frac{I_1}{I_2} - 1 \tag{163c}$$

$$N = 2 I_2 [f''(0) - \beta (I_1 + I_2)] \tag{163d}$$

The family of straight lines in figure 1 represents a simple curvefit to the Dewey and Gross Data:

$$N(n, S_w) = A + B(S_w)\, n \tag{164}$$

where

$$B(S_w) = 2.14 + 1.28 (1 + S_w) + 0.93 (1 + S_w)^4 \tag{165a}$$

and

$$A = 0.38 \tag{165b}$$

The linear dependence of (164) upon n is required for further progress in the analysis. The figure shows that the linear fit is reasonably accurate. At $n = 0$, the correct value of $N(n, S_w)$ is 0.441 for all S_w, whereas the analytical fit (164), (165) gives a value of 0.38. The coefficients (165) have been chosen to optimize the accuracy for $n \lesssim 0.1$, i.e., for rather strongly favorable pressure gradients, because this is the region of most frequent use and greatest importance in NATA calculations.

Substitution of the curvefit (164) into the differential equation (159) gives

$$- U_e \frac{d}{dX} \left(\frac{n}{dU_e/dX} \right) = A + B(S_w)\, n \tag{166}$$

For constant wall temperature (S_w = const.), equation (166) has the solution

$$n = - A U_e^{-B} \frac{dU_e}{dX} \int_{X_0}^{X} U_e^{B-1}\, dX \tag{167}$$

where X_0 is the value of X at the point where the boundary layer starts. Initial conditions on the boundary layer will be discussed below.

The external flowfield $U_e(X)$ is assumed known. Thus, n can be calculated at each point X by a running quadrature, using (167). Then the incompressible momentum thickness θ_i can be obtained from (158):

$$\theta_i = \sqrt{- \frac{\nu_0\, n}{dU_e/dX}} \tag{168}$$

Because the shear parameter ℓ is assumed to be given as a function of n and S_w, and because S_w is known, the shear can then be calculated from equation (157). Similarly, the displacement thickness can be evaluated from $H_{inc}(n, S_w)$, and the heat flux to the wall from a Reynolds analogy factor. Thus, equation (167), together with Cohen and Reshotko's correlation assumption, provides an explicit description of the boundary layer.

5.5 Momentum Thickness

Substitution of the Stewartson-Illingworth transformation formulas (142a) and (145a) gives the solution (167) for n in terms of the variables for a compressible two-dimensional boundary layer:

$$n = - \frac{A M_e^{-B}}{\frac{a_e}{a_0}\frac{P_e}{P_0}} \frac{dM_e}{d\bar{x}} \int_{\bar{x}_0}^{\bar{x}} M_e^{B-1} \frac{a_e}{a_0}\frac{P_e}{P_0} d\bar{x} \tag{169}$$

Then substitution of the Mangler transformation formulas (140a) and (140c) gives the expression for n in the case of an axisymmetric compressible boundary layer:

$$n = - \frac{A M_e^{-B}}{r^2 \frac{a_e}{a_0}\frac{P_e}{P_0}} \frac{dM_e}{dx} \int_{x_0}^{x} r^2 M_e^{B-1} \frac{a_e}{a_0}\frac{P_e}{P_0} dx \tag{170}$$

To introduce a more compact notation, let

$$\Phi \equiv r^{2j} M_e^{B-1} \frac{a_e}{a_0}\frac{P_e}{P_0} \tag{171}$$

$$I = \int_0^{\xi} \Phi \, d\xi \tag{172}$$

$$n' = AI/L\Phi \tag{173}$$

where L is a characteristic length and the index j is 0 for a two-dimensional boundary layer and 1 for an axisymmetric layer. Then

$$n = - \frac{L n'}{M_e} \frac{dM_e}{d\xi} \tag{174}$$

where ξ is the streamwise coordinate along the surface (equal to $x - x_0$ for the axisymmetric case and to $\bar{x} - \bar{x}_0$ for the two-dimensional case). Both n' and n are non-dimensional.

The momentum thickness for a compressible two-dimensional boundary layer is defined by

$$\bar{\theta} = \int_0^{\bar{\delta}} \frac{\rho u}{\rho_e u_e} \left(1 - \frac{u}{u_e}\right) d\bar{y} \tag{175}$$

Equations (142b), (145a), (155a), and (175) show that $\bar{\theta}$ is related to the incompressible momentum thickness θ_i by

$$\bar{\theta} = \frac{\rho_0 a_0}{\rho_e a_e} \theta_i \tag{176}$$

Application of the Stewartson-Illingworth formulas (142a) and (145a) to equation (168), followed by use of (176), gives the following explicit formula for the momentum thickness of a two-dimensional compressible boundary layer:

$$\bar{\theta} = L \sqrt{-\frac{n M_e}{dM_e/d\bar{x}} \cdot \frac{1}{N_{ReL}} \cdot \frac{\lambda}{L} \frac{\mu_0}{\mu_e} \frac{\rho_0}{\rho_e} \frac{P_e}{P_0}} \tag{177}$$

where

$$N_{ReL} \equiv \frac{\rho_e u_e L}{\mu_e} \tag{178}$$

is the Reynolds number based on the characteristic scale length L. The value of $\bar{\theta}$ is independent of L. Because λ is defined by (143), and since the pressure gradient through the thickness of the boundary layer is negligible ($P_w = P_e$), for a perfect gas

$$\lambda \frac{\mu_0}{\mu_e} \frac{\rho_0}{\rho_e} \frac{P_e}{P_0} = \frac{\rho_w \mu_w}{\rho_e \mu_e} \tag{179}$$

Hence, (177) becomes

$$\bar{\theta} = L \sqrt{-\frac{n M_e}{dM_e/d\bar{x}} \cdot \frac{1}{L\, Re_L} \cdot \frac{\rho_w \mu_w}{\rho_e \mu_e}} \tag{180}$$

The momentum thickness for an axisymmetric boundary layer is

$$\theta = \int_0^{\delta} \frac{\rho u}{\rho_e u_e} \left(1 - \frac{u}{u_e}\right) dy \tag{181}$$

From the Mangler transformation (140),

$$\theta = \frac{L}{r}\,\bar{\theta} \tag{182}$$

and

$$\frac{dM_e}{d\bar{x}} = \frac{L^2}{r^2}\,\frac{dM_e}{dx} \tag{183}$$

Substitution of these relations into (180) gives

$$\theta = L\sqrt{-\frac{n\,M_e}{dM_e/dx}\cdot\frac{1}{LN_{ReL}}\cdot\frac{\rho_w\,\mu_w}{\rho_e\,\mu_e}} \tag{184}$$

which is of the same form as (180). Thus, based on this formulation, the difference in momentum thickness between axisymmetric and two-dimensional boundary layers with the same external flow $M_e(\xi)$ arises entirely from the difference in n resulting from use of equation (169) in the 2D case and (170) in the axisymmetric case. In both cases, the momentum thickness can be expressed, with the aid of (174), in the form

$$\theta = L\sqrt{\frac{n'}{N_{ReL}}\cdot\frac{\rho_w\,\mu_w}{\rho_e\,\mu_e}} \tag{185}$$

The above formulation assumes, in the axisymmetric case, that the boundary layer thickness is everywhere negligible compared with the distance r of the wall from the axis of symmetry. This assumption is not necessarily valid far downstream in an axisymmetric nozzle, where the local Reynolds number N_{ReL} can become quite low owing to the rarefaction of the gas. Accordingly, for axisymmetric nozzles, NATA applies an approximate transverse curvature correction to the momentum and displacement thicknesses. This correction is based upon the following reasoning (reference 30). Figure 2 shows a portion of an axisymmetric nozzle, in cross section, near a location where the nozzle radius is r and the tangent to the nozzle surface is inclined at an angle b to the nozzle axis. The actual momentum thickness θ', including the effects of transverse curvature, is shown. The flow area in the boundary layer, based on the thickness θ', is the area of the conical frustum whose cross section is represented by the line segment AB in the figure. This area is given by

$$A = \pi\,(2r - \theta'\cos b)\,\theta' \tag{186}$$

It is assumed that this flow area is equal to the flow area $2\pi r\theta$, where θ is the momentum thickness (184) or (185) based on the thin-layer analysis. This assumption gives the relation

$$\theta' = \frac{r}{\cos b}\left[1 - \sqrt{1 - \frac{2\theta\cos b}{r}}\right] \tag{187}$$

This correction increases the calculated momentum thickness for axisymmetric nozzles.

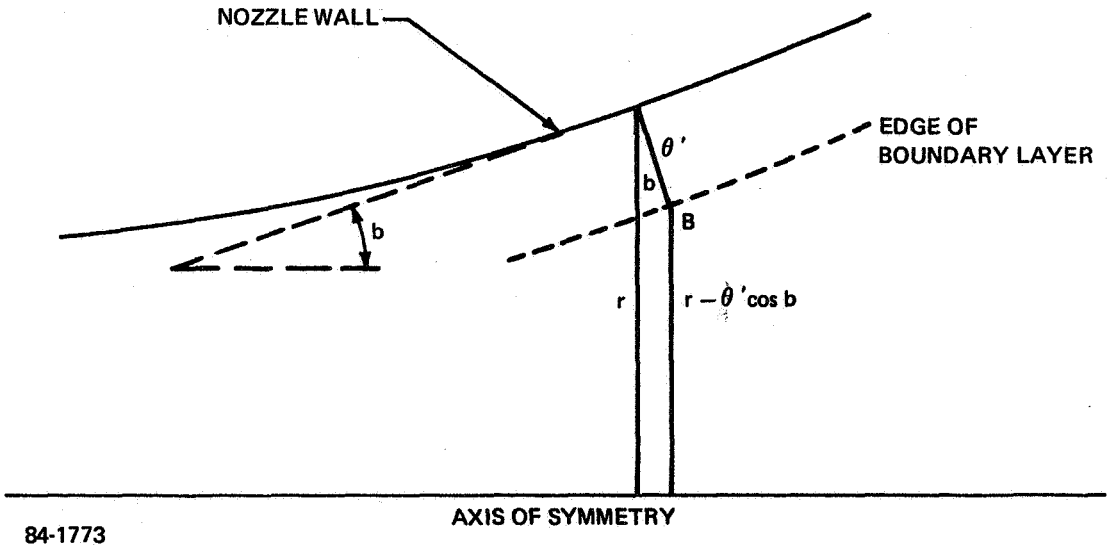

Figure 2 GEOMETRY OF TRANSVERSE CURVATURE CORRECTION

5.6 Displacement Thickness

Cohen and Reshotko (ref. 23) give the following relation between the displacement and momentum thicknesses:

$$\frac{\delta^*}{\theta} = (H_{inc} + 1)\frac{T_0}{T_e} - 1 \tag{188}$$

where H_{inc} is defined by (160). This relation can also be derived from relations given by Dewey and Gross (ref. 26) for similar boundary layers with arbitrary Prandtl number, free-stream Mach number, and viscosity-temperature index ω, for zero sweep angle. NATA calculates δ^* from (188), using an analytical curvefit to H_{inc} based on the Dewey-Gross data. For axisymmetric boundary layers, NATA uses the momentum thickness θ' corrected for the transverse curvature effect, equation (187), in (188).

The curvefit to the incompressible form factor is

$$H_{inc} + 1 = \{0.25 + 0.75\, e^{4.6\,n}\,[1 + (3 - 15.6\,n)\,(1 + S_w)]\} \cdot$$

$$\cdot\,[(1 + S_w)^{-0.4\,\ell n\, N_{Pr}} - 0.47\,\sigma\,\ell n\, N_{Pr}] \tag{189}$$

where N_{Pr} represents the Prandtl number and σ is the hypersonic parameter

$$\sigma = \frac{u_e^2}{2\,h_0} \tag{190}$$

This formula contains two main factors. The first, enclosed in braces, gives the dependence of H_{inc} upon n and S_w for Prandtl number unity and $\omega = 1$. The second factor, in brackets, gives the dependence on N_{Pr} and σ. The dependence of H_{inc} upon the viscosity-temperature index ω, defined by

$$\frac{\mu}{\mu_w} = \left(\frac{T}{T_w}\right)^{\omega} \tag{191}$$

is weak and is neglected in (189). Figures 3 to 5 compare the curvefit (189) with data on H_{inc} calculated from Dewey and Gross's tabulation of similar solutions. The abscissa in these plots is $1 + H_{inc}$ as calculated from (189), while the ordinate is $1 + H_{inc}$ based on the Dewey and Gross data. The plots include data for $N_{Pr} = 0.5$, 0.7, and 1.0, for $\omega = 0.5$, 0.7, and 1, for $\sigma = 0$, 0.5, and 1, for $(1+S_w) = T_w/T_0$ from 0 to 1, and for values of β (the Falkner-Skan parameter) from 0 to 5. The root-mean-square percentage error in $(1+H_{inc})$ based on the curvefit, for the 405 data points considered in the fitting analysis, is 5 percent. The largest individual error is 17 percent.

In the limiting case of an infinite favorable pressure gradient ($\beta \to \infty$), Dewey and Gross's integral I_1 is zero (reference 26). Thus, from (163c), $H_{inc} \to -1$. The curvefit (189) does not reproduce this limit exactly. For $\beta \to \infty, n \to -\infty$ according to

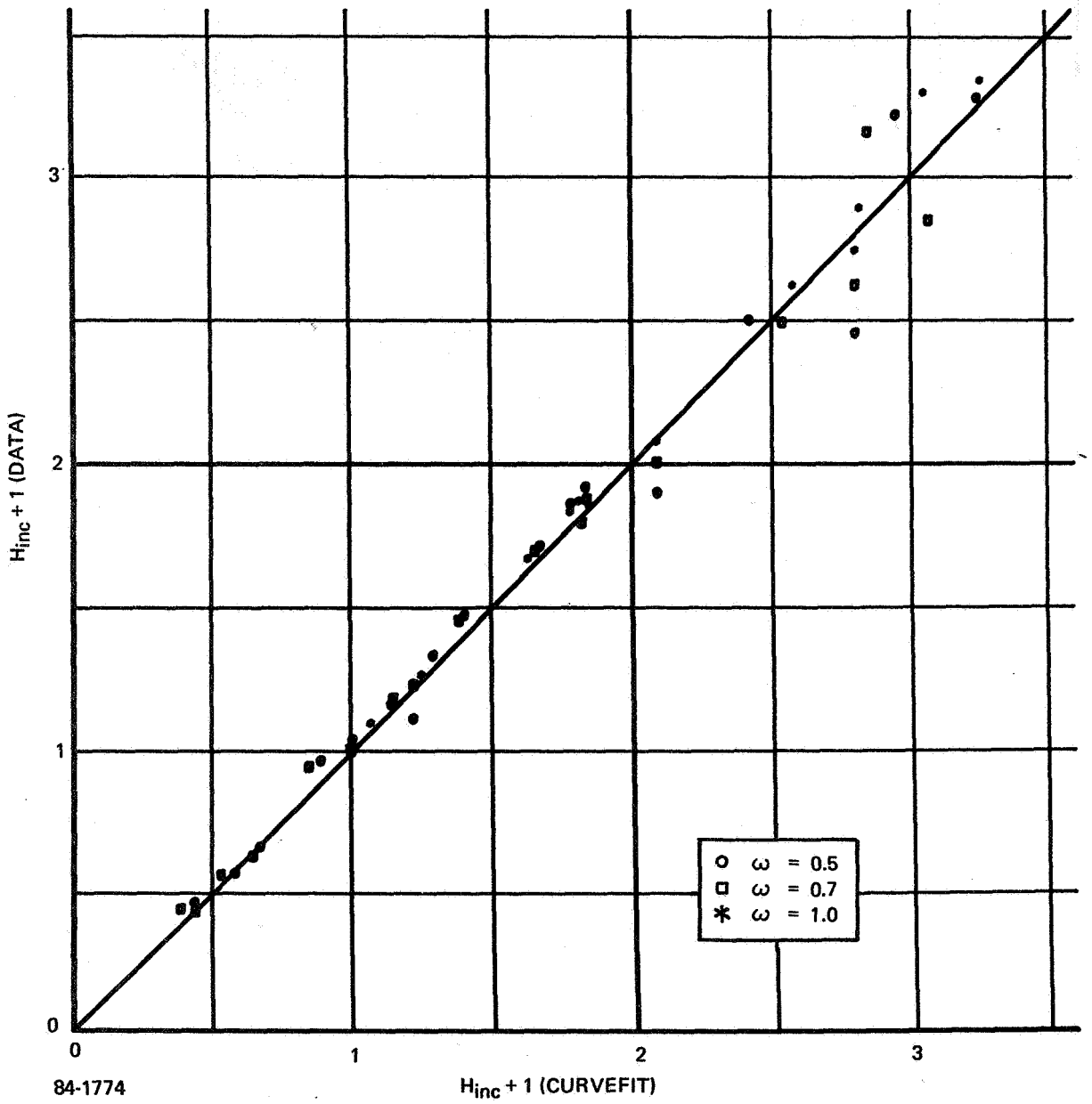

Figure 3 COMPARISON OF INCOMPRESSIBLE FORM FACTOR CURVEFIT WITH DEWEY-GROSS DATA (N_{Pr} = 0.5)

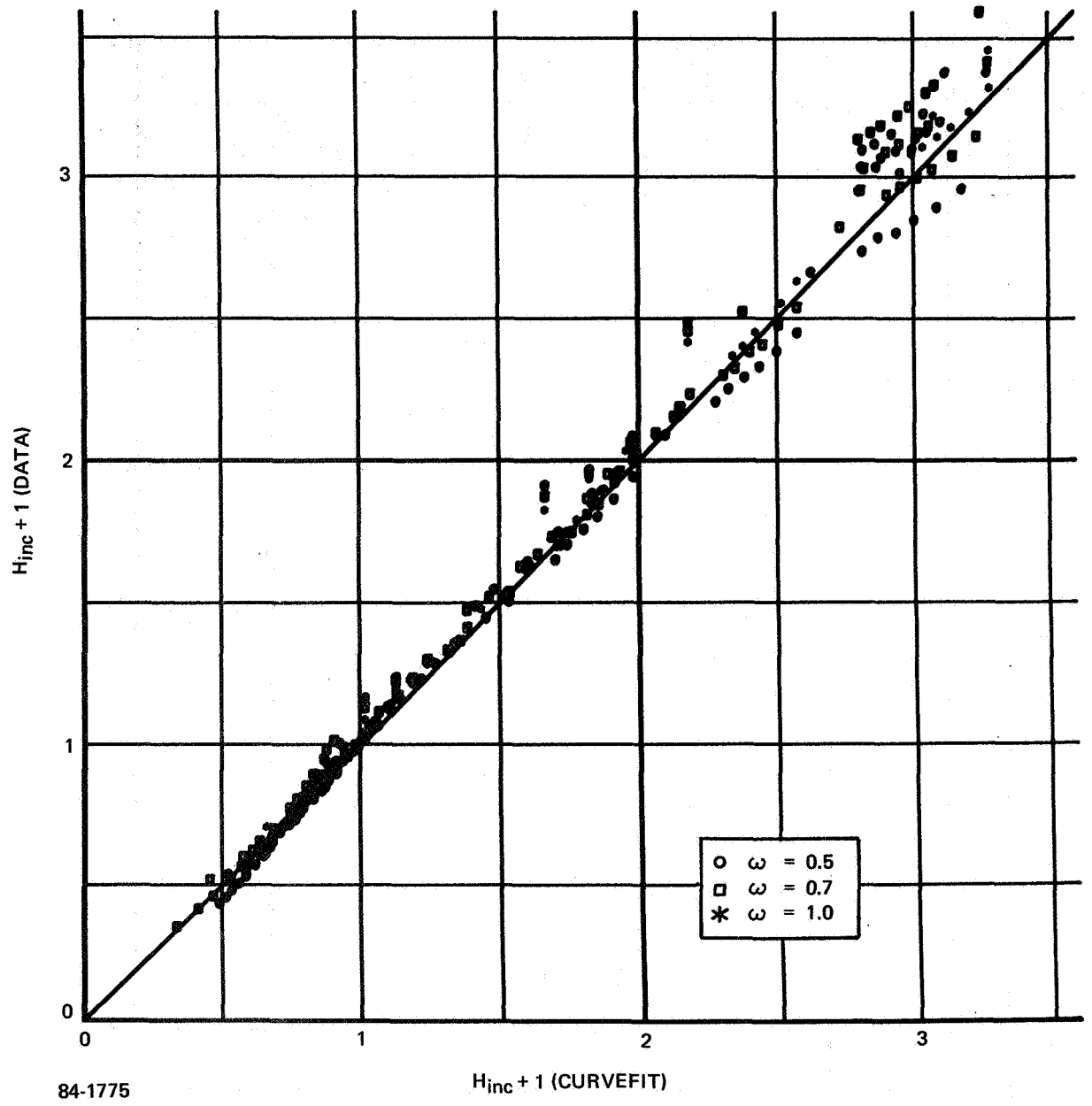

Figure 4 COMPARISON OF INCOMPRESSIBLE FORM FACTOR CURVEFIT WITH DEWEY-GROSS DATA (N_{Pr} = 0.7)

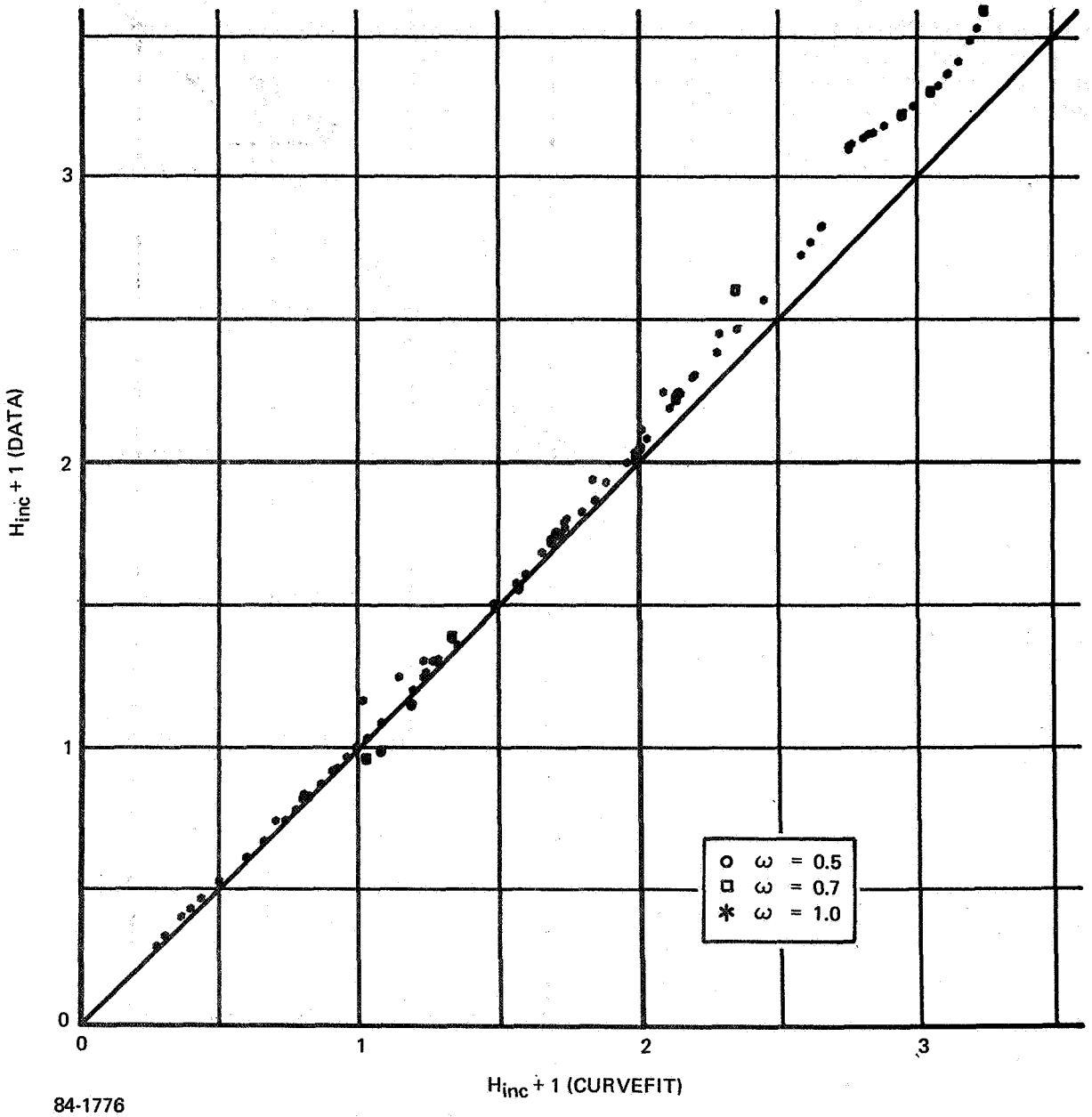

84-1776

Figure 5 COMPARISON OF INCOMPRESSIBLE FORM FACTOR CURVEFIT WITH DEWEY-GROSS DATA (N_{Pr} = 1.0)

(163a); thus, the term containing the factor $e^{4.6n}$ in (189) has a limit of zero, and the limit of $(1+H_{inc})$ is

$$\lim_{\beta\to\infty} [1 + H_{inc}(fit)] = 0.25 \left[(1+S_w)^{-0.4 \ell n N_{Pr}} - 0.47 \sigma \ell n N_{Pr} \right] \tag{192}$$

For example, if $N_{Pr} = 0.7$, $(1+S_w) = 0.1$, and $\sigma = 1$, this limit has the value 0.22. The correct value for $\beta\to\infty$ would be zero. However, the Dewey-Gross data show that the approach to this limit is very gradual. For the pressure gradients encountered in NATA runs, (189) is of acceptable accuracy.

5.7 Shear Stress

The shear stress τ_w at the wall can be calculated from the definition and value of the shear parameter ℓ. From equations (157), (142b), (145a), (140b), and (182),

$$\tau_w = \frac{\rho_w \mu_w \ell u_e}{\rho_e \theta} \tag{193}$$

for either an axisymmetric or a two-dimensional boundary layer.

Values of ℓ can be obtained from Dewey and Gross's tabulated similar solutions using equation (163b). Values of the shear parameter thus obtained have been curvefitted by the following expression:

$$\ell = \left[0.2205 + \frac{1 + 4.5\,(1+S_w)^{0.9}}{\frac{2.7}{(-n)} + \frac{5.06}{(-n)^{0.224}}} \right] \cdot \left[\phi_0 + 0.45\,(1-\omega) \left(1 - e^{3.5n/\phi_0^{1.57}} \right) + \phi_1 \right] \tag{194a}$$

where

$$\phi_0 = \exp\left\{ -0.427 \left[(1+S_w)^{-(1-\omega)} - 1 \right] \right\} \tag{194b}$$

$$\phi_1 = \frac{0.76\,(1-\omega)^{1.2}\,(1-\sqrt{1-\sigma})}{1 + a(-n)^b} \tag{194c}$$

$$a = 15.5\, e^{-29(1+S_w)} + 0.67\, e^{4.37(1+S_w)} \tag{194d}$$

$$b = 0.7 + 0.47\,(1+S_w) \tag{194e}$$

The first factor in (194a) gives ℓ as a function of n and S_w for $\omega = 1$. The second factor gives the dependence on ω and σ. The dependence on Prandtl number is weak and is neglected. Thus, equations (194) represent ℓ as varying with the hypersonic parameter σ even for $N_{Pr} = 1$. In theory, the boundary layer properties should be independent of σ for $N_{Pr} = 1$. The Dewey-Gross data indicate little

dependence of ℓ on N_{Pr} in the range from $N_{Pr} = 0.5$ to 0.7, and thus provide no basis for fitting a Prandtl number dependence which would cause the dependence on σ to vanish for $N_{Pr} = 1$. These formulas should, in any event, be satisfactory for air, in which the Prandtl number is about 0.7.

In typical applications of NATA, the enthalpy ratio parameter $(1 + S_w)$ is small of order 10^{-2}. The smallest value of $(1 + S_w)$ in the Dewey-Gross data, for $\omega < 1$, is 0.05. Thus, application of these data in the code normally requires an extrapolation to $(1 + S_w)$ values beyond the range investigated by Dewey and Gross. Unfortunately, the data for $(1 + S_w) = 0.05$ and 0.1 indicate that ℓ has a strong dependence on $(1 + S_w)$ for small $(1 + S_w)$ and $\omega < 1$. As a result, the extrapolation to still smaller values of $(1+S_w)$ is a potential source of sizeable errors. The rather complex curvefit (194) was developed in an effort to minimize such extrapolation errors by fitting the Dewey-Gross data for small $(1 + S_w)$ as closely as possible.

Figures 6 through 8 compare the curvefit (194) with ℓ values obtained from Dewey and Gross's tabulated similar solutions. The 405 cases used in the comparison include Prandtl numbers of 0.5, 0.7, and 1, ω values of 0.5, 0.7 and 1, values of the hypersonic parameter σ of 0, 0.5, and 1, several temperature ratios $1 + S_w$ in the range from 0 to 1, and values of the Falkner-Skan parameter β ranging from 0 to 5. The root-mean-square percentage error is 2 percent. The largest individual percentage error is 17 percent.

5.8 Heat Flux

Because the energy equation is not used in the Cohen-Reshotko correlation method, the heat flux q_w is calculated from the shear stress τ_w using a Reynolds analogy factor based upon similar solutions. The formula is

$$\frac{q_w}{\tau_w} = \frac{h_r - h_w}{R_A u_e N_{Prw}} \tag{195}$$

where h_r denotes the recovery enthalpy and R_A the Reynolds analogy factor. The expression for recovery enthalpy recommended in the literature (ref. 25, p. 296) is

$$h_r = h_e + \sqrt{N_{Pr}}\,(h_0 - h_e) \tag{196}$$

However, the data tabulated by Dewey and Gross are fitted more accurately by

$$h_r = h_e + N_{Pr}^{0.56}\,(h_0 - h_e) \tag{197}$$

which is the formula used in NATA. The Reynolds analogy factor is given, in terms of quantities tabulated by Dewey and Gross, by

$$R_A = \frac{f''(0)}{\theta'(0)} \cdot \frac{t_{aw} - t_w}{1 - t_w} \tag{198}$$

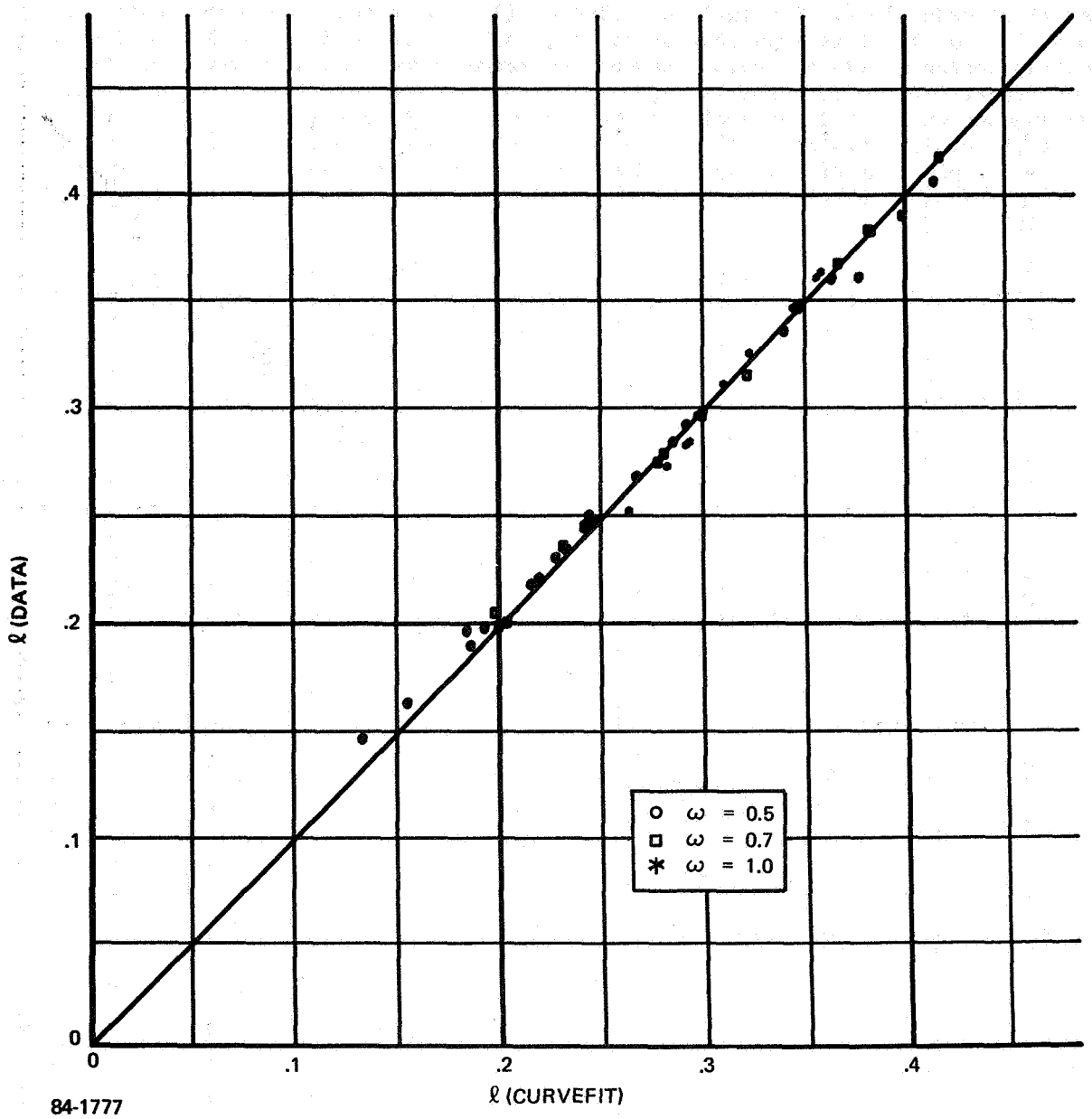

Figure 6 COMPARISON OF SHEAR PARAMETER CURVEFIT WITH DEWEY-GROSS DATA ($N_{Pr} = 0.5$)

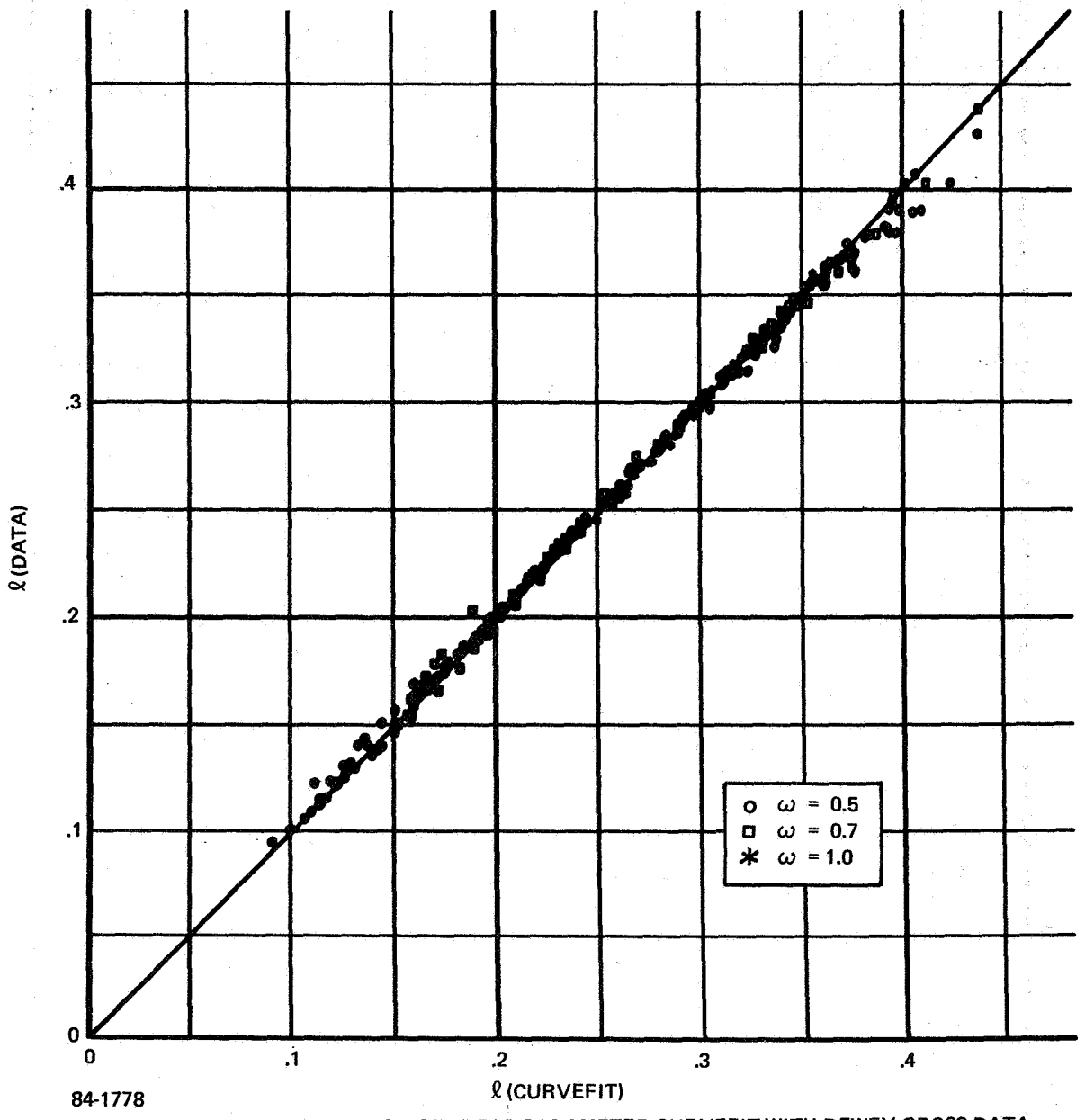

Figure 7 COMPARISON OF SHEAR PARAMETER CURVEFIT WITH DEWEY-GROSS DATA (N_{Pr} = 0.7)

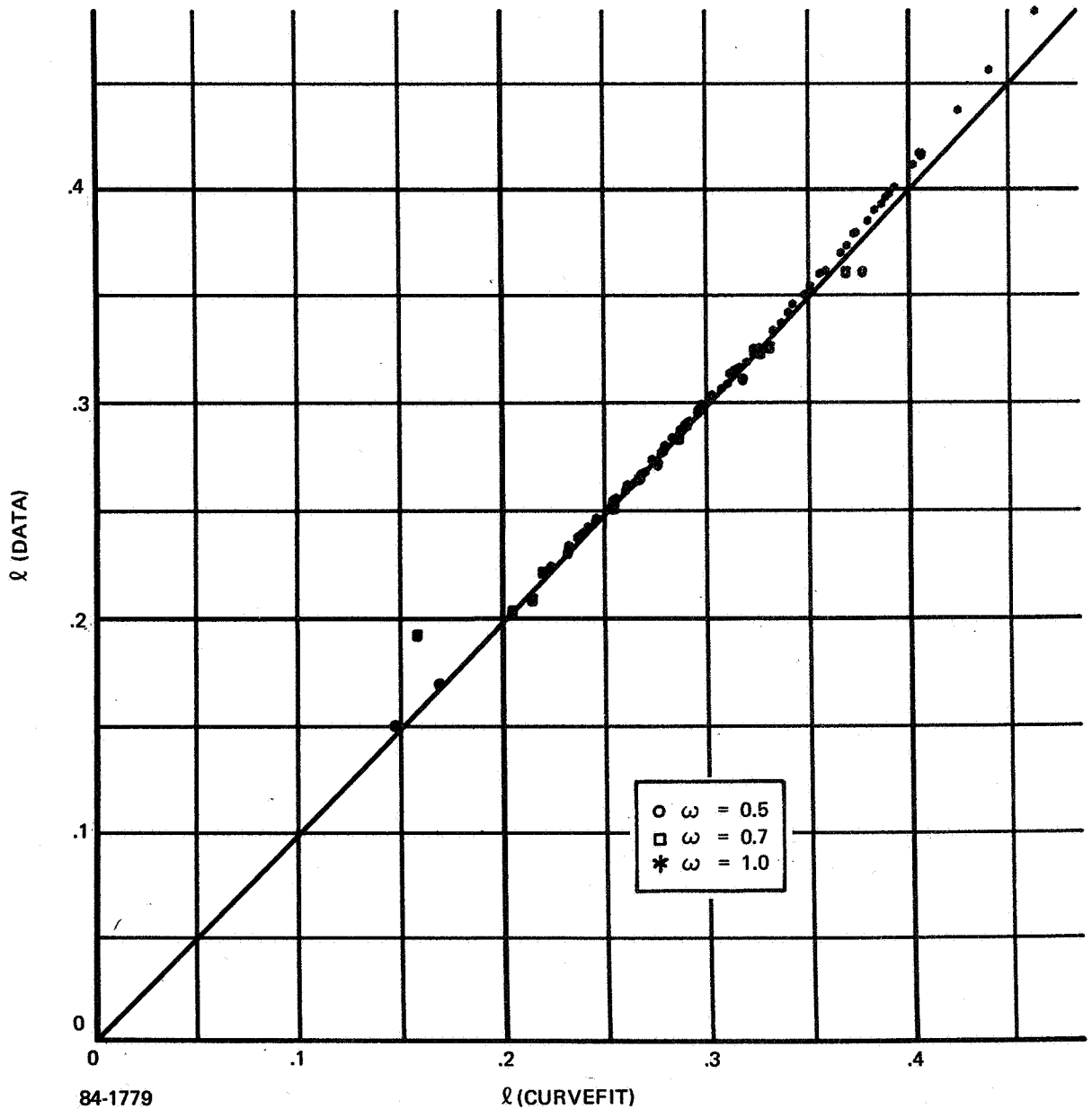

Figure 8 COMPARISON OF SHEAR PARAMETER CURVEFIT WITH DEWEY-GROSS DATA (N_{Pr} = 1.0)

Here, $t_{aw} = h_r / h_0$. A curvefit to t_{aw}, based upon equation (197), is

$$t_{aw} = 1 - \sigma (1 - N_{Pr}^{0.56}) \tag{199}$$

The Reynolds analogy factor based upon Dewey and Gross's tables has been curvefitted in the following form:

$$R_A = N_{Pr}^{-0.35} \left[1 - \frac{n}{a_R - b_R n} \right] \tag{200a}$$

where

$$a_R = (1 + S_w)^{-0.86\omega} \left\{ \frac{1}{6.2 + 2.35 (1 + S_w)^{-0.86}} + (1 - N_{Pr})^2 [-0.185 (1 + 2S_w) + 0.29 (1 + S_w)^{0.38} \sigma/\omega] \right\} \tag{200b}$$

$$b_R = 0.94 - 1.31 (1 + S_w)^{0.486} - \ln N_{Pr} \{0.62 (1 + S_w) + [3.5 (1 - \omega) - 0.49 - 3.61 (1 + S_w)] \sigma \} \tag{200c}$$

As in the case of the shear parameter, a relatively complex analytical form is used in an attempt to minimize the errors resulting from extrapolation to values of $(1 + S_w)$ below the range covered by the Dewey-Gross data.

Figures 9 through 11 compare the curvefit (200) with data from Dewey and Gross. The ordinate in these figures is $\theta'(0) / f''(0)$, computed from values in their tabulation of similar solutions. The abscissa is the quantity $[(t_{aw} - t_w)/(1 - t_w)] / R_A$ (fit), calculated from equations (199) and (200). Equation (198) shows that the ordinate and abscissa would be equal if the curvefit were exact. This manner of plotting the comparison tests the curvefit (197) for the recovery enthalpy together with the fit (200) for the Reynolds analogy factor. Figures 9 through 11 do not include the Dewey-Gross points for which $t_w = 1$ or $t_w = t_{aw}$. Such points were excluded because it was difficult to fit both the high-wall-temperature and low-wall-temperature heat transfer data accurately using a single analytical formula. The fit to R_A thus applies only to cases in which the wall temperature is lower than the adiabatic wall temperature, which is always the case in typical applications of NATA. The plots in figures 9 through 11 contain a total of 321 points. The root-mean-square percentage error for these points is 9 percent. The largest individual percentage error is 127 percent, in a case with $t_w = 0.6$ and $t_{aw} = 0.67$. The error arises partly from inaccuracy in the curvefit to the adiabatic wall temperature. Another similar point has an error of 79 percent. If these two points were excluded, the maximum percentage error would be 24 percent and the root-mean-square percentage error would be 3 percent.

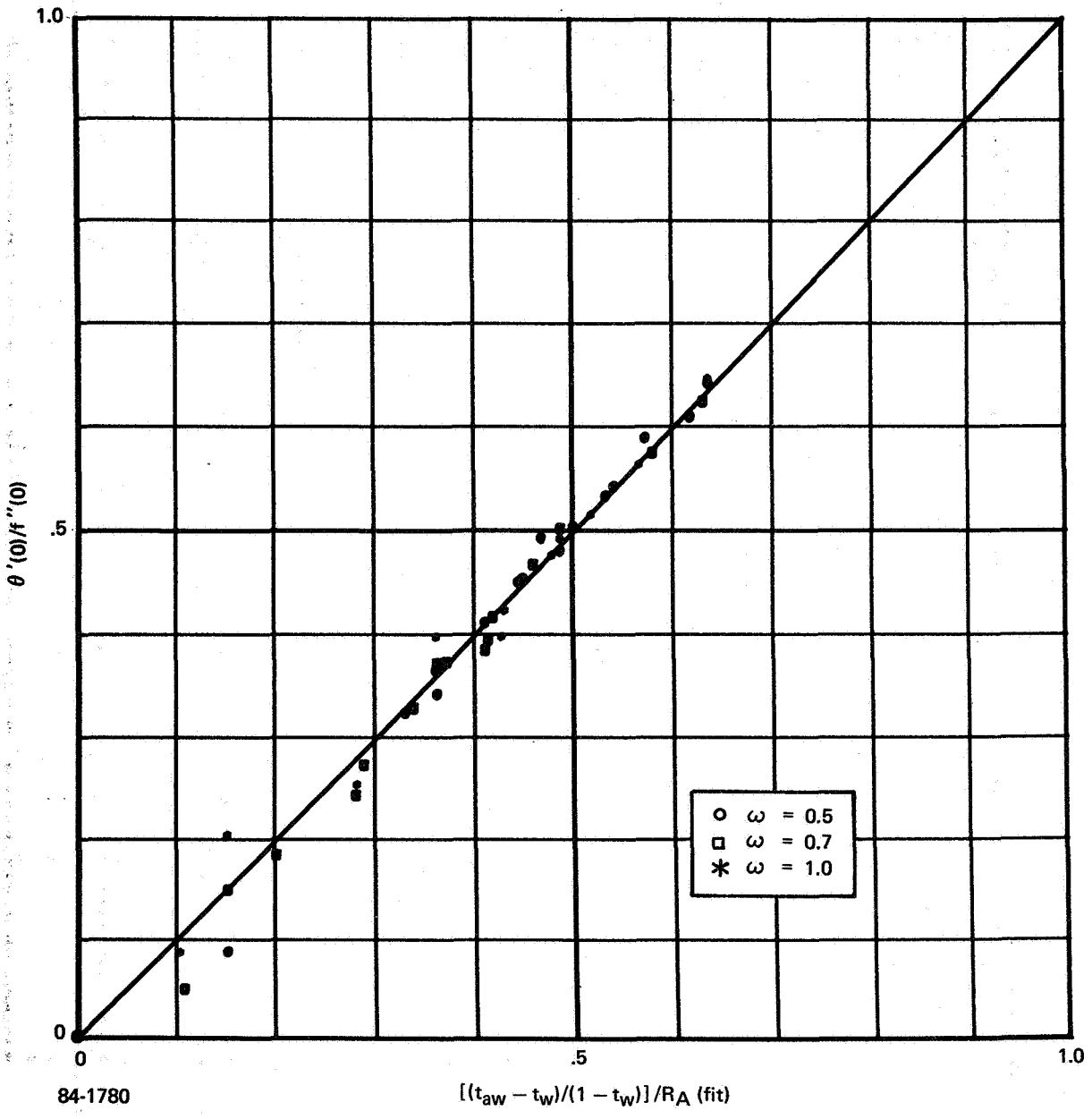

Figure 9 COMPARISON OF REYNOLDS ANALOGY FACTOR CURVEFIT WITH DEWEY-GROSS DATA ($N_{Pr} = 0.5$)

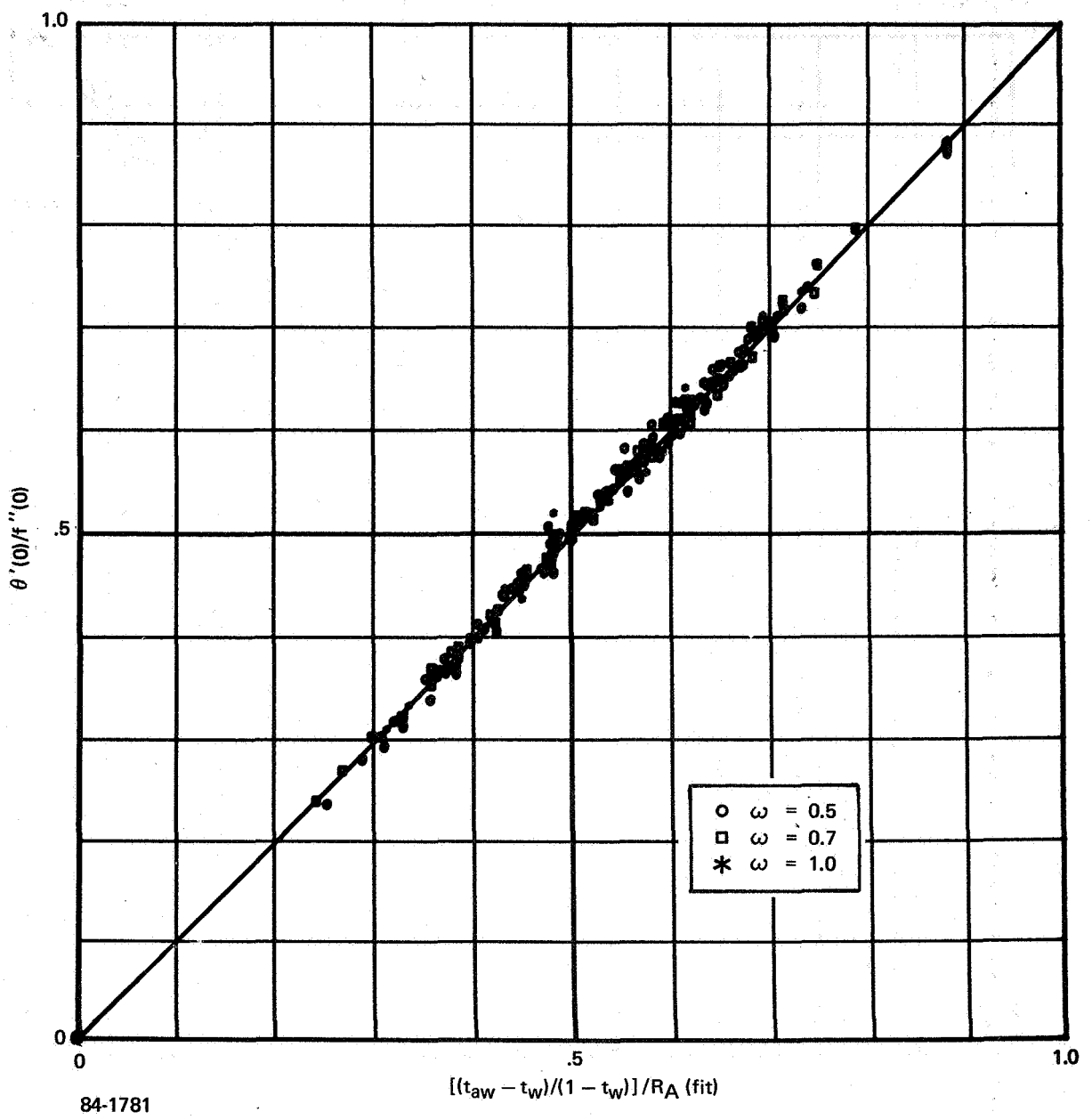

Figure 10 COMPARISON OF REYNOLDS ANALOGY FACTOR CURVEFIT WITH DEWEY-GROSS DATA ($N_{Pr} = 0.7$)

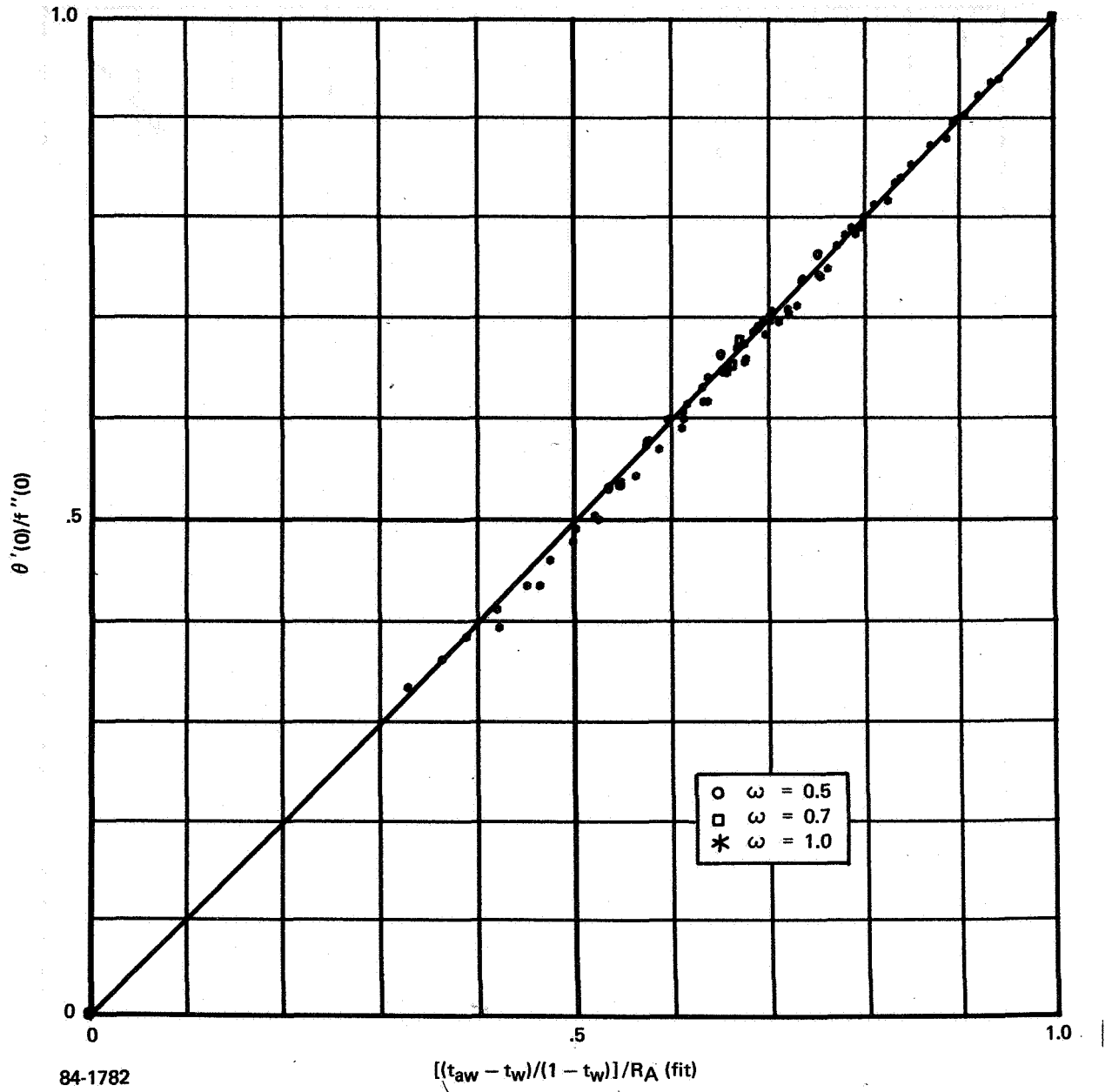

Figure 11 COMPARISON OF REYNOLDS ANALOGY FACTOR CURVEFIT WITH DEWEY-GROSS DATA (N_{Pr} = 1.0)

5.9 Dependence of the Momentum Parameter N Upon N_{Pr} and ω

Cohen and Reshotko assumed the parameter N, appearing in the form (162) of the boundary layer momentum equation, to be a function only of n and S_w. When N is evaluated from the Dewey-Gross data using (163d) it is found to vary with N_{Pr}, ω, and σ as well as with n and S_w. Cohen and Reshotko neglected the dependence upon these additional parameters because they determined N from similar solutions for $N_{Pr} = \omega = 1$. For these conditions, the boundary layer properties are independent of σ.

Because the solutions tabulated by Dewey and Gross include the dependence upon N_{Pr}, ω, and σ, it appears desirable to determine whether this information can be used to improve the accuracy and range of applicability of the Cohen-Reshotko correlation method. The solution (167) of equation (166) is valid only if the coefficients A and B in the linear curvefit (164) are constant for each problem. Since σ varies within each problem, from zero in the upstream reservoir to nearly 1 at the downstream nozzle exit, including the dependence on σ would lead to inadmissible variation of A and B. Thus, the dependence on σ must be neglected.

Inclusion of the dependence of N upon the Prandtl number leads to no inconsistency or difficulty so long as N_{Pr} is constant for each problem. However, inclusion of the dependence upon ω involves a logical inconsistency, because the derivation of equation (162) involves the assumption of the viscosity law (146), which is equivalent to (191) with $\omega = 1$. Nevertheless, a dependence of A and B upon ω is compatible with the solution (167), so long as ω is constant for each problem and the inclusion of such a dependence can be justified by comparison with Dewey and Gross's similar solutions (see below).

The variation of N with N_{Pr} and ω can be fitted approximately by retaining the analytical form (164) and the expression (165b) for B, but replacing (165a) by

$$A = 0.38 - 0.76\, N_{Pr}\,(1-\omega)\, e^{-6.67\,(1+S_w)} \tag{201}$$

Figures 12 through 14 compare the curvefit given by (164), (165a) and (201) with the Dewey-Gross data. The straight line in the figure is the locus of agreement between the fit and the data. The curvefit represents the data reasonably well for N values less than about 0.2, but is systematically too low at higher N. This is the same discrepancy seen near the right-hand edge of figure 1, where the linear curvefit $N = A + Bn$ lies beneath the upward-curving relationship $N(n, S_w)$ given by the Dewey-Gross data. The region of N values where the curvefit is most accurate corresponds to values of the correlation number n less than about -0.05, i.e., to the range of strongly favorable pressure gradients which is important in NATA runs for axisymmetric nozzles. For channels, smaller values of n of order -0.01 are encountered on the expanding face.

The validity of treating the parameter A in equation (166) as a function of ω and N_{Pr}, in accordance with (201), can be tested by applying the Cohen-Reshotko integral method to some of the similar solutions tabulated by Dewey and Gross. These similar solutions assume that the Falkner-Skan parameter β is constant. By definition

$$\beta = \frac{2\xi}{u_e}\,\frac{du_e}{d\xi}\cdot\frac{T_0}{T_e} \tag{202}$$

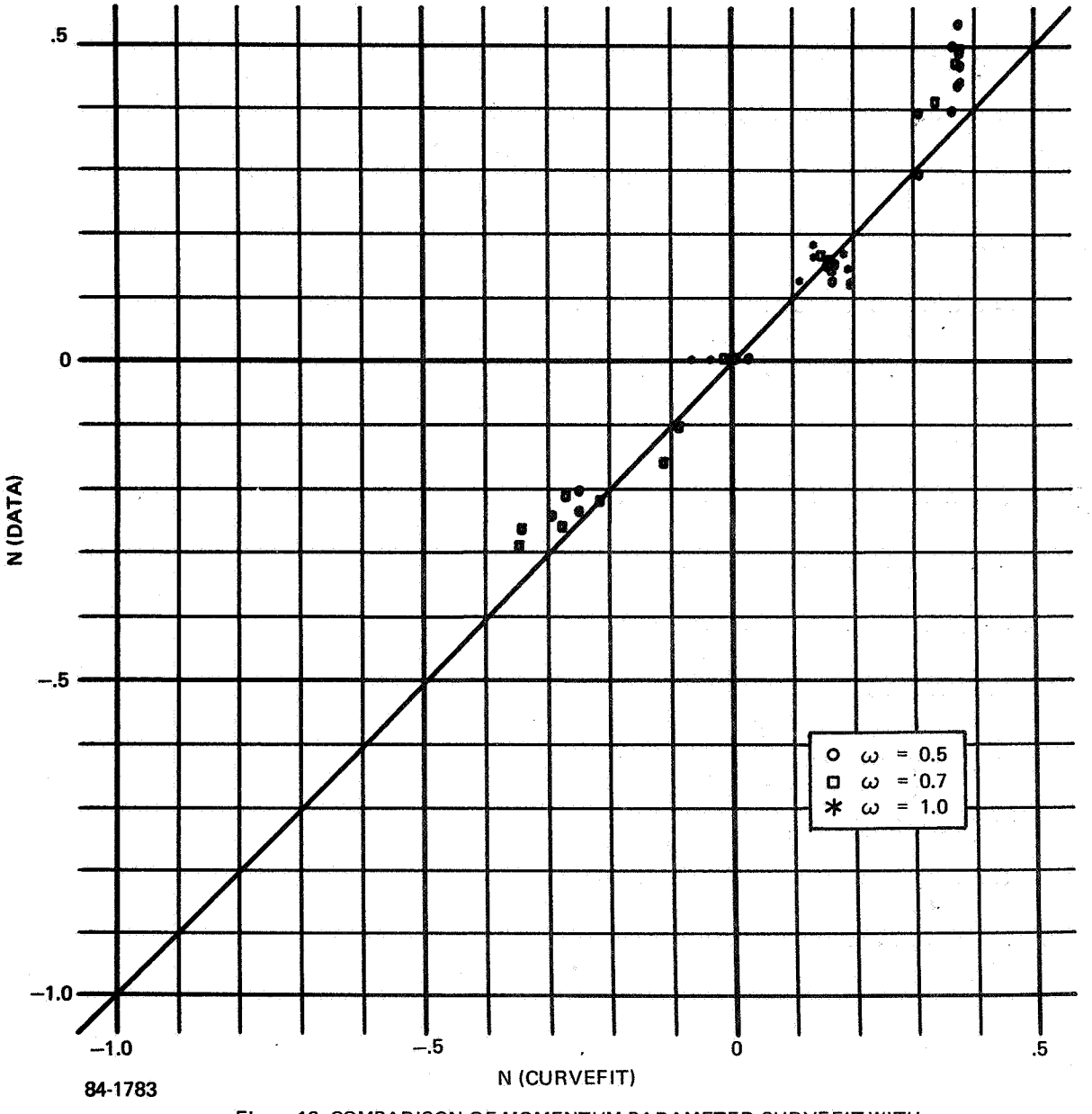

Figure 12 COMPARISON OF MOMENTUM PARAMETER CURVEFIT WITH DEWEY-GROSS DATA ($N_{Pr} = 0.5$)

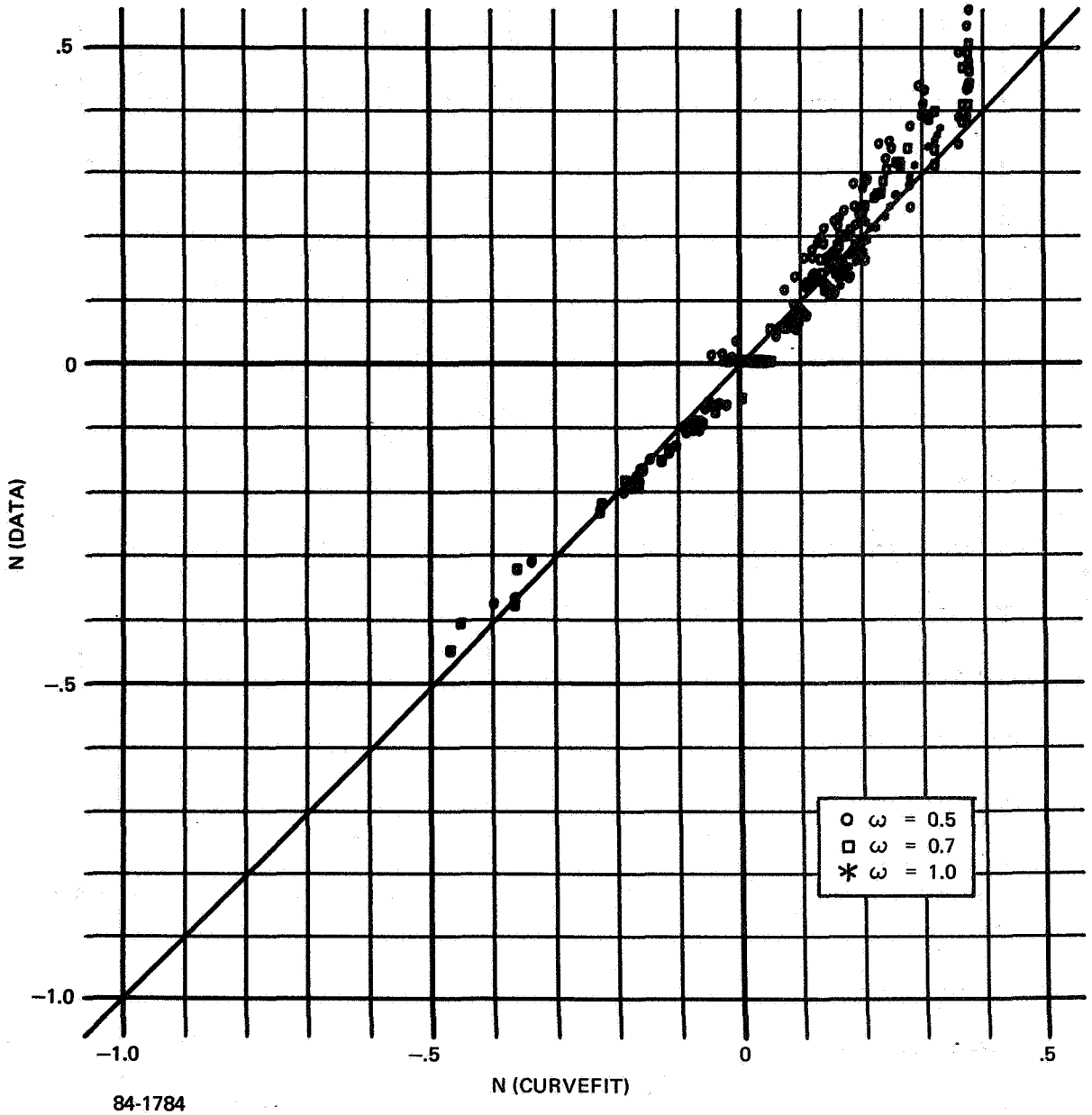

Figure 13 COMPARISON OF MOMENTUM PARAMETER CURVEFIT WITH DEWEY-GROSS DATA (N_{Pr} = 0.7)

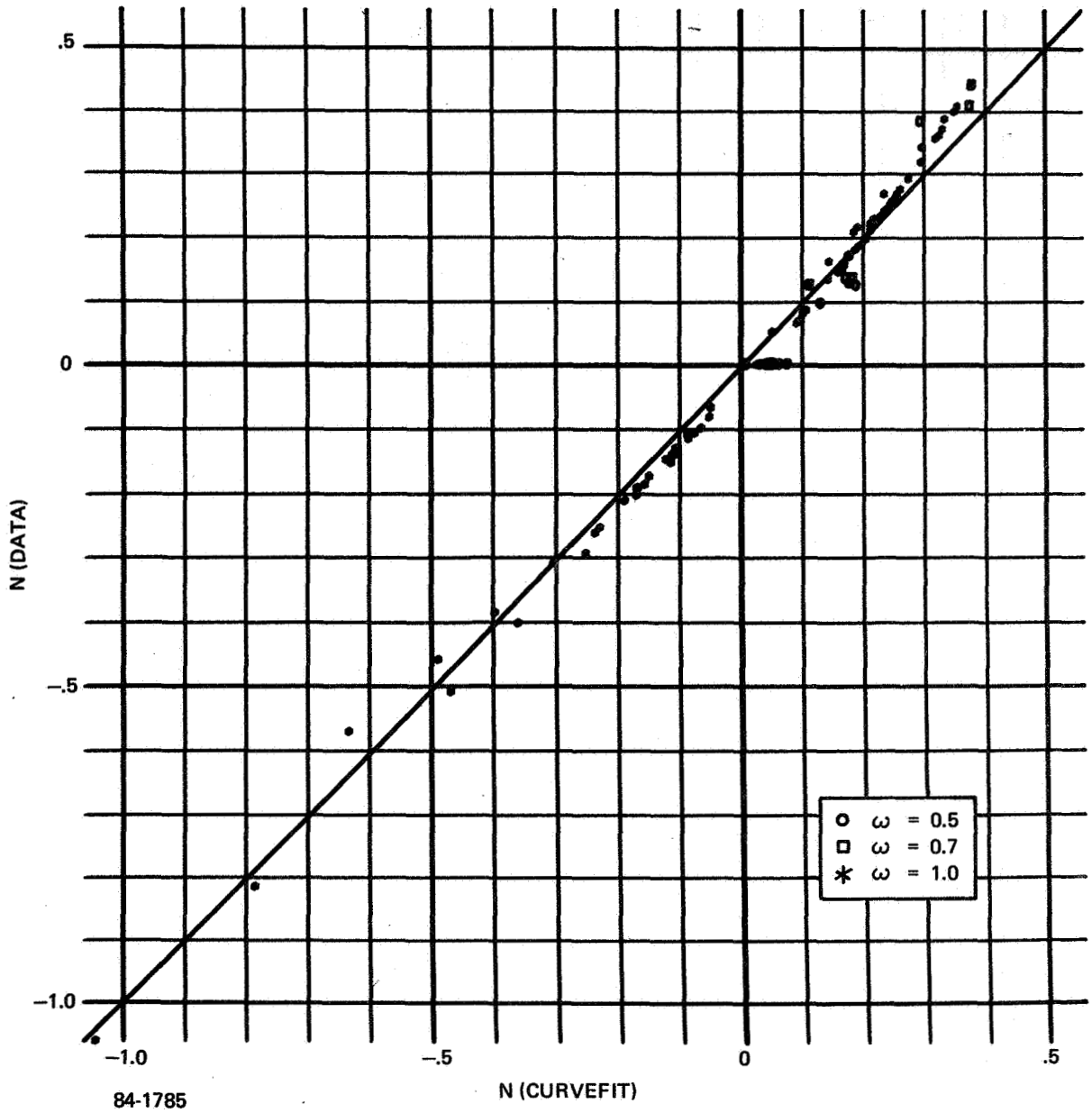

Figure 14 COMPARISON OF MOMENTUM PARAMETER CURVEFIT WITH DEWEY-GROSS DATA ($N_{p_r} = 1.0$)

$$\xi \equiv \int_0^x \rho_w \mu_w u_e r^{2j} dx \tag{203}$$

For $\rho_w \mu_w$ = constant and $j = 0$, (203) becomes

$$\xi = \rho_w \mu_w \int_0^x u_e dx \tag{204}$$

To simplify the analysis, cases with $\sigma << 1$ are considered. Then (202) gives, upon integration with $T_0 / T_e = 1$,

$$\xi = K u_e^{2/\beta} \tag{205}$$

With the aid of (204) and (205), equation (202) can be converted into a differential equation with x as the independent variable:

$$dx = \frac{2K u_e^{(2/\beta)-2} du_e}{\rho_w \mu_w \beta} \tag{206}$$

For $\sigma << 1$,

$$\frac{a_e}{a_0} \simeq 1 \tag{207a}$$

$$\frac{P_e}{P_0} \simeq 1 \tag{207b}$$

$$M_e \simeq u_e / a_0 \tag{207c}$$

Thus, for the cases under consideration, the quadrature in equation (169) can be performed analytically with the aid of (206) and (207). The result is

$$n = - \frac{A}{B - 2 + (2/\beta)} \tag{208}$$

With equation (164), this can be written in the form

$$n = - \frac{N(fit)}{2\left(\frac{1}{\beta} - 1\right)} \tag{209}$$

Figure 15 compares values of n calculated from (209) with values obtained directly from (163a), for a number of the similar solutions tabulated by Dewey and Gross. The filled circles represent data for $\omega = 1$, $N_{Pr} = 1$. The other symbols refer to cases with $\omega \neq 1$. Cases with $\beta = 1$, for which the denominator in (209) is zero and N(fit) is small, are omitted. The line is the locus of agreement. The figure shows that the n values calculated from (209) agree reasonably well with the correct values based on (163a). The agreement is nearly as good for $\omega \neq 1$ as for $\omega = 1$. If the dependence of A upon ω and N_{Pr}, as given by (201), had not been included in the calculation, the agreement would have been poorer for the cases with $\omega \neq 1$, especially for smaller-magnitude values of n. Thus, the use of (201) to determine the coefficient A in equation (166) appears justified.

The data in figure 15 are all for $\sigma = 0$. If data for other values of σ had been included, the scatter would have been greater, especially for small $|n|$.

It is also of interest to compare the predictions of momentum thickness based on the Cohen-Reshotko integral method with the exact results for the similar solutions. Substitution of equations (204) to (208) into the formula (177) for the two-dimensional momentum thickness gives, with use of (179),

$$\bar{\theta}_{CR} = \sqrt{\frac{A}{B-2+2/\beta} \cdot \frac{2K u_e^{(2/\beta)-2}}{\beta \rho_e^2}} \tag{210}$$

The momentum thickness for similar solutions, based on relations given by Dewey and Gross, is

$$\bar{\theta}_{DG} = \frac{I_2 \sqrt{2\xi}}{\rho_e u_e} = \sqrt{\frac{2 I_2^2 K u_e^{(2/\beta)-2}}{\rho_e^2}} \tag{211}$$

where ξ has been expressed using (205). From (210) and (211),

$$\frac{\bar{\theta}_{CR}}{\bar{\theta}_{DG}} = \sqrt{\frac{A}{B-2+2/\beta} \cdot \frac{1}{\beta I_2^2}} \tag{212}$$

According to equations (163a) and (208), the quantity under the radical is simply the ratio of the correlation number n, as evaluated using the Cohen-Reshotko method with the curvefit (164), to the correct value of n for the similar solution. Thus, to the extent that (208) agrees with (163a), the Cohen-Reshotko integral method gives the correct momentum thickness when applied to similar boundary layer problems, at least in the limit $\sigma << 1$ that is treated by the preceding analysis.

The remaining boundary layer properties, δ^*, τ_w, and q_w, are all calculated from the momentum thickness using curvefits to relations based on similar solutions. Thus, their accuracy should be comparable with that of the momentum thickness.

5.10 Initial Condition

The initial condition on the solution (167) of the Cohen-Reshotko differential equation (166) is embodied in the lower limit of integration, X_0. If U_e is

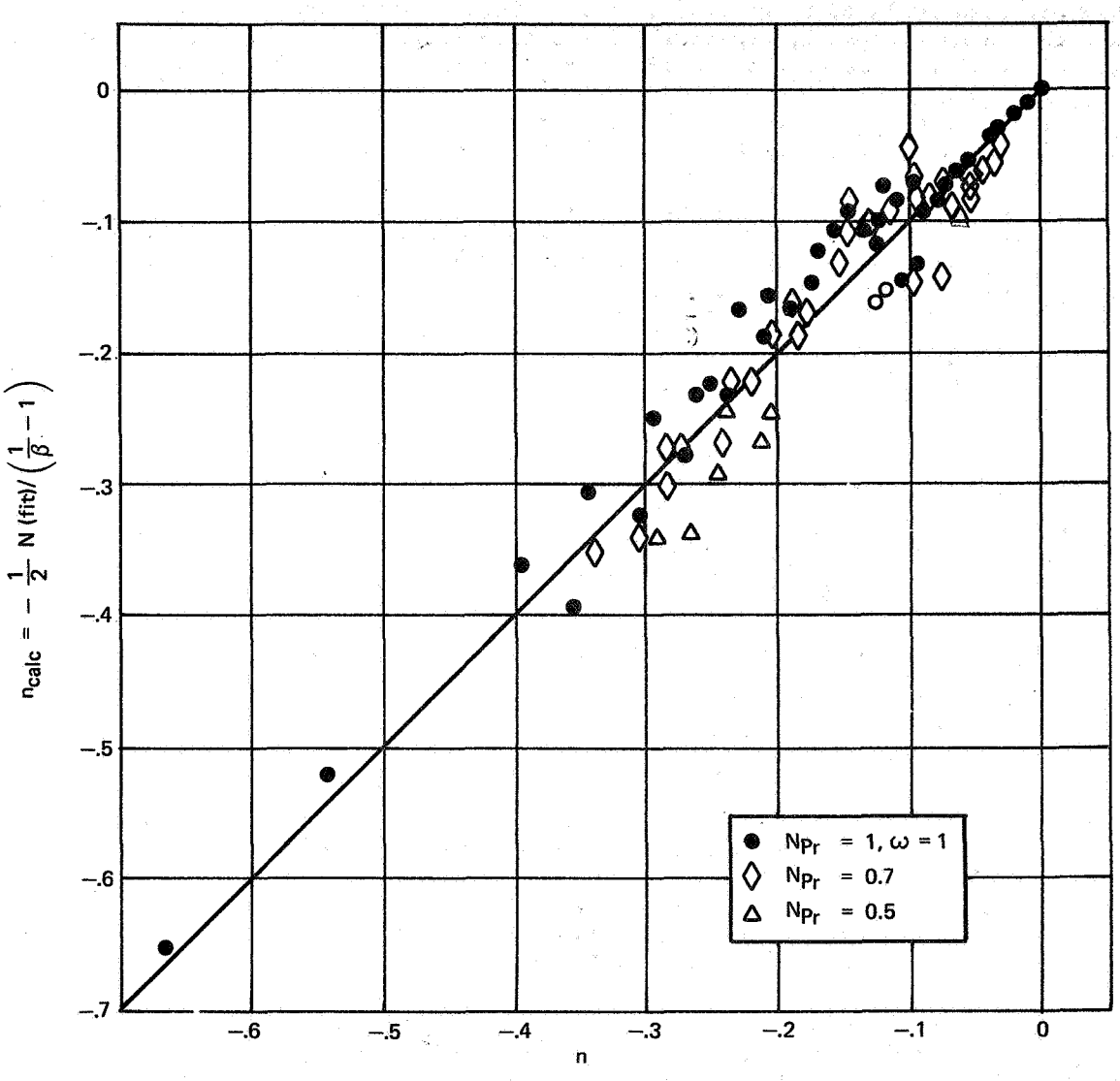

84-1786

Figure 15 COMPARISON OF THE CORRELATION NUMBER n (CALCULATED USING THE COHEN-RESHOTKO APPROXIMATION) WITH DATA FROM SIMILAR SOLUTIONS

non-zero at $X = X_0$, then $n = 0$ at that point. In that case, the incompressible momentum thickness θ_i is also zero at X_0. If $X = X_0$ is a stagnation point ($U_e = 0$) then $n(X_0)$ is not zero and the boundary layer starts with a finite thickness.

It is difficult to specify a fully satisfactory initial condition for the boundary layer in an internal flow system such as an arc-heated wind tunnel. Under some circumstances the boundary layer might extend upstream along the wall confining the flow, through the plenum chamber (if any) and the arc heater. The conditions in these regions upstream of the nozzle are poorly known and generally chaotic because of the presence of the arc column, swirl caused by tangential gas injection and, in some cases, free-stream turbulence. In general, the cross sectional area of the flow is finite everywhere, and any stagnation point which may exist in a "corner" of the wall profile is likely to receive an influx of boundary layer gas from further upstream.

In NATA, no attempt is made to model the detailed geometry of the plenum and arc chamber. The boundary layer is assumed to start at a somewhat arbitrary point near the juncture between the nozzle and the plenum. The uncertainty in x_0 due to the arbitrariness in the choice of this starting point affects the value of the integral I (172). The resulting uncertainty in I, in turn, affects n' (173), n (174), and thus θ (185), δ^* (188), τ_w (193), and q_w (195). The percentage errors in these boundary layer properties, due to an error in x_0, decrease downstream as the value of I increases.

Some insight into the dependence of these errors upon x can be obtained by examining the behavior of the integral I in the limits of low and high Mach number. At the assumed boundary layer starting point x_0, the Mach number is much less than unity. Thus, $a_e/a_0 \simeq p_e/p_0 \simeq 1$, and I is approximately

$$I \simeq \frac{1}{a_0^{B-1}} \int_0^{\xi} r^{2j} u_e^{B-1} \, d\xi \tag{213}$$

In the two-dimensional case ($j = 0$), the contributions to I from points near $\xi = 0$ are relatively small because u_e is low in that region and, according to (165a), $B-1$ is a little greater than 1. Thus, for two-dimensional boundary layers, the results in the throat region and downstream should be rather insensitive to the value of x_0 chosen, so long as it defines a point well upstream of the throat where the Mach number is low.

In the axisymmetric case ($j = 1$), however, the continuity equation $\rho u_e A' =$ constant shows that $r^{2j} u_e^{B-1}$ is roughly constant in the subsonic part of the flow, because r^{2j} is proportional to the cross sectional flow area A', $B-1$ is approximately 1, and ρ is almost constant. Thus, the results for an axisymmetric boundary layer are more sensitive to the choice of x_0 than those in the two-dimensional case.

For flow over a flat plate at zero angle of attack, the integrand Φ (171) of I is constant, so that $I \propto (x - x_0)$. In that case, the relative error in I due to

an error in x_0 decreases as $(x-x_0)^{-1}$. For flow of a perfect gas in an axisymmetric nozzle, the integral can be expressed in the form

$$I = R_0^2 \left(\frac{2}{\gamma+1}\right)^{0.5(\gamma+1)/(\gamma-1)} \int_0^{\xi} \left[1 + \frac{\gamma-1}{2} M_e^2\right]^{-1} M_e^{B-3} \, d\xi \qquad (214)$$

In the limit of high Mach number, the integrand varies as M_e^{B-5}. Since $B \simeq 2.2$ for cases with a low wall temperature, the integrand decreases more rapidly with increasing ξ, at high Mach number, than in the case of a flat plate, and the effects of an error in x_0 vanish more slowly.

5.11 Coupling with the Inviscid Flow

The method by which the boundary layer is coupled with the inviscid flow in NATA has been explained in Section 4. Briefly, the boundary layer solution is generated step by step along with the inviscid solution. The inviscid flow variables at each point are used in determining the boundary layer parameters n, θ, δ^*, etc., and the displacement thickness δ^* at each point is used in the inviscid solution to provide a relation between the geometric area ratio A_g and the effective area ratio A_e (Section 4.4).

A fundamental problem in the calculation of coupled solutions for a confined inviscid flow and the boundary layer on the confining wall is that the system of equations for the coupled flow is unstable at supersonic Mach numbers (ref. 27, p. 377). If the boundary layer is computed using the Cohen-Reshotko integral method, as in the NATA code, this instability arises as follows: Assume that there is a small initial error in the Mach number gradient, $dM_e/d\xi$. If this gradient is too high, then the correlation parameter n (174) has too large a negative value. Then the exponential factor $e^{4.6n}$ in the correlation (189) for the incompressible form factor H_{inc} is too small, and as a result, $(1 + H_{inc})$ is too small. Correspondingly, the displacement thickness δ^* calculated from (188) is too low. When this erroneous δ^* is used in the inviscid flow calculation, the effective area ratio computed is too high, so that the corresponding Mach number is too high. Then the next-computed value of the Mach number gradient, $dM_e/d\xi$, is too high. Under some conditions, the error in the new $dM_e/d\xi$ can be larger than the previous error which led to it. In such cases, the error is amplified from step to step, and the solution becomes unstable. Such instabilities were actually observed in some solutions run during the development of the NATA code.

To avoid such instabilities, NATA uses a computational artifice. The incompressible form factor (189) is calculated from a smoothed value $\bar{n}$ of the correlation parameter n, rather than from the actual current value of n. In some earlier versions of the code, $\bar{n}$ was defined as an unweighted average of n over the entire portion of the boundary layer upstream of the current flow point:

$$\bar{n} = \frac{1}{x - x_0} \int_{x_0}^{x} n \, dx'$$

However, this has been found to be an unnecessarily severe approximation. In the current version of the code, $\bar{n}$ is defined as an exponentially weighted average over the upstream part of the solution:

$$\bar{n} = b \int_{x_0}^{x} n(x') \, e^{-(x-x')/a} \, dx' \tag{215}$$

Here a represents a characteristic averaging distance, such that $\bar{n}$ depends mainly upon the values of n at points lying between $x-a$ and x. The coefficient b is chosen such that, for n = constant, (215) gives $\bar{n} = n$. For $x - x_0 >> a$, the value $b = 1/a$ gives accurate results. The algorithm actually used in the code is derived from (215) as follows: Let $\bar{n}_p$ be the $\bar{n}$ at the previous point of the solution, and let Δx denote the current step size. Then application of (215) to the current solution point gives, with $b = 1/a$,

$$\bar{n} = \bar{n}_p \, e^{-\Delta x/a} + \frac{1}{a} \int_{x-\Delta x}^{x} n(x') \, e^{-(x-x')/a} \, dx' \tag{216}$$

The integral on the right is approximated by treating n as constant over the step. Then

$$\bar{n} = \bar{n}_p \, e^{-\Delta x/a} + n\,(1 - e^{-\Delta x/a}) \tag{217}$$

This relation gives $\bar{n}$ as a weighted average of the $\bar{n}$ for the previous step and the n for the current step.

The step size in NATA solutions is typically small in the throat region and quite large in the downstream region of high Mach numbers. An a value of a few times the local step size is required for stability. If a is many times the local step size, the solution remains stable but is affected to an inordinate extent by the use of $\bar{n}$ in place of n. Therefore, the averaging distance used in NATA is varied according to the following rule:

$$a = R_0 \, A_g / w \tag{218}$$

where R_0 denotes the throat radius, A_g the geometric area ratio, and w a constant. Over a large part of the supersonic region, $A_g/\Delta x$ is approximately constant for frozen NATA inviscid solutions. In this region, (218) gives $a/\Delta x \simeq$ constant.

Averaging of n over a fixed number of previous points in the solution would be simpler than (218), but would cause the solution to depend upon the step size used in running the problem. The averaging prescribed by (217) and (218) makes the solution approximately independent of step size.

The smoothed value $\bar{n}$ of the correlation parameter is used only in calculating the form factor (and thus the displacement thickness). The shear parameter ℓ and Reynolds analogy factor R_A are computed from the actual current value of n. Thus, the shear stress and heat flux are unaffected by the smoothing procedure, apart from any resulting errors in the inviscid solution itself.

5.12 Geometric Options

The basic geometric options available in NATA (two-dimensional nozzle, axisymmetric nozzle, and rectangular channel) have been described and discussed in Section 4. The present section deals with the treatment of these options in the boundary layer calculations.

The application of the Cohen-Reshotko integral method to two-dimensional and axisymmetric boundary layers has been discussed explicitly in preceding parts of the present section. The entire difference between these two cases is contained in the exponent j appearing in equation (171). If n' is calculated from equations (171), (172) and (173), and θ from (185), then all of the boundary layer properties are obtained simply by setting $j = 0$ for the two-dimensional case and $j = 1$ for the axisymmetric case.

However, the third option (the rectangular channel) requires some further discussion. A channel has two pairs of nominally identical faces. If a channel face is of constant width, the boundary layer on it can be approximated as two-dimensional. If a face has variable width, the streamlines in the boundary layer converge or diverge. The effects of such a flow geometry upon the continuity equation for the boundary layer can be taken into account by treating the boundary layer as axisymmetric in this case, but omitting the transverse curvature correction. For example, a channel face which is widening in the downstream direction can be regarded as equivalent to the surface of a diverging axisymmetric nozzle whose circumference is equal to the width of the actual face at each axial position.

Since the widths of the two sets of faces of a channel vary differently with axial position, two independent boundary layer calculations are performed in channel flow solutions. Both boundary layers are treated formally as if they were axisymmetric, i.e., using equation (170) to calculate n. For each layer, the equivalent radius r in (170) is taken to be the half-width of the channel face upon which the layer lies. No attempt is made to correct for the interaction of the boundary layers on adjoining channel faces in the corner regions.

5.13 Examples and Discussion

The present section exhibits selected results of NATA flow solutions including the boundary layer. These examples are intended to illustrate certain aspects of the NATA boundary layer calculations and to provide, by comparisons with experimental data, some indication as to the accuracy of the results.

Figures 16 through 20 show some of the results of a non-equilibrium solution of the flow in a rectangular channel. The channel has a 2.54 x 5.08 cm (1 x 2 inch) cross section at the throat. In the downstream region, the 5.08 cm dimension is constant, and the other dimension increases from 2.54 to 53 cm at the exit, 145 cm

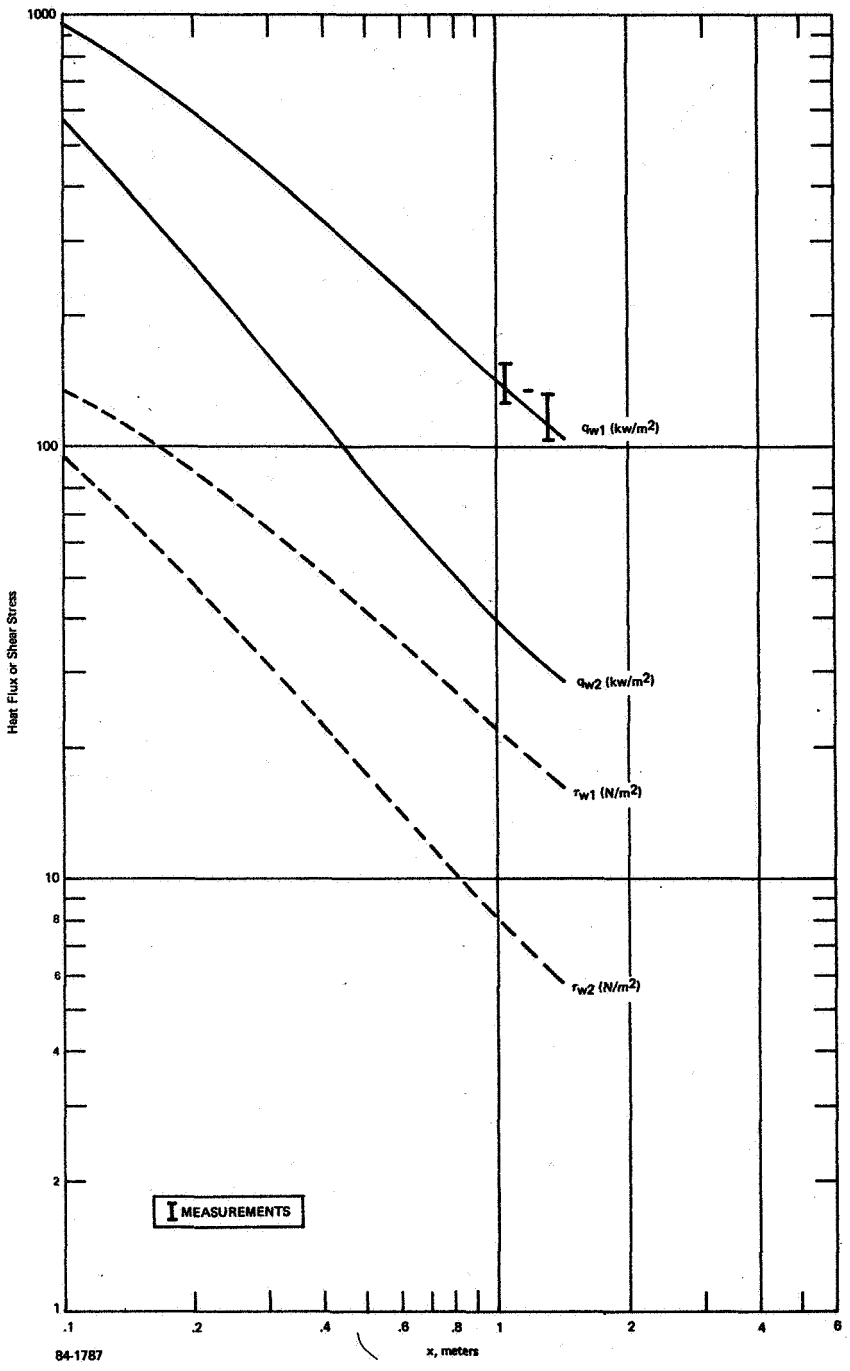

Figure 16 HEAT FLUX AND SHEAR STRESS FOR THE CHANNEL TEST CASE

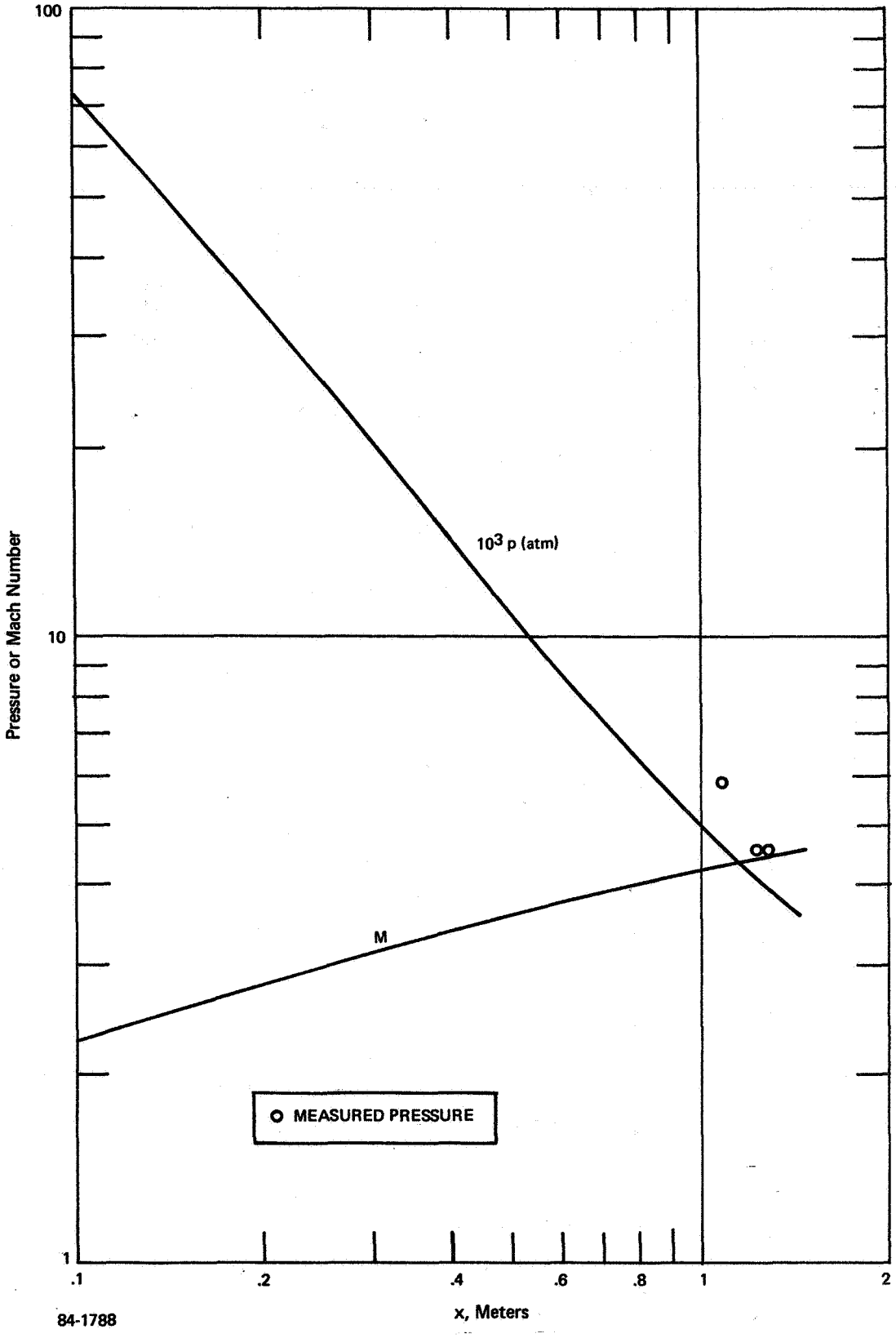

Figure 17 PRESSURE AND MACH NUMBER FOR THE CHANNEL TEST CASE

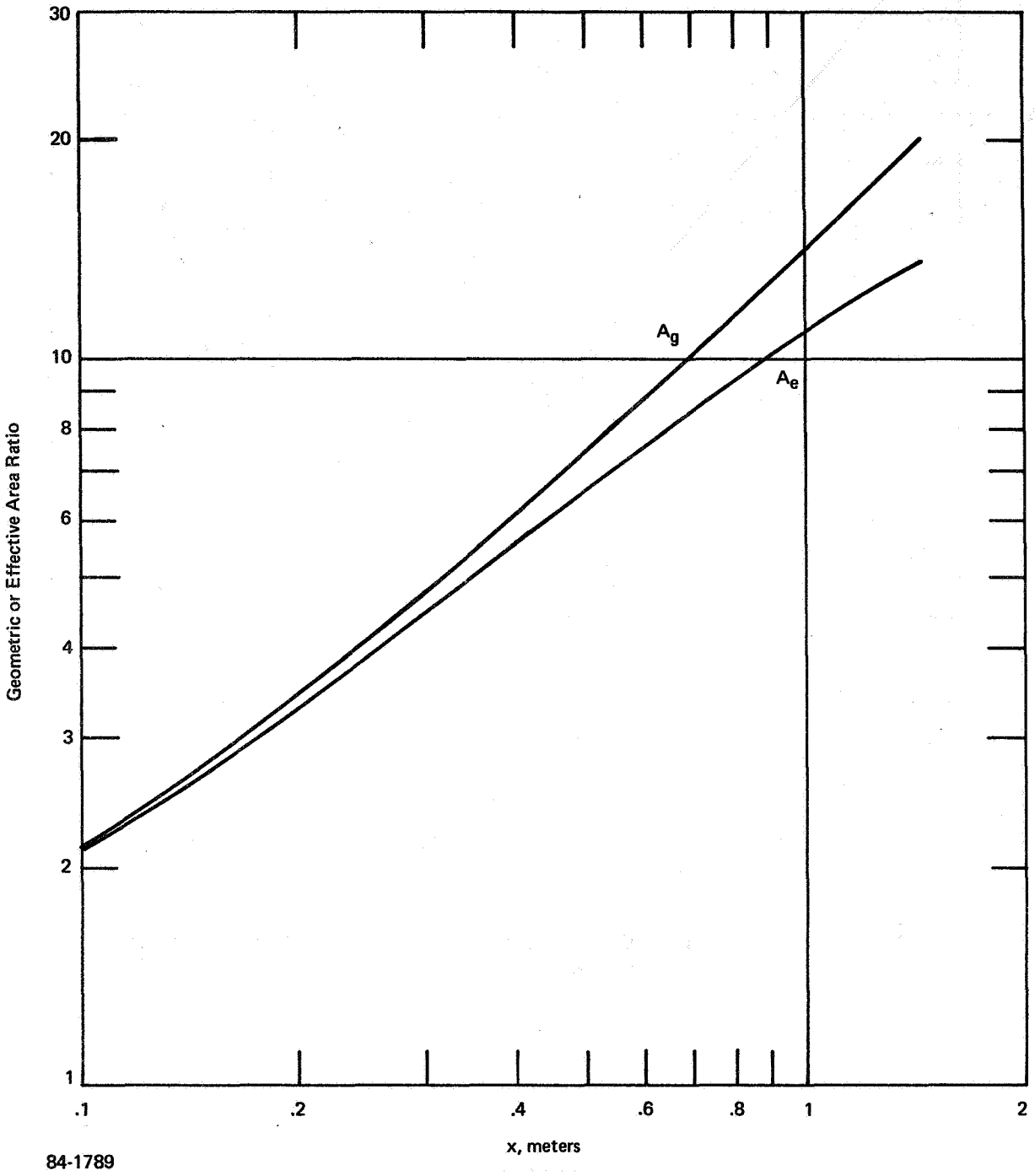

Figure 18 GEOMETRIC AND EFFECTIVE AREA RATIOS FOR THE CHANNEL TEST CASE

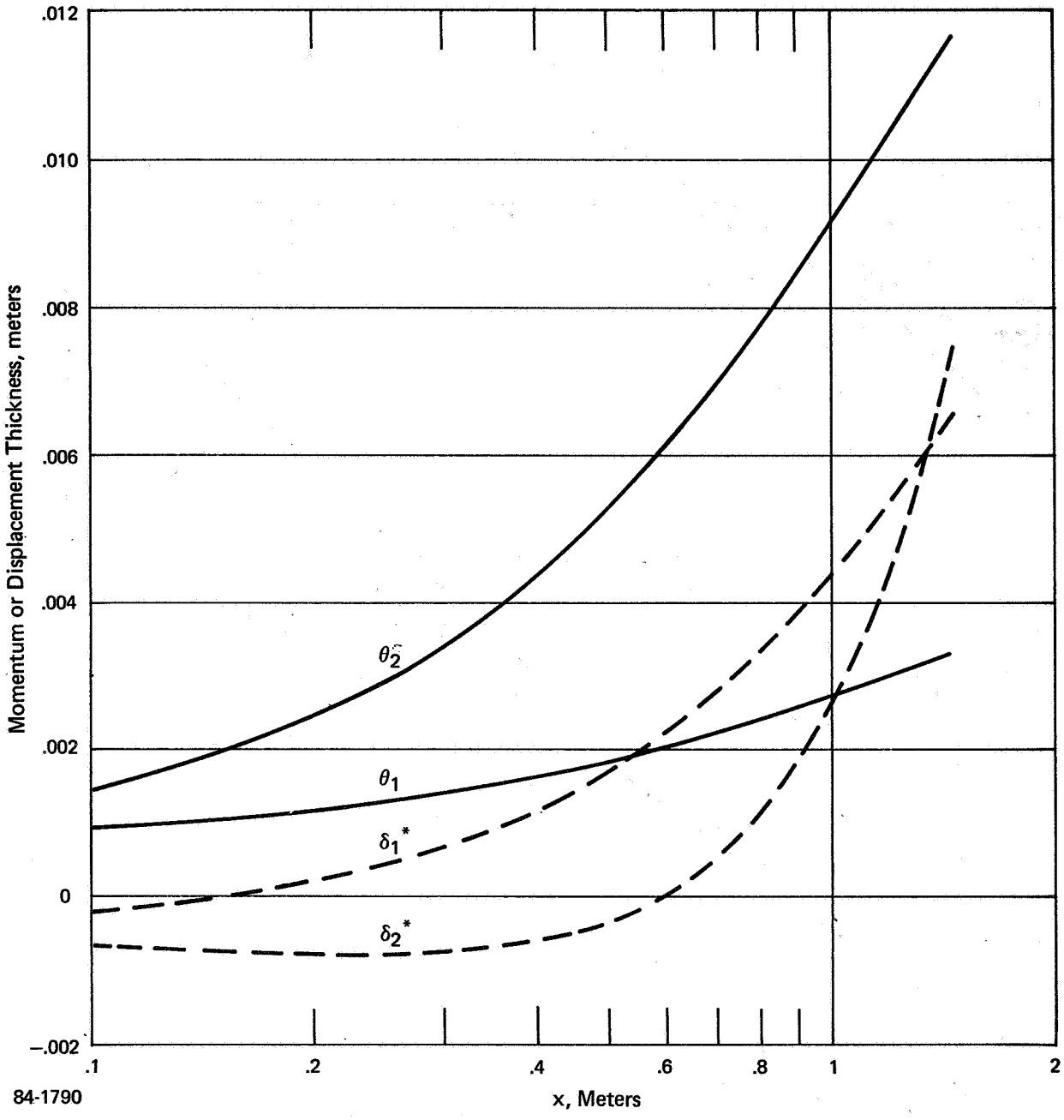

Figure 19 MOMENTUM AND DISPLACEMENT THICKNESSES FOR THE CHANNEL TEST CASE

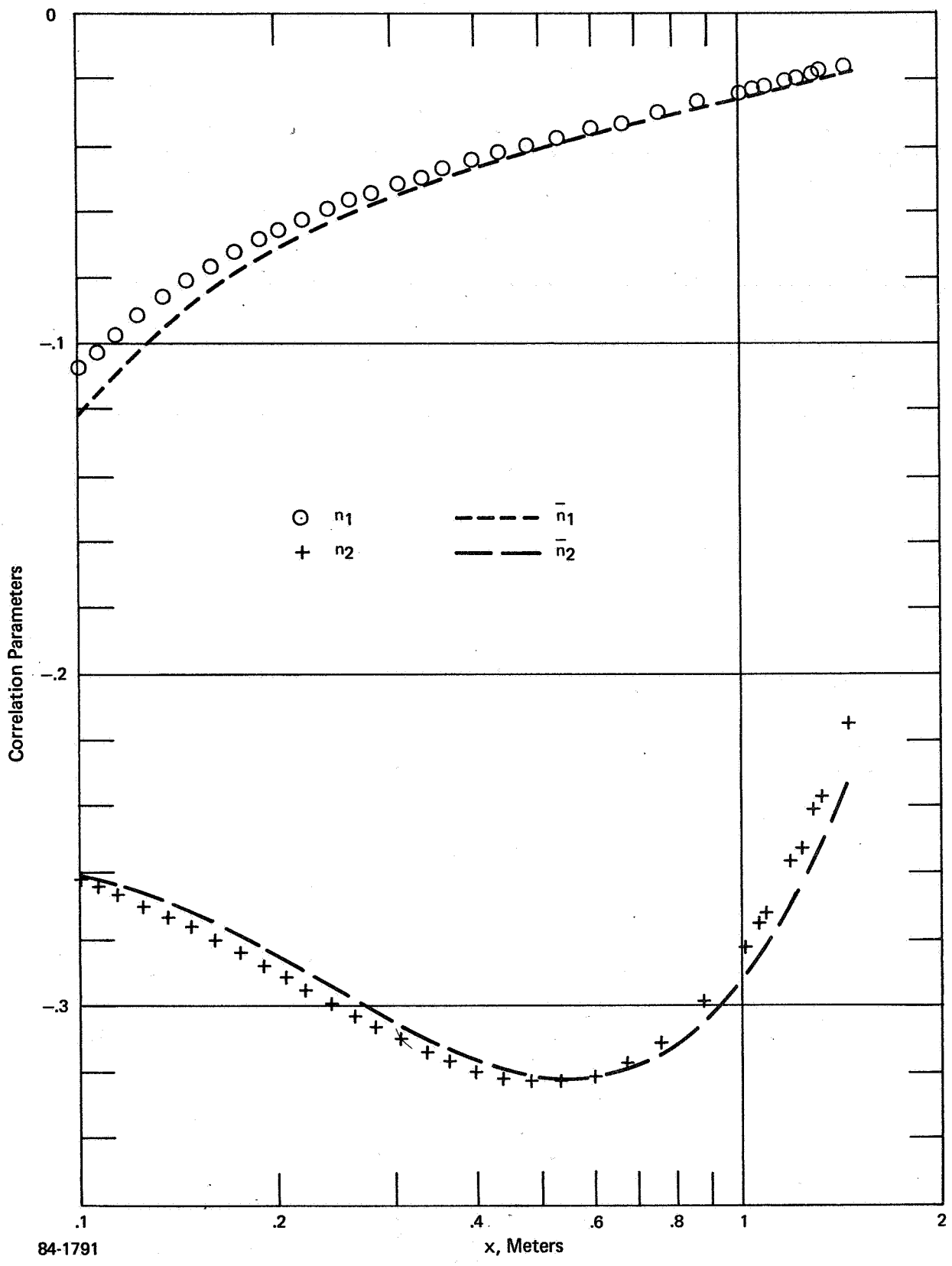

Figure 20 BOUNDARY LAYER CORRELATION PARAMETERS FOR THE CHANNEL TEST CASE

beyond the throat. In the region between 103 and 143 cm downstream of the throat, one of the wide faces of the channel is instrumented with pressure taps and flush-mounted heat transfer gages.

The flow solution illustrated in figures 16 through 20 simulates a test with an actual channel at the NASA Johnson Space Center ARMSEF facility. The heated air flow was supplied by the Dual-Constrictor Arc. The conditions of the test were as follows:

Mass flow = 0.0454 kg/sec (0.1 lb/sec)

Plenum pressure = 0.919 atm

Reservoir temperature = 6879° K

Stagnation enthalpy = 25.1 MJ/kg (10799 Btu/lb)

Reservoir molecular weight = 18.36 gm/mole

The mass flow and plenum pressure are measurements. The other values were computed by NATA from these data.

Figure 16 shows the variation of heat flux and shear stress with the axial coordinate, x, for this case, for the region from 0.1 m beyond the throat to the end of the channel. The curve labeled q_{w1} represents the calculated heat flux to one of the broad faces of the channel. The three vertical bars represent heat flux measurements. Experimental data were available from three heat transfer gages at each of three axial positions. The ranges of values indicated by the vertical bars show the lateral variation of heat flux at each axial station. In most cases, the heat flux measured on the centerline of the channel face was higher than the values obtained from the off-axis gages. The main source of the variation in heat flux was lateral non-uniformities in the flow.

The curve labeled q_{w2} represents the calculated heat flux to the narrow (5.08 cm wide) face of the channel. q_{w2} is smaller than q_{w1} because the boundary layer on the narrow face is thicker than that on the wide face. The curves labeled τ_{w1} and τ_{w2} represent the calculated shear stresses on the wide and narrow faces of the channel, respectively. No experimental measurements of q_{w2}, τ_{w1}, or τ_{w2} are available.

Figure 17 shows the variation of the static pressure and the Mach number with axial position for the same case. The three circles represent experimental measurements of the pressure on the centerline of one of the wide channel faces. The Mach number at the channel exit is about 4.5.

Figure 18 shows the geometric area ratio A_g and the effective area ratio A_e as functions of axial position. At the exit, A_e is about 30 percent smaller than A_g. Figure 19 shows the momentum and displacement thicknesses. The momentum thickness θ_1 on the broad face is smaller than that (θ_2) on the narrow face of the channel because of flow-divergence in the boundary layer on the broad face. For x less than 0.155 meter, both displacement thicknesses, δ_1^* and δ_2^* are negative. In this region, the effective cross sectional area of the flow (A_e') is larger than the geometric cross section (A_g'). However, as shown in figure 18,

the effective area ratio A_e is smaller than the geometric area ratio A_g. These data are mutually consistent because the effective flow cross section A'_{e*} at the sonic point is larger than the geometric cross section A'_{g0} at the throat. (See equations (113) and (114).)

Figure 20 shows the correlation parameters, n_1 and n_2, for the boundary layers on the broad and narrow channel faces, respectively, together with the corresponding smoothed values $\bar{n}_1$ and $\bar{n}_2$, calculated from equation (217). The smoothed values track the local values quite well. The local values n_1 and n_2 are shown for every step of the non-equilibrium solution in the region covered by the graph. Irregularities in step size between x = 1 m and the exit are due to insertion of steps at specified channel widths corresponding to the locations of heat transfer gages and pressure taps.

Figure 21 presents a comparison of NATA heat flux calculations with experimental data on heat flux to the channel wall for eleven cases. The mass flows for these cases ranged from 0.028 to 0.091 kg/sec, the plenum pressures from 0.544 to 1.985 atm, and the stagnation enthalpies from 10 to 47 MJ/kg. The vertical bars indicate the range of heat flux values observed at different lateral positions at each axial station. The dashed line is the locus of agreement between the calculations and the experimental data. The unbroken line is a fit by eye to all of the data bars shown. Based on the unbroken line, the heat flux as given by NATA is too low by 28 percent, on the average.

Figure 22 is a similar comparison of NATA static pressure calculations with experimental measurements using the centerline pressure taps in the channel. The flow cases are the same as in figure 22. Based on the curvefit provided by the unbroken line, the static pressures given by NATA are too low by 20 percent, on the average.

One possible explanation of this discrepancy in static pressure would be that the effective area ratio, as computed in NATA, is too large because of errors in the boundary layer displacement thicknesses. To test this hypothesis, the ratio of experimental and calculated pressures is plotted versus the calculated displacement thickness on the broad face in figure 23 for a single station in the channel. If the errors in pressure were due to a systematic error in displacement thickness, this ratio would be close to 1 for small δ_1^*, and would diverge from unity as δ_1^* increased. Figure 23, however, shows that the ratio has no significant correlation with displacement thickness. Thus, the hypothesized explanation is rejected. The apparent systematic error in static pressure is probably a result of lateral non-uniformities in the flow. The pressure data were all taken on the centerline of the channel face. If the off-axis pressures were lower than the centerline pressure, then the average pressure would be more nearly in agreement with the results of the NATA calculations, which are based on a uniform-flow model.

The boundary layer calculations in NATA involve many approximations, including those listed below:

(1) The assumption of uniform inviscid flow

(2) The correlation assumptions in Cohen and Reshotko's method

(3) The analytical curvefits (164), (165), (189), (194), (200), (201) to the results of similar solutions

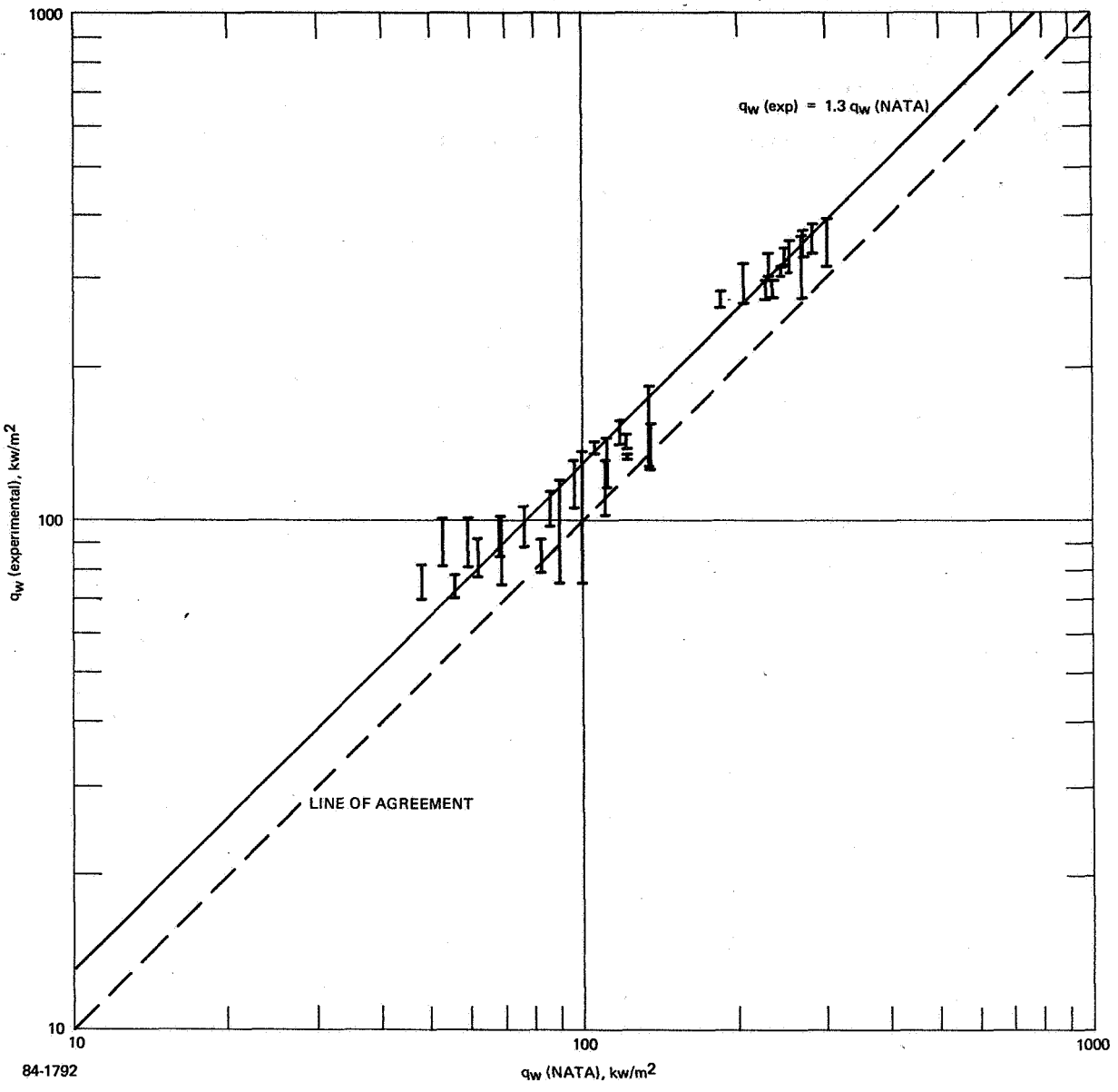

Figure 21 COMPARISON OF EXPERIMENTAL AND CALCULATED VALUES OF HEAT FLUX TO THE CHANNEL WALL

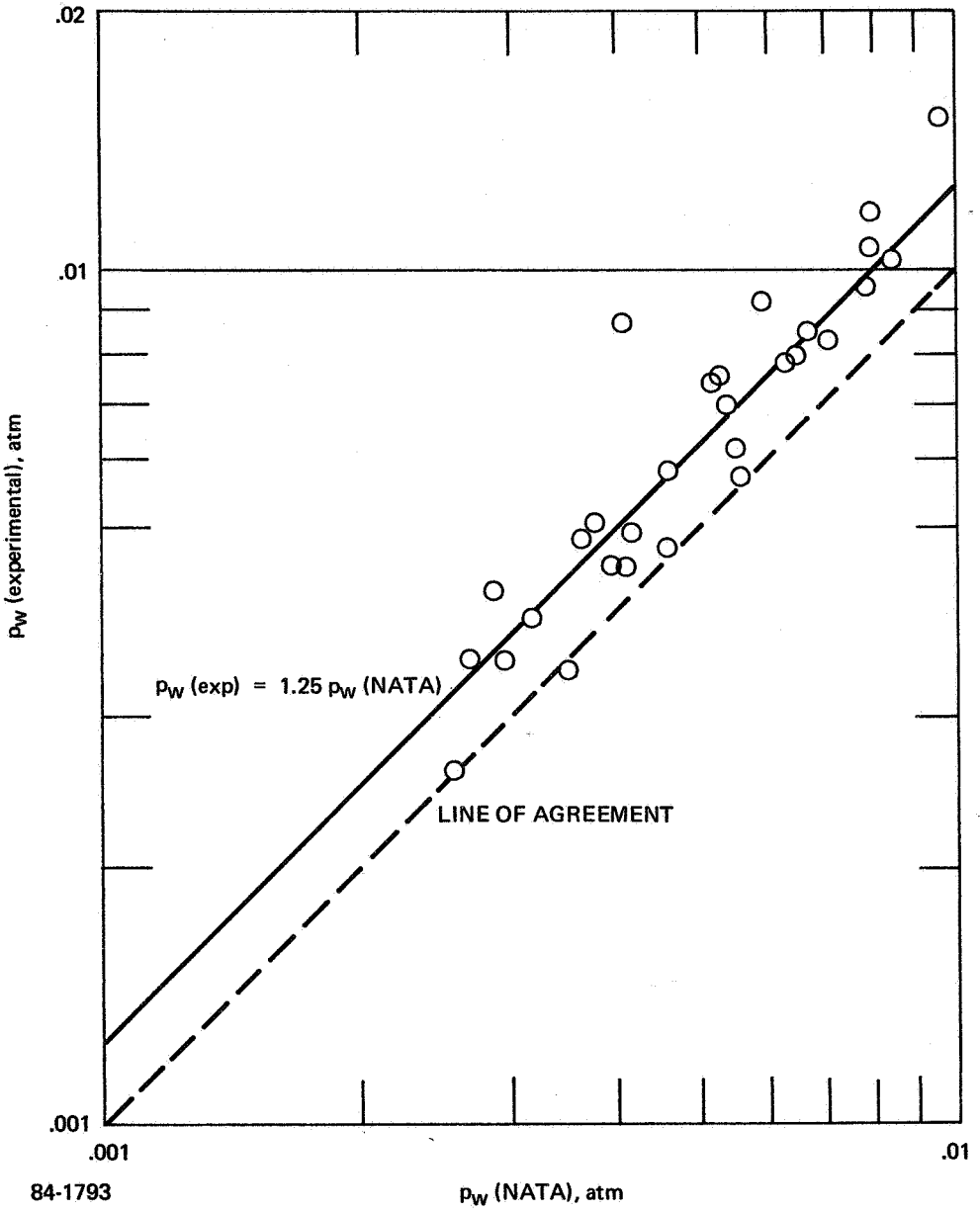

Figure 22 COMPARISON OF EXPERIMENTAL AND CALCULATED VALUES OF STATIC PRESSURE

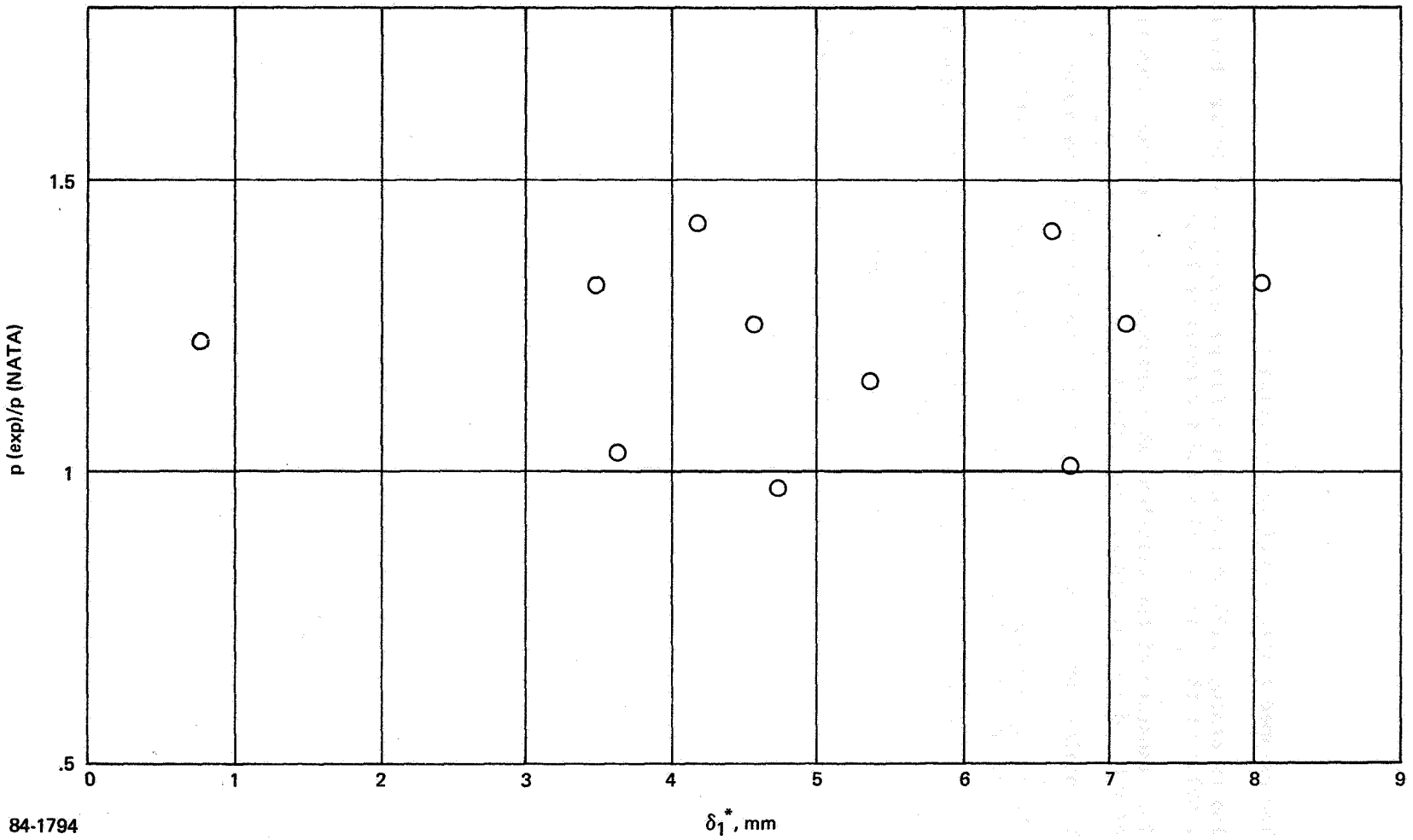

Figure 23 RATIO OF EXPERIMENTAL AND CALCULATED STATIC PRESSURE AS A FUNCTION OF CALCULATED DISPLACEMENT THICKNESS ON THE BROAD CHANNEL FACE

(4) The assumed initial condition (Section 5.10)

(5) The smoothing (217) of the correlation parameter to stabilize the coupled problem of the inviscid flow and the boundary layer

(6) The linearity of the relation (164) assumed between the momentum parameter N and the correlation parameter n

(7) The neglect of the dependence of N upon the hypersonic parameter

(8) The use of a Reynolds analogy factor, based on similar solutions, to calculate the heat flux

(9) Approximations to gas properties used in the analysis, i.e., the perfect gas law and the viscosity-temperature relation (143).

The combined effects of these approximations could account for sizeable errors in the results of the boundary layer calculations. In the context of these approximations, the discrepancies actually seen in figures 21 and 22 appear moderate in magnitude.

6. EQUILIBRIUM AND FROZEN FLOW

NATA performs two types of thermochemical equilibrium calculation:

(1) Equilibrium at specified temperature and pressure. This calculation is done by subroutine EQCALC. It is used in the determination of the reservoir conditions and in the computation of conditions behind an equilibrium normal shock on a model.

(2) Equilibrium at specified temperature and entropy. This calculation is done by subroutine NEWRAP and is used in generating the solution for equilibrium flow of the gas through the nozzle.

The technique used in the thermochemical equilibrium calculations at specified temperature and pressure is explained in Section 6.1. Section 6.2 discusses the inviscid equilibrium flow calculation. Section 6.3 discusses the coupling of the inviscid flow with the boundary layer on the nozzle or channel wall. Section 6.4 discusses the frozen flow solution, which is generated using techniques similar to those used in the equilibrium solution, with the constraint that the species mole fractions are constant at their reservoir values. Finally, Section 6.5 explains the three options available in NATA for specifying the reservoir conditions, based on input of reservoir temperature and pressure, of reservoir pressure and total mass flow, and of stagnation enthalpy and total mass flow.

6.1 Thermochemical Equilibrium at Specified Temperature and Pressure

A chemical reaction can be specified symbolically in the form

$$\sum_{\text{reactants}} \nu_i M_i = \sum_{\text{products}} \nu'_j M_j \tag{219}$$

where the M_i, M_j represent chemical species and the ν_i, ν'_j are the stoichiometric coefficients. The condition for equilibrium of the reaction is (ref. 2, pp. 284-285 and 952-953)

$$\sum_{\text{reactants}} \nu_i \mu_i = \sum_{\text{products}} \nu'_j \mu_j \tag{220}$$

in which μ_i, μ_j represent the chemical potentials of the reactant and product species. From equation (21) and the relation

$$p_i = p X_i \tag{221}$$

between partial pressures p_i, mole fractions X_i, and the gas pressure p, the chemical potentials can be expressed in the form

$$\mu_i = \mu_i^o + \ell n\, p + \ell n\, X_i \tag{222}$$

in which the chemical potential μ_i^o at the standard pressure is a function only of temperature.

Application of the equilibrium condition (220) to the reactions (5) for forming the dependent species ($i = c + 1, \ldots, n$) from the independent species ($m = 1, \ldots, c$) gives

$$\mu_i = \sum_{m=1}^{c} \bar{\nu}_{i-c,\,m} \mu_m \qquad (i = c+1, \ldots, n) \tag{223}$$

Substitution of equation (222) for the chemical potentials appearing in this relation gives an explicit expression for the mole fraction X_i of the i^{th} dependent species in equilibrium with the independent species:

$$X_i = K_i\, p^{\nu^*_{i-c}-1} \prod_{k=1}^{c} X_k^{\bar{\nu}_{i-c,\,k}} \tag{224}$$

where

$$K_i \equiv \exp\left[-\frac{\mu_i^o}{R_0 T} + \sum_{k=1}^{c} \bar{\nu}_{i-c,\,k} \frac{\mu_k^o}{R_0 T} \right] \tag{225}$$

is the equilibrium constant.

Conservation of the chemical elements can be formulated using equation (16):

$$X_j = q_j - \sum_{i=c+1}^{n} X_i \left[\bar{\nu}_{i-c,\,j} - q_j \left(\nu^*_{i-c} - 1 \right) \right] \tag{226}$$

Here the q_j are the normalized coefficients (10) expressing the elemental composition of the gas in terms of the independent species, and the X_j (for $j = 1, \ldots, c$) are the mole fractions of those species. The $(n-c)$ equations (224) together with

the c equations (226) provide a system of n equations for determining the mole fractions X_m ($m = 1, \ldots, n$) of all the species. However, if equations (224) are used to eliminate the mole fractions X_i of the dependent species from (226), equations (226) become a system of c equations for the mole fractions X_j of the c independent species. This formulation of the thermochemical equilibrium problem thus reduces the number of equations to be solved from n (the number of species) to c (the number of elements). Since the right-hand side of (224) contains a product of mole fractions X_m raised to various powers $\bar{\nu}_{i-c,m}$, the system of equations is, in general, non-linear.

In NATA, these equations for the mole fractions of the independent species are solved using the Newton-Raphson method. Equations (226) are rewritten in the form

$$F_j(X_1, \ldots, X_c) = q_j - \sum_{i=c+1}^{n} X_i \left[\bar{\nu}_{i-c,j} - q_j \left(\nu^*_{i-c} - 1 \right) \right] - X_j = 0 \tag{227}$$

The component mole fractions in the r^{th} iteration will be denoted by X_j^r. Then, to first order,

$$F_j(X_k^{r+1}) = F_j(X_k^r) + \sum_{m=1}^{c} \left(\frac{\partial F_j}{\partial X_m} \right)^r (X_m^{r+1} - X_m^r) \tag{228}$$

where $(\partial F_j / \partial X_m)^r$ denotes the derivative of F_j with respect to X_m, evaluated using the mole-fraction values of the r^{th} iteration. This derivative can be determined analytically by differentiating (227):

$$\frac{\partial F_j}{\partial X_m} = - \sum_{i=c+1}^{n} \left[\bar{\nu}_{i-c,j} - q_j \left(\nu^*_{i-c} - 1 \right) \right] \frac{\partial X_i}{\partial X_m} - \frac{\partial X_j}{\partial X_m} \tag{229}$$

since the q_j, $\bar{\nu}_{i-c,j}$, and ν^*_{i-c} are all independent of the mole fractions for a given gas model. The subscripts j and m refer to independent species, while i refers to a dependent species. Thus

$$\frac{\partial X_j}{\partial X_m} = \delta_{jm} \equiv \begin{cases} 1 & \text{for} \quad j = m \\ 0 & \text{for} \quad j \neq m \end{cases} \tag{230}$$

and from logarithmic differentiation of (224),

$$\frac{\partial X_i}{\partial X_m} = X_i \sum_{k=1}^{c} \frac{\bar{\nu}_{i-c,k}\ \delta_{km}}{X_k} = \frac{X_i\ \bar{\nu}_{i-c,m}}{X_m} \tag{231}$$

Substitution of these expressions into (229) gives

$$\frac{\partial F_j}{\partial X_m} = -\sum_{i=c+1}^{n} \left[\bar{\nu}_{i-c,j} - q_j\ (\nu^*_{i-c} - 1)\right] \frac{X_i}{X_m}\ \bar{\nu}_{i-c,m} - \delta_{jm} \tag{232}$$

The object of the Newton-Raphson iteration is to make the $F_j\ (X_k)$ all equal to zero. Hence, in equations (228), the $F_j\ (X_k{}^{r+1})$ are set equal to zero, for $j = 1$ to c. This gives the following system of equations:

$$-\sum_{m=1}^{c} X_m{}^r \left(\frac{\partial F_j}{\partial X_m}\right)^r h_m{}^r = F_j\ (X_k{}^r) \tag{233a}$$

where the $h_m{}^r$ are the relative corrections to the mole fractions:

$$h_m{}^r \equiv \frac{X_m{}^{r+1} - X_m{}^r}{X_m{}^r} \tag{234}$$

such that the corrected mole fractions are given by

$$X_m{}^{r+1} = X_m{}^r\ (1 + h_m{}^r) \tag{235}$$

(233a) is a system of c linear, inhomogeneous equations for the $h_m{}^r$. Substitution of (232) into (233a) gives the matrix of coefficients in the form

$$-X_m{}^r \left(\frac{\partial F_j}{\partial X_m}\right)^r = \sum_{i=c+1}^{n} \left[\bar{\nu}_{i-c,j} - q_j\ (\nu^*_{i-c} - 1)\right] X_i{}^r\ \bar{\nu}_{i-c,m} + \delta_{jm} X_m{}^r \tag{233b}$$

In the special case of a gas model in which there are no dependent species (i.e., in which the number of species n is equal to the number of chemical elements c), the above formulas remain valid if the sums running over the dependent species are eliminated. These are the sums in which the summation index runs

from $c + 1$ to n. Equation (226) shows that, in this special case, the mole fractions X_j are equal to q_j and thus are constant. Equations (227), (233a), and (233b), with the sums over dependent species eliminated, show that the Newton-Raphson procedure gives this solution for the independent mole fractions correctly on the first iteration.

In NATA, the system of equations (233) is solved for the corrections h_m^r, at each stage of the iteration, by calling a subroutine (DSMSØL) for simultaneous solution of a system of linear equations. The iteration is continued until the h_m^r are all less than or equal to 10^{-6} in absolute magnitude. Once the iteration has converged, the entropy, enthalpy, and mean molecular weight of the equilibrium gas mixture are computed from equations (30b), (26), and

$$\mathbb{W} = \sum_{j=1}^{n} X_j \mathbb{W}_j \tag{236}$$

The gas density is then computed from the ideal gas relation

$$\rho = \frac{p \mathbb{W}}{R_0 T} \tag{237}$$

Finally, the density and enthalpy are corrected for gas imperfections using equations (79b) and (81).

It should be noted that the mixture enthalpy given by (26),

$$H = \sum_{j=1}^{n} X_j H_j \tag{238}$$

is the enthalpy per mole of mixture. The specific enthalpy (enthalpy per unit mass) is

$$h = \frac{H}{\mathbb{W}} \tag{239}$$

where $\mathbb{W}$ is the mean molecular weight (236). In the internal calculations of NATA, the species molar enthalpies H_j are computed in the non-dimensional form

$$SHJ(J) = \frac{H_j}{R_0 T_0} \tag{240}$$

where R_0 is the universal gas constant and T_0 the reservoir temperature, and the specific enthalpy is given as

$$CH = \frac{W_0 h}{R_0 T_0} \tag{241}$$

where W_0 is the molecular weight in the reservoir. From equations (238) to (241),

$$CH = \frac{W_0}{W} \sum_{J=1}^{n} X_J \cdot SHJ(J) \tag{242}$$

6.2 Inviscid Equilibrium Flow

The governing equations for steady, one-dimensional adiabatic inviscid flow are

$$\rho u A_e' = \rho_* u_* A_{e*}' = \text{const.} \tag{243}$$

$$u\,du + \frac{dp}{\rho} = 0 \tag{244}$$

$$h + \frac{1}{2} u^2 = h_0 = \text{const.} \tag{245}$$

where ρ denotes the density, u the flow velocity, A_e' the cross sectional area, p the pressure, and h the specific enthalpy. In the continuity equation (243), the asterisks indicate sonic-point values. The Euler equation (244) assumes that viscous stresses and body forces (such as electromagnetic and gravitational forces) are negligible. The energy equation (245) assumes that the flow is adiabatic. Subject to these assumptions, these equations are applicable to any steady, one-dimensional flow whether the gas is chemically frozen, in equilibrium, or undergoing reactions with finite rates.

Equations (244) and (245) can be combined to give

$$dh - \frac{dp}{\rho} = 0 \tag{246}$$

From the first law of thermodynamics,

$$T\,ds \geq d\epsilon + p\,d\left(\frac{1}{\rho}\right) \tag{247}$$

and the definition of enthalpy,

$$h = \epsilon + \frac{p}{\rho} \tag{248}$$

it may be shown that

$$Tds \geq dh - \frac{dp}{\rho} \tag{249}$$

Equation (246) thus implies that

$$Tds \geq 0 \tag{250}$$

i.e., the specific entropy of the gas either remains constant or increases in a flow obeying equations (244) and (245). The condition for $ds = 0$ is that the flow be reversible in the thermodynamic sense. This means that if the flow retraces its sequence of velocities (without passing through a shock), the gas is restored to its initial state. The flow is reversible, in this sense, if the gas obeys a rate-independent equation of state, $\rho = \rho(p, h)$, such that the density is uniquely determined when the pressure and enthalpy are specified. A gas which is everywhere in local thermochemical equilibrium obeys a constitutive relation of this type. A gas whose chemical composition is frozen also obeys a rate-independent equation of state. Thus, both equilibrium and frozen flows governed by equations (243) to (245) are isentropic ($ds = 0$). On the other hand, non-equilibrium flows with finite reaction rates are irreversible, because the gas composition depends not only upon the pressure and enthalpy but also upon the past history of the gas sample. Thus, from (250), the entropy increases in such non-equilibrium flows.

All of the flow solutions calculated by NATA are assumed to start from a state of thermochemical equilibrium in an upstream reservoir. The composition and state of the gas in the reservoir are computed using the method described in Section 6.1. If the reservoir temperature and pressure are input-specified, this method is applied directly. If other options for input specification of the reservoir conditions are employed, the reservoir temperature and pressure are determined using the iterative techniques explained in Section 6.5, and the method of Section 6.1 is again used to compute the gas composition and state in the reservoir.

The flow conditions that can be reached by an equilibrium expansion from a specified reservoir condition form a one-parameter family of states. In NATA, the gas temperature is taken to be the independent variable. A sequence of equilibrium flow states is generated by decrementing the temperature, starting from the reservoir value. At each temperature, the species mole fractions and the static pressure are determined from a thermochemical equilibrium calculation with the supplementary condition that the gas specific entropy s be equal to its value s_0 in the reservoir. The conditions for thermochemical equilibrium are equations (224) and (227). The specific entropy may be obtained by dividing the molar entropy (30b) by the local molecular weight W:

$$s = \frac{1}{W}\left\{\sum_{j=1}^{n} X_j S_j^o - R_0 \ell n\, p - R_0 \sum_{j=1}^{n} X_j \ell n\, X_j\right\} \tag{251}$$

Thus, the condition $s = s_0$ can be written, with the aid of (236), in the form

$$F_{c+1} \equiv \sum_{j=1}^{n} X_j \left[\frac{S_j^o}{R_0} - \frac{s_0 W_j}{R_0} - \ell n\, X_j\right] - \ell n\, p = 0 \tag{252}$$

in which X_j is the mole fraction of the j^{th} species, W_j the species molecular weight, S_j^o the species molar entropy at standard pressure, and R_0 the universal gas constant. Equations (227) and (252) constitute a system of $c + 1$ equations to be solved for the equilibrium mole fractions and the static pressure p at the specified temperature and specific entropy. As in Section 6.1, these equations are solved by the Newton-Raphson method. The solution is carried out by subroutine NEWRAP. The additional derivatives required by incorporation of the additional equation (252) and the additional unknown p are as follows, for $j = 1, \ldots, c$ and $m = 1, \ldots, c$:

$$\frac{\partial F_j}{\partial p} = -\sum_{i=c+1}^{n} \left[\bar{\nu}_{i-c,j} - q_j\,(\nu^*_{i-c} - 1)\right] \frac{X_i}{p}\,(\nu^*_{i-c} - 1) \tag{253}$$

$$\frac{\partial F_{c+1}}{\partial X_m} = \frac{S_m^o}{R_0} - \frac{s_0 W_m}{R_0} - \ell n\, X_m - 1$$

$$+ \sum_{i=c+1}^{n} \frac{X_i}{X_m}\left[\frac{S_i^o}{R_0} - \frac{s_0 W_i}{R_0} - \ell n\, X_i - 1\right] \bar{\nu}_{i-c,m} \tag{254}$$

$$\frac{\partial F_{c+1}}{\partial p} = \frac{1}{p}\left\{-1 + \sum_{i=c+1}^{n} X_i \left[\frac{S_i^o}{R_0} - \frac{s_0 W_i}{R_0} - \ell n\, X_i - 1\right](\nu^*_{i-c} - 1)\right\} \tag{255}$$

Equation (253) is derived by differentiating equation (227) with respect to the pressure, p . For the independent species (j) ,

$$\frac{\partial X_j}{\partial p} = 0 \tag{256}$$

since the mole fractions X_j (j = 1, ..., c) and the pressure p are all independent variables. For the dependent species (i) , from (224),

$$\frac{\partial X_i}{\partial p} = (\nu^*_{i-c} - 1) \frac{X_i}{p} \tag{257}$$

Equation (254) is obtained by differentiating (252) with respect to the mole fraction X_m of an independent species, and using equations (230) and (231). Equation (255) results from differentiation of (252) with respect to p , when (256) and (257) are taken into account.

The system of Newton-Raphson equations for the state of the gas at a point in an equilibrium flow may be written

$$-\sum_{m=1}^{c+1} Y_m{}^r \left(\frac{\partial F_j}{\partial Y_m}\right)^r h_m{}^r = F_j(Y_k{}^r) \tag{258}$$

where j and k run from 1 to c + 1 ,

$$Y_m{}^r = X_m{}^r \qquad (m = 1, \ldots, c) \tag{259a}$$

$$Y_{c+1}{}^r = p^r \tag{259b}$$

and

$$h_m{}^r \equiv \frac{Y_m{}^{r+1} - Y_m{}^r}{Y_m{}^r} \tag{260}$$

For m = 1 to c and j = 1 to c, the matrix of coefficients in (258) is given by (233b). For m = c + 1 and j = 1 to c ,

$$-Y_{c+1}{}^r \left(\frac{\partial F_j}{\partial Y_{c+1}}\right)^r = \sum_{i=c+1}^{n} \left[\bar{\nu}_{i-c,j} - q_j (\nu^*_{i-c} - 1)\right] X_i (\nu^*_{i-c} - 1) \tag{261a}$$

For $m = 1$ to c and $j = c + 1$, from (254),

$$-Y_m^r \left(\frac{\partial F_{c+1}}{\partial Y_m}\right)^r = Y_m^r \left(1 - \frac{S_m^o}{R_0} + \frac{s_0 W_m}{R_0} + \ell n\ Y_m^r\right)$$

$$+ \sum_{i=c+1}^{n} X_i \left(1 - \frac{S_i^o}{R_0} + \frac{s_0 W_i}{R_0} + \ell n\ X_i\right) \bar{\nu}_{i-c,m} \qquad (261b)$$

Finally, for $m = c + 1$ and $j = c + 1$, from (255),

$$-Y_{c+1}^r \left(\frac{\partial F_{c+1}}{\partial Y_{c+1}}\right)^r = 1 + \sum_{i=c+1}^{n} X_i \left(1 - \frac{S_i^o}{R_0} + \frac{s_0 W_i}{R_0} + \ell n\ X_i\right)(\nu^*_{i-c} - 1) \qquad (261c)$$

At each stage of the Newton-Raphson iteration, the system of $c + 1$ linear equations (258) is solved for the relative corrections h_m^r by calling subroutine DSMSØL. The improved estimates for the independent species mole fractions X_n and the pressure are then obtained from

$$Y_m^{r+1} = Y_m^r\ (1 + h_m^r) \qquad (m = 1, \ldots, c + 1) \qquad (262)$$

The iteration is continued until all of the h_m^r are smaller than or equal to 10^{-6}.

Once the equilibrium mole fractions and the static pressure have thus been determined, the molecular weight, density, and specific enthalpy are computed from equations (236), (237), and (242). The density and enthalpy are corrected for effects of gas imperfections using equations (79b) and (81). The flow velocity is then determined from equation (245):

$$u = \sqrt{2(h_0 - h)} \qquad (263)$$

and the mass flux

$$m = \rho u \qquad (264)$$

is computed.

Up to this point, the calculations have proceeded without reference to the nozzle geometry or to the location in the nozzle at which the computed flow conditions occur. The flow conditions are related to the nozzle geometry only through the continuity equation (243). This equation can be solved for the area ratio A_e:

$$A_e \equiv \frac{A'_e}{A'_{e_*}} = \frac{\rho_*\ u_*}{\rho u} \equiv \frac{m_*}{m} \qquad (265)$$

Thus, if the sonic mass flux $m_* = \rho_* u_*$ is known, the area ratio can be calculated from the local mass flux (264). The location of the flow point within the nozzle can then be determined by inverting the area ratio relation $A_e = f(x)$, based on the nozzle or channel geometry (Section 4), to obtain the axial position x corresponding to the calculated area ratio.

Since the area ratio A_e has a minimum at the sonic point, the sonic mass flux m_* is the maximum mass flux occurring anywhere in the flow. It is determined from a preliminary calculation (performed in subroutine NRMAX), before the main equilibrium flow solution. In NRMAX, the temperature is repeatedly decremented, and the equilibrium mass flux is computed at each stage, until m passes its maximum value. An iteration is then carried out to determine the temperature and other flow conditions corresponding to the maximum mass flux. The resulting m_* value is then used in the determination of the area ratio from (265) during the main equilibrium flow solution.

6.3 Boundary Layer Effects

Inviscid flow is, of course, only an idealization of the behavior of real gases. In an actual wind tunnel, there is a boundary layer on the nozzle wall, within which viscous stresses and heat transfer are important. Upstream of the throat and in the throat region, this boundary layer is thin and has small (but not negligible) effects upon the free stream flow. Downstream, in the region of high Mach number and low density, the boundary layer thickness can become comparable with the nozzle radius or the gap between channel faces. In such cases, the effects of the boundary layer upon the free-stream flow can become quite important.

Depending on the flow conditions, the boundary layer can be either laminar or turbulent. Within the operating envelopes of existing NASA/JSC arc-heated wind tunnels, the layer is usually laminar. NATA contains an approximate calculation of laminar boundary layer development on the nozzle wall, based on the Cohen-Reshotko integral method (Section 5). The boundary layer properties, including the displacement thickness δ^*, are computed step-by-step, beginning at an upstream starting point, along with the inviscid flow solution. The displacement thickness alters the effective geometry of the nozzle or channel.* If it is positive, it reduces the effective cross sectional area of the flow. If it is negative, as it normally is upstream and in the throat region, it increases the effective area.

Relations between the effective area ratio (allowing for the displacement thickness) and the geometric area ratio have been given in Section 4. These relations involve the displacement thickness δ^*_* at the nozzle throat. This quantity is not known until the inviscid flow solution and the boundary layer calculation have reached the throat. Thus, the solution in the region upstream of the throat must be generated without accurate knowledge of the relation between the effective and geometric area ratios in this region. Several different techniques for circumventing this difficulty have been tried during the

*In the case of a channel, the flow is confined by two pairs of walls with different geometry. In this case, NATA performs two separate boundary layer calculations, and there are two displacement thicknesses at each flow point.

development of NATA. Most of these techniques involved the use of an approximate value for the displacement thickness at the throat, based upon some type of preliminary solution up to the throat. Techniques of this type involved relatively complex programming and, in some cases, led to unreliable code operation in the throat region, where the solution is extremely sensitive to small errors in the area ratio.

The technique used in the current version of NATA is simple and reliable, and gives results of acceptable accuracy. Upstream of the throat, the relation between the effective area ratio and the axial coordinate x is approximated by neglecting the difference between the effective and geometric area ratios in this region. Since the boundary layer is thin in comparison with the nozzle diameter upstream and near the throat, this approximation is equivalent to a small change in the nozzle shape in the upstream region. Such a change has little effect on the displacement thickness at the throat. Downstream of the throat, in the region where the boundary layer thickness can become large, the relation between the geometric and effective area ratios is calculated using the local displacement thickness, so that the boundary layer and the inviscid flow are coupled.

The effect of the displacement thickness upon calculations of reservoir conditions from the total mass flow using sonic flow analysis is discussed below, in Section 6.5. This effect is not negligible, and is taken into account by an iteration.

The preceding discussion of boundary layer effects is phrased in general terms, and is applicable to all three types of flow solution. In the specific case of equilibrium free-stream flow, the solution including boundary layer effects is generated in the following way:

(1) As in the purely inviscid case discussed in Section 6.2, the gas temperature is taken as the independent flow variable. The temperature is repeatedly decremented, starting from the reservoir, and at each stage the composition, thermodynamic properties, and flow velocity are determined by a Newton-Raphson solution of equations (227) and (252).

(2) Upstream of the throat (i.e., for temperatures above the sonic temperature T_*), the axial coordinate corresponding to each flow point is determined from equation (265) by assuming that the effective area ratio A_e is equal to the geometric area ratio A_g. That is, x is determined by solving the equation

$$A_g(x) \simeq A_e = \frac{m_*}{m} \tag{266}$$

with the aid of subroutine FINDX.

(3) For each flow point, after x has thus been determined, the boundary layer calculation for the point is carried out as described in Section 5.

(4) This procedure is continued until the throat ($x = 0$) is reached. The displacement thickness at the throat (δ_*^*) is thus determined approximately.

(5) Beyond the throat, the flow conditions are again determined by decrementing the temperature and solving equations (227) and (252), but the geometric area ratio A_g is obtained from equation (127), (131), or (135), depending on the type of nozzle geometry. The axial coordinate x is then determined by inverting the geometric area ratio relation $A_g(x)$ for the nozzle or channel. These operations are performed in subroutine AGSØLN. Since the formulas relating A_g and A_e involve the displacement thickness δ^*, and since δ^* is obtained from the boundary layer calculation which requires the coordinate x, the computation of A_g is based on the effective area ratio A_e for the current flow point and the displacement thickness δ^* at the preceding flow point. After the boundary layer calculation for the flow point has been performed, subroutine AGSØLN is called again with the effective area ratio and displacement thickness for the current flow point. The resulting improved value of x is the one printed by the code. The error resulting from use of this approximation is small so long as the change in δ^* in one step of the flow calculation is sufficiently small in comparison with the nozzle diameter.

6.4 Frozen Flow

Equilibrium flow is the limiting case of the flow of a reacting gas mixture in which the reaction rates are infinitely high. Frozen flow is the opposite limit, in which the reaction rates are zero. Thus, in frozen flow, the species mole fractions are assumed to be constant and equal to their values in the upstream reservoir.

As in the case of equilibrium flow, the frozen flow solution is generated in NATA by decrementing the temperature, starting from the reservoir value. At each temperature, the flow conditions are computed as follows: The enthalpy is computed from (242). The static pressure is determined from the condition that the flow be isentropic; from (251), this condition can be formulated

$$p = \exp\left\{ \frac{1}{R_0} \sum_{j=1}^{n} X_j \hat{S}_j^{\circ} - \sum_{j=1}^{n} X_j \ell n\, X_j - \frac{s_0 W_0}{R_0} \right\} \tag{267}$$

in which s_0 denotes the specific entropy in the reservoir and W_0 the molecular weight, which is everywhere equal to the reservoir value since the flow is frozen. Once the pressure is known, the perfect-gas density can be calculated from (237). For a frozen flow, (237) becomes

$$\frac{\rho}{\rho_0} = \frac{p}{p_0} \cdot \frac{T_0}{T} \tag{268}$$

The density is calculated from (268), and the density and enthalpy are then corrected for the effects of gas imperfections using equations (79b) and (81). These calculations are all performed in subroutine PRØP.

As in the equilibrium case, the inviscid flow conditions are all computed without reference to the nozzle geometry. The sonic mass flux for frozen flow is determined by a preliminary calculation, performed before the main frozen flow solution, in which the temperature is adjusted repeatedly to find the value corresponding to the maximum mass flux. During the main frozen solution, at each temperature, the flow conditions are computed as described above and the effective area ratio A_e is then calculated from the continuity equation in the form (265). The location in the nozzle at which the calculated flow conditions occur is then determined from the effective area ratio. If a solution neglecting the boundary layer is being generated, the geometric area ratio A_g is equal to A_e, and the axial coordinate x is obtained by inverting the area ratio relation $A_g = A_g(x)$ for the nozzle. If the solution includes boundary layer effects, the technique for determining x from A_e and the displacement thickness δ^* is exactly the same as in the case of the equilibrium solution, described in Section 6.3.

6.5 Determination of Reservoir Conditions

NATA provides three options for input specification of the reservoir conditions. In all three cases, it is assumed that the gas in the reservoir is in thermochemical equilibrium. In the first option, the code user specifies the reservoir temperature and pressure directly. The composition and thermodynamic properties of the gas in the reservoir are then computed as described in Section 6.1.

In the second option, the input quantities are the reservoir pressure and the total mass flow. The rationale supporting this choice of parameters is that the total mass flow is much easier to measure than the reservoir temperature. A meaningful reservoir pressure measurement can also be obtained easily in wind tunnels equipped with a plenum chamber within which a condition of flow stagnation is approximated. In this second option, the reservoir temperature is determined, by an iteration, based on the condition that the product of the effective throat area and the equilibrium sonic mass flux be equal to the input total mass flow. For each successive trial value of the reservoir temperature, the equilibrium reservoir conditions are calculated as explained in Section 6.1, and the equilibrium sonic mass flux m_* is then computed as described in Section 6.2. If boundary layer effects are to be neglected in the flow solution, the effective throat area is equal to the known geometric cross section of the nozzle at the throat. If boundary layer effects are to be included, the effective throat area involves the displacement thickness at the throat, as shown in equations (125), (129), and (133). In this case, the reservoir temperature is determined initially neglecting boundary layer effects. A preliminary equilibrium flow solution from the reservoir to the throat is then computed to determine an approximation to the displacement thickness at the throat. The calculation of the reservoir temperature is then repeated, using an effective throat area which includes the effect of the boundary layer displacement thickness. The main flow solutions for frozen, equilibrium, and non-equilibrium flow are then carried out assuming this revised reservoir temperature.

The third option for specifying the reservoir conditions is based on input of the total mass flow and the stagnation enthalpy. The enthalpy can be determined from energy-balance data, and is a more meaningful piece of information than the upstream pressure in wind tunnel configurations lacking a stagnation region between the arc heater and the throat, especially if the upstream flow is highly rotational. When this option is used, NATA determines the stagnation temperature and pressure in a fictitious upstream reservoir by a double iteration, based on the conditions that the reservoir enthalpy be equal to the input stagnation enthalpy, and that the product of the effective throat area and the equilibrium sonic mass flux be equal to the input total mass flow. If boundary layer effects are to be included in the flow solution, a preliminary calculation to determine the displacement thickness at the throat is performed prior to the main flow solutions, as in the second option.

In the second and third options, the determination of the reservoir conditions is based in part on calculations of equilibrium flow from the reservoir to the throat, regardless of whether the main flow solutions to be generated are to be equilibrium, frozen, non-equilibrium, or some combination of these. The rationale for this procedure may be outlined as follows:

(1) When two or three different types of flow solution are computed for the same problem, the user's purpose is to assess the importance of the reactions by comparing solutions based on infinite, finite, and zero reaction rates. Such an assessment would be obscured if the different types of solution started from different reservoir conditions, as they would if separate reservoir calculations were performed for frozen, non-equilibrium, and equilibrium flow.

(2) The equilibrium-flow reservoir calculations for the second and third options already consume a significant amount of computer time, ranging from a few seconds to over a minute per case, depending on the gas model and the option. Similar calculations assuming non-equilibrium flow would use a great deal more time, especially since the non-equilibrium solution is often forced, by stability requirements, to take very small steps in the upstream region.

(3) In most of the cases to which NATA is applied, the non-equilibrium solution (which simulates the actual flow most closely) is approximated reasonably well by the equilibrium solution in the region upstream of the throat, because the flow starts from an equilibrium state in the reservoir and the pressure remains fairly high until the throat has been passed.

The reservoir condition calculations for the second and third options are controlled by subroutine RESTMP.

7. NON-EQUILIBRIUM FLOW

The chemical reaction rates in a real, high-temperature gas mixture are finite. Thus, equilibrium and frozen flow are only limiting cases, which under some circumstances may approximate the flow in portions of the nozzle. The actual flow in an arc-heated wind tunnel is a non-equilibrium expansion. The present section explains how non-equilibrium flow is calculated in the NATA code.* Section 7.1 presents the flow relations and reaction rate equations which are assumed to govern the flow, both for the normal case of chemical non-equilibrium and for the case in which the free electrons and bound electronic excited states are also assumed to be out of equilibrium with the heavy species. Section 7.2 outlines the overall method of solution used in NATA. Special techniques used to calculate portions of the non-equilibrium flow are then described and analyzed in Sections 7.3 to 7.5. These techniques are an inverse method used in the upstream region, a perturbation method used to start the solution in the region just downstream of the reservoir, where the flow is still nearly in equilibrium, and the numerical integration method used to compute the flow farther downstream, where some of the reactions are appreciably out of equilibrium. Finally, Section 7.6 explains how the non-equilibrium inviscid flow is coupled with the boundary layer on the nozzle or channel wall.

7.1 Governing Equations

The NATA code contains two different treatments of non-equilibrium flow. The first is a conventional single-temperature model in which, at each station in the nozzle, the kinetic translational temperatures and the excitation temperatures of all species are assumed equal. In this model, only the species concentrations are allowed to depart from equilibrium. The compiled-in air models and planetary atmosphere models are of this type. For brevity, these may be referred to as chemical non-equilibrium models.

The second type of non-equilibrium treatment implemented in NATA is a two-temperature model. In this case, in addition to non-equilibrium of the species concentrations, the electronic degrees of freedom are assumed to be out of equilibrium with the translational and vibrational motions of the atoms, ions, and molecules. The velocity distributions of these heavy particles are assumed to be Maxwellian at a temperature T, while the translational temperature of the free electrons is allowed to have a different value, T_e. The electronic excited states of some chemical species are treated as separate physical species, so that the populations of these states need not be in equilibrium at either of the temperatures, T or T_e. The governing equations include terms representing energy transfer between the electrons and heavy particles. In addition, radiative losses from the plasma are taken into account. The compiled-in models for helium and argon are of this type. Such models will be referred to as electronic non-equilibrium models.

The first part of this section presents and discusses the governing equations for the chemical non-equilibrium models. The second part deals with the electronic non-equilibrium models. Part 3 explains the technique used to maintain the elemental composition of the gas mixture.

*Available techniques for analyzing non-equilibrium nozzle flows have been reviewed by Bray (ref. 31) and by Hall and Treanor (ref. 32).

7.1.1 Chemical Non-equilibrium

The gas flowing through the nozzle is assumed to consist of n chemical species which can undergo r chemical reactions. The reactions can be represented in the form

$$\sum_{j=1}^{n} \nu_{ij} M_j \underset{k_{ri}}{\overset{k_{fi}}{\rightleftharpoons}} \sum_{k=1}^{n} \nu'_{ik} M_k \tag{269}$$

In this formula, the M_j symbols represent the chemical species, and the matrices ν_{ij} , ν'_{ik} are the stoichiometric coefficients. The forward and reverse reaction rate constants are denoted by k_{fi} , k_{ri} , respectively. The gas is assumed to obey the equations of steady, one-dimensional, adiabatic inviscid flow, namely equations (243) through (245). These equations may be written in differential form as

$$\frac{d\,\ell n\,\rho}{dx} + \frac{d\,\ell n\,u}{dx} + \frac{d\,\ell n\,A'_e}{dx} = 0 \tag{270}$$

$$u\frac{du}{dx} + \frac{1}{\rho}\frac{dp}{dx} = 0 \tag{271}$$

$$\frac{dh}{dx} + u\frac{du}{dx} = 0 \tag{272}$$

Equations (270) to (272) are the continuity, momentum, and energy equations, respectively. The gas mixture is assumed to be ideal, so that the equation of state is

$$p = \frac{\rho R_0 T}{W} \tag{273}$$

in which the molecular weight W is given by equation (236):

$$W = \sum_{j=1}^{n} X_j W_j \tag{274}$$

in terms of the mole fractions X_j and molecular weights W_j of the individual species. Also, the specific enthalpy h is given by

$$h = \frac{1}{W}\sum_{j=1}^{n} X_j H_j = \sum_{j=1}^{n} \gamma_j H_j \tag{275}$$

where H_j is the molar enthalpy of the j^{th} species, a function of temperature.

Inspection of equations (270) through (275) reveals the presence of $n+6$ dependent variables: ρ, u, p, h, T, W, and X_j for $j = 1$ to n. (The flow area A'_e is assumed, for now, to be a known function, $A'_e(x)$ of the position coordinate x.) Since there are just six equations, it may be seen that n additional relations are required, to yield a determinate system. The required additional relations are the rate equations specifying the changes in the species mole fractions, X_j, or concentrations, γ_j. According to equation (61), the net rate of change of the molar concentration $[M_j]$ of species j due to the i^{th} reaction is

$$\left\{\frac{d[M_j]}{dt}\right\}_i = (\nu'_{ij} - \nu_{ij}) \left\{ k_{fi} \prod_{k=1}^{n} [M_k]^{\nu_{ik}} - k_{ri} \prod_{k=1}^{n} [M_k]^{\nu'_{ik}} \right\} \tag{276}$$

In this equation, $[M_k]$ has units of moles/cm^3. The forward and reverse rate constants, k_{fi} and k_{ri}, are assumed to be connected by the detailed balancing relation (62),

$$k_{ri} = \frac{k_{fi}}{K_i} \tag{277}$$

in which the equilibrium constant K_i is given by equation (68):

$$K_i = \frac{1}{(R_0 T)^{\beta_i}} \exp\left\{ - \frac{1}{R_0 T} \sum_{j=1}^{n} \beta_{ij} \mu_j^o \right\} \tag{278}$$

Here

$$\beta_{ij} \equiv \nu'_{ij} - \nu_{ij} \tag{279}$$

$$\beta_i \equiv \sum_{j=1}^{n} \beta_{ij} \tag{280}$$

Some manipulation is required to bring equation (276) into a form suitable for use in the non-equilibrium flow calculations. First, in the NATA non-equilibrium solution, the amounts of the species are expressed in terms of the specific molar concentrations γ_j, which are related to the mole fractions by equation (1) and which have units of moles per gram of mixture. The volume concentrations $[M_j]$ are related to the γ_j by

$$[M_j] = \rho \gamma_j \tag{281}$$

in which ρ is the gas density. Second, since NATA deals with steady flows, the time derivative in (276) must be converted into a space derivative using

$$\frac{d}{dt} = u \frac{d}{dx} \tag{282}$$

Substitution of equations (279), (281) and (282) into (276) gives

$$\rho u \left\{\frac{d\gamma_j}{dx}\right\}_i = \beta_{ij} \left\{ k_{fi} \rho^{\nu_i} \prod_{k=1}^{n} \gamma_k^{\nu_{ik}} - k_{ri} \rho^{\nu'_i} \prod_{k=1}^{n} \gamma_k^{\nu'_{ik}} \right\} \tag{283}$$

in which

$$\nu_i = \sum_{j=1}^{n} \nu_{ij} \tag{284a}$$

$$\nu'_i = \sum_{j=1}^{n} \nu'_{ij} \tag{284b}$$

Equation (276) gives only the changes in $[M_j]$ due to the chemical reaction, not those resulting from changes in the volume of the gas sample. Thus, the $\{d/dt\}_i$ operator on the left in (276) refers to changes in species concentrations at constant gas density, and it is correct to set

$$\left\{\frac{d}{dt}(\rho\gamma_j)\right\}_i = \rho \left\{\frac{d\gamma_j}{dt}\right\}_i \tag{285}$$

as was done in the derivation of equation (283)*.

The total rate of change of the specific concentration γ_j for the j^{th} species may now be obtained by summing equation (283) over all of the reactions:

$$\rho u \frac{d\gamma_j}{dx} = \sum_{i=1}^{r} \beta_{ij} \left\{ k_{fi} \rho^{\nu_i} \prod_{k=1}^{n} \gamma_k^{\nu_{ik}} - k_{ri} \rho^{\nu'_i} \prod_{k=1}^{n} \gamma_k^{\nu'_{ik}} \right\} \tag{286}$$

*See Section 7.1.2 (below) for a more detailed derivation of (283).

With the aid of the detailed balancing relation (277), equation (286) can be rewritten in the form used in NATA:

$$\frac{d\gamma_j}{dx} = \sum_{i=1}^{r} \beta_{ij} P_i \chi_i \tag{287}$$

where

$$P_i = \frac{\rho^{\nu_i - 1}}{u} k_{fi} \prod_{k=1}^{n} \gamma_k^{\nu_{ik}} \tag{288}$$

$$\chi_i = 1 - \frac{\rho^{\beta_i}}{K_i} \prod_{k=1}^{n} \gamma_k^{\beta_{ik}} \tag{289}$$

The five flow equations (270) to (273) and (275) can be reduced to two by eliminating the derivatives du/dx , dp/dx, and dh/dx. Combination of the continuity equation (270) with the energy equation (272) gives

$$\frac{d \ln \rho}{dx} + \frac{d \ln A'_e}{dx} - \frac{1}{u^2} \frac{dh}{dx} = 0 \tag{290}$$

From (275),

$$\frac{dh}{dx} = \sum_{j=1}^{n} \left[\gamma_j \frac{dH_j}{dx} + H_j \frac{d\gamma_j}{dx} \right] \tag{291}$$

Also, from (31),

$$\frac{dH_j}{dx} = \frac{dH_j}{dT} \frac{dT}{dx} = C_{pj} \frac{dT}{dx} \tag{292}$$

Hence, (290) can be rewritten in the form

$$\sum_{j=1}^{n} \gamma_j C_{pj} \frac{dT}{dx} + H_j \frac{d\gamma_j}{dx} - u^2 \frac{d \ln \rho}{dx} - u^2 \frac{d \ln A'_e}{dx} = 0 \tag{293}$$

Differentiation of the equation of state (273) gives

$$\frac{dp}{dx} = \frac{R_0 T}{W}\frac{dp}{dx} + \frac{R_0 \rho}{W}\frac{dT}{dx} - \frac{\rho R_0 T}{W^2}\frac{dW}{dx} \tag{294}$$

Substitution of (272) and (294) into the momentum equation (271) gives

$$-\frac{dh}{dx} + \frac{R_0 T}{W}\frac{d\ell n \rho}{dx} + \frac{R_0}{W}\frac{dT}{dx} - \frac{R_0 T}{W^2}\frac{dW}{dx} = 0 \tag{295}$$

The quantity dW/dx can be expressed in terms of the concentration gradients $d\gamma_j/dx$ by differentiating the relation

$$\sum_{j=1}^{n} \gamma_j = \frac{1}{W} \tag{296}$$

which can be derived simply by summing equation (1) over the species. Differentiation of (296) gives

$$\sum_{j=1}^{n} \frac{d\gamma_j}{dx} = -\frac{1}{W^2}\frac{dW}{dx} \tag{297}$$

Substitution of (291), (292), (296), and (297) into (295) gives

$$\sum_{j=1}^{n} (R_0 T - H_j)\frac{d\gamma_j}{dx} + \sum_{j=1}^{n} \gamma_j (R_0 - C_{pj})\frac{dT}{dx} + \frac{R_0 T}{W}\frac{d\ell n \rho}{dx} = 0 \tag{298}$$

Addition of equations (293) and (298) gives, finally,

$$\sum_{j=1}^{n}\left[T\frac{d\gamma_j}{dx} + \gamma_j\frac{dT}{dx}\right] + \left(\frac{T}{W} - \frac{u^2}{R_0}\right)\frac{d\ell n \rho}{dx} - \frac{u^2}{R_0}\frac{d\ell n A_e'}{dx} = 0 \tag{299}$$

The basic system of differential equations for the chemical non-equilibrium model is (287), (293), and (299). This is a system of $n+2$ equations for the dependent variables ρ, T, and γ_j for $j = 1$ to n.

In NATA, these equations are expressed in finite difference form and solved numerically. The integration technique is discussed in Section 7.5. At each point x in the flow, the concentration derivatives $d\gamma_j/dx$ are computed from equations (287), and the derivatives dT/dx and $d\ell_n \rho/dx$ are obtained by simultaneous solution of equations (293) and (299). The conditions at a point $x+\Delta x$ are then calculated from the flow variables and their first-order derivatives at x, using a modified Runge-Kutta technique. Once T, ρ, and the γ_j have thus been determined at the new point, the specific enthalpy is computed from (275) and the velocity from the integral form of the energy equation (245). To ensure accurate conservation of mass, the density is recalculated from the flow velocity and the area ratio at the current flow position x, using the continuity equation (265). The molecular weight is then computed from (296), and the pressure from the equation of state (273). Also, the specific entropy is calculated from equation (251), and a Mach number is calculated based on a "speed of sound" given by $[(dp/dx)/(d\rho/dx)]^{1/2}$. From (270) and (271),

$$M = \frac{u}{\sqrt{(dp/dx)/(d\rho/dx)}} = \frac{1}{\sqrt{1 + \dfrac{d\ell_n A'_e/dx}{d\ell_n \rho/dx}}} \qquad (300)$$

The above defined speed of sound is not, in general, the speed of propagation of small disturbances in a relaxing medium (ref. 33).

7.1.2 Electronic Non-equilibrium

Measurements of the electron temperature T_e in ionized nozzle flows generally show that the equilibrium between T_e and the gas temperature breaks down at some point in the expansion. (See ref. 34, for example.) The importance of including this phenomenon in flow calculations depends upon the intended application of the results. Aerodynamic forces and heating are not likely to be much affected by electronic non-equilibrium, but the electron density, the populations of excited states, and the spectrally resolved radiation emitted by the gas all depend sensitively on the electron temperature.

Equations for steady-state, quasi-one-dimensional flow of a plasma with unequal electron and heavy-particle temperatures have been formulated and solved in several previous studies (refs. 35 through 37). Since there appears to be some disagreement in the literature as to the correct form of such equations, the applicable relations are derived here by formulating conditions for mass, momentum, and energy conservation for each species.

Mass Conservation. - Let $\dot{r}_j$ represent the mass of the j^{th} species produced per unit volume per unit time by reactions occurring in the flow. Then the mass conservation equation for species j may be written by considering the mass balance for a small volume element in the flow of thickness Δx. The total mass of the j^{th} gas entering this volume element per unit time through the upstream boundary at $x = x$ is then given by $\rho_j u_j A'_e$ evaluated at x, while the mass leaving the volume through the downstream boundary at $x = x + \Delta x$ is $\rho_j u_j A'_e$ evaluated at $x = x + \Delta x$, where ρ_j is the mass density of the j^{th} species in the gas, u_j is its mean flow velocity, and A'_e is the cross-sectional area of the flow at the given value of x.

Since the net mass of species j leaving the volume element between x and $x + \Delta x$ due to flow through the ends must be just equal to the mass of j produced in the volume element by the source term $\dot{r}_j$, the mass balance for the volume element becomes

$$(\rho_j u_j A'_e)_{x+\Delta x} - (\rho_j u_j A'_e)_x = \int_x^{x+\Delta x} \dot{r}_j A'_e \, dx \tag{301}$$

Taking the limit of equation (301) as $\Delta x \to 0$ yields the mass conservation equation for the j^{th} species in steady quasi-one-dimensional flow,

$$\frac{d}{dx} (\rho_j u_j A'_e) = \dot{r}_j A'_e \tag{302}$$

Momentum Conservation. - To derive the momentum conservation equation for the j^{th} species, consider a test mass of the j^{th} gas which is instantaneously located between the planes x and $x + \Delta x$ and which is moving with the local flow velocity u_j. The total momentum of this gas element is then

$$P = \int_x^{x+\Delta x} \rho_j u_j A'_e \, dx \tag{303}$$

while the force acting on the element is

$$F = (p_j A'_e)_x - (p_j A'_e)_{x+\Delta x} + \int_x^{x+\Delta x} p_j \frac{dA'_e}{dx} dx + \int_x^{x+\Delta x} f_j A'_e \, dx \tag{304}$$

Here, the first two terms on the right hand side of equation (304) are the net pressure force of the j^{th} gas acting across the end planes of the volume element at x and $x + \Delta x$, the third term is the x-component of the force between the nozzle wall and the j^{th} gas and the final term is the total force on the test mass of the j^{th} gas due to interactions with other gaseous species, where f_j represents the total body force per unit volume on the j^{th} gas due to the interactions. Applying the momentum conservation condition $F = dP/dt$ to the test mass then yields the momentum balance for the element as

$$(p_j A'_e)_x - (p_j A'_e)_{x+\Delta x} + \int_x^{x+\Delta x} p_j \frac{d A'_e}{dx} dx + \int_x^{x+\Delta x} f_j A'_e dx \qquad (305)$$

$$= (\rho_j A'_e u_j^2)_{x+\Delta x} - (\rho_j A'_e u_j^2)_x$$

where the right-hand-side of equation (305) follows directly from equation (303), since the limits of integration in (304) are assumed to move with the local flow velocity u_j. Taking the limit of equation (305) as $\Delta x \to 0$ now yields the momentum conservation equation for the j^{th} species in steady, quasi-one-dimensional flow,

$$\frac{d}{dx}(\rho_j u_j^2 A'_e) = - A'_e \frac{dp_j}{dx} + f_j A'_e \qquad (306)$$

Energy Conservation. - Now consider the energy balance for the same test mass of the j^{th} gas discussed in the previous paragraph. Let ϵ_j be the internal energy per unit mass of the j^{th} gas and $\dot{q}_j$ be the total heat energy added to this gas per unit volume per unit time. $\dot{q}_j$ is thus assumed to include all sources of energy addition to the j^{th} gas in the test volume except for the work energy supplied by the partial pressure p_j on the ends of the volume and by the body force f_j. Thus, the energy balance for the test volume may be written as

$$\frac{d}{dt}\int_x^{x+\Delta x} (\epsilon_j + \frac{1}{2} u_j^2) A'_e \rho_j dx$$

$$= \int_x^{x+\Delta x} \dot{q}_j A'_e dx + (p_j A'_e u_j)_x - (p_j A'_e u_j)_{x+\Delta x} + \int_x^{x+\Delta x} f_j A'_e u_j dx \qquad (307)$$

Taking the limit of equation (307) as $\Delta x \to 0$ and rearranging the result slightly yields the energy conservation equation for the j^{th} gas in the form

$$\frac{d}{dx}\left[\rho_j u_j A'_e (h_j + \frac{1}{2} u_j^2)\right] = (\dot{q}_j + f_j u_j) A'_e \qquad (308)$$

where the specific enthalpy h_j of the j^{th} gas is defined by

$$h_j \equiv \epsilon_j + \frac{p_j}{\rho_j} \qquad (309)$$

Equations (302), (306), and (308) are the basic conservation equations which must be satisfied by the individual components of a gas mixture in steady quasi-one-dimensional flow. In general, the flow velocities u_j of the individual species in these equations may be different; however, in the present analysis it is assumed that the flow velocity

$$u_j = u \tag{310}$$

is the same for all species. For the heavy particles this should be a good approximation for pressures at least down to the order of 10^{-4} atmospheres, while for the electrons the condition (310) will be met provided there is no net flow of electrical current in the gas. It is further assumed that

$$\sum_{j=1}^{n} \dot{r}_j = \sum_{j=1}^{n} f_j = 0 \tag{311}$$

so that there is no net production of mass and no net body force on the flow. Then equations (302), (306), and (308) may be summed for all species j in the gas to obtain the usual quasi-one-dimensional conservation equations for the total flow

$$\frac{d}{dx} (\rho u A_e') = 0 \tag{312a}$$

$$\rho u \frac{du}{dx} = - \frac{dp}{dx} \tag{312b}$$

$$\rho u \frac{d}{dx} (h + \frac{1}{2} u^2) = \dot{q} \tag{312c}$$

where

$$\rho \equiv \sum_{j=1}^{n} \rho_j \tag{313a}$$

is the total density of the gas mixture,

$$p \equiv \sum_{j=1}^{n} p_j \tag{313b}$$

is the total pressure,

$$h \equiv \frac{1}{\rho} \sum_{j=1}^{n} \rho_j h_j \tag{313c}$$

is the total enthalpy of the gas mixture per unit mass, and

$$\dot{q} \equiv \sum_{j=1}^{n} \dot{q}_j \tag{313d}$$

is the total energy addition to the flow per unit volume per unit time from external sources. For the present analysis, the only external source term to be considered will be the radiative energy loss from the gas, so that the source term (313d) becomes simply

$$\dot{q} = - \dot{q}_r \tag{314}$$

where $\dot{q}_r$ is the radiated power per unit volume lost from the gas.

For the most general type of one-dimensional flow, the species densities ρ_j, flow velocities u_j, and internal energies ϵ_j would all be independent variables, so that the species mass, momentum, and energy conservation equations (302), (306), and (308) would all be required to obtain the complete flow solution. Because of the assumption (310) made in the present analysis, however, these equations are no longer all independent, so that the body force f_j may be eliminated between the momentum and energy equations (306) and (308) to obtain the single equation

$$\frac{d}{dx} (\rho_j u A'_e \epsilon_j) + p_j \frac{d}{dx} (u A'_e) - \frac{1}{2} u^2 \frac{d}{dx} (\rho_j u A'_e) = \dot{q}_j A'_e \tag{315}$$

for the species internal energy ϵ_j. Further, it will be assumed in the present analysis that the exchange of translational energy among the heavy particles in the gas is sufficiently rapid to maintain thermal equilibrium among them, so that equation (315) is required only for the electrons. Thus, for a gas mixture containing n species, there are $n + 3$ independent flow equations (namely, the n species conservation equations (302), the overall momentum and energy conservation equations (312b) and (312c) for the mixture, and the electron energy equation (315) to determine the n species densities ρ_j, the flow velocity u, and the electron and heavy-particle temperatures T_e and T for the mixture.

For use in the NATA code, it is convenient to express the above flow equations in terms of the species concentrations γ_j in moles/gm, defined by

$$\gamma_j \equiv \frac{\rho_j}{\rho W_j} \tag{316}$$

where W_j is the molecular weight of the j^{th} species and ρ is the total density of the mixture defined by equation (313a). When this notation is introduced into equation (302) and the result simplified by the use of equations (310) and (312a), one obtains the species conservation equations in the form

$$\rho u \frac{d\gamma_j}{dx} = \frac{\dot{r}_j}{W_j} \tag{317}$$

Similarly, the electron energy equation (315) becomes

$$\rho u W_e \left[\frac{d}{dx} (\gamma_e \epsilon_e) - \frac{\rho_e}{W_e \rho^2} \frac{d\rho}{dx} - \frac{1}{2} u^2 \frac{d\gamma_e}{dx} \right] = \dot{q}_e \tag{318}$$

or, introducing the ideal gas equation of state for the electrons and noting that the flow energy term $u^2/2$ will be negligible compared to the random thermal energy ϵ_e for electrons because of their small mass,

$$\rho u \left[\frac{d}{dx} \left(\frac{3}{2} \gamma_e R_0 T_e \right) - \gamma_e R_0 T_e \frac{d \ell n \rho}{dx} \right] = \dot{q}_e \tag{319}$$

where $R_0 = 1.9872$ cal/mole-^oK is the gas constant per mole.

To complete the specification of the problem, it is now necessary to specify the source terms $\dot{r}_j$, $\dot{q}_r$, and $\dot{q}_e$ occurring in equations (312), (317), and (319). In general, these terms may be written as sums of contributions from the individual collisional and radiative processes occurring in the gas. Thus if the i^{th} reaction process occurring in the gas is represented by the chemical formula (269), then the total number of reactions of the type (269) occurring per unit volume of the gas per unit time in the forward and reverse directions will be respectively

$$N_{fi} = N_0 k_{fi} \prod_{j=1}^{n} (\rho \gamma_j)^{\nu_{ij}} \tag{320a}$$

and

$$N_{ri} = N_0 k_{ri} \prod_{j=1}^{n} (\rho \gamma_j)^{\nu'_{ij}} \tag{320b}$$

where $N_0 = 6.0225 \times 10^{23}$ is Avogadro's number and k_{fi} and k_{ri} are respectively the forward and reverse reaction rates for process i in units of $(\text{mole/cm}^3)^{(1-\nu_i)}$ sec^{-1}. The source terms $\dot{r}_j$, $\dot{q}_r$, and $\dot{q}_e$ are then given in terms of the numbers of reactions (320) by

$$\frac{\dot{r}_j}{W_j} = \sum_{i=1}^{r} \beta_{ij} \left(\frac{N_{fi}}{N_0} - \frac{N_{ri}}{N_0} \right) \tag{321a}$$

$$\dot{q}_r = \sum_{i=1}^{r} \left[q_{fi} \frac{N_{fi}}{N_0} - q_{ri} \frac{N_{ri}}{N_0} \right] \tag{321b}$$

$$\dot{q}_e = \sum_{i=1}^{r} \left[\epsilon_{fi} \frac{N_{fi}}{N_0} - \epsilon_{ri} \frac{N_{ri}}{N_0} \right] \tag{321c}$$

where the sum is over all reactions i occurring in the gas, $\beta_{ij} = \nu_{ij} - \nu_{ij}$ is the net number of molecules of species j which are formed in a single reaction of type i in the forward direction, q_{fi} and $-q_{ri}$ are the mean energies lost from the gas by radiation in N_0 reactions of type i in the forward and reverse directions, respectively, and ϵ_{fi} and $-\epsilon_{ri}$ are similarly the mean energies gained by the electron gas in N_0 reactions of type i in the forward and reverse directions. In general, the reaction rates k_{fi} and k_{ri} in equations (320) and the parameters q_{fi}, q_{ri}, ϵ_{fi} and ϵ_{ri} in equations (321) depend on the reaction under consideration and must be evaluated individually for each gas. The rate constants and parameters used in the standard gas models for argon and helium will be documented in Volume II of this final report (The NATA Code - User's Manual).

Substitution of (321a) into (317) gives the species production equation (286) used in the chemical non-equilibrium model. Also, (312a) and (312b) are identical with equations (270) and (271), respectively. The set of governing equations for the electronic nonequilibrium model differs from that for the previously considered chemical non-equilibrium model in the following respects:

(1) The electronic non-equilibrium model contains one additional dependent variable, the electron temperature, T_e.

(2) There is one additional governing equation, the electronic energy equation (319).

(3) The global energy equation (312c) contains the radiative loss term (314) on the right, whereas the corresponding equation (272) in the chemical non-equilibrium model has zero in the right-hand side. Thus, in the electronic non-equilibrium model the total enthalpy decreases in the downstream direction.

(4) The equation of state (273) is replaced by (313b), in which the partial pressure p_j for the j^{th} species is

$$p_j = R_0 N_j T_j \tag{322}$$

Here $N_j = p\gamma_j$ is the number of moles of the j^{th} species per unit volume, and T_j is the translational temperature for the species. Since T_j is assumed to be equal to T for all of the heavy species, equations (313b) and (322) give

$$p = R_0 \rho (\gamma_e T_e + \gamma_h T) \tag{323}$$

in which

$$\gamma_h = \sum_{j=2}^{n} \gamma_j \tag{324}$$

is the total molar concentration of the heavy species.*

For use by the code, the species production equations are rewritten in the form (287). The only modification of these equations in the electronic non-equilibrium model is that the equilibrium constant K_i in the expression (289) for the quantities χ_i may be calculated from the electron temperature T_e instead of the gas temperature T, for some of the reactions. In such cases, K_i is computed from

$$K_i = \frac{1}{(R_0 T_e)^{\beta_i}} \exp\left\{ - \frac{1}{R_0 T_e} \sum_{j=1}^{n} \beta_{ij} \mu_j^{\circ}(T_e) \right\} \tag{325}$$

in place of equation (278).

Elimination of the derivative du/dx of the flow velocity between the continuity and energy equations (312a) and (312c) gives

$$\frac{d\ell n\, \rho}{dx} + \frac{d\, \ell n\, A_e'}{dx} - \frac{1}{u^2}\left[\frac{dh}{dx} + \frac{\dot{q}_r}{\rho u}\right] = 0 \tag{326}$$

when (314) is taken into account. For the electrons, equation (292) is replaced by

$$\frac{dH_e}{dx} = C_{pe} \frac{dT_e}{dx} \tag{327}$$

If (291) is used to eliminate dh/dx from (326), and (292) and (327) are used for the heavy species and the electrons, respectively, there results

$$\gamma_e C_{pe} \frac{dT_e}{dx} + \sum_{j=2}^{n} \gamma_j C_{pj} \frac{dT}{dx} + \sum_{j=1}^{n} H_j \frac{d\gamma_j}{dx} \tag{328}$$

$$+ \frac{\dot{q}_r}{\rho u} - u^2 \frac{d\ell n \rho}{dx} - u^2 \frac{d\, \ell n\, A_e'}{dx} = 0$$

This is the electronic non-equilibrium analog of equation (293).

*Equation (324) is based on the NATA convention that the electrons, if present, are species number 1.

Differentiation of the equation of state in the form (323) gives

$$\frac{dp}{dx} = R_0 \frac{d\rho}{dx} (\gamma_e T_e + \gamma_h T) + R_0 \rho \left(\gamma_e \frac{dT_e}{dx} + \gamma_h \frac{dT}{dx} \right)$$
$$+ R_0 \rho \left(T_e \frac{d\gamma_e}{dx} + T \frac{d\gamma_h}{dx} \right) \tag{329}$$

Substitution of (312c) and (329) into the momentum equation (312b) gives

$$- \frac{dh}{dx} - \frac{\dot{q}_r}{\rho u} + R_0 (\gamma_e T_e + \gamma_h T) \frac{d\ell n \rho}{dx} + R_0 \left(\gamma_e \frac{dT_e}{dx} + \gamma_h \frac{dT}{dx} \right)$$
$$+ R_0 \left(T_e \frac{d\gamma_e}{dx} + T \frac{d\gamma_h}{dx} \right) = 0 \tag{330}$$

Elimination of dh/dx using (291), (292), and (327), followed by addition of (328), gives

$$\gamma_e \frac{dT_e}{dx} + \gamma_h \frac{dT}{dx} + T_e \frac{d\gamma_e}{dx} + T \frac{d\gamma_h}{dx}$$
$$+ \left[\gamma_e T_e + \gamma_h T - \frac{u^2}{R_0} \right] \frac{d\ell n \rho}{dx} - \frac{u^2}{R_0} \frac{d\ell n A'_e}{dx} = 0 \tag{331}$$

which is the electronic non-equilibrium analog of equation (299). The electron energy equation (319) may be rewritten as

$$\frac{3R_0}{2} \left(T_e \frac{d\gamma_e}{dx} + \gamma_e \frac{dT_e}{dx} \right) - \gamma_e R_0 T_e \frac{d\ell n \rho}{dx} - \frac{\dot{q}_e}{\rho u} = 0 \tag{332}$$

The total enthalpy, $h_0 = h + u^2/2$, obeys equations (312c) and (314), i.e.,

$$\frac{dh_0}{dx} = - \frac{\dot{q}_r}{\rho u} \tag{333}$$

To follow the changes in this quantity accurately, NATA treats h_0 as an additional dependent variable in the numerical integration. Thus, there are $n + 3$ dependent variables, T, T_e, h_0, and the γ_j, in the electronic non-equilibrium model. At each point x in the flow, the concentration derivatives $d\gamma_j/dx$ are computed from equations (287), and the derivatives dT/dx, dT_e/dx, and dh_0/dx are obtained by simultaneous solution of equations (328), (331), (332), and (333).* The conditions at the point $x + \Delta x$ are then calculated from the flow variables and their first-order derivatives at x, using the modified Runge-Kutta technique described in Section 7.5. Once T, T_e, H_0, and the γ_j have thus been determined at the new point, the specific enthalpy is computed from (275), which here takes the form

$$h = \gamma_e H_e (T_e) + \sum_{j=2}^{n} \gamma_j H_j (T) \tag{334}$$

*Either $d\ell n\rho/dx$ or $d\ell n A'_e/dx$ is also obtained from the simultaneous solution, but these quantities are not integrated numerically. Section 7.4 discusses the reasons for this procedure.

The flow velocity u is then calculated from

$$u = \sqrt{2\,(h_0 - h)} \tag{335}$$

Either the area A_e or the density ρ is assumed known as a function of x. The other quantity is calculated from the continuity equation (243). The pressure is calculated from the equation of state (323), the entropy from (251), and the Mach number from (300).

7.1.3 Conservation of Chemical Elements

Each of the individual chemical reactions (269) must be "balanced", i.e., must conserve the chemical elements. If this is true, the entire reaction system conserves the elemental composition of the gas mixture, regardless of the rates at which the individual reactions proceed. However, truncation errors in the finite-difference solution of the chemical rate equations lead to small changes in the elemental composition in each integration step. If allowed to accumulate, such errors could become objectionably large. In NATA, such gradual shifts in the elemental composition of the gas are prevented by adjusting the species concentrations after each successful integration step. This adjustment is based on the following relations.

The number of gram-atoms of the j^{th} element per gram of the gas mixture is given by

$$c_j = \sum_{i=1}^{n} \gamma_i \alpha_{ij} = \sum_{i=1}^{n} (\gamma_i)_0 \alpha_{ij} = \text{constant} \tag{336}$$

In this equation, α_{ij} is the number of atoms of the j^{th} element per molecule of the i^{th} species, γ_i is the concentration of the i^{th} species (moles/gm) at the current flow point, and $(\gamma_i)_0$ is the concentration in the upstream reservoir. The equation (336) can be solved to give the concentrations of the independent species in terms of the c_j and the concentrations of the dependent species. (See Section 2.1.) From (336),

$$\sum_{i=1}^{c} \gamma_i \alpha_{ij} = c_j - \sum_{i=c+1}^{n} \gamma_i \alpha_{ij} \tag{337}$$

Multiplication of (337) by the inverse A_{jk} of the square submatrix of α_{ij} with i = 1 to c, followed by summation over j, gives

$$\gamma_k = \sum_{j=1}^{c} c_j A_{jk} - \sum_{i=c+1}^{n} \gamma_i \bar{\nu}_{i-c,k} \tag{338}$$

for $k = 1$ to c, where $\bar{\nu}_{i-c,k}$ is defined by equation (6).

In some earlier versions of NATA, the elemental composition was maintained by recomputing the concentrations γ_k of the independent species, using (338), after every integration step. This procedure proved to be unreliable. If the concentration of one of the independent species is very much smaller than the concentrations of some dependent species containing the same chemical elements, the loss of accuracy on the subtractions indicated in (338) can become so severe that the independent species in question fluctuates wildly or even goes to a negative concentration. To avoid this problem, the present version of the code uses a more elaborate element-conservation algorithm which spreads the corrections over all of the species, more or less in proportion to their concentrations, instead of adjusting only the independent species. The adjustments $\delta\gamma_i$ to the concentrations γ_i' computed in an integration step are selected so as to minimize the sum of squares of the relative adjustments,

$$D = \sum_{i=1}^{n} \left(\frac{\delta\gamma_i}{\gamma_i'} \right)^2 \tag{339}$$

subject to the constraint that equation (338) be satisfied by the adjusted concentrations

$$\gamma_i = \gamma_i' + \delta\gamma_i \tag{340}$$

Prior to the adjustment, the concentrations of the elements have the incorrect values

$$c_j' = \sum_{i=1}^{n} \gamma_i' a_{ij} \tag{341}$$

instead of the correct values c_j based on the gas composition in the reservoir. Thus, before the adjustment

$$\gamma_k' = \sum_{j=1}^{c} c_j' A_{jk} - \sum_{i=c+1}^{n} \gamma_i' \bar{\nu}_{i-c,k} \tag{342}$$

Subtraction of (342) from (338) gives

$$\delta\gamma_k = \sum_{j=1}^{c} \delta c_j \, A_{jk} - \sum_{i=c+1}^{n} \delta\gamma_i \cdot \bar{\nu}_{i-c,k} \tag{343}$$

where

$$\delta c_j \equiv c_j - c_j' \tag{344}$$

Thus, the sum of squares (339) of the relative adjustments can be written in terms of the adjustments for the dependent species:

$$D(\delta\gamma_{c+1}, \ldots, \delta\gamma_n) = \sum_{k=1}^{c} \left(\frac{\delta\gamma_k}{\gamma_k'}\right)^2 + \sum_{i=c+1}^{n} \left(\frac{\delta\gamma_i}{\gamma_i'}\right)^2$$

$$= \sum_{k=1}^{c} \left\{ \frac{\sum_{j=1}^{c} \delta c_j \cdot A_{jk} - \sum_{i=c+1}^{n} \delta\gamma_i \cdot \bar{\nu}_{i-c,k}}{\gamma_k'} \right\}^2 + \sum_{i=c+1}^{n} \left(\frac{\delta\gamma_i}{\gamma_i'}\right)^2$$

The conditions $\partial D/\partial(\delta\gamma_i) = 0$ for minimum D can be written in the form

$$\sum_{m=c+1}^{n} a_{im} \, \delta\gamma_m = b_i \tag{346a}$$

where

$$a_{im} = \delta_{im} + (\gamma_i')^2 \sum_{k=1}^{c} \frac{\bar{\nu}_{i-c,k} \, \bar{\nu}_{\ell-c,k}}{(\gamma_k')^2} \tag{346b}$$

$$b_i = (\gamma_i')^2 \sum_{k=1}^{c} \frac{\bar{\nu}_{i-c,k}}{(\gamma_k')^2} \sum_{j=1}^{c} \delta c_j \cdot A_{jk} \tag{346c}$$

In NATA, the system of linear equation (346) is solved for the adjustments to the concentrations $\delta\gamma_m$ of the dependent species using subroutine DSMSØL. The adjusted concentrations of the independent species are then computed using equation (338). The entire element-conservation calculation is done in double precision to avoid excessive loss of accuracy in the final evaluation of the independent species concentrations using (338).

7.2 Method of Solution

The basic method for calculating the non-equilibrium solution in NATA is numerical integration of the rate equations derived in Section 7.1. However, there are two difficulties which prevent immediate application of this method when the solution is started in the upstream reservoir:

(1) Startup of integration near equilibrium. - The gas in the reservoir is assumed to be in equilibrium, with zero flow gradients. Also, for the kinds of nozzle profiles that are used in NATA, the derivative of the flow area, dA_e'/dx, is finite everywhere; thus, the flow velocity is quite low in the far upstream region of the nozzle, and in consequence the gradients of the flow variables dT/dx , $d\rho/dx$, $d\gamma_j/dx$ are quite small in that region, and the flow is close to equilibrium. For flows which are nearly in equilibrium, the numerical integration procedure is stable only for extremely small step sizes. Thus, it is impracticable to start the integration far upstream in the nozzle.

(2) Flow upstream of the throat. - The gas conditions in the reservoir, together with the nozzle geometry, determine what the mass flow must be. However, the correct mass flow for a given non-equilibrium flow problem is not known when the solution is started. The mass flow for the corresponding equilibrium flow problem is known, but typically differs slightly from the non-equilibrium value. If an attempt were made to compute a non-equilibrium solution by straightforward integration of the rate equations, assuming the equilibrium-flow value of the mass flow, most probably the solution would fail. Either the Mach number would reach unity before the throat was reached, in which case the solution would blow up because of the flow gradients becoming extremely large; or the Mach number at the throat would be less than unity, in which case the transition from subsonic to supersonic flow would be impossible. To obtain a valid solution in this way, an iteration to determine the correct mass flow would be required.* However, repeated numerical integrations of the flow equations from the reservoir to the throat would be extremely time consuming.

These two problems are dealt with, in NATA, using methods which were evolved over a period of several years at Cornell Aeronautical Laboratory (refs. 1, 38). The difficulty in starting the integration near an equilibrium flow condition is avoided by treating the initial portion of the non-equilibrium solution by a perturbation method, in which the unperturbed solution is the infinite-reaction-rate equilibrium flow. This perturbation method is explained in Section 7.3. The problem of calculating the non-equilibrium flow in the region upstream of the throat is handled using an inverse method which is documented in Section 7.4.

*Methods of dealing with this problem are discussed by Bray (ref. 31).

Beyond the throat, and beyond the near-equilibrium region in which the perturbation method is employed, the solution is calculated by direct numerical integration of the rate equations, using the modified Runge-Kutta technique described in Section 7.5.

Figure 24 shows, in flowchart form, how these three methods are combined to generate the entire non-equilibrium solution. The solution is always begun using the perturbation method. In this method, the step from one flow point to the next is taken by decrementing the gas temperature, as in the equilibrium flow solution (Section 6.2). After each step, certain quantities $\delta\chi_i$, which measure the departures of the reactions from equilibrium, are tested. When any one of these quantities reaches a specified size, the perturbation method is abandoned and the numerical integration is started. During the integration, the step from one flow point to the next is taken by incrementing the position coordinate, x. If the solution has not yet reached the "downstream region" (bounded by a point somewhat beyond the throat, at which the flow is already supersonic), the inverse method is used. Once the downstream region has been reached, the solution is generated using the direct method. If the downstream region is reached in the perturbation solution, then the inverse method is never used at all.

7.3 Perturbation Method

The flow in the far upstream portion of the nozzle, where the conditions differ only slightly from those in the reservoir, is nearly in equilibrium. The species concentrations and flow variables can therefore be expressed in the form

$$\gamma_j = \bar{\gamma}_j + \delta\gamma_j \tag{347a}$$

$$T = \bar{T} + \delta T \tag{347b}$$

$$\rho = \bar{\rho} + \delta\rho \tag{347c}$$

in which the barred quantities are values for the equilibrium flow and $\delta\gamma_j$, δT, $\delta\rho$ are small perturbations due to departures from equilibrium.

7.3.1 Perturbation of the Rate Equations

A system of equations for determining the perturbations is needed. Such a set of relations can be derived from the chemical rate equations (287) and the flow equations, as follows. Substitution of (347) into the rate equations (287) gives, to first order,

$$\frac{d\bar{\gamma}_j}{dx} + \frac{d(\delta\gamma_j)}{dx} = \sum_{i=1}^{r} \beta_{ij} \left(\bar{P}_i \bar{\chi}_i + \bar{\chi}_i \, \delta P_i + \bar{P}_i \, \delta\chi_i \right) \tag{348}$$

The bar symbol in $\bar{\chi}_i$, $\bar{P}_i$ denotes that a quantity is to be evaluated using the equilibrium flow values of the dependent variables, γ_j, T, and ρ. Thus, for

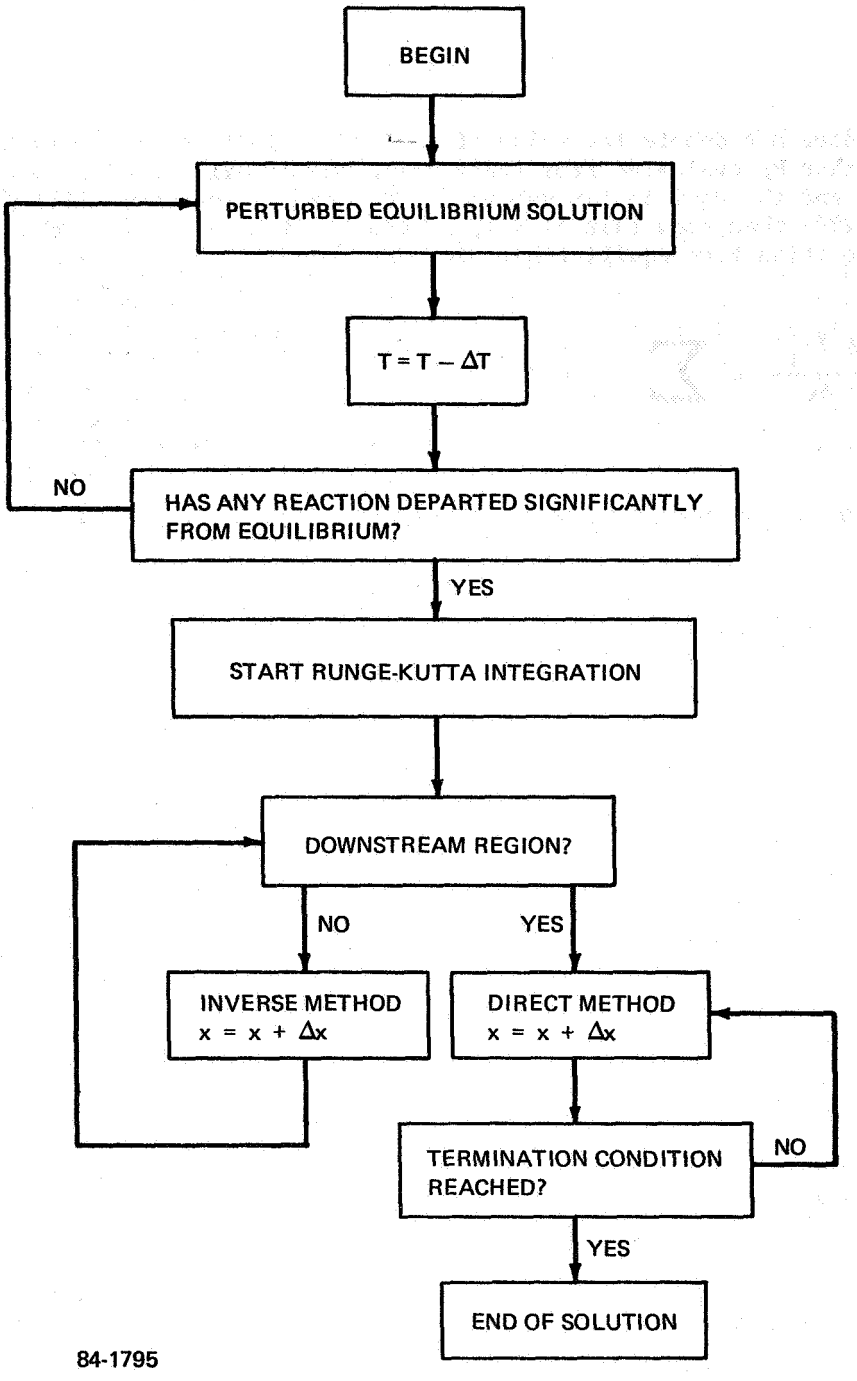

Figure 24 FLOW CHART OF METHODS USED IN THE NON-EQUILIBRIUM SOLUTION

example, $\bar{P}_i$ does not denote the value of P_i for the infinite-rate equilibrium flow, but rather P_i evaluated from (288) using the actual value of the rate constant k_{fi} and the equilibrium values $\bar{\gamma}_j$, $\bar{T}$, and $\bar{\rho}$. Equations (277), (279), (283), and (289) then show that $\bar{\chi}_i = 0$, so that χ_i is a measure of the departure of the i^{th} reaction from equilibrium. Setting $\bar{\chi}_i = 0$ in (348) gives

$$\frac{d\bar{\gamma}_j}{dx} + \frac{d(\delta\gamma_j)}{dx} = \sum_{i=1}^{r} \beta_{ij} \bar{P}_i \delta\chi_i \tag{349}$$

To first order in the perturbations, $\delta\chi_i$ is given by

$$\delta\chi_i = \left(\overline{\frac{\partial\chi_i}{\partial T}}\right) \delta T + \left(\overline{\frac{\partial\chi_i}{\partial \rho}}\right) \delta\rho + \sum_{j=1}^{n} \left(\overline{\frac{\partial\chi_i}{\partial\gamma_j}}\right) \delta\gamma_j \tag{350}$$

Here, $\overline{(\partial\chi_i / \partial T)}$ is the derivative $\partial\chi_i / \partial T$ of (289), evaluated at equilibrium. From (289),

$$\frac{\partial\chi_i}{\partial T} = \frac{\beta_i}{\rho} \prod_{k=1}^{n} \gamma_k^{\beta_{ik}} \frac{dK_i}{dT} \tag{351}$$

At equilibrium, $\bar{\chi}_i = 0$ or

$$\frac{\bar{\rho}^{\beta_i}}{K_i(\bar{T})} \prod_{k=1}^{n} \bar{\gamma}_k^{\beta_{ik}} = 1 \tag{352}$$

Thus, (351) implies that

$$\left(\overline{\frac{\partial\chi_i}{\partial T}}\right) = \frac{1}{K_i(\bar{T})} \left(\overline{\frac{dK_i}{dT}}\right) = \frac{d}{d\bar{T}} [\ell n\, K_i(\bar{T})] \tag{353}$$

From (278),

$$\ell n\, K_i = -\beta_i (\ell n\, R_0 + \ell n\, T) - \frac{1}{R_0 T} \sum_{j=1}^{n} \beta_{ij} \mu_j^o \tag{354}$$

Hence

$$\frac{d\ell n\, K_i}{dT} = -\frac{\beta_i}{T} - \sum_{j=1}^{n} \beta_{ij} \frac{d}{dT}\left(\frac{\mu_j^o}{R_0 T}\right) \tag{355}$$

Now, from equation (25),

$$\frac{d}{dT}\left(\frac{\mu_j^o}{R_0 T}\right) = -\frac{H_j}{R_0 T^2} \tag{356}$$

Therefore, from (280), (353), (355), and (356),

$$\left(\overline{\frac{\partial \chi_i}{\partial T}}\right) = \frac{1}{\bar{T}} \sum_{j=1}^{n} \beta_{ij} \left[\frac{H_j(\bar{T})}{R_0 \bar{T}} - 1\right] \tag{357}$$

Similarly, differentiation of (289) with respect to ρ and γ_j, followed by use of (352), shows that

$$\left(\overline{\frac{\partial \chi_i}{\partial \rho}}\right) = -\frac{\beta_i}{\bar{\rho}} \tag{358}$$

$$\left(\overline{\frac{\partial \chi_i}{\partial \gamma_j}}\right) = -\frac{\beta_{ij}}{\bar{\gamma}_j} \tag{359}$$

Thus, (350) becomes

$$\delta\chi_i = \left\{\frac{1}{\bar{T}} \sum_{j=1}^{n} \beta_{ij} \left[\frac{H_j(\bar{T})}{R_0 \bar{T}} - 1\right]\right\} \delta T - \frac{\beta_i}{\bar{\rho}}\, \delta\rho - \sum_{j=1}^{n} \frac{\beta_{ij}}{\bar{\gamma}_j}\, \delta\gamma_j \tag{360}$$

From (349) and (360), the entire right-hand side of (349) is of first order in the perturbations. Thus, $d\bar{\gamma}_j / dx$ is small of first order, and $d(\delta\gamma_j) / dx$ is therefore of second order and can be neglected to within the accuracy of the perturbation calculation. Equation (349) is therefore rewritten as

$$\frac{d\bar{\gamma}_j}{dx} = \sum_{i=1}^{r} \beta_{ij}\, \bar{P}_i\, \delta\chi_i \tag{361}$$

Substitution of (360) then gives

$$\sum_{i=1}^{r} \beta_{ij} \bar{P}_i \left\{ - \sum_{k=1}^{n} \frac{\beta_{ik}}{\bar{\gamma}_k} \delta\gamma_k + \frac{1}{\bar{T}} \sum_{k=1}^{n} \beta_{ik} \left(\frac{\bar{H}_k}{R_0 \bar{T}} - 1 \right) \delta T - \frac{\beta_i}{\bar{\rho}} \delta\rho \right\} = \frac{d\bar{\gamma}_j}{dx} \tag{362}$$

7.3.2 Equilibrium Derivatives of the Flow Variables

The right-hand side of equation (362), $d\bar{\gamma}_j/dx$, denotes the gradient of the concentration of the j^{th} species in the equilibrium flow. The equilibrium concentration gradients depend upon $d\bar{T}/dx$ and $d\bar{\rho}/dx$. Thus, all of the derivatives $d\bar{\gamma}_j/dx$ for $i = 1$ to n, $d\bar{T}/dx$, and $d\bar{\rho}/dx$ have to be determined. The relations (293) and (299), which are based on the one-dimensional steady flow equations, are valid for the equilibrium flow as well as for the non-equilibrium case. However, the rate equations (287) cannot be used for the equilibrium case because P_i is infinite and χ_i is zero in this case. Thus, for the determination of the derivatives of the flow variables, n relations are needed to replace the n rate equations (287). The relations used for this purpose, in NATA, are the c element-conservation relations (336), which give

$$\sum_{i=1}^{n} a_{ij} \frac{d\bar{\gamma}_i}{dx} = 0 \qquad (j = 1, \ldots, c) \tag{363}$$

and the $n-c$ equations (224) for the equilibrium mole fractions X_j of the dependent species. From equations (1) and (273), equation (224) can be written in terms of the equilibrium molar concentrations $\bar{\gamma}_j$ in place of the mole fractions X_j, in the form

$$\bar{\gamma}_j = K_j \, (\rho R_0 T)^{\nu^*_{j-c} - 1} \prod_{\ell=1}^{c} \bar{\gamma}_\ell^{\,\bar{\nu}_{j-c,\ell}} \tag{364}$$

where K_j is the equilibrium constant (225) for the reaction forming the j^{th} dependent species from the independent species. Logarithmic differentiation of (364) gives

$$\frac{1}{\bar{\gamma}_j}\frac{d\bar{\gamma}_j}{dx} - \sum_{\ell=1}^{c}\frac{\bar{\nu}_{j-c,\ell}}{\bar{\gamma}_\ell}\frac{d\bar{\gamma}_\ell}{dx} - \frac{d\ell_n K_j}{d\bar{T}}\frac{d\bar{T}}{dx}$$

$$-(\nu^*_{j-c}-1)\left[\frac{1}{\bar{\rho}}\frac{d\bar{\rho}}{dx} + \frac{1}{\bar{T}}\frac{d\bar{T}}{dx}\right] = 0 \qquad (365)$$

From (225) and (356),

$$\frac{d\ell_n K_j}{d\bar{T}} = \frac{\bar{H}_j}{R_0\bar{T}^2} - \sum_{\ell=1}^{c}\bar{\nu}_{j-c,\ell}\frac{\bar{H}_\ell}{R_0\bar{T}^2} \qquad (366)$$

With the aid of equations (15) and (366), equation (365) can be rewritten in the form

$$\frac{1}{\bar{\gamma}_j}\frac{d\bar{\gamma}_j}{dx} - \sum_{m=1}^{c}\frac{\bar{\nu}_{j-c,m}}{\bar{\gamma}_m}\frac{d\bar{\gamma}_m}{dx} + \frac{1}{\bar{T}}\frac{d\bar{T}}{dx}\cdot\sum_{m=1}^{c}\bar{\nu}_{j-c,m}\left(\frac{\bar{H}_m}{R_0\bar{T}}-1\right)$$

$$-\frac{1}{\bar{T}}\frac{d\bar{T}}{dx}\left(\frac{\bar{H}_j}{R_0\bar{T}}-1\right) - (\nu^*_{j-c}-1)\cdot\frac{1}{\bar{\rho}}\frac{d\bar{\rho}}{dx} = 0 \quad (\text{for } j = c+1,\ldots,n) \qquad (367)$$

Equations (293), (299), (363), and (367) are $n+2$ linear relations among the $n+2$ derivatives $d\bar{\gamma}_j/dx$, $d\bar{T}/dx$, and $d\bar{\rho}/dx$ for the equilibrium flow. In NATA, this system of equations is solved using subroutine DSMSØL.

7.3.3 Unperturbed Equilibrium Solution

Equations (293) and (299) contain the derivative $d\ell_n A_e/dx$ of the effective nozzle cross sectional area. During the non-equilibrium solution by the perturbation method, this geometric quantity is determined as follows. As in the NATA equilibrium flow solution (Section 6.2), the temperature is the independent variable. Successive points in the solution are generated by decrementing the equilibrium temperature, $\bar{T}$. At each $\bar{T}$, all of the equilibrium flow variables are computed just as in the equilibrium solution, using subroutine NEWRAP. From the equilibrium-flow values $\bar{\rho}$ and $\bar{u}$ of the density and flow velocity, the flow area ratio A_e is calculated using the continuity equation in the form (265). Then the geometric position x of the flow point in the nozzle is determined by solving equation (266) using subroutine FINDX. Finally, $d\ell_n A'_e/dx$ is calculated from the known nozzle geometry and the position x by calling subroutine GEØMAR.*

*Note that $d\ell_n A'_e/dx = d\ell_n A_e/dx$.

7.3.4 Equations Determining the Perturbations

There are $n+2$ perturbations $\delta\gamma_j$, δT, $\delta\rho$ to be determined at each flow point in the perturbation solution. Thus, $n+2$ independent linear algebraic relations among these perturbations are needed. Perturbation of the element conservation equations (336) gives c relations,

$$\sum_{i=1}^{n} a_{ij}\,\delta\gamma_i = 0 \qquad (j = 1, \ldots, c) \tag{368}$$

Equations (362) are an additional n relations involving the $\delta\gamma_i$, but these relations are not all independent. Equations (362) were derived by perturbing the rate equations (287). As pointed out in Section 7.1.3, these rate equations automatically conserve the chemical elements provided the individual reactions (269) are balanced. Thus, the system of $n+c$ equations (362) and (368) contains the same information as the n equations (362) alone. Since the c equations (368) are used*, only $n-c$ of the equations (362) provide independent relations among the $\delta\gamma_j$. The equations (362) with $j = c+1$ to n are the ones used.

Another requirement for solvability of the equations for the $\delta\gamma_j$ is that the reaction system provide independent chemical pathways for the formation and destruction of all the species. If there is no reaction for forming one of the species, then its concentration cannot change and no choice of the $\delta\gamma_j$ will allow the left hand side of (362) to match the equilibrium concentration gradient $d\bar{\gamma}_j/dx$ on the right. If there are reactions involving a particular pair of species, but these reactions do not allow the two species to be formed or destroyed independently, then the species concentrations change in a fixed relationship and it is not possible for the left hand sides of equations (362) to match the independent equilibrium gradients $d\bar{\gamma}_j/dx$ on the right. This requirement on the reaction system can be expressed in quantitative terms by considering the chemical reaction formula (269) in the form

$$\sum_{j=1}^{n} \beta_{ij}\,M_j = 0 \tag{369}$$

which may be obtained by combining (279) with (269). In (369), M_j denotes the j^{th} species and β_{ij} is the number of molecules of this species produced in the i^{th} reaction. Since each individual reaction conserves the chemical elements, the β_{ij} satisfy the c conditions for each reaction

$$\sum_{j=1}^{n} \beta_{ij}\,a_{jk} = 0 \qquad \begin{matrix}(k = 1, \ldots, c)\\ (i = 1, \ldots, r)\end{matrix} \tag{370}$$

*An alternative approach would be to omit equations (368) and use all of the equations (362). The method used in NATA has the advantage that equations (368) involve less computation and ensure accurate element conservation in the perturbation solution.

Equation (370) states that the net number of atoms of the k^{th} element produced in the i^{th} reaction is zero. Because of (370), only $n-c$ of the β_{ij} values defining a given (i^{th}) reaction can be chosen independently; once these have been selected, the remaining values are all determined by conservation of elements. For example, if the β_{ij} for the "dependent species" $j = c + 1$ to n (Section 2.1) are specified, then the β_{ij} for the "independent species" $j = 1$ to c are all determined by element conservation.

Now, if the species M_j are considered to define the directions in an n-dimensional vector space, then the β_{ij} for each i are the components of a vector. The number of linearly independent reactions is then equal to the rank of the β_{ij} matrix (ref. 39). According to (370), the rank of β_{ij} can be no larger than $n-c$, regardless of how many reactions are included in the gas model. The rank can be smaller than $n-c$ if there are too few linearly independent reactions, but in this case the perturbation solution will not work for reasons explained above. Thus, the reaction system is required to contain exactly $n-c$ linearly independent reactions. In NATA, this requirement is applied by computing the rank of β_{ij} using a standard technique (ref. 40). If the rank is found to be less than $n-c$, the case is terminated. Of course, all of the compiled-in gas models satisfy this requirement on the rank of β_{ij}.

Equations (368) together with equations (364) for $j = c + 1$ to n provide n relations among the $n+2$ perturbations $\delta\gamma_j$, δT, $\delta\rho$. Two additional independent relations are required. One such relation may be obtained by perturbing the energy equation in its integral form (245):

$$\delta h + \bar{u}\, \delta u = 0 \tag{371}$$

From (275),

$$\delta h = \sum_{j=1}^{n} \left[H_j(\bar{T})\, \delta\gamma_j + \bar{\gamma}_j \bar{C}_{pj}\, \delta T \right] \tag{372}$$

Perturbation of the continuity equation (243) gives

$$\bar{\rho}\, \delta u + \bar{u}\, \delta\rho = 0 \tag{373}$$

since the reactions do not affect the nozzle geometry. Use of (372) and (373) to eliminate δh and δu from (371) gives

$$\frac{1}{\bar{u}^2} \sum_{j=1}^{n} \left[\bar{H}_j\, \delta\gamma_j + \bar{\gamma}_j\, \bar{C}_{pj}\, \delta T \right] - \frac{\delta\rho}{\bar{\rho}} = 0 \tag{374}$$

7.3.5 The Condition $\delta s = 0$

Equations (362) for $j = c + 1$ to n, equations (368) for $j = 1$ to c, and equation (374) are a system of $n+1$ relations among the $n+2$ perturbations $\delta\gamma_j$, δT, $\delta\rho$. One additional relation is required to give a determinate system. Logically, this relation should be based on the momentum equation (244) or (271), which has not yet been applied to the determination of the perturbations. However, the momentum equation is a differential equation; substitution of (347) into it would give a relation between the derivatives of the perturbations, whereas what is desired is an additional linear algebraic relation between $\delta\gamma_j$, δT, and $\delta\rho$. To obtain such an algebraic relation, Cornell Aeronautical Laboratory (ref. 1) chose to introduce the approximation $\delta\rho \simeq 0$ in the computer program from which NATA has been developed. In other versions of the same program, Cornell Aeronautical Laboratory used the alternative approximation that the perturbation in entropy is negligible,

$$\delta s = 0 \tag{375}$$

which is slightly more accurate (ref. 1). The current version of NATA uses (375) as the required additional relation between the perturbations $\delta\gamma_j$, δT, and $\delta\rho$. Since both the infinite-reaction-rate equilibrium flow and the zero-reaction-rate frozen flow are isentropic (Section 6.2), it is plausible that the finite-reaction-rate non-equilibrium flow should be nearly isentropic in the initial region where the departures from equilibrium are still small. Thus, the perturbation in entropy from the equilibrium flow value, δs, should be small in the region to which the perturbation technique is applicable. This supposition is amply confirmed by the results of integration of the rate equations using NATA. In general, the increase in entropy in non-equilibrium flow solutions is quite small, not only in the initial region but even in the region beyond the throat.

The condition (375) can be expressed as a relation between δT, $\delta\rho$, and the $\delta\gamma_j$ as follows. From equations (1) and (296), the specific entropy (251) of the gas mixture can be written as

$$s = \sum_{j=1}^{n} \gamma_j \left[S_j^o - R_0 \ln (\rho R_0 T) - R_0 \ln \gamma_j \right] \tag{376}$$

To first order, the perturbation δs is given by

$$\delta s = \left(\overline{\frac{\partial s}{\partial T}}\right) \delta T + \left(\overline{\frac{\partial s}{\partial \rho}}\right) \delta\rho + \sum_{j=1}^{n} \left(\overline{\frac{\partial s}{\partial \gamma_j}}\right) \delta\gamma_j \tag{377}$$

From (376),

$$\left(\frac{\overline{\partial s}}{\partial \gamma_j}\right) = S_j^o(\bar{T}) - R_0 \left[1 + \ell n \left(R_0 \bar{\rho} \bar{T} \bar{\gamma}_j\right)\right] \tag{378a}$$

$$\left(\frac{\overline{\partial s}}{\partial T}\right) = \sum_{j=1}^{n} \bar{\gamma}_j \left[\left(\frac{\overline{dS_j^o}}{dT}\right) - \frac{R_0}{\bar{T}}\right] = \frac{1}{\bar{T}} \sum_{j=1}^{n} \bar{\gamma}_j \left[C_{pj}(\bar{T}) - R_0\right] \tag{378b}$$

$$\left(\frac{\overline{\partial s}}{\partial \rho}\right) = -\frac{R_0}{\bar{\rho}} \sum_{j=1}^{n} \bar{\gamma}_j = -\frac{R_0}{\bar{\rho}\bar{W}} \tag{378c}$$

The final form of (378b) is obtained using the relation

$$\frac{dS_j^o}{dT} = \frac{C_{pj}}{T} \tag{379}$$

which can easily be derived from equations (29), (31), and (356), and also follows directly from the thermodynamic definitions of entropy and specific heat. The final form of equation (378c) is obtained using (296). Substitution of (378) into (375) and (377) gives

$$\begin{aligned} \delta s = & \sum_{j=1}^{n} \left\{S_j^o(\bar{T}) - R_0 \left[1 + \ell n \left(R_0 \bar{\rho} \bar{T} \bar{\gamma}_j\right)\right]\right\} \delta\gamma_j \\ & + \frac{1}{\bar{T}} \left\{\sum_{j=1}^{n} \bar{\gamma}_j \left[\bar{C}_{pj} - R_0\right]\right\} \delta T \\ & - \frac{R_0}{\bar{\rho}\bar{W}} \delta\rho = 0 \end{aligned} \tag{380}$$

7.3.6 Conditions for Starting the Numerical Integration

Equations (368) for j = 1 to c, equations (362) for j = c + 1 to n, equation (374), and equation (380) are the n+2 equations which are solved simultaneously for the perturbations $\delta\gamma_j$, δT, $\delta\rho$. These equations are set up in subroutine PERT and solved by calling subroutine DSMSØL. Once these perturbations have thus been determined, $\delta\chi_i$ is computed from equation (360) for each of the reactions. These $\delta\chi_i$ values are used to determine the point in the flow solution at which the perturbation technique is abandoned and the numerical

integration of the chemical rate equations is started. The rule for selecting this point is based on the following considerations:

1) The accuracy of the perturbation calculation decreases with increasing distance down the nozzle, as the perturbations $\delta\gamma_j$, δT, $\delta\rho$ become larger. The numerical integration must be started before the errors become excessively large.

2) Each $\delta\chi_i$ is an approximate measure of the departure of the corresponding reaction from equilibrium, since $\chi_i \simeq \bar{\chi}_i + \delta\chi_i = \delta\chi_i$. When any one of the $\delta\chi_i$ is very small, the numerical integration is stable only for extremely small step size, Δx. Thus, it is desirable to carry out the switchover to numerical integration as far downstream as possible, to avoid having to compute a large number of very small integration steps.

The criterion for switching from perturbation to integration is

$$C_\chi \leq |\delta\chi_i|_{max} \leq 1.2\, C_\chi \tag{381}$$

in which $|\delta\chi_i|_{max}$ is the largest absolute magnitude $|\delta\chi_i|$ for any of the reactions, and C_χ is an input criterion value which is preset to 0.1. If $|\delta\chi_i|_{max}$ turns out to be greater than $1.2\, C_\chi$ at a point in the perturbation solution, a new point is computed for a temperature half way between this point and the preceding one. If necessary, the temperature interval is thus subdivided repeatedly in order to determine a point at which $|\delta\chi_i|_{max}$ satisfies both of the inequalities in (381).

Once a point satisfying the criterion (381) has been found, the perturbations $\delta\gamma_j$, δT, $\delta\rho$ are added to the corresponding equilibrium-flow quantities in accordance with equations (347), and the numerical integration is begun.

Figure 25 illustrates the effect of the switching criterion C_χ on the nonequilibrium solution. Three NATA cases were run for the flow of air through standard nozzle 1, starting from reservoir conditions of 7000° K and 1 atm. In one run, C_χ had its standard value of 0.1; in the other two cases, C_χ values half and twice as large were used. Figure 25 shows the air temperature as a function of position along the nozzle, in the upstream region covered by the perturbation solution and the beginning of the numerical integration. The continuous curve shown in the figure is drawn through points of the perturbation solution. Each trace of unconnected graph symbols represents the results of the numerical integration of the rate equations for one of the cases. The equilibrium and frozen flow solutions are also shown for comparison. The figure shows that increasing C_χ causes the code to begin the integration farther downstream. The differences between the three solutions provide an indication of the errors resulting from use of the perturbation technique. The vertical scale has been greatly expanded in figure 25 to show these small differences clearly. The solution for $C_\chi = 0.05$ is the most accurate, and should lie very close to the correct curve over most of the region shown. At the beginning of the integration for the $C_\chi = 0.1$ case, the temperature as given by the perturbation solution is too low by about 15 degrees or 0.2 percent. For $C_\chi = 0.2$, the corresponding error is 38 degrees or 0.5 percent. After the integration has begun, each solution tends to relax toward the correct solution. For the cases shown in figure 25, at $x = +1.27$ cm the three solutions are separated by differences of about 1 degree out of 3770° K, or 0.03 percent.

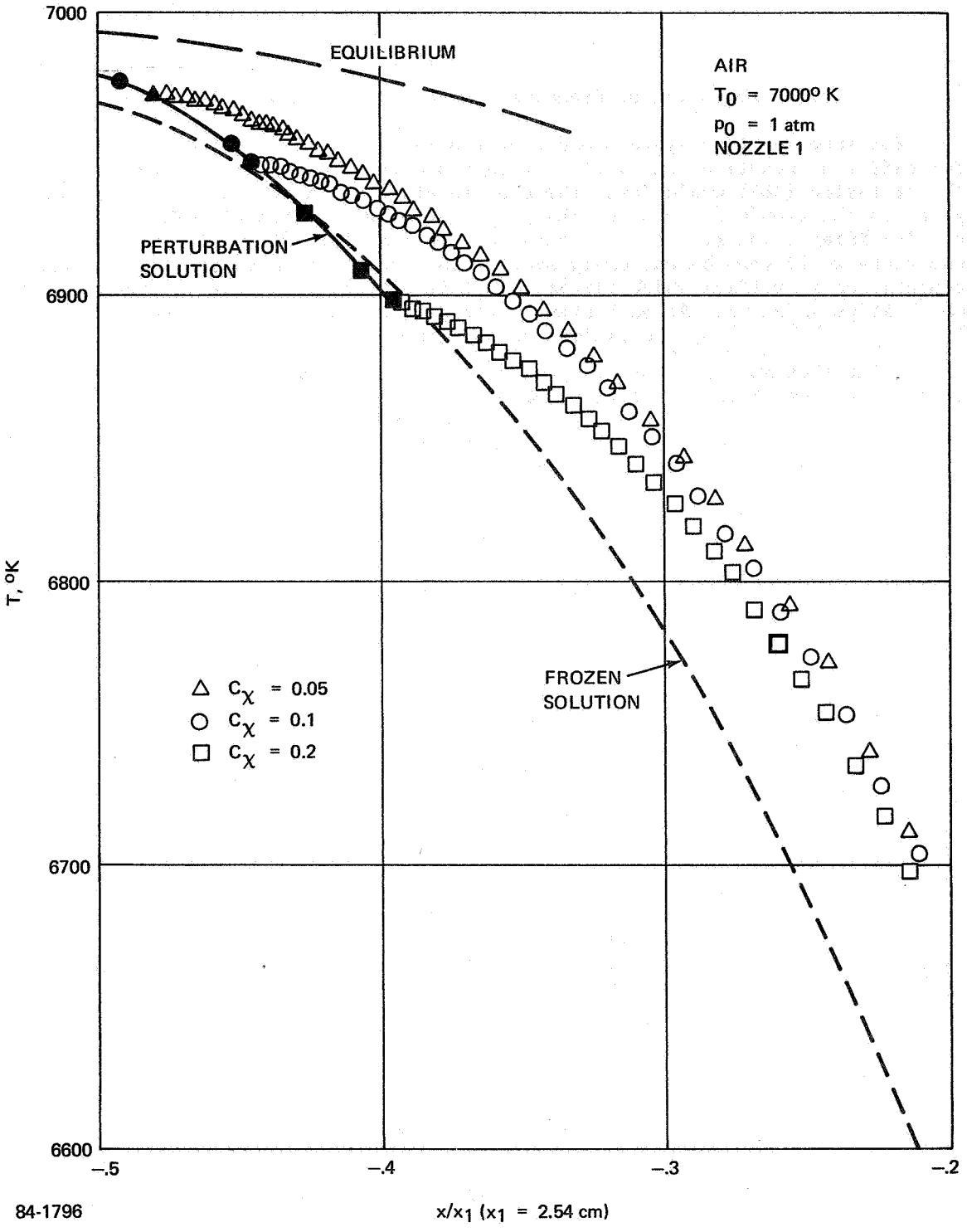

Figure 25 TEMPERATURE VERSUS POSITION IN THE UPSTREAM REGION FOR NON-EQUILIBRIUM SOLUTIONS WITH DIFFERENT C_χ

7.3.7 Prevention of Premature Switch to Numerical Integration

For some reaction systems and some reservoir conditions, the $|\delta\chi_i|$ values for different reactions can differ by many orders of magnitude. When this occurs, the criterion (381) would force the code to start the numerical integration at a point in the flow where some of the $|\delta\chi_i|$ values were extremely small. The resulting integration step size Δx required for stability of the finite difference equations would then be extremely small. The present version of NATA contains a computational artifice which circumvents this difficulty in most of the cases in which it would occur. At each step in the perturbation solution, the ratio $R = |\delta\chi_i|_{min} / |\delta\chi_i|_{max}$ of the minimum and maximum $|\delta\chi_i|$ values is computed. If R is smaller than an input DCHRAT, preset to 10^{-4}, the code applies the following tests to the reaction i_{max} giving the maximum $|\delta\chi_i|$:

1. Does any species j appearing in the reaction have a concentration γ_j which is less than or equal to a value GAMIN (preset to 10^{-10} mole/gm)?

2. Is the reaction running in such a direction as to further reduce the concentration of this species; i.e., is $\beta_{i_{max}\,j}\, P_{i_{max}}\, \chi_{i_{max}} < 0$?

If both of these conditions are satisfied, then the computational artifice is applied. It consists simply of increasing the rate constant for the i_{max}^{th} reaction by a factor of $1.1 \times 10^{-4}/R$ for the duration of the perturbation solution. This increase should make $|\delta\chi_i|_{max}$ equal to about 10^4 times $|\delta\chi_i|_{min}$, which is a ratio allowing normal operation of the code. The justification for this artifice is as follows: First, it cannot affect the overall flow solution significantly, because it simply causes more rapid destruction of a species whose concentration is already negligible. Second, it is efficacious in most cases because the most common cause for an exceptionally high $|\delta\chi_i|$ value is the presence of a species of high formation enthalpy H_0° whose equilibrium concentration is very low because the temperature is relatively low. Under these circumstances the equilibrium constant (225) for formation of the species, which contains a factor $e^{-H_0^\circ / R_0 T}$, is very sensitive to the temperature because the exponent $H_0^\circ / R_0 T$ is large. Thus, the equilibrium flow solution demands a rapid decrease in the species concentration. The inability of the actual reaction rate to follow this rapid equilibrium change is responsible for a large departure of the reaction from equilibrium and thus a large $|\delta\chi_i|$. For example, this situation arises when a gas model including Ar, Ar^+, and the 3-body recombination reaction

$$Ar^+ + e^- + e^- \rightarrow Ar + e^-$$

is used at relatively low temperatures where the equilibrium concentration of Ar^+ is very low and the electron concentration may also be low.

7.3.8 Neglect of Electronic Non-equilibrium Effects

In runs based on gas models including electronic non-equilibrium, the inequality of the electron and gas temperatures and the loss of energy by radiation are neglected in the perturbation solution. These features are "switched on" together with the numerical integration. The neglect of temperature non-equilibrium in the perturbation solution appears to be a reasonable approximation, since the gas is assumed to be nearly in equilibrium in the region where the perturbation

solution is used. The neglect of radiative losses is a poorer approximation, since the radiated power per unit volume is greatest in the high-temperature, high-density region near the reservoir. However, because of geometric approximations used in NATA, inclusion of the radiative losses in the perturbation solution would give radically incorrect results. In the upstream region, for $x \to -\infty$, NATA nozzle profile curvefits open out in conical fashion rather than going to infinite area at a finite distance upstream of the throat. Thus, the reservoir is, in effect, assumed to be an infinite distance upstream. Since the flow velocity is finite everywhere, the transit time of an element of gas from the reservoir to the throat is also infinite. This geometric idealization causes no difficulties in adiabatic flows. However, if the gas were allowed to emit radiation for an infinite time, it would lose all of its energy. Thus, the neglect of radiative losses in the perturbation solution allows the code to simulate the actual flow of a radiating gas which is heated in a region a finite distance upstream of the throat.

7.4 Inverse Method for the Upstream Region

The perturbation method used to start the non-equilibrium solution is based upon the equilibrium solution, and thus assumes the equilibrium-flow value of the sonic mass flux, m_* (Section 6.2). When the numerical integration of the rate equations is started, the initial density ρ, velocity u, and effective area ratio A_e at the switchover point thus have values which are consistent with the equilibrium sonic mass flux: $\rho u A_e = m_*$. If the integration is started downstream of the throat, in the supersonic portion of the flow, it is carried out in a straightforward manner as outlined in Section 7.1. However, if the integration is started upstream of the throat, a straightforward numerical integration of the flow equations would almost certainly fail in the throat region because the sonic mass flux required to allow a smooth passage from subsonic to supersonic flow at the throat would differ slightly from the equilibrium value. To avoid this difficulty, NATA uses an inverse procedure when the integration is started upstream of the throat. This inverse method assumes, on the basis of previous studies (ref. 41), that the non-equilibrium density distribution upstream of the throat and the sonic mass flux differ only slightly from the equilibrium flow values. The $\rho(x)$ and m_* for equilibrium flow are assumed to determine the flow, in place of the specified nozzle geometry. To obtain a smooth representation of $\rho(x)$ with smooth derivatives, an analytical curvefit to $\rho(x)$ is used in place of the data at discrete flow points provided by the NATA equilibrium solution. The form of the curvefit is based on the approximation of isentropic flow of a perfect gas with constant specific-heat ratio, γ. In any standard elementary text on aerodynamics (ref. 42), the following relations are shown to apply to such a flow:

$$\frac{1}{2} u^2 + \frac{\gamma}{\gamma-1} \frac{p}{\rho} = \frac{\gamma}{\gamma-1} \frac{p_0}{\rho_0} \tag{382a}$$

$$\frac{p}{\rho^\gamma} = \frac{p_0}{\rho_0{}^\gamma} \tag{382b}$$

$$\rho u A_e = \rho_* u_* = \text{constant} \tag{382c}$$

$$\frac{\rho_*}{\rho_0} = \left(\frac{2}{\gamma + 1}\right)^{1/(\gamma-1)} \tag{382d}$$

$$u_* = a_* = \sqrt{\frac{2}{\gamma + 1} \cdot \frac{\gamma p_0}{\rho_0}} \tag{382e}$$

where subscript 0 denotes reservoir conditions and * denotes sonic conditions. Elimination of u, p, and u_* from these four equations gives a relation between the density and the effective area ratio:

$$\left(\frac{\rho}{\rho_0} A_e\right)^2 \left[1 - \left(\frac{\rho}{\rho_0}\right)^{\alpha}\right] = C \tag{383}$$

where

$$\alpha = \gamma - 1 \tag{384a}$$

$$C = \frac{\gamma - 1}{2} \left(\frac{2}{\gamma + 1}\right)^{(\gamma+1)/(\gamma-1)} \tag{384b}$$

The value of α is determined from equations (382d) and (384a), which give

$$(\alpha + 2)\left(\frac{\rho_*}{\rho_0}\right)^{\alpha} = 2 \tag{385}$$

The ratio ρ_*/ρ_0 is known from the equilibrium solution. Equation (385) is solved for α using the Newton-Raphson method. The object of the iteration is to make

$$g(\alpha) \equiv (\alpha + 2)\left(\frac{\rho_*}{\rho_0}\right)^{\alpha} - 2 = 0 \tag{386}$$

From the n^{th} estimate, α_n, of α, the $(n+1)^{th}$ estimate is calculated as

$$\alpha_{n+1} = \alpha_n - \frac{g(\alpha_n)}{(dg/d\alpha)_{\alpha=\alpha_n}} \tag{387}$$

The derivative in the denominator of (387) is obtained by evaluating

$$\frac{dg}{d\alpha} = \left(\frac{\rho_*}{\rho_0}\right)^{\alpha} \left[(\alpha + 2)\, \ell n \left(\frac{\rho_*}{\rho_0}\right) + 1\right] \tag{388}$$

at $\alpha = \alpha_n$. The iteration is continued until both $|g|$ and $|\alpha_{n+1} - \alpha_n|$ are less than or equal to 10^{-5}. Then C is evaluated by substituting α and ρ_*/ρ_0 into (383).

Figure 26 illustrates the accuracy with which equation (383) fits the results of actual equilibrium-flow calculations. The flow problem is the same one on which figure 25 was based. The curve represents equation (383), and the points are results of NATA equilibrium calculations.

The non-equilibrium solution by the inverse method proceeds as follows. At each new value of x in the numerical integration, the geometric area ratio $A_g(x)$

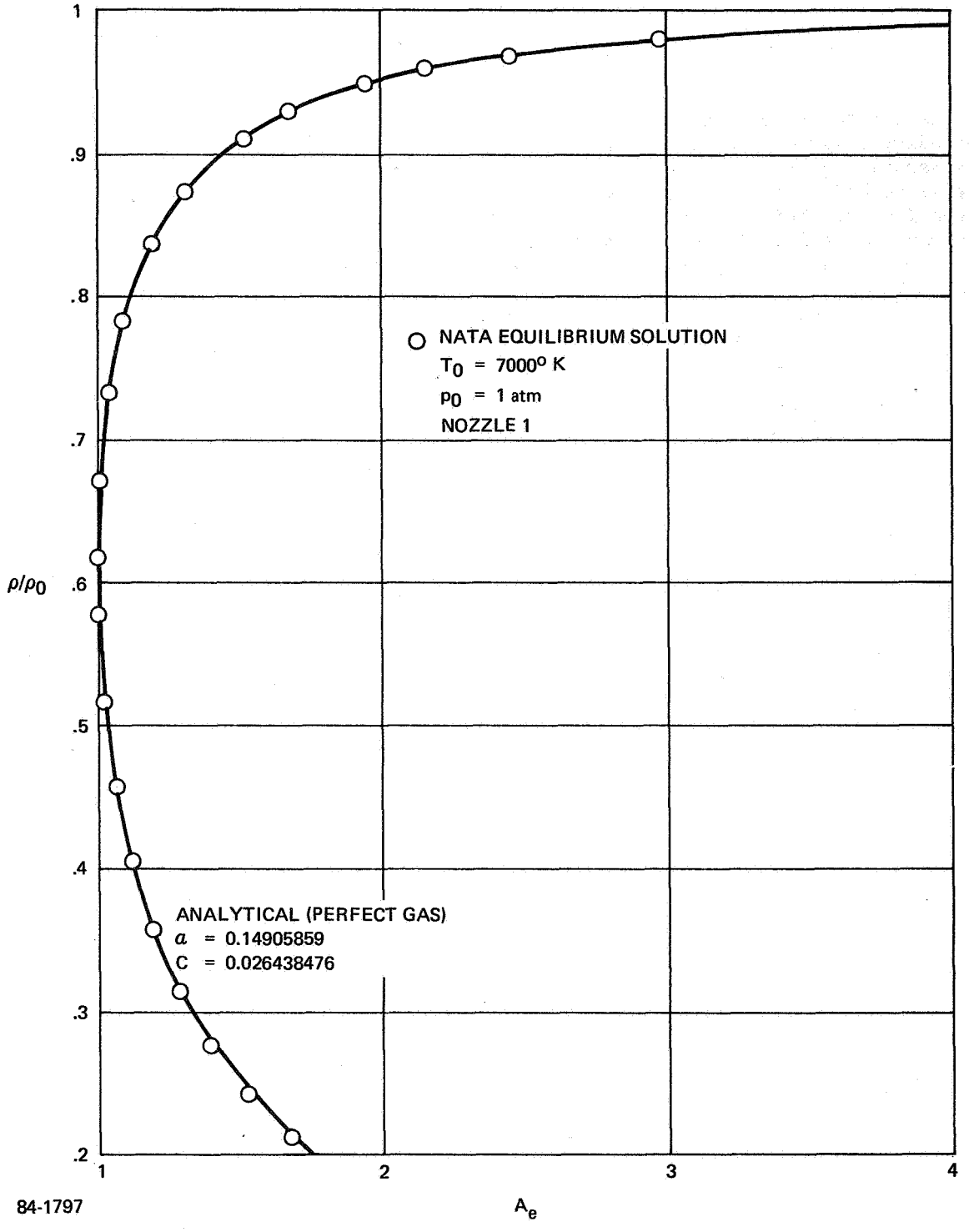

Figure 26 COMPARISON OF ANALYTICAL DENSITY-AREA RELATION WITH EQUILIBRIUM FLOW RESULTS

is calculated by calling subroutine GEØMAR. Even if the run is one in which the boundary layer on the nozzle wall is to be included, the effective area ratio A_e is assumed equal to the geometric area ratio A_g during the solution by the inverse method. Then the density ratio ρ/ρ_0 is calculated by solving equation (383) numerically. This computation is performed in subroutine GEØM. Thus, ρ/ρ_0 is determined as a function of the position x in the nozzle. The derivative $d\ell n\,\rho/dx$ is also calculated from the relation

$$\frac{d\ell n\,\rho}{dx} = \frac{2C}{a\left(\frac{\rho A_e}{\rho_0}\right)^2 - (a+2)C} \cdot \frac{d\ell n\,A_e}{dx} \qquad (389)$$

which can be derived by taking the logarithm of (383), differentiating, solving for the derivative, and using (383) to re-express the result in somewhat simpler form.

The flow equations (293) and (299) for the chemical non-equilibrium model, which are integrated during the non-equilibrium solution, contain both $d\ell n\,\rho/dx$ and $d\ell n\,A_e'/dx$. The same is true of the equations (328) and (331) for the electronic non-equilibrium model. Either of these derivatives could easily be eliminated from the equations. Both are retained in order to accommodate both the normal, direct integration and the inverse procedure in the same set of formulas. In the direct solution, $d\ell n\,A_e'/dx$ is obtained from the nozzle geometry and $d\ell n\,\rho/dx$ is determined by solving the flow equations. In the inverse method, $d\ell n\,\rho/dx$ is determined from the given nozzle geometry and the area-density relation (383), as described above, and $d\ell n\,A_e'/dx$ is determined by solving the equations.

Neither $d\ell n\,\rho/dx$ nor $d\ell n\,A_e'/dx$ is actually integrated in the Runge-Kutta routine (RNKT, Section 7.5). The quantities obtained from the integration at each flow point are T and γ_j (and T_e and h_0 in the electronic non-equilibrium model). From these quantities the enthalpy h is computed using (275). The velocity u is obtained from the integral form of the energy equation (245). The continuity equation (265) is then used to calculate the density ρ in the direct solution or the area ratio A_e in the inverse procedure. The effective area ratio $\tilde{A}_e$ thus determined in the solution by the inverse method is slightly different from the actual area ratio at the flow point, $A_g(x)$, which was used in determining the density from (383). This difference results from deviations of the non-equilibrium temperature and concentrations from the corresponding equilibrium values, which produce a difference in the calculated flow velocity. Typically, $\tilde{A}_e$ is a little smaller than $A_g(x)$ and drops below unity in the vicinity of the throat.

$\tilde{A}_e$ has its minimum at the point where the non-equilibrium flow velocity is equal to $a = \sqrt{(dp/dx)/(d\rho/dx)}$. This point is near, but not necessarily at, the geometric throat of the specified nozzle geometry. In a reacting gas, there is a second sound speed besides a, the so-called "frozen" sound speed, c. The point in the nozzle at which the flow velocity is equal to c is a branch point; beyond the branch point, the governing equations permit two solutions, a supersonic solution (which is the one desired) and a subsonic solution. In nozzle flow of a non-reacting gas, a and c are equal and the branch point and the point of minimum area both lie at the geometric throat. In a reacting gas, the frozen sound speed is a little larger than a (refs. 31, 41), and thus the branch point is slightly downstream of the point of minimum area.

In NATA, the solution by the inverse method is continued beyond the throat until the calculated area ratio $\tilde{A}_e$ reaches a value (1.01) which typically occurs downstream of the branch point. Then the specified nozzle geometry is adjusted to make the actual effective area ratio A_e continuous with the value $\tilde{A}_e$ computed in the inverse-method solution, and the solution is continued by direct integration of the rate equations. The adjustment of the nozzle geometry is carried out by setting an area rescaling factor, R_a, equal to the value of

$$R_a = \frac{\tilde{A}_e}{A_e} \tag{390}$$

at the switchover point from the inverse method to the direct solution. This factor typically has values in the range 0.95 to 1.00.

After the direct integration has been begun, the value of $d\ell n\,\rho/dx$ computed at each point is checked for sign. If $d\ell n\,\rho/dx$ goes positive slightly downstream of the switch point, it is assumed that the program has started to follow the subsonic downstream solution instead of the desired supersonic solution. This condition could arise if the branch point were actually downstream of the switch point. To recover the correct solution, the program restarts the inverse-method solution at the switch point, using previously stored data, and extends it farther downstream to a new switch point. If the $d\ell n\,\rho/dx > 0$ condition is encountered well downstream of the switch point, or if more than four restarts prove to be required, the case is abandoned.

7.5 Numerical Integration

7.5.1 Treanor Integration Technique

The governing equations (287), (293), (299), (328), (331), (332) for the non-equilibrium nozzle flow problem are first-order differential equations of the form

$$\frac{dy}{dx} = f(x, y) \tag{391}$$

Here the dependent variable y represents a concentration γ_j, the gas temperature T, the electron temperature T_e, or the stagnation enthalpy h_0, and x is the axial position coordinate in the nozzle. Actually there are $n+1$ or $n+3$ dependent variables y and functions f, and each function f depends upon all of the y's. The subscripts needed to distinguish the different variables and functions are omitted in (391) to simplify the notation in the following discussion.

Numerous numerical integration methods for systems of equations like (391) are available (ref. 43). The earliest version of the Cornell Aeronautical Laboratory program from which NATA was derived used a fourth-order Runge-Kutta method based on the equations

$$\Delta y = \frac{1}{6}\,\Delta x\,(f_1 + 2\,f_2 + 2\,f_3 + f_4) \tag{392}$$

where

$$f_i = f(x_i, y_i) \tag{393}$$

and

$$x_2 = x_1 + \frac{1}{2}\,\Delta x \qquad y_2 = y_1 + \frac{1}{2}\,f_1\,\Delta x \tag{394a}$$

$$x_3 = x_1 + \frac{1}{2}\,\Delta x \qquad y_3 = y_1 + \frac{1}{2}\,f_2\,\Delta x \tag{394b}$$

$$x_4 = x_1 + \Delta x \qquad y_4 = y_1 + f_3\,\Delta x \tag{394c}$$

Here x_1 is a value of x at which the value y_1 of y is already known, and $y_1 + \Delta y$ is the computed value of y at $x = x_1 + \Delta x$. This integration algorithm is generally satisfactory. The truncation error in one step is of order $(\Delta x)^5$, so that high accuracy can be achieved by suitable choice of the step size, Δx. Like other explicit integration methods, it is conditionally stable, i.e., stability can be maintained by using a sufficiently small Δx. However, a special problem arises in the application of this fourth-order Runge-Kutta technique to the non-equilibrium flow problem. The P_i factors (288) for the various reactions can differ by several orders of magnitude because of differences in the rate constants k_{fi} and the concentrations γ_k of the participating species. Consequently, some of the species concentrations may relax toward equilibrium very rapidly while others do so very slowly. For a species which is near equilibrium, the rate equation (287) takes the approximate form

$$\frac{dy}{dx} \simeq -P(y - \bar{y}) \tag{395}$$

where $\bar{y}$ is the local equilibrium concentration and P is an inverse relaxation distance. Differentiation of (395) shows that each derivative of y is P times larger than the derivative of previous order. Thus if P is large (i.e., if the relaxation distance is small), the higher order derivatives $d^n y/dx^n$ are very large. Under these circumstances, the Runge-Kutta technique is unstable except for very small step sizes Δx such that $P \cdot \Delta x \leq O(1)$.

To deal with this problem, NATA uses a modification of the fourth-order Runge-Kutta technique developed by Treanor (ref. 44). When one of the P's is large, Treanor's technique normally allows the use of a much larger step size than is possible in the Runge-Kutta method. When the P's are all small, it reduces to the Runge-Kutta method.

Treanor's technique is based on the assumption that, over the interval Δx, equation (391) can be approximated in the form

$$\frac{dy}{dx} = f(x, y) = -P(y - y_1) + A + B(x - x_1) + \frac{1}{2}\,C(x - x_1)^2 \tag{396}$$

This relation can be integrated analytically from $x = x_1$ to $x = x_1 + \Delta x$ to give the change in y over the interval:

$$\Delta y = \Delta x \left[A F_1 + (B \Delta x) F_2 + (C \Delta x^2) F_3 \right] \tag{397}$$

where

$$F_1 \equiv \frac{1 - e^{-P\Delta x}}{P \Delta x} \tag{398a}$$

$$F_2 \equiv \frac{P\Delta x - 1 + e^{-P\Delta x}}{(P\Delta x)^2} \tag{398b}$$

$$F_3 \equiv \frac{(P\Delta x)^2 - 2(P\Delta x) + 2 - 2e^{-P\Delta x}}{2(P\Delta x)^3} \tag{398c}$$

The four coefficients P, A, B, C in (396) are determined by fitting this relation to data at the following four (x, y) points:

$$x = x_1 \qquad y = y_1 \tag{399a}$$

$$x = x_1 + \frac{1}{2}\Delta x \qquad y = y_2 \tag{399b}$$

$$x = x_1 + \frac{1}{2}\Delta x \qquad y = y_3 \tag{399c}$$

$$x = x_1 + \Delta x \qquad y = y_4 \tag{399d}$$

The y_i will be chosen at a slightly later stage in the analysis. Substitution of (399) into (396) gives four linear equations for P, A, B, C. The solution of these equations gives

$$P = -\frac{f_3 - f_2}{y_3 - y_2} \tag{400a}$$

$$A = f_1 \tag{400b}$$

$$B\Delta x = -3(f_1 + Py_1) + 2(f_2 + Py_2) + 2(f_3 + Py_3) - (f_4 + Py_4) \tag{400c}$$

$$C\Delta x^2 = 4\left[(f_1 + Py_1) - (f_2 + Py_2) - (f_3 + Py_3) + (f_4 + Py_4)\right] \tag{400d}$$

Substitution of (400) into (397) gives

$$\begin{aligned} \Delta y = \Delta x \{ & f_1 F_1 \\ & + \left[-3(f_1 + Py_1) + 2(f_2 + Py_2) + 2(f_3 + Py_3) - (f_4 + Py_4)\right] F_2 \\ & + 4\left[(f_1 + Py_1) - (f_2 + Py_2) - (f_3 + Py_3) + (f_4 + Py_4)\right] F_3 \} \end{aligned} \tag{401}$$

The quantities y_2 and y_3 are chosen to be the values given by (394a) and (394b). Based on these values, the formula (400a) for P becomes

$$P = -\frac{2}{\Delta x} \cdot \frac{f_3 - f_2}{f_2 - f_1} \tag{402}$$

When $(P\ \Delta x)$ is large, the y_4 value given by (394c) can be considerably different from the correct value on the solution curve. To avoid the errors in B and C which would result from the use of (394c), a better approximation to y_4 is obtained by evaluating (397) with $C = 0$; i.e.,

$$y_4 = y_1 + \Delta y = y_1 + \Delta x\ [A' F_1 + (B' \Delta x) F_2] \tag{403}$$

where the coefficients A' and B' are determined by fitting equation (396) to the three points (x_1, y_1), $(x_1 + \Delta x/2, y_2)$, and $(x_1 + \Delta x/2, y_3)$. The expression (402) for P remains valid, since it depends only on the evaluation of y_2 and y_3. A and $(B' \Delta x)$ are found to be

$$A' = f_1 \tag{404a}$$

$$B' \Delta x = 2\ [(f_3 + P y_3) - (f_1 + P y_1)] \tag{404b}$$

Hence, (403) gives

$$y_4 = y_1 + \Delta x\ [2 f_3 F_2 + f_1 (F_1 - 2F_2) + f_2 (P \Delta x) F_2] \tag{405}$$

This result is used, in place of equation (394c), for evaluating $(B\ \Delta x)$ and $(C \Delta x^2)$ from (400) and in the final integration formula (401).

For $(P\ \Delta x) \to 0$, equations (398) show that

$$\lim_{P \Delta x \to 0} F_1 = 1 \tag{406a}$$

$$\lim_{P \Delta x \to 0} F_2 = \frac{1}{2} \tag{406b}$$

$$\lim_{P \Delta x \to 0} F_3 = \frac{1}{6} \tag{406c}$$

Hence, for $(P\ \Delta x) \to 0$, equation (405) for y_4 reduces to (394c), and the Treanor integration formula (401) reduces to the fourth-order Runge-Kutta formula (392). Thus, in a region of the integration where $(P\ \Delta x)$ is small, Treanor's technique behaves like the fourth-order Runge-Kutta method, which is known to perform well under such circumstances. On the other hand, for large $(P\ \Delta x)$, Treanor's technique allows the use of a much larger step size without instability.

Equation (402) specifies the evaluation of P as the ratio of two differences. If f_1, f_2, and f_3 are nearly equal, the loss of accuracy on the indicated subtractions can produce large errors in P, or even a negative value of P. However, when these slopes are nearly equal the fourth-order Runge-Kutta method is satisfactory. Thus, if the magnitude of $(f_2 - f_1)/f_1$ is found to be smaller than 10^{-4}, or if P is computed to be negative, the Runge-Kutta formula is used.

The preceding discussion has been phrased in terms of the solution of a single differential equation. The non-equilibrium flow problem, of course, involves a system of n+1 (or n+3) coupled equations for the concentrations γ_j and temperature T (and for T_e and h_0 in the case of an electronic non-equilibrium model). In NATA, Treanor's integration technique is applied to each of these differential equations individually. This procedure is the same as the one used when the Runge-Kutta method is applied to a system of differential equations.

Lomax and Bailey (ref. 45) have studied the stability and accuracy of several integration methods, including Treanor's, when applied to the equations of steady, one-dimensional, non-equilibrium flow. Their principal findings with regard to Treanor's method were as follows:

1. When applied to a single differential equation, the method is stable for large step sizes, provided the parameter P is sufficiently close to the eigenvalue of the linearized equation.

2. When the method is applied to a system of coupled equations, its stability depends on the coefficients. It works very well if the equations are nearly uncoupled, but the coupling is difficult to assess a priori. The allowable step size for a system of coupled equations depends upon the eigenvalues of the system.

3. With proper step size control, the method is stable and gives accurate results.

On the whole, Lomax and Bailey preferred an implicit integration technique to Treanor's method. However, the advantages of the implicit technique were most apparent in non-equilibrium shock wave calculations, in which the system under consideration approaches an equilibrium state downstream. Treanor's explicit integration formula has to use a small step size in near-equilibrium regions. In the nozzle flow problem, the departures from equilibrium generally increase in the downstream direction, so that the step size can be increased as the calculation proceeds. Thus, Treanor's method is expected to be more satisfactory for nozzle flow problems than for shock wave problems.

7.5.2 Step-Size Controls

Proper control of the step size is extremely important in any numerical integration using an explicit finite difference scheme. If the step is just a little too large, the solution becomes noisy and inaccurate. If the step is increased still further, the solution becomes unstable and small errors are amplified without limit. On the other hand, if the step is much smaller than necessary, the solution requires a needlessly large number of steps and wastes computer time. In nozzle flow calculations, the step must be small initially, where the gas mixture is still near an equilibrium state, but becomes stable for much larger steps far downstream where the reactions are nearly frozen. Thus, a procedure for determining and maintaining the proper step size in each part of the calculation is needed.

The step size controls in NATA are based on those described in ref. 1 for the Cornell Aeronautical Laboratory program from which NATA was derived. The

controls in NATA are somewhat more elaborate and restrictive to meet the needs of the electronic non-equilibrium models, which are distinctly less stable than conventional chemical non-equilibrium models. The controls are based on tests for the acceptability and accuracy of the computed results, both at intermediate points in each Treanor-Runge-Kutta integration step and at the end of each step. The tests at the end of each step in conventional chemical non-equilibrium models are as follows:

$$\gamma_j \geq 0 \qquad (j = 1, \ldots, n) \tag{407a}$$

$$x \cdot \frac{d \ell n A_e}{dx} \geq -0.01 \tag{407b}$$

$$\left| \frac{\Delta \gamma_j}{\gamma_{jb}} \right| \leq \text{GTEST} \qquad (j = 1, \ldots, n) \tag{407c}$$

$$\left| \frac{\Delta T}{T_b} \right| \leq \text{TTEST} \tag{407d}$$

Here the subscript b denotes values at the beginning of the integration step. The criterion values GTEST and TTEST are under input control. They are preset to the values GTEST = 0.1 and TTEST = 0.05.

The first test, (407a), requires that the concentrations be positive. The second requires that dA_e/dx be negative upstream of the throat and positive downstream of the throat; this test is effective only during the solution by the inverse method, in which $\rho(x)$ is assumed given and $d \ell n A_e/dx$ is computed from the flow equations. The small negative value (-0.01) on the right allows for possible slight displacement of the non-equilibrium sonic point from the geometric throat. The last two tests (407c, d) set limits on the changes in the dependent variables in any one step.

In the case of an electronic non-equilibrium model, the following additional tests are performed at the end of each integration step:

$$\left| \frac{\Delta T_e}{T_{eb}} \right| \leq \text{TETEST} \tag{408a}$$

$$\left| \frac{\Delta h_0}{h_{0b}} \right| \leq \text{HTEST} \tag{408b}$$

$$|\Delta \dot{q}_e| \leq \max \left\{ \text{QTEST} \cdot |\dot{q}_{eb}|, D_{qm} \right\} \tag{408c}$$

where TETEST, HTEST, and QTEST are inputs preset to 0.05, 0.01 and 0.1, respectively, and D_{qm} is the maximum value of $\text{QTEST} \cdot |\dot{q}_{eb}|$ computed previously in the case. The tests (408a) and (408b) set limits to the changes in the electron temperature T_e and the total enthalpy h_0 in each step. The test (408c) controls the fluctuations in the energy transfer $\dot{q}_e$ to the electron gas. This test is needed in the electronic non-equilibrium model because in the upstream region, where some of the reactions are near equilibrium, $\dot{q}_e$ is extremely sensitive to small changes in the temperatures T and T_e and some of the mole fractions γ_j. In turn, $\dot{q}_e$ affects the electron temperature through equation (332). The sensitivity of $\dot{q}_e$ to the dependent flow variables is the principal cause of the

poor stability of the electronic non-equilibrium models, which requires the use of small step sizes in non-equilibrium flow calculations based on such models. The form of the test (408c) allows for the possibility that $\dot{q}_e$ may pass through zero at some point in the solution.

The tests performed at intermediate points in the Treanor-Runge-Kutta integration step are generally more lenient than those done at the end of the step. In the chemical non-equilibrium models, the tests at intermediate points are (407a), (407b), and

$$T \geq 0 \tag{409a}$$

$$h \leq h_0 \tag{409b}$$

In electronic non-equilibrium models, the following additional tests are performed at intermediate points.

$$T_e \geq 0 \tag{409c}$$

$$h_0 \geq 0 \tag{409d}$$

$$| \Delta \dot{q}_e | \leq 2 D_{qm} \tag{409e}$$

At the start of each integration step, the values of γ_j, T, T_e, x, h_0, A_e, ρ, and s are saved in a separate set of storage locations. If any of the conditions (407) to (409) is violated at any point where it is applied, the flow variables are reset to their values at the start of the step, the step size is reduced, and the step is repeated. If the step fails again, this procedure is repeated until a successful step which passes all of the tests is obtained, or until the step size falls below 10^{-10} cm. If the step size goes below this limit, or if a successful step has not been achieved after 30 tries, diagnostic data are printed out and the case is abandoned.

Changes in the step size are based on two factors, SC (used for increasing the step) and SCD (used for decreasing the step). SC is initially 1.1. If NQS successful integration steps have been taken without the need for a step size reduction, the step size Δx is multiplied by SC. If the step has thus increased NQS times without the need for a reduction, SC is increased by 0.1. NQS is an input (with input name NQSI), preset to 4. Thus, so long as the integration proceeds with no failures of the tests, the step size is increased repeatedly, and the factor SC by which Δx is multiplied is also increased.

When a failure of one of the tests occurs, the following actions are taken:

1. The counters for successful steps and successful increases in step size are both reset to zero.
2. SC is decreased by 0.1 (but not below 1.1).
3. Δx is divided by SCD.
4. SCD is multiplied by 1.1.
5. The step is restarted from its beginning.

If repeated failures of the same step occur, the increase in SCD on each attempt allows the program to reduce the step size very sharply in a small number of cycles. However, once the step has been taken successfully, Δx is reset from its (possibly very small) value used in the integration to $\max(\Delta x , 0.7\,\Delta x_{old})$, where Δx_{old} is the step size used in the previous successful step. Also, after a successful step, SCD is reset to the current SC value.

The initial step size at the beginning of the numerical integration is an input (DELTXI). It is preset to 0.01 cm. However, if

$$\Delta x_m = 100\,|\delta \gamma_i|_{min} \tag{410}$$

is less than the input value of Δx, the step size is reset to Δx_m. This provision takes account of the smaller step size required when the switch from the perturbation technique to numerical integration occurs in a region where one or more of the reactions are still very close to equilibrium.

The preset values for TTEST and GTEST do not imply that the program allows errors of 10 percent in the concentrations or of 5 percent in the temperature. In fact, the cumulative truncation errors which occur when the step size is controlled by (407) are typically of the order of 0.1 percent or smaller.

7.5.3 Freezing of Minor Species

Previous versions of NATA were subject to a mode of failure which typically occurred far downstream of the nozzle throat. The symptoms of this type of failure were as follows: The concentration of a minor species, already very low, would begin to decrease more and more rapidly, until changes in the concentration of this species were controlling the step size in the non-equilibrium integration. The decrease in concentration would continue to accelerate, forcing successive decreases in the step size. Thus, the rate of progress of the solution would become quite low. In some cases, the step size would become so small that loss of accuracy on subtractions would lead to major fluctuations in some of the flow quantities, and the code would be unable to proceed with the non-equilibrium solution.

The mechanism of this type of behavior is as follows. The gas models used in NATA contain numerous reactions of the type

$$S + A \rightleftharpoons B + C \tag{411}$$

Equation (283) for the rate of change of species S due to this reaction is

$$\frac{d\gamma_S}{dx} = -\frac{\rho}{u}\left(k_f \gamma_S \gamma_A - k_r \gamma_B \gamma_C\right) \tag{412}$$

since $\nu_i = \nu_i' = 2$ for the reaction (411). Now, the reverse rate constant k_r is given in terms of k_f and the equilibrium constant K by equation (277). Hence (412) can be rewritten

$$\frac{1}{\gamma_S}\frac{d\gamma_S}{dx} = -\frac{k_f \rho}{u}\left(\gamma_A - \frac{\gamma_B \gamma_C}{K \gamma_S}\right) \tag{413}$$

The equilibrium constant (278) for the reaction (411) is

$$K = \exp\left\{ -\frac{1}{R_0 T} \sum_{j=1}^{n} \beta_{ij} \mu_j^{o} \right\} \tag{414}$$

Now, assume that the reaction (411) has been written so that products (B and C) are much more stable than the reactants (S and A) at low temperatures. Then the exponent in (414) is positive. Because of its factor 1/T, this exponent can become large in magnitude as the temperature falls. In such a case, the equilibrium constant K itself can become exceedingly large. Moreover, under such circumstances, K increases very rapidly as the temperature decreases. Even though γ_S is decreasing, the increase in K can be so rapid that the second term on the right in (413) becomes and remains small in comparison with the first term. If the concentration γ_A of the second reactant A is large compared with γ_S, the reaction has little effect on γ_A. Under these conditions, $d\ell_n \gamma_S/dx$ is negative and varies only slowly with x. Thus, γ_S approaches zero in an approximately exponential fashion,

$$\gamma_S \sim e^{-x/L}, \qquad L = u/k_f \rho \gamma_A \tag{415}$$

The type of failure described above would occur under these circumstances if the characteristic relaxation length L were small. For some of the reactions used in NATA gas models, the rate constant k_f is sufficiently high to produce such failures in some cases.

The current version of NATA contains a procedure designed to prevent failures of this type. Whenever the following three conditions are satisfied:

(1) An excessive change in the concentration γ_j of a species, over a complete integration step, has forced a reduction in the step size;

(2) The concentration γ_{jb} of the species at the start of the integration step was less than an input value GAMIN, preset to 10^{-10} mole/gm;

(3) The concentration γ_j decreased during the step,

then the concentration of the species j is frozen by switching off all of the reactions which produce or destroy the species. The rationale for this procedure may be outlined as follows:

(1) It prevents failures of the type described above by switching off the reaction causing the rapid destruction of the minor species S (along with the other reactions affecting the concentration of the species).

(2) Because the concentration of S is very low, and since the net effect of the reaction system is to transform S into other species, freezing the concentration of S cannot significantly affect the concentrations of the other species during the remainder of the non-equilibrium flow solution.

When this procedure is used, NATA prints out a message identifying the species whose concentration is being frozen and the reactions which are being switched off.

7.6 Boundary Layer Effects

The method used in the approximate calculation of laminar boundary layer development on the nozzle wall has been documented in Section 5. The boundary layer calculation for the non-equilibrium solution follows an approach similar to that used for the frozen and equilibrium calculations (Section 6.3). In the upstream and throat regions, the boundary layer is computed but is not coupled to the inviscid flow. A short distance beyond the throat, the coupling is "switched on". The motivation and justification for this approach have been explained in Section 6.3.

In the frozen and equilibrium flow solutions, the coupling of the inviscid flow to the boundary layer is turned on at the third point beyond the geometric throat. In the non-equilibrium solution, the uncoupled solution is carried a little farther downstream, to the point at which the switch from the inverse solution to the direct integration is made. This procedure allows the effect of the displacement thickness on the area ratio at the switch point to be included in the area rescaling factor R_a equation (390). Also, it avoids stability problems which might result from switching the coupling on very close to the throat, where the solution is extremely sensitive to the area ratio.

In the uncoupled region upstream of the switch point, the effect of the boundary layer upon the effective area ratio A_e is neglected;i.e., A_e is assumed equal to the geometric area ratio, $A_g(x)$. Downstream of the switch point, A_e is calculated from $A_g(x)$ and the displacement thickness δ^* using equation (126), (130), or (134) depending upon the type of nozzle geometry. Also, $d\ell n\, A_e'/dx = d\ell n\, A_e/dx$ in equations (293) and (299) is calculated from the derivative of the applicable area ratio formula. The derivative $d\delta^*/dx$ appearing in these formulas is evaluated by the simple first-order difference expression

$$\left(\frac{d\delta^*}{dx}\right)_c = \frac{\delta^* - \delta_0^*}{x - x_0} \tag{416}$$

in which δ^* and x are the displacement thickness and axial coordinate at the current flow point, and δ_0^*, x_0 the corresponding values at the preceding flow point. To avoid an abrupt discontinuity in $d\ell n\, A_e/dx$ at the point where the coupling is switched on, $d\delta^*/dx$ is built up gradually from zero over 29 integration steps, according to the formula.

$$\frac{d\delta^*}{dx} = w\left(\frac{d\delta^*}{dx}\right)_c + (1-w)\left(\frac{d\delta^*}{dx}\right)_0 \tag{417}$$

where

$$w = \frac{1}{30 - i} \tag{418}$$

and i is an integration step counter which is initialized to zero in the step in which the coupling is switched on. Also, $(d\delta^*/dx)_0$ is the final $d\delta^*/dx$ calculated in the preceding step using (417). If $(d\delta^*/dx)_c$ were constant, equations (417) and (418) would give a linear variation of $d\delta^*/dx$ with the counter i, from 0.0333

$(d\delta^*/dx)_c$ at $i = 0$ to 0.9667 $(d\delta^*/dx)_c$ at $i = 28$. For $i > 28$, equation (418) is no longer used. Instead, the weight factor w in (417) is calculated from

$$w = \frac{1}{2} \min \left[1, \left(\frac{\Delta x}{\Delta x_0} \right)^2 \right] \tag{419}$$

in which Δx is the integration step size in the current step and Δx_0 that in the preceding step. Thus, w never exceeds 0.5, and equation (417) provides some smoothing of fluctuations in $(d\delta^*/dx)_c$. If the current step size Δx is much smaller than the value Δx_0 for the preceding integration step, which can happen if the current flow point is a model point or if the numerical integration of the flow equations is encountering severe convergence problems, then the weight w applied to the current $(d\delta^*/dx)_c$ value is very small. This algorithm avoids difficulties which could result from loss of accuracy in the subtractions indicated in (416) when x and x_0 are very nearly equal.

The above-described procedure for switching on the coupling between the boundary layer and the inviscid flow is found to work reliably in flow calculations based on conventional chemical non-equilibrium models. However, when attempts are made to compute flow solutions including the boundary layer for gases represented by the electronic non-equilibrium model, the solutions usually fail at the point where the coupling is switched on. Such failures occur because the disturbance produced by increasing $d\delta^*/dx$ in accordance with (417) and (418), small though it is, upsets the precarious stability of the electronic non-equilibrium model.

Boundary layer calculations are performed both at the intermediate points in the Treanor-Runge-Kutta integration step and at the end of each successful step. Now, the method used in the boundary layer calculations involves the evaluation of a definite integral, equation (170) or (172), in which the variable of integration is the streamwise coordinate ξ lying along the nozzle surface. Also, ξ itself is evaluated as a definite integral. To avoid contaminating these integrals with inaccurate data from unsuccessful integration steps and intermediate points in successful steps, the "permanent" values of the integrals are incremented only following successful full steps. At intermediate points in a step, the integrals are incremented on a temporary basis for use in computing the boundary layer displacement thickness, but are restored to their initial values. Also, $d\delta^*/dx$ is not computed at intermediate points.

The calculation of the displacement thickness δ^* (Sections 5.5 and 5.6) involves the quantity $d\ell n\, M/dx$, in which M denotes the Mach number. During the non-equilibrium solution, this derivative is evaluated as follows:

$$\frac{d\ell n\, M}{dx} = \frac{1}{u}\frac{du}{dx} - \frac{1}{a}\frac{da}{dx} = \frac{1}{u}\frac{du}{dx} - \frac{1}{2T}\frac{dT}{dx} \tag{420}$$

where the second form is based on the approximation $a \propto T^{1/2}$ for the sound speed a. The velocity derivative is obtained from equation (245):

$$\frac{du}{dx} = \frac{1}{u}\left(\frac{dh_0}{dx} - \frac{dh}{dx} \right) \tag{421}$$

For chemical non-equilibrium gas models, $dh_0/dx = 0$ and dh/dx is given by (291). For electronic non-equilibrium models, dh_0/dx is given by (333) and, from (334),

$$\frac{dh}{dx} = \gamma_e C_{pe} \frac{dT_e}{dx} + H_e \frac{d\gamma_e}{dx} + \sum_{j=2}^{n} \left[\gamma_j C_{pj} \frac{dT}{dx} + H_j \frac{d\gamma_j}{dx} \right] \tag{422}$$

Thus, $d\ell n\, M/dx$ is evaluated from the current values of dT/dx, $d\gamma_j/dx$, and, in the case of electronic non-equilibrium models, dT_e/dx and dh_0/dx. These derivatives, in turn, are obtained by solving equations (293) and (299) (or (328), (331), (332), and (333) for electronic non-equilibrium models). These equations for the derivatives involve A_e and $d\ell n\, A_e/dx$, which depend on δ^* and $d\delta^*/dx$. Thus, the calculation of δ^* at any flow point requires knowledge of the value of δ^* at the same flow point. This impasse is broken by using an iterative self-consistent solution for δ^* and the derivatives dT/dx, $d\gamma_j/dx$, dT_e/dx, dh_0/dx of the flow variables. The convergence criterion in the iteration is that the newly computed δ^* differ by no more than 1 percent from the previous value. Whenever calculations of the derivatives are required, in a non-equilibrium solution including the boundary layer, the derivatives are first computed assuming the δ^* value δ_p^* left in storage by the last previous calculation. Then a new value δ_1^* for the thickness is computed by calling the boundary layer routine, and is compared with the previous one. If δ_1^* and δ_p^* differ by no more than 1 percent, the new value is accepted and used. If they differ by more than this amount, the entire calculation is repeated, using δ_1^* in the rate calculation, to obtain a further improved estimate δ_2^*. If the convergence test is satisfied, δ_2^* is accepted as the displacement thickness. If not, the following rapidly converging algorithm is used to obtain a more accurate estimate of δ^*. Denote the input value of displacement thickness assumed in the rate calculation by δ_i^*, and the output value obtained from the boundary layer routine by δ_o^*. Then the calculational procedure defines a functional relationship $\delta_o^* = f(\delta_i^*)$. The condition for a self-consistent solution is that $\delta_o^* = \delta_i^*$. The functional relation is approximated by a straight line passing through the two points already computed (or the two most recent points if the algorithm is applied more than once). The equation of the straight line is

$$\frac{\delta_o^* - \delta_{o2}^*}{\delta_{o2}^* - \delta_{o1}^*} = \frac{\delta_i^* - \delta_{i2}^*}{\delta_{i2}^* - \delta_{i1}^*} \tag{423}$$

The intersection of (423) with the self-consistent solution line is found to be at $\delta_o^* = \delta_i^* = \delta^*$, where

$$\delta^* = \frac{\delta_{o2}^* \delta_{i1}^* - \delta_{o1}^* \delta_{i2}^*}{\delta_{i1}^* - \delta_{i2}^* - \delta_{o1}^* + \delta_{o2}^*} \tag{424}$$

Figure 27 illustrates the geometry of this solution. The first application of (424) almost always gives a δ^* value which satisfies the self-consistency condition to within 1 percent. The program allows a maximum of four iterations using (424).

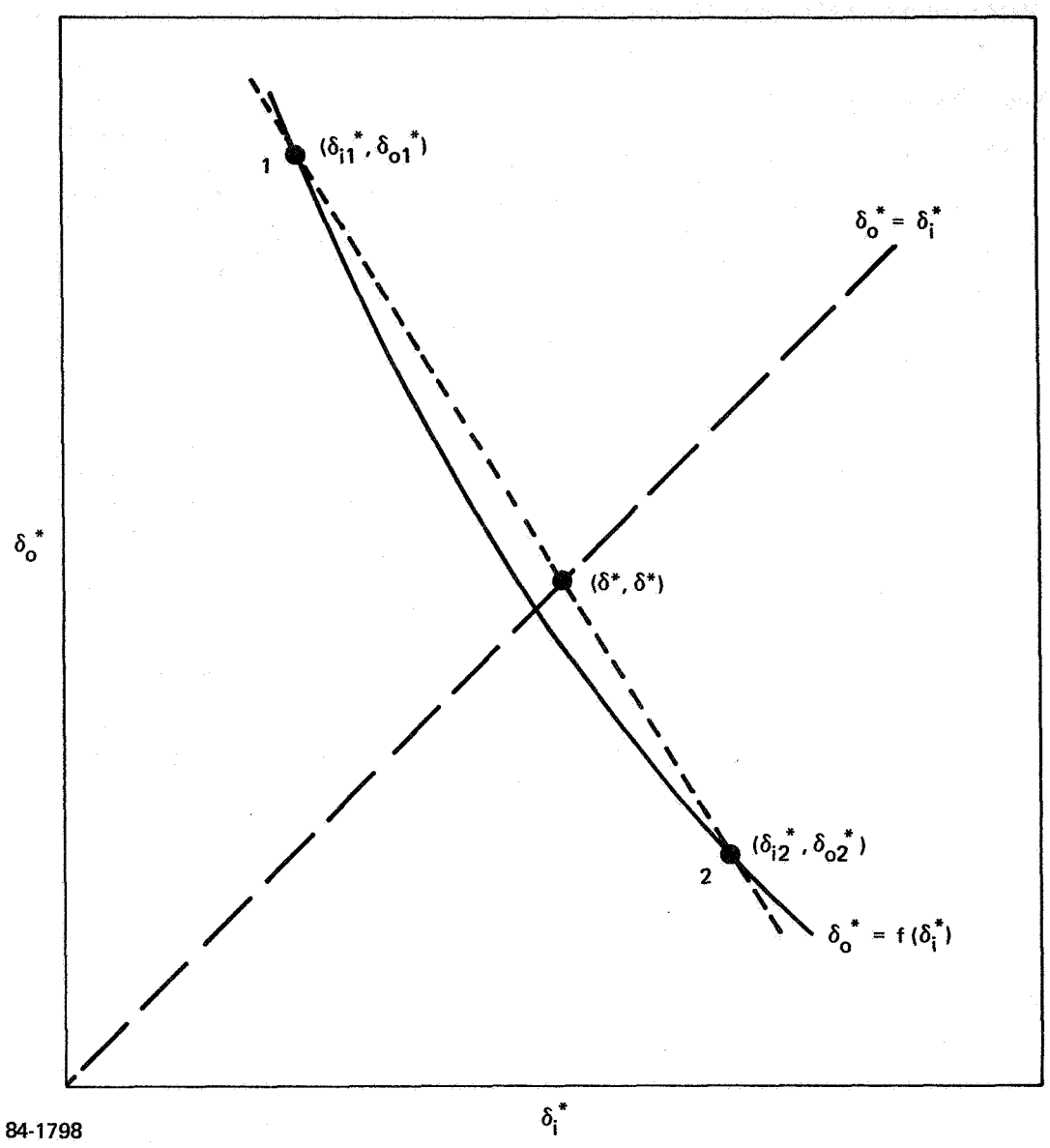

Figure 27 SELF-CONSISTENT SOLUTION FOR THE DISPLACEMENT THICKNESS

7.7 Example - NO_2 Recombination

To illustrate the non-equilibrium flow calculations performed by NATA, the code has been used to compute the flow and concentration changes in two of Wegener's classic experiments (refs. 46, 47) on the three-body recombination of nitrogen dioxide,

$$2\ NO_2 + N_2 \rightleftharpoons N_2O_4 + N_2 \tag{425}$$

Wegener's experiments were performed in a small wind tunnel of rectangular cross section. The flow geometry was modeled in NATA as a two-dimensional nozzle with the profile shown in figure 28. The flow in this tunnel was found to be one-dimensional to within the accuracy of the measurements. The experiments analyzed were those designated C and F in reference 46. The conditions in these experiments were as summarized below:

Experiment	$(X_{NO_2})_0$ percent	p_0 atm	T_0 ^oK
C	0.0100	2.00	400
F	0.0500	2.16	402

Of the three gas species appearing in (425) only N_2 is a standard species in NATA. Thermo fits for NO_2 and N_2O_4 were obtained by fitting the data in the JANAF tables (ref. 48) over the temperature range 200° to 400° K. The coefficients obtained for use in equations (33) and (34) were as follows:

Coefficient	NO_2	N_2O_4
a	4.003	3.553
b	-3.75×10^{-4}	1.1625×10^{-2}
c	2.45×10^{-6}	-4.55×10^{-6}
d	0	0
e	0	0
k	5.945	10.028
H_0^o (kcal/mole)	8.586	4.473

The rate constant for the reaction (425) was taken to be 3×10^{14} $cm^6/mole^2$-sec (ref. 47).

Frozen, equilibrium, and non-equilibrium flow calculations were performed for each of the two experiments. The results are compared with Wegener's data in figures 29 and 30. The abscissa in these figures is distance along the nozzle. The ordinate is the ratio $[NO_2]/[NO_2]_0$ of the NO_2 concentration to its value in the upstream reservoir. This was calculated from quantities available in the NATA output as

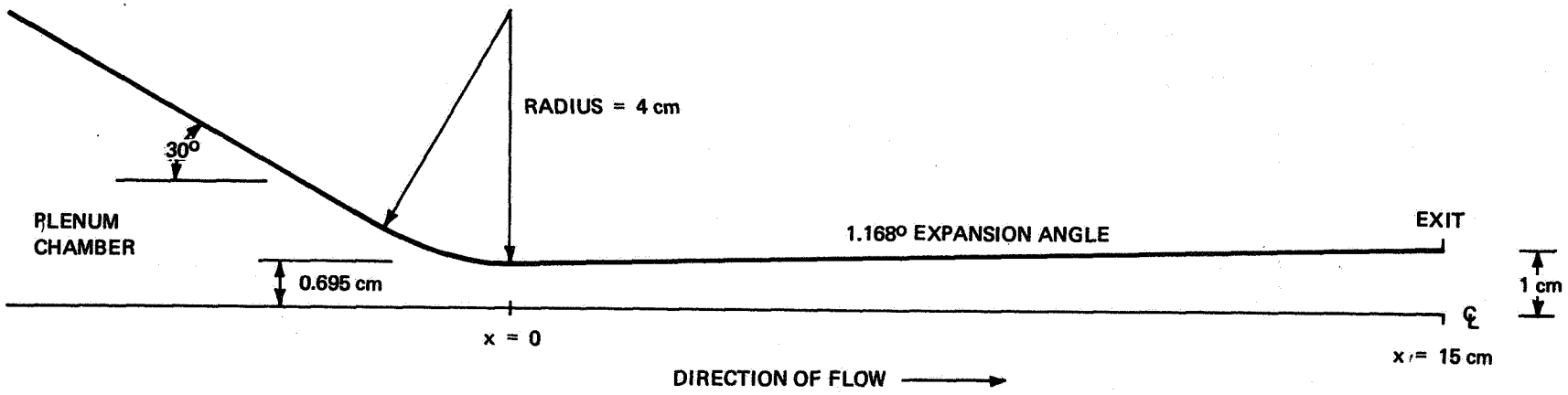

Figure 28 PROFILE OF WIND TUNNEL USED IN NO_2 RECOMBINATION EXPERIMENTS

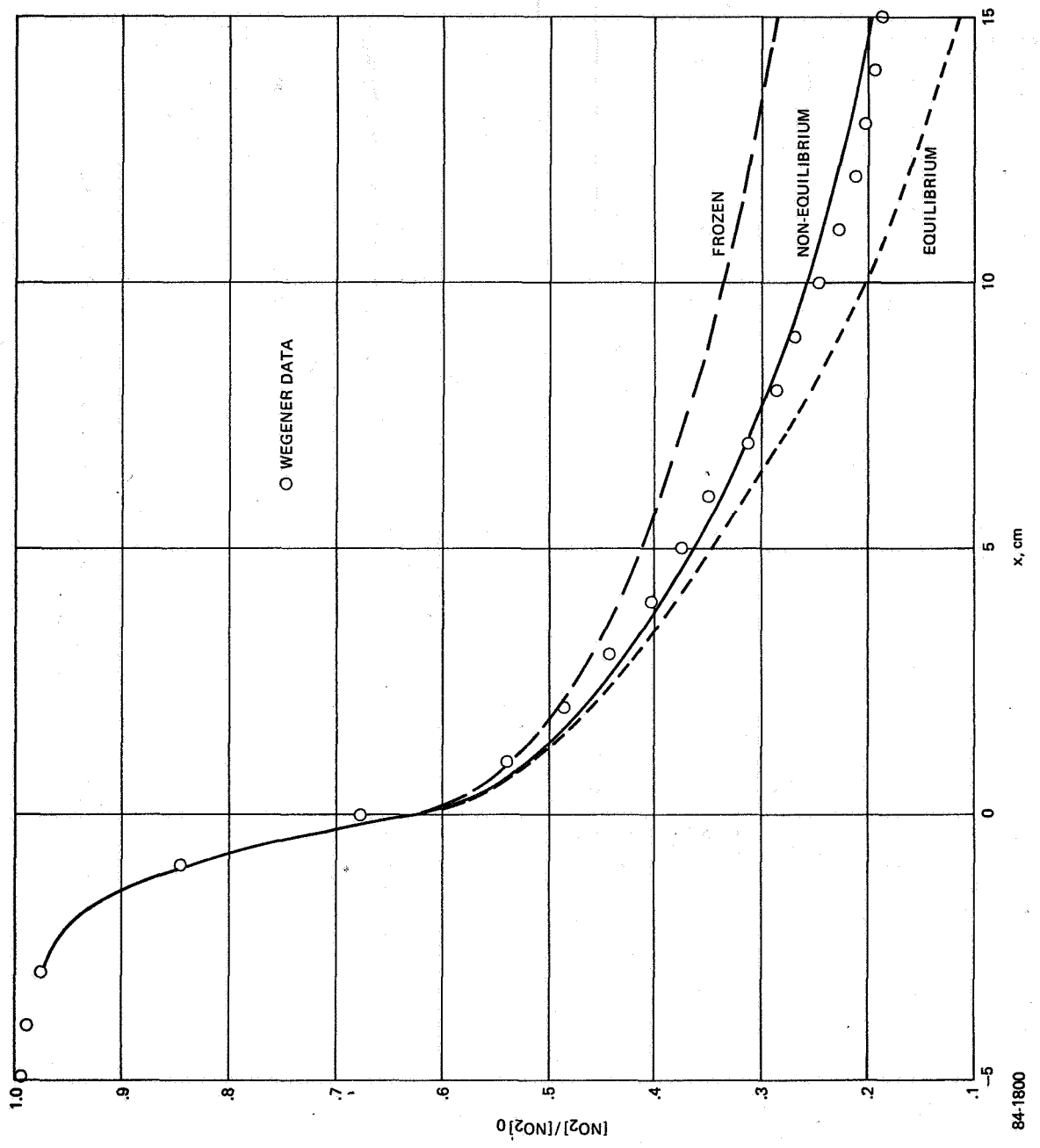

Figure 29 COMPARISON OF NATA RESULTS WITH WEGENER'S DATA ON NO_2 RECOMBINATION (EXPERIMENT C)

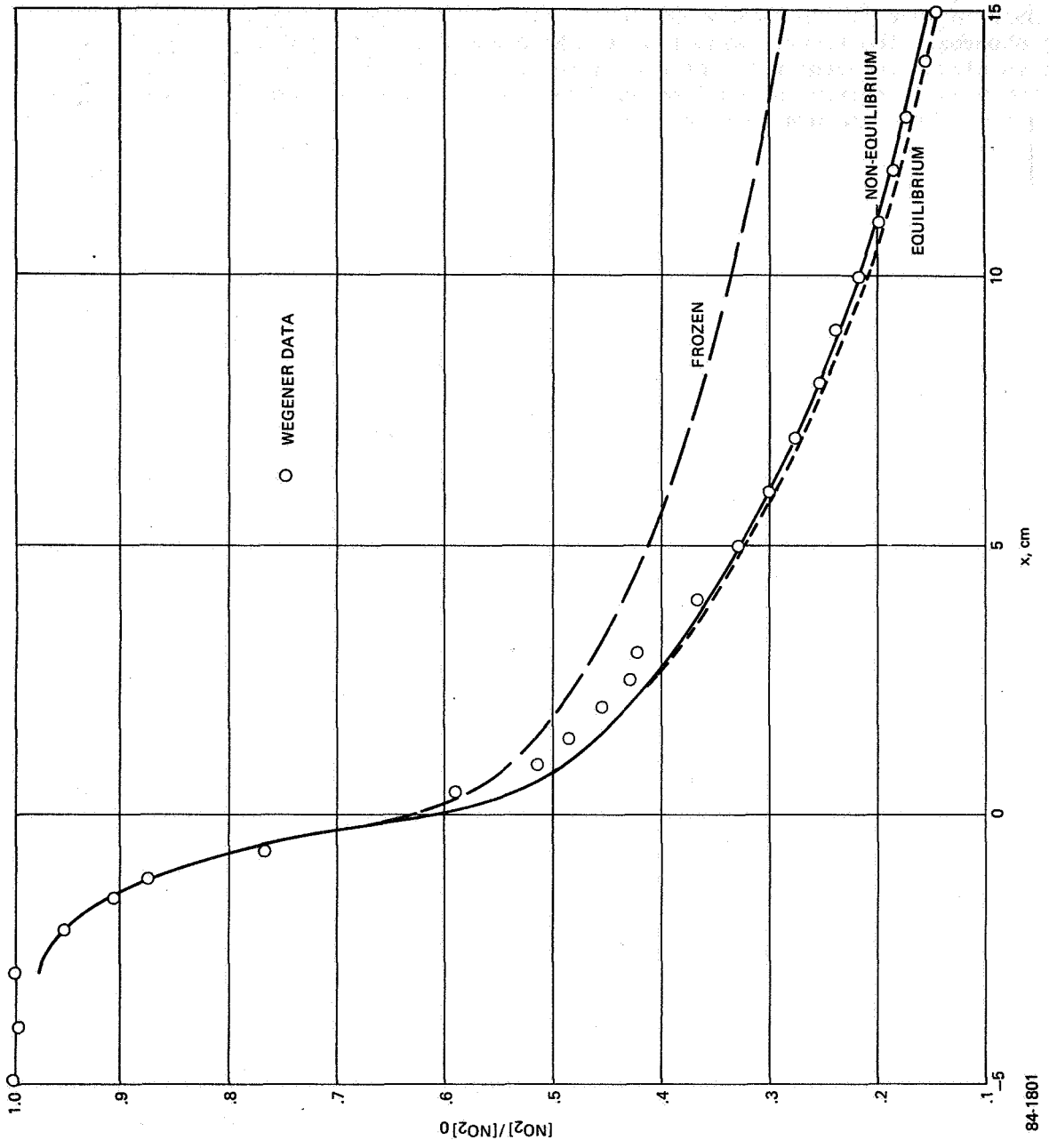

Figure 30 COMPARISON OF NATA RESULTS WITH WEGENER'S DATA ON NO_2 RECOMBINATION (EXPERIMENT F)

$$\frac{[NO_2]}{[NO_2]_0} = \frac{\rho}{\rho_0} \cdot \frac{X_{NO_2}}{(X_{NO_2})_0} \cdot \frac{W_0}{W} \qquad (426)$$

The curves in the figures give the NATA results. The points are Wegener's data (ref. 46), which are based on measurements of optical transmission at wavelengths of 3950 to 4750 Å. In this wavelength range, N_2 and N_2O_4 are transparent, while NO_2 absorbs. The figures show that the NATA non-equilibrium flow calculations are in close agreement with the experimental data in both cases. In experiment F, the flow is nearly in equilibrium throughout the tunnel, but a major departure from equilibrium occurs in experiment C.

8. CONDITIONS ON MODELS

The NATA code provides calculations of the heat flux and pressure on models inserted into the free-stream flow at specified locations. The code treats two general types of model configurations: the stagnation point of an axisymmetric or two-dimensional probe, and the flat surface of a blunt wedge.

The points in the free-stream flow at which model condition calculations are to be done may be specified in either or both of two ways:

(1) A list of up to 20 test section diameters (TSDIAM) may be read in. Model condition calculations are done at the positions (downstream of the throat) at which the nozzle diameter has the values thus specified.

(2) An initial axial coordinate value (XMØDP1), a final value (CXMAXI), and a number of model points (NMØDPT) may be read in. Model condition calculations are then done at the specified number of points, including the initial and final positions and a sequence of intermediate points whose axial coordinates form a geometric progression. For NMØDPT = 1, calculations are done only at the initial point.

The influence of the test models upon the free-stream flow is not considered. Thus, when calculations are done for several model locations, each model is assumed to be inserted into the previously undisturbed free stream.

8.1 Stagnation-Point Calculations

The calculation of stagnation-point conditions begins with an approximate normal shock solution. The heat flux and shock standoff distance are then calculated for both flat-faced and hemispherical axisymmetric models. Optionally, the calculations can be done instead for two-dimensional models with flat and cylindrical leading edges. These calculations are carried out assuming either equilibrium flow behind the shock or a frozen shock with the species mole fractions behind the shock equal to those ahead of it. Optionally, both types of normal shock calculation can be done.

Section 8.1.1 discusses the normal shock solutions, Section 8.1.2 the heat flux calculations, and Section 8.1.3 the stagnation-point velocity gradient. Section 8.1.4 specifies the model heat flux outputs provided, and Section 8.1.5 discusses low-density effects which limit the validity and accuracy of the stagnation-point heat flux calculations.

8.1.1 Normal Shock Solutions

The main purpose of the stagnation-point model-condition calculations is to predict the stagnation point heat flux and the stagnation pressure on the model. The objective of the normal shock solution is to determine the conditions at the stagnation point of the inviscid flow, just outside the boundary layer on the model. The free stream conditions ahead of the shock will be designated by subscript 1, conditions just behind the shock by subscript 2, and stagnation conditions by subscript s.

The conservation relations for the normal shock are:

$$p_1 + \rho_1 u_1^2 = p_2 + \rho_2 u_2^2 \tag{427a}$$

$$\rho_1 u_1 = \rho_2 u_2 \tag{427b}$$

$$h_1 + \frac{1}{2} u_1^2 = h_2 + \frac{1}{2} u_2^2 \tag{427c}$$

The conditions ahead of the shock are known from the nozzle flow solution. The conditions at the inviscid stagnation point are assumed to be related to those just behind the shock by

$$h_s = h_2 + \frac{1}{2} u_2^2 \tag{428a}$$

$$p_s \simeq p_2 + \frac{1}{2} \rho_2 u_2^2 \tag{428b}$$

The first of these relations (428) is exact. The incompressible Bernoulli equation (428b) is only an approximation to the actual compressible isentropic flow relation, but is reasonably accurate as long as the shock Mach number is not too low. In NATA, model condition calculations are not done for points at which the free-stream Mach number is less than 1.5. At this Mach number, for a perfect gas with $\gamma = 1.4$ (for example), equation (428b) is accurate to within about 3.5 percent. For higher free-stream Mach numbers, the accuracy is still better because the Mach number behind the shock is lower. For example, at Mach 5 the error is only 0.5 percent for a perfect gas with $\gamma = 1.4$.

The gas equation of state has the form

$$\rho = \rho(T, p) \tag{429a}$$

$$h = h(T, p) \tag{429b}$$

In the case of a frozen shock, the relations (429) are assumed to be the equations for a thermally perfect but calorically imperfect gas:

$$\rho = \frac{Wp}{RT} \tag{430a}$$

$$h = h(T) \tag{430b}$$

For the equilibrium shock, the relations (429) are embodied in a subroutine (EQCALC) which computes the thermochemical equilibrium state of a gas mixture at specified temperature and pressure. In this case, neither of the equation of state relations can be expressed in analytical form.

NATA calculations of the stagnation conditions on a model are carried out in two stages. First, the conditions immediately behind the shock are computed by simultaneous solution of the Rankine-Hugoniot conservation relations (427) and the equation of state (429). Then the stagnation conditions are calculated by simultaneous solution of equations (428) and (429).

The equations (427) for the normal shock can be rewritten in terms of the density ratio

$$\epsilon_\rho \equiv \rho_1/\rho_2 \tag{431}$$

in the following form:

$$p_2 = p_1 + \rho_1 u_1^2 (1 - \epsilon_\rho) \tag{432a}$$

$$h_2 = h_1 + \frac{1}{2} u_1^2 (1 - \epsilon_\rho^2) \tag{432b}$$

In (432), equation (427b) has been used to eliminate the velocity u_2 from the remaining two equations (427a), (427c).

For both the equilibrium shock and the frozen shock, the solution involves an iteration on the temperature T_2 of the gas immediately behind the normal shock. For each estimate of T_2, the static enthalpy h_2 is calculated both from (432b) and from the equation of state relation (429b) or (430b). The correct temperature T_2 is the one for which these two enthalpy values are equal.

In the case of a frozen shock, the gas enthalpy (430b) depends on temperature only, not on pressure. It is computed from the species enthalpies $H_j(T_2)$ using equation (275). In the solution for the frozen shock, the mole fractions are assumed constant across the shock, so that the free stream values are used. To calculate the second h_2 value from (432b), the density ratio ϵ_ρ must be known. In the case of the frozen shock, since the gas is assumed thermally perfect and since the molecular weight $\mathbb{W}$ behind the shock is the same as that ahead of the shock, the density ρ_2 behind the shock is given by

$$\rho_2 = \rho_1 \cdot \frac{p_2}{p_1} \cdot \frac{T_1}{T_2} \tag{433}$$

From (431) and (433)

$$\epsilon_\rho = \frac{p_1}{p_2} \cdot \frac{T_2}{T_1} \tag{434}$$

Substitution of (434) into (432a) gives a quadratic equation for the pressure p_2:

$$p_2^2 - p_T p_2 + A_p = 0 \tag{435}$$

where

$$p_T = p_1 + \rho_1 u_1^2 \tag{436a}$$

$$A_p = \frac{\rho_1 u_1^2 p_1 T_2}{T_1} \tag{436b}$$

The applicable solution of (435) is

$$p_2 = \frac{1}{2}\left[p_T + \sqrt{p_T^2 - 4 A_p} \right] \tag{437}$$

For each estimate of the temperature T_2 in the iterative solution of the equations for the frozen normal shock, p_2 is calculated from (437) and ϵ_ρ is then obtained from (434). This ϵ_ρ value is then used to compute h_2 from (432b). The resulting h_2 value is compared with the one from (275) to determine whether convergence has been achieved and if not, to select an improved estimate of T_2 for the next iteration.

In the case of an equilibrium shock, the solution is slightly more complicated because the enthalpy (429b) depends upon the pressure p_2, and because the calculation of ϵ_ρ for each estimate of T_2 cannot be performed analytically but requires an inner iteration. For each trial value of T_2, the corresponding pressure p_2 and density ratio ϵ_ρ are obtained by solving equations (429), (431) and (432a), as follows:

1. An initial estimate of ϵ_ρ is chosen and is used to calculate an initial estimate of p_2 from (432a).

2. The equilibrium equation of state (429a) is used to compute

   $$\rho_2 = \rho(T_2, p_2)$$

3. The new density ratio

   $$\epsilon'_\rho = \rho_1/\rho_2$$

   is calculated.

4. The new ratio ϵ'_ρ is compared with the old value ϵ_ρ to determine whether the inner iteration has converged. The criterion is that the two values be equal to within 0.1 percent.

5. If not, the quantity

   $$a = p_2/\rho_2$$

   is computed, and a new estimate of p_2 is obtained from

   $$p_2 = \frac{1}{2}\left[p_T + \sqrt{{p_T}^2 - 4{\rho_1}^2 {u_1}^2 a}\right] \qquad (438)$$

   Equation (438) is equivalent to (437) with

   $$A_p = {\rho_1}^2 {u_1}^2 a$$

   Thus, (438) is an approximation to the pressure p_2 corresponding to the assumed temperature T_2, based on neglecting the pressure dependence of the gas composition.

6. The steps beginning with (2) are repeated using the new p_2 from step (5).

This inner iteration to obtain ϵ_ρ and p_2 is repeated for each step of the main iteration on T_2. The logic of the iteration to determine T_2 is the same as for the frozen shock.

Once the conditions p_2, T_2, ρ_2 behind the shock have been obtained, the conditions at the inviscid stagnation point on the model are calculated by solving equations (428) and (429). The stagnation pressure is calculated directly from (428b), which is rewritten in the form

$$p_s = p_2 + \frac{1}{2}\rho_1 u_1^2 \epsilon_\rho \tag{439}$$

The stagnation temperature T_s is then obtained by an iterative solution of (428a) and (429b) or (430b).

8.1.2 Stagnation-Point Heat Flux

NATA calculations of stagnation-point heat transfer to models are based on a correlation formula which incorporates results of analyses by Fay and Riddell (ref. 49), Bade (ref. 50), Finson and Kemp (ref. 51) and Goulard (whose work is reviewed by Dorrance, ref. 52, pp. 92-93). Fay and Riddell's correlation

$$\frac{N_{Nu,w}}{\sqrt{N_{Re,w}}} = 0.763\, N_{Pr}^{0.4} \left(\frac{\rho_e \mu_e}{\rho_w \mu_w}\right)^{0.4} \left[1 + (N_{Le}^{f} - 1)\frac{h_D}{h_e}\right] \tag{440}$$

(ref. 49) is widely used for calculating stagnation point heat transfer in high-temperature air. The non-dimensional groups appearing in this formula are defined as follows:

Nusselt number based on property values at the wall

$$N_{Nu,w} = \frac{q_s \times c_{pw}}{K_w(h_e - h_w)} \tag{441}$$

Reynolds number based on property values at the wall

$$N_{Re,w} = \frac{\rho_w u_e x}{\mu_w} \tag{442}$$

Frozen Prandtl number (assumed constant)

$$N_{Pr} = \frac{c_p \mu}{K} \tag{443}$$

Lewis number (assumed constant)

$$N_{Le} = \frac{D_{12} \rho c_p}{K} \tag{444}$$

The other notations used in (440) to (444) are:

c_p = specific heat (chemically frozen)

D_{12} = binary diffusion coefficient for atoms and molecules

f = 0.52 for an equilibrium boundary layer, 0.63 for a frozen one

h = enthalpy

h_D = enthalpy of dissociation per unit mass for the gas in the external flow

K = thermal conductivity (chemically frozen)

q_s = stagnation point heat flux

u = velocity component in the direction parallel to the body surface

x = radial distance along the body surface from the stagnation point

μ = viscosity

ρ = density

The subscript notation is

e = conditions at the stagnation point of the external flow

w = conditions at the body surface

It is easy to show from the above definitions that

$$\frac{N_{Nu,e}}{\sqrt{N_{Re,e}}} = \frac{N_{Pr,e}}{N_{Pr,w}} \sqrt{\frac{\rho_w \mu_w}{\rho_e \mu_e}} \frac{N_{Nu,w}}{\sqrt{N_{Re,w}}} \tag{445}$$

Thus, for constant Prandtl number the Fay-Riddell formula (440) can be rewritten in terms of Nusselt and Reynolds numbers based on property values at the edge of the boundary layer in the form

$$\frac{N_{Nu,e}}{\sqrt{N_{Re,e}}} = 0.763\ N_{Pr}^{0.4} \left(\frac{\rho_w \mu_w}{\rho_e \mu_e}\right)^{0.1} \left[1 + (N_{Le}^{f} - 1)\frac{h_D}{h_e}\right] \tag{446}$$

The Fay-Riddell correlation (440) or (446) is a curvefit to the results of 49 numerical solutions of the stagnation-point laminar boundary layer equations. The solutions included cases in which the boundary layer was assumed to be in chemical equilibrium, cases in which finite rates were used for the dissociation/recombination reactions, and cases with a chemically frozen boundary layer. In all cases, the viscosity was assumed to be given by a Sutherland formula,

$$\mu = \mu_0 \left(\frac{T}{T_0}\right)^{3/2} \frac{T_0 + T_S}{T + T_S} \tag{447}$$

with $\mu_0 = 1.72 \times 10^{-4}$ poise, $T_0 = 273^o$ K, and $T_S = 113^o$ K, and the Prandtl number was assumed to have the constant value 0.71. The Fay-Riddell formula (440) or (446), with these gas transport properties, with f = 0.52 (equilibrium boundary layer), and with a Lewis number $N_{Le} = 1.4$, has been found to correlate measurements of stagnation-point heat transfer in air to within the experimental accuracy of about ±20 percent (ref. 52, p. 91; ref. 53), at temperatures up to the onset of ionization effects.

Although the Fay-Riddell correlation was developed specifically for dissociated air, it can also be used to estimate stagnation-point heat transfer in other gas mixtures. This is done in NATA. The transport properties μ, K, N_{Pr}, N_{Le}, appearing in (446) and in the defining equations (441) and (442) for the Nusselt and Reynolds numbers, are computed by the NATA transport subroutine package (Section 3).

Air is treated in the same way as other gases; i.e., transport properties computed by the code are used in place of the properties, such as (447), assumed by Fay and Riddell in their calculations. For this reason, a minor modification of the correlation formula (446) is required. The Sutherland formula (447) for the viscosity of air is quite inaccurate at high temperatures. For example, at 7000° K and 1 atm pressure, the value based on (447) is 35 percent lower than the value given by Yos' calculations (ref. 54). At high temperatures, the Sutherland formula is practically equivalent to a power-law viscosity formula, $\mu = A T^{\omega}$, with the exponent $\omega = 0.5$, whereas realistic calculations for equilibrium air (ref. 54) can be approximated by the power law with $\omega \simeq 0.7$ in the range from room temperature up to 5000° K. At higher temperatures, the viscosity first increases still more rapidly, then passes through a maximum and falls off.

The value of the exponent ω affects the dependence of the stagnation-point heat flux upon the enthalpy ratio $g_w = h_w/h_e$ across the boundary layer (ref. 50). For $\omega = 0.5$, the correlation parameter $N_{Nu,e}/\sqrt{N_{Re,e}}$ decreases with increasing enthalpy ratio. This is the dependence which Fay and Riddell fitted using the factor $(\rho_w \mu_w/\rho_e \mu_e)^{0.1}$ in (446). However, their representation of this dependence is valid only for $\omega = 0.5$ (or for the Sutherland law). For $\omega = 1$, $(\rho_w \mu_w/\rho_e \mu_e)$ is equal to unity for all values of the enthalpy ratio, but $N_{Nu,e}/\sqrt{N_{Re,e}}$ increases slightly with increasing g_w. For $\omega \simeq 0.7$ to 0.8, $(\rho_w \mu_w/\rho_e \mu_e)$ varies with g_w but $N_{Nu,e}/\sqrt{N_{Re,e}}$ is practically independent of g_w.

Since the viscosity of air, as calculated in NATA, is approximated by a power law with $\omega \simeq 0.7$ for temperatures up to 5000° K, the results of reference 50 indicate that the dependence of the correlation parameter $N_{Nu,e}/\sqrt{N_{Re,e}}$ upon the enthalpy ratio should be weak. For this reason, the Fay-Riddell correlation (446) is adjusted for the use of the real air viscosity in place of the Sutherland law (447) by omitting the factor $(\rho_w \mu_w/\rho_e \mu_e)^{0.1}$ representing the dependence on the enthalpy ratio across the boundary layer:

$$\frac{N_{Nu,e}}{\sqrt{N_{Re,e}}} = \left(\frac{N_{Nu}}{\sqrt{N_{Re}}}\right)_0 \left[1 + (N_{Le}^{f} - 1)\frac{h_D}{h_e}\right] \tag{448}$$

where

$$\left(\frac{N_{Nu}}{\sqrt{N_{Re}}}\right)_0 = C(j)\, N_{Pr,w}^{0.4} \tag{449}$$

is the laminar heat transfer parameter for a low-temperature flow with constant Prandtl number and $\rho\mu$ = constant through the boundary layer. In (449), C(j) is a coefficient which depends upon body geometry. For a stagnation point in two-dimensional flow (j=0), according to Squire (ref. 55),

$$C(0) = 0.570 \tag{450a}$$

For an axisymmetric stagnation point (j = 1), from Sibulkin (ref. 56),

$$C(1) = 0.763 \tag{450b}$$

These values (450) can also be obtained from the results of Dewey and Gross (ref. 26).*

Equation (448) shows that the laminar heat transfer parameter, evaluated using gas properties in the external flow, may be approximated as the product of the low-temperature correlation function (449) and a correction factor representing the effects of heat transfer by diffusion and recombination of atoms. Substitution of the definitions for $N_{Nu,e}$ and $N_{Re,e}$ (analogous to equations (441) and (442) for $N_{Nu,w}$ and $N_{Re,w}$) into (448) gives the following expression for the stagnation-point heat flux:

$$q_s = \frac{C(j)}{N_{Pr}^{0.6}} \left[\rho_e \mu_e \left(\frac{du_e}{dx} \right)_s \right]^{1/2} (h_e - h_w) \left[1 + (N_{Le}^{f} - 1) \frac{h_D}{h_e} \right] \tag{451}$$

In the vicinity of the stagnation point, the velocity u_e is proportional to the radial distance x from the stagnation point. Thus, in (451) the ratio u_e/x has been replaced by the stagnation-point velocity gradient, $(du_e/dx)_s$.

A further minor modification of the Fay-Riddell formula has been made to permit inclusion of the effects of surface catalytic efficiency in the calculations. In the case of a frozen boundary layer, (446) and (451) assume that the model surface is perfectly catalytic for recombination of atoms. In NATA, (451) has been modified to allow for surface catalytic efficiency less than 1, using an approach suggested by Goulard (ref. 52, pp. 92-93):

$$q_s = \frac{C(j)}{N_{Pr}^{0.6}} \left[\rho_e \mu_e \left(\frac{du_e}{dx} \right)_s \right]^{1/2} \left[1 + (\Phi N_{Le}^{f} - 1) \frac{h_D}{h_e - h_w} \right] (h_e - h_w) \tag{452}$$

Here Φ is a catalytic factor which can take values between 0 (no catalysis) and an upper limit which is less than 1 for a perfectly catalytic surface. Equation (452) is used only for the frozen boundary layer. For the equilibrium boundary layer, the factor Φ is omitted because, in that case, recombination of atoms is accomplished by reactions in the boundary layer regardless of the properties of the model surface. For $\Phi = 0$, (452) makes the heat flux proportional to $(h_e - h_D - h_w)$. According to Goulard's analysis, Φ is given by

$$\Phi = \left\{ 1 + \frac{0.47 \, (N_{Le}/N_{Pr})^{2/3} \, [2(du_e/dx)_s \rho_e \mu_e]^{1/2}}{\rho_w k_{Rw}} \right\}^{-1} \tag{453}$$

*To get (450) from the data in Dewey and Gross, it is necessary to note that the Falkner-Skan parameter β is 1 for j=0 and 0.5 for j=1, and that $N_{Nu}/\sqrt{N_{Re}} = \sqrt{j+1}\ \theta'(0)$ for $t_w = 1$.

where k_{Rw} is the surface recombination rate constant, defined such that the mass of atoms recombining on the surface per unit area per unit time is k_{Rw} times the concentration of atoms in mass per unit volume in the gas at the surface. The units of k_{Rw} are cm/sec.

In NATA, the dissociation enthalpy h_D is calculated as

$$h_D = \frac{1}{W} \sum_{\text{atoms}} X_i H_{i0}^{\circ} \tag{454}$$

in which W is the mean molecular weight, X_i is the mole fraction for the ith species, and H_{i0}° is the molar enthalpy of formation for the species. Only neutral atoms are included in the sum. The Lewis number N_{Le} is calculated for an atom-molecule diffusion process which is assumed to be dominant or characteristic; in the standard air models, N_{Le} is computed based on the $O\text{-}N_2$ diffusion coefficient. Thus, the significant recombination process is assumed to be $2O \longrightarrow O_2$. In the planetary atmosphere (CO_2-N_2-Ar) models, the bracketed factor containing the Lewis number in (448), (451), and (452) is omitted since there is no theoretical support for applying it to a gas mixture so different from air.

The boundary layer solutions of Fay and Riddell did not include effects of ionization of the air. Flows with copious free-stream ionization are within the intended scope of application of the NATA code. Gas ionization affects the structure and properties of a laminar boundary layer primarily through its effects on the gas transport properties. The main changes in transport properties due to ionization are as follows:

(1) The chemically frozen thermal conductivity K_f increases greatly as a result of the high conductivity of the free electrons.

(2) Energy transport by ambipolar diffusion and recombination of electron-ion pairs occurs. This process further increases the effective thermal conductivity. However, this reaction conductivity is considerably less important than the corresponding effect due to dissociation and recombination of diatomic molecules in air, because the large charge exchange cross sections impede the diffusion.

(3) The viscosity decreases as a result of the large momentum-transfer cross section for collisions of charged particles.

As a result of these changes, the (frozen) Prandtl number $N_{Pr} = c_{pf}\,\mu/K_f$ decreases markedly as the amount of ionization increases. Thus, when the external flow is ionized to a substantial extent, the frozen Prandtl number is considerably smaller at the outer edge of the boundary layer than at the cold surface, where the ionization is negligible. This variation of the frozen Prandtl number is a new feature, not previously encountered in studies of lower temperature boundary layers. In air, for example, the equilibrium Prandtl number $(c_p)_{eq}\,\mu/K_{eq}$ (where K_{eq} includes the reaction conductivity) has peaks and dips due to the reactions, but the frozen Prandtl number varies by only a few percent in the temperature region below the onset of ionization.

Available stagnation point boundary layer solutions have been studied to obtain a correlation of the effects of free-stream ionization upon stagnation-point heat transfer. These solutions include the calculations of Finson and Kemp (refs. 51, 57) for the noble gases, those of DeRienzo and Pallone (ref. 58) for air, and those of Fay and Kemp (ref. 59) for nitrogen.

Finson and Kemp (refs. 51, 57) computed solutions of the laminar stagnation-point boundary layer equations in axisymmetric and two-dimensional flows of ionized argon and xenon. They included energy transport by ambipolar diffusion and recombination, and obtained two sets of solutions, one based on local thermochemical equilibrium through the boundary layer, the other based on frozen chemistry but assuming a perfectly catalytic wall. The cases computed were chosen to simulate situations for which experimental data were available in the literature.

Figure 31 presents a correlation of Finson and Kemp's results for the equilibrium boundary layer. The abscissa in this figure is the ratio of the frozen Prandtl number across the boundary layer. In all cases, the wall temperature was 300° K; thus, $N_{Pr,\,w}$ was constant at its low-temperature value of 2/3 for monatomic gases. The frozen Prandtl number $N_{Pr,\,e}$ in the external flow was calculated from the transport property formulas assumed in Finson and Kemp's calculations, rather than from other, possibly more accurate data, because the object of the study was to correlate the calculated heat flux with the transport properties upon which it was based.

The ordinate in figure 31 is the ratio of the non-dimensional laminar heat transfer parameter, $(N_{Nu}/\sqrt{N_{Re}})_e$, based on gas properties in the external flow, to the value $(N_{Nu}/\sqrt{N_{Re}})_0$ for a low-temperature flow, given by (449). Bade (ref. 50) has shown that this ratio is approximately equal to unity for stagnation point boundary layers in helium, neon, argon, krypton, and xenon at temperatures up to the onset of free-stream ionization. Figure 31 shows that, in the ionization region, this ratio varies over a wide range. The straight line drawn to fit the data points in the figure represents the equation

$$\frac{(N_{Nu}/\sqrt{N_{Re}})_e}{(N_{Nu}/\sqrt{N_{Re}})_0} = \left(\frac{N_{Pr,\,e}}{N_{Pr,\,w}}\right)^{0.7} \tag{455}$$

Substitution of (441), (442), and (449) into (455) gives the following formula for stagnation point heat transfer in a noble gas, valid from low temperatures up to and including the ionization region:

$$q_s = C(j)\,\frac{\sqrt{\rho_e \mu_e (du_e/dx)_s}}{(N_{Pr,\,w}\,N_{Pr,\,e})^{0.3}}\,(h_e - h_w) \tag{456}$$

This formula is used in NATA for calculations of stagnation point heat transfer in helium and argon. Since the effect of ionization is to decrease $N_{Pr,\,e}$, equation (456) shows that free-stream ionization increases the stagnation point heat flux above the value predicted by the theory of reference 50 for a gas of neutral atoms at the same enthalpy.

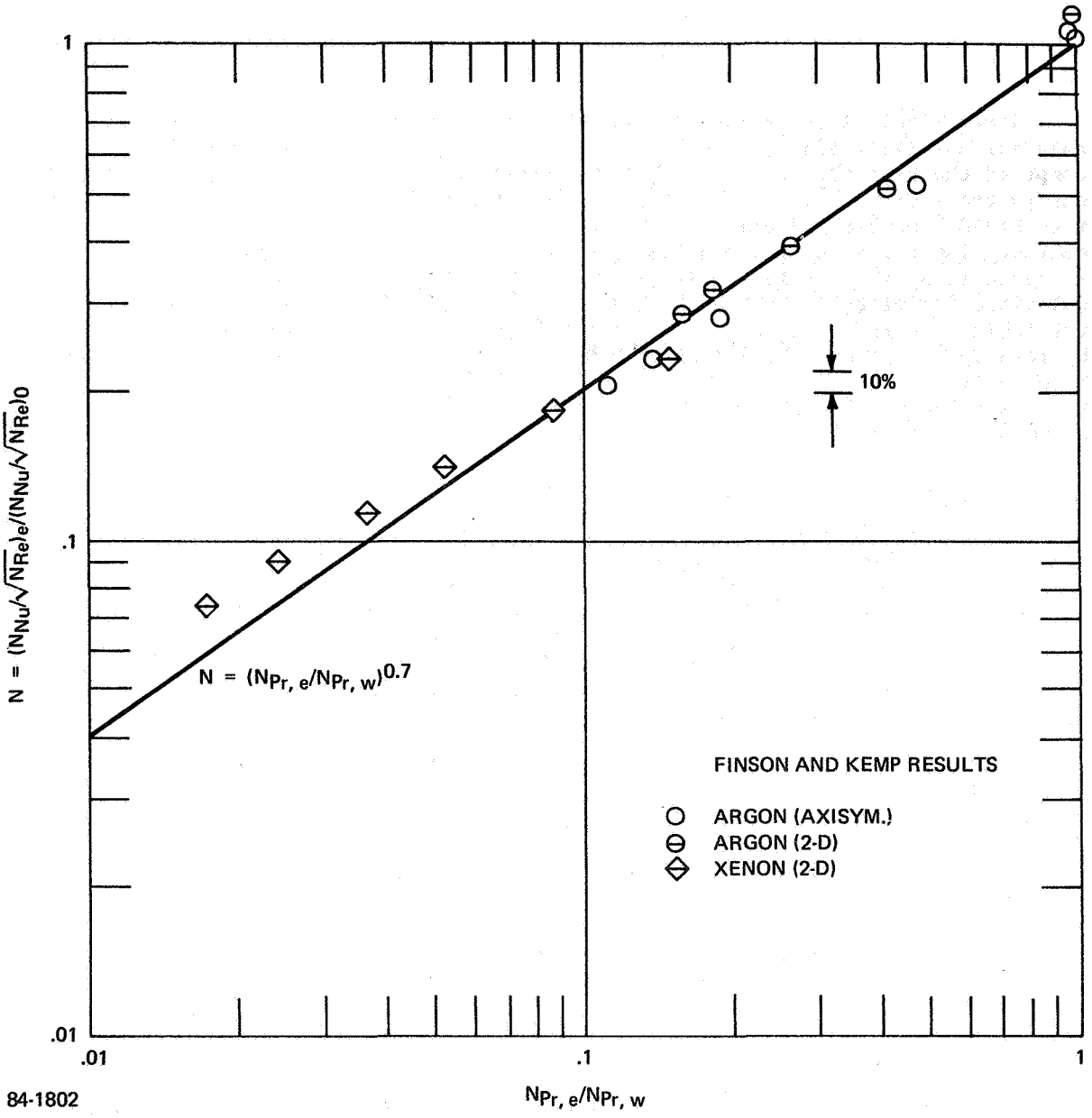

Figure 31 CORRELATION OF STAGNATION-POINT HEAT TRANSFER IN IONIZED NOBLE GASES

Theoretical calculations of stagnation point heat transfer are also available for partially ionized air and nitrogen. DeRienzo and Pallone (ref. 58) computed the heat flux through an equilibrium boundary layer in air. They took energy transport by diffusion and reactions into account by using the equilibrium Prandtl number and omitting the diffusion equations from the system to be solved. Their results for equilibrium air with no blowing at the wall are represented by the circles in figure 32. Fay and Kemp (ref. 59) performed calculations for nitrogen, using a model in which the reaction conductivity due to the ionization reaction $N \rightleftharpoons N^+ + e$ was neglected. This approximation was justified by reference to the large charge-exchange cross section for nitrogen. Fay and Kemp explicitly included energy transport by diffusion of neutral atoms and their recombination to form diatomic molecules. Their results are represented by the diamonds and triangles in figure 32.

Both reference 58 and reference 59 tabulate their results in terms of the parameter $(N_{Nu}/\sqrt{N_{Re}})_w$, based on gas properties at the cold wall. For the preparation of figure 32, these data were converted into $(N_{Nu}/\sqrt{N_{Re}})_e$ values with the aid of equation (445). In each case, the transport properties assumed in the reported boundary layer solutions were used in equation (445) and in evaluating the abscissa of figure 32, since the object of the study was to correlate calculated heat transfer data with the transport properties upon which the calculations were based. In the case of reference 58, the surviving documentation is not sufficient to specify the assumed transport properties exactly, so that there is some uncertainty as to where the points should lie. Fay and Kemp provided enough information to permit reconstructing the transport property values for each of their solutions.

The scatter of the points in figure 32 is considerably greater than that in figure 31, but the overall trend is similar. The straight line in figure 32 again represents equation (455). The fit would be a little better if the exponent of 0.7 in (455) were replaced by a slightly lower value, e.g., 0.65. However, (455) accounts for the main part of the variation of the ordinate. The uncorrelated variations probably result mainly from energy transport by diffusion and recombination of atoms. Trend lines drawn through the Fay-Kemp results for L = 0.3 and L = 1 (triangles and inverted triangles) bracket nearly all of the data from both references 58 and 59. The parameter L is not the Lewis number as defined by (444), but is a related quantity which (unlike N_{Le}) is approximately constant over the temperature range in which nitrogen molecules dissociate. Fay and Kemp's results indicate that the stagnation point heat flux varies roughly as $L^{0.37}$.

In NATA, stagnation point heat transfer in air and other molecular gases under conditions of free stream ionization is calculated by combining the ionization effect represented by equation (455) with the atom diffusion and recombination effect given by (448) (and adjusted for surface catalytic efficiency in (452)). This combination of correlations gives

$$\frac{(N_{Nu}/\sqrt{N_{Re}})_e}{(N_{Nu}/\sqrt{N_{Re}})_0} = \left(\frac{N_{Pr,e}}{N_{Pr,w}}\right)^{0.7} \left[1 + (\Phi\, N_{Le}{}^f - 1)\, \frac{h_D}{h_e - h_w}\right] \qquad (457)$$

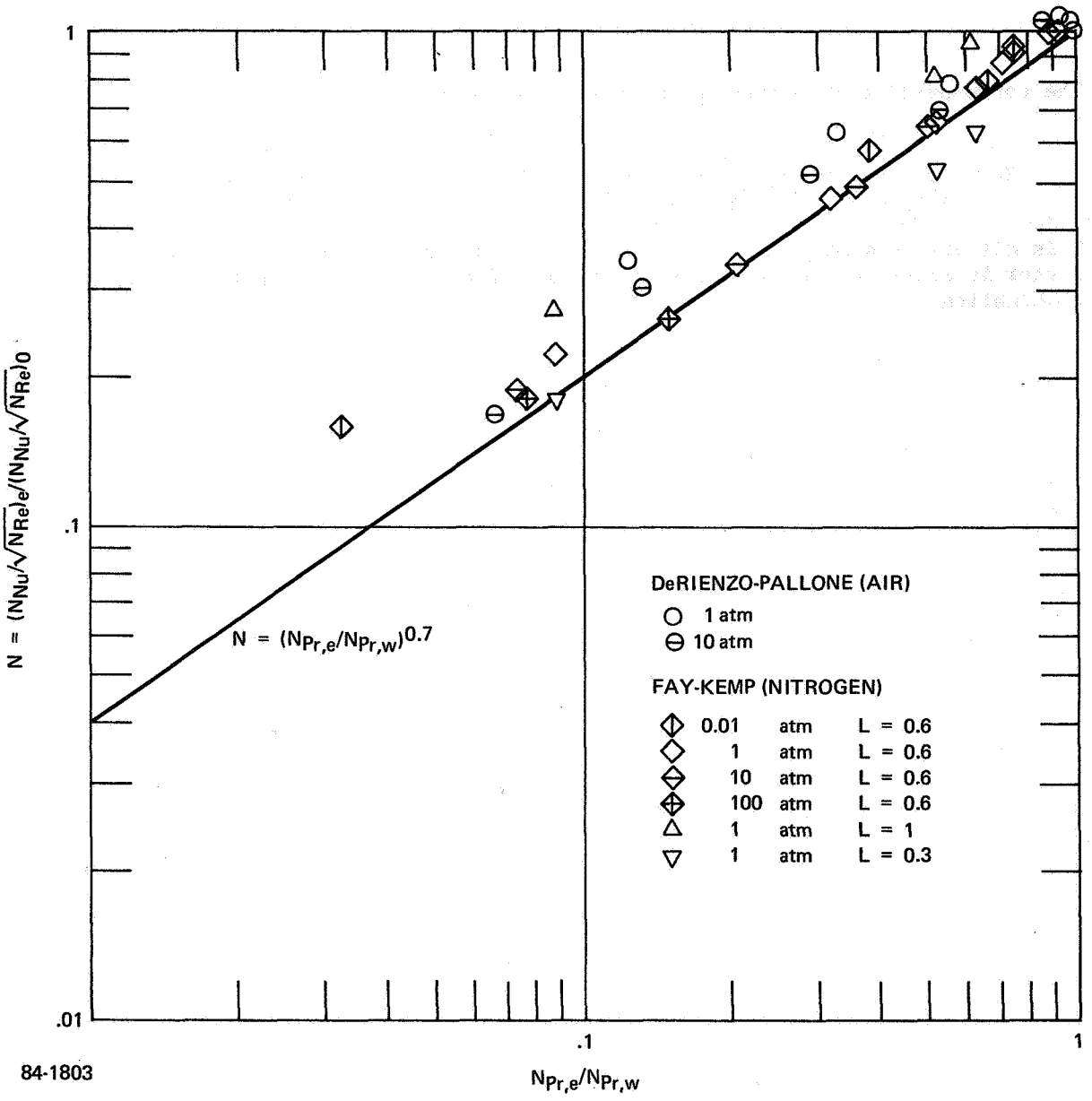

Figure 32 CORRELATION OF STAGNATION-POINT HEAT TRANSFER IN IONIZED AIR AND NITROGEN

The corresponding stagnation point heat flux formula is

$$q_s = \frac{C(j)}{(N_{Pr,\,w}\, N_{Pr,\,e})^{0.3}} \sqrt{\rho_e \mu_e \left(\frac{du_e}{dx}\right)_s} \left[1 + (\Phi\, N_{Le}{}^{f} - 1) \frac{h_D}{h_e - h_w}\right] (h_e - h_w) \qquad (458)$$

This differs from equation (456), which is used for the noble gases, only by the factor in square brackets representing the effects of atom diffusion and recombination.

8.1.3 Stagnation Point Velocity Gradient

The stagnation-point velocity gradient $(du_e/dx)_s$ appearing in (452), (456), and (458) depends upon the free-stream velocity u_1, the model nose radius R_b, the shock density ratio ϵ_ρ, and the model shape. It also depends weakly upon the gas equation of state, i.e., the effective specific heat ratio, γ.

For hemispherical models in axisymmetric flow and cylindrical models in two-dimensional flow, NATA computes the velocity gradient using the modified Newtonian approximation (ref. 60):

$$\frac{p - p_1}{p_s - p_1} = \cos^2 \beta \qquad (459)$$

where p is the local pressure on the body surface at a point where the incident flow ahead of the shock makes an angle β with the normal to the surface. As before, p_1 is the free-stream static pressure ahead of the shock and p_s the stagnation pressure on the body. Near the stagnation point, the pressure and flow velocity are related by the incompressible Bernoulli equation

$$p_s = p + \frac{1}{2} \rho_s\, u_e{}^2 \qquad (460)$$

and the distance along the surface from the stagnation point is given by

$$x = R_n\, \beta \simeq R_n \sin \beta \qquad (461)$$

where R_n is the body radius of curvature at the stagnation point. Combination of (459), (460) and (461) gives

$$\left(\frac{du_e}{dx}\right)_s \simeq \frac{1}{R_n} \sqrt{\frac{2\, p_s}{\rho_s} \left(1 - \frac{p_1}{p_s}\right)} \qquad (462)$$

Equation (459) is an empirical pressure distribution which is reasonably accurate for spheres. Figure 33 compares the non-dimensional velocity gradient parameter.

$$\frac{R_n}{u_1} \left(\frac{du_e}{dx}\right)_s = \frac{1}{u_1} \sqrt{\frac{2\, p_s}{\rho_s} \left(1 - \frac{p_1}{p_s}\right)} \qquad (463)$$

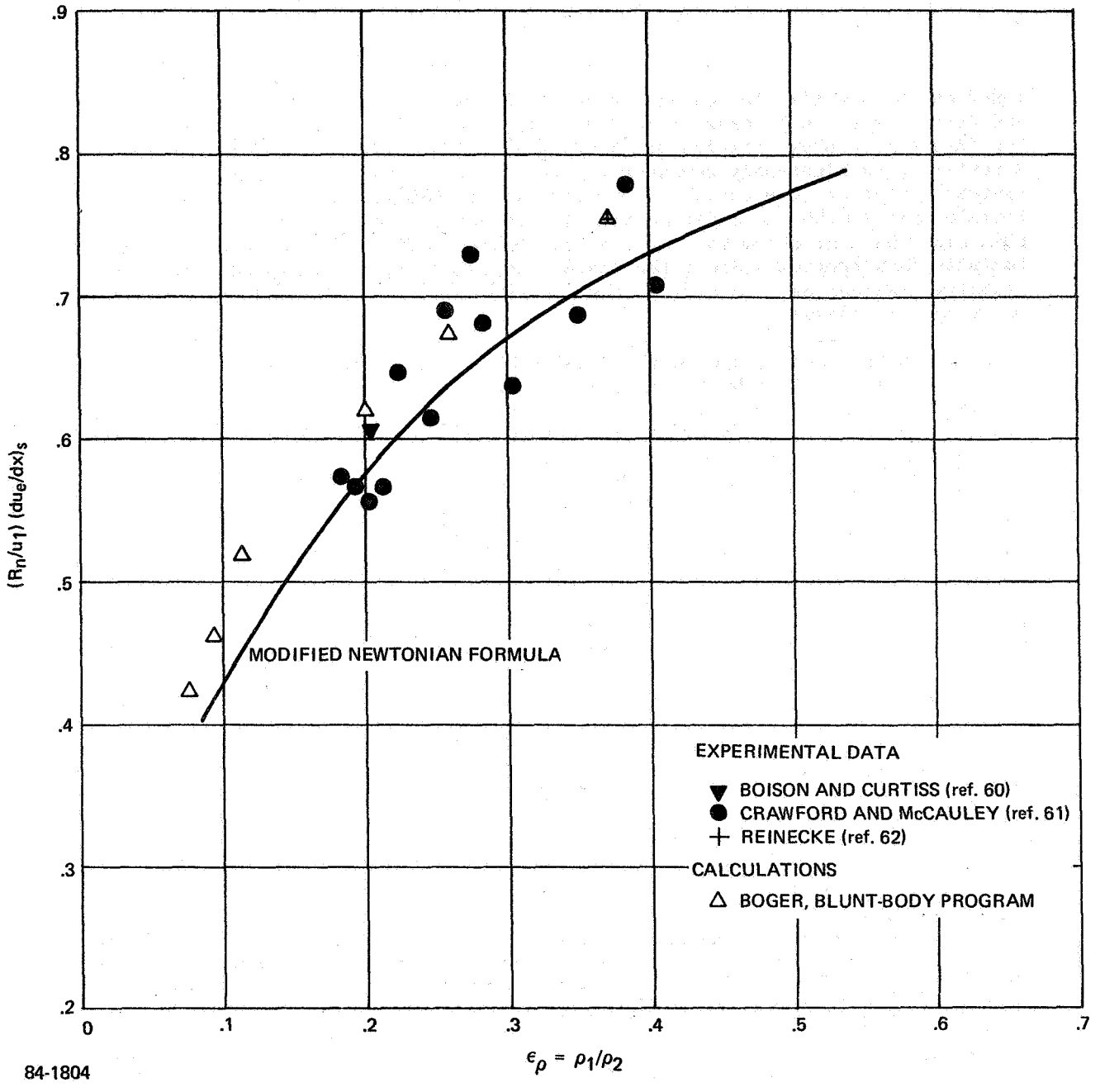

Figure 33 STAGNATION-POINT VELOCITY GRADIENT PARAMETER FOR SUPERSONIC FLOW OF AIR OVER A SPHERE

based on the modified Newtonian formula (462), with experimental data from Boison and Curtiss (ref. 60), Crawford and McCauley (ref. 61), and Reinecke (ref. 62).* The figure also shows results of unpublished calculations carried out with the Moretti-Bleich blunt-body computer program (ref. 63) by R. C. Boger of Avco Systems Division. The curve represents equation (463). The modified Newtonian formula agrees with the experimental data to within their scatter, and lies less than eight percent below the trend of the theoretical results from the blunt-body inviscid flow program. Since the stagnation point heat flux depends upon the velocity gradient as $(du_e/dx)_s^{1/2}$, the accuracy of (463) for models with spherical noses appears adequate.

Information surveyed by Hayes and Probstein (ref. 64, pp. 422-423) suggests that the pressure distribution in two-dimensional hypersonic flow over a circular cylinder is given approximately by equation (459). The velocity gradient parameter $(R_n/u_1)(du_e/dx)_s$ is apparently a little lower for cylinders than for spheres. This difference, if real, is neglected in NATA.

Figure 34 summarizes some available data on the stagnation point velocity gradient in axisymmetric flow over a flat-faced cylinder. The experimental data from reference 60 lie about 20 percent below the results of Vinokur's (refs. 65, 66) approximate constant density solution. The unbroken curve shown represents the analytical relation

$$\frac{R_b}{u_1}\left(\frac{du_e}{dx}\right)_s = \frac{\epsilon_\rho}{1.34 + 4.2\,(\sqrt{\epsilon_\rho} - 0.4)^2} \tag{464}$$

which is a curvefit to Vinokur's results for the flat-faced cylinder, divided by a factor of 1.2 to improve the fit to Boison and Curtiss's experimental data. In (464), R_b denotes the radius of the circular flat face.

Two-dimensional flow over a flat-faced plate has been analyzed by Cole and Brainerd (ref. 67) using the constant density approximation. According to Hayes and Probstein (ref. 64, p. 310), Cole and Brainerd's calculations give the stagnation point velocity gradient in the form

$$\frac{R_b}{u_1}\left(\frac{du_e}{dx}\right)_s = 0.64\,\epsilon_\rho \tag{465}$$

where R_n is the half width of the flat face. Hayes and Probstein (ref. 64, pp. 426-428) have compared Cole and Brainerd's results with those from other calculations.

Since the body radius R_b is equal to the nose radius of curvature R_n for spherical and cylindrical models, equations (463), (464), and (465) all indicate that the stagnation point velocity gradient $(du_e/dx)_s$ is equal to (u_1/R_b) times a non-dimensional function of the inviscid flow parameters on the stagnation streamline. Thus, the stagnation point heat flux (458) can be expressed in the form

$$q_s\sqrt{R_b} = \frac{C(j)}{(N_{Pr,w}N_{Pr,e})^{0.3}}\sqrt{\rho_e\mu_e u_1 G}\left[1 + (\Phi N_{Le}^{\,f} - 1)\frac{h_D}{h_e - h_w}\right](h_e - h_w) \tag{466}$$

*The authors are indebted to W. G. Reinecke of Avco Systems Division for assembling the data plotted in the figure.

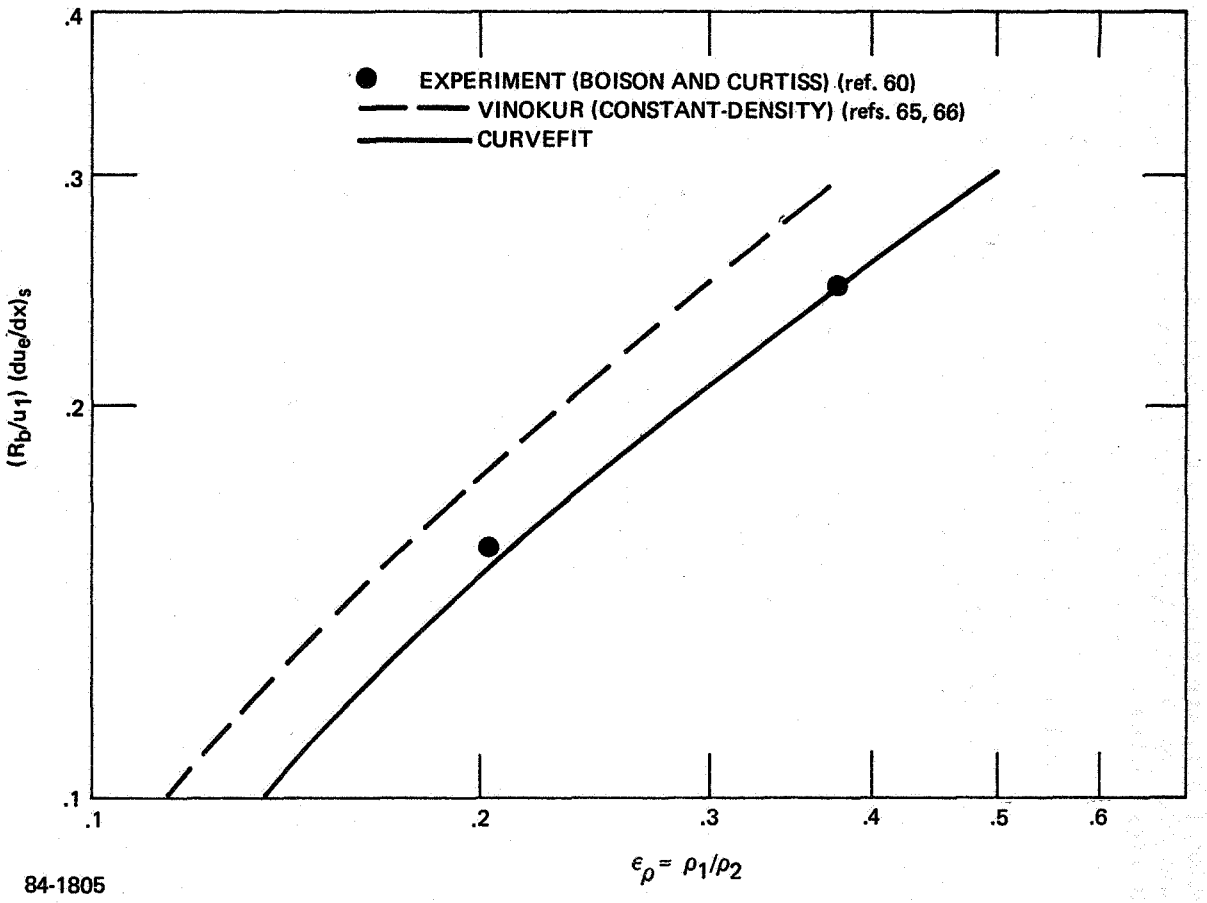

Figure 34 STAGNATION-POINT VELOCITY GRADIENT PARAMETER FOR AXISYMMETRIC SUPERSONIC FLOW OF AIR OVER A FLAT-FACED CYLINDER

where G denotes the non-dimensional velocity gradient parameter:

$$G = \frac{R_b}{u_1}\left(\frac{du_e}{dx}\right)_s \tag{467}$$

If the catalytic factor Φ is considered to be a given constant, then the right-hand side of (466) is independent of body radius. However, if Φ were assumed to be given by equation (453), the right-hand side of (466) would depend explicitly on R_b. The present version of NATA treats Φ as an input constant, so that (466) is independent of body radius.

8.1.4 Model Heat Flux Outputs

The stagnation point heat flux on the model is printed out as $q_s\sqrt{R_b}$, for up to eight cases. The following four values are printed when equilibrium shock calculations are done:

$[q_s\sqrt{R_b}]_{EFE}$	Equilibrium shock, flat-faced model, equilibrium boundary layer
$[q_s\sqrt{R_b}]_{EFF}$	Equilibrium shock, flat-faced model, frozen boundary layer
$[q_s\sqrt{R_b}]_{EHE}$	Equilibrium shock, hemispherical model, equilibrium boundary layer
$[q_s\sqrt{R_b}]_{EHF}$	Equilibrium shock, hemispherical model, frozen boundary layer

If frozen shock calculations are requested, the following four values are printed:

$[q_s\sqrt{R_b}]_{FFE}$	Frozen shock, flat-faced model, equilibrium boundary layer
$[q_s\sqrt{R_b}]_{FFF}$	Frozen shock, flat-faced model, frozen boundary layer
$[q_s\sqrt{R_b}]_{FHE}$	Frozen shock, hemispherical model, equilibrium boundary layer
$[q_s\sqrt{R_b}]_{FHF}$	Frozen shock, hemispherical model, frozen boundary layer

In addition to these values, NATA provides two other heat fluxes at each model point. One is based on a simple formula proposed by Hiester of Stanford Research Institute (ref. 68):

$$[q_s\sqrt{R_b}]_{SRI} = 0.0417\sqrt{p_s}\,(h_e - h_w) \tag{468}$$

where p_s is assumed expressed in atmospheres, h_e and h_w are in Btu/lb, and the left hand side is given in Btu/ft$^{3/2}$ sec. Equation (468) is an approximation to the Fay-Riddell formula for hemispherical models. The other additional value printed is an estimate of the heat flux to a flat plate with a sharp leading edge at zero angle of attack:

$$[q_w\sqrt{x}]_{FP} = \frac{0.332}{(N^*_{Pr})^{2/3}}\,(\rho^*\mu^* u_1)^{1/2}\,(h_r - h_w) \tag{469}$$

Here x represents the distance from the leading edge, and the gas properties N_{Pr}^*, ρ^*, μ^* are evaluated at a reference temperature T^* defined by

$$T^* = \frac{h^*}{h_s} \cdot T_0 \tag{470a}$$

$$h^* = \frac{1}{2}(h_e + h_w) + 0.22\,(h_r - h_e) \tag{470b}$$

$$h_r = h_e + Pr^{1/2}\,(h_s - h_e) \tag{470c}$$

where h^* is the reference enthalpy and h_r the recovery enthalpy. These formulas were obtained from Schlichting (ref. 21, p. 286), Jakob (ref. 69, pp. 428-430), and the first edition of Hayes and Probstein (ref. 25, pp. 296-297). Since they do not take low Reynolds number effects into account, they are expected to become inaccurate at large nozzle expansion ratios where the gas density becomes very low.

8.1.5 Low-Density Effects

The preceding stagnation point heat flux formulas are based on boundary layer theory and assume the existence of an inviscid shock layer. At large nozzle expansion ratios, the flow becomes highly rarefied and this system of approximations breaks down. According to Cheng (ref. 70), the influences of low-density effects upon the flow in the stagnation region of a blunt body can be classified into the following regimes of continuum flow based upon the value of a parameter $\mathfrak{E}\,K^2$:

Regime 0: Inviscid shock layer plus boundary layer

$\mathfrak{E}\,K^2$ extremely large

Regime 1: Vorticity-interaction and viscous-layer effects

$$\mathfrak{E}\,K^2 \geq O(1) \tag{471}$$

Regime 2: Merged-layer regime

$$O(\epsilon_\rho) \leq \mathfrak{E}\,K^2 \leq O(1) \tag{472}$$

The notation O(x) means "order of x". For $\mathfrak{E}\,K^2$ less than $O(\epsilon_\rho)$, the continuum flow description becomes inappropriate. The parameters $\mathfrak{E}$ and K^2 are defined by

$$\mathfrak{E} = \frac{\gamma - 1}{2\gamma} \tag{473a}$$

$$K^2 = \mathfrak{E}\,\frac{\rho_1 u_1 R_b}{\mu_s}\left(\frac{T^*}{T_0}\,\frac{\mu_0}{\mu^*}\right) \tag{473b}$$

where γ denotes the specific heat ratio and quantities with an asterisk superscript are evaluated at a reference temperature behind the shock.

The quantity $\tilde{\varepsilon} K^2$ is computed by NATA to provide a basis for evaluating the importance of low-density effects upon the stagnation-point heat flux. Based on a survey of experimental data given in figure 4.1 of reference 70, the increase in q_s due to vorticity-interaction and viscous-layer effects should be less than 10 percent for $\tilde{\varepsilon} K^2 \gtrsim 15$, and less than 20 percent for $\tilde{\varepsilon} K^2 \gtrsim 8$. For $\tilde{\varepsilon} K^2 \lesssim 1.5$, the heat flux decreases with further decreases in $\tilde{\varepsilon} K^2$ as a result of merged-layer effects. However, the heat flux should be within about 30 percent of the value based on boundary layer theory so long as $\tilde{\varepsilon} K^2 \gtrsim 0.1$.

In the calculation of $\tilde{\varepsilon} K^2$ by the code, $\tilde{\varepsilon}$ is computed from the shock density ratio ϵ_ρ:

$$\tilde{\varepsilon} = \frac{\epsilon_\rho}{1 + \epsilon_\rho} \tag{474}$$

which is based on the formula $\epsilon_{\rho_{lim}} = (\gamma - 1)/(\gamma + 1)$ for the density ratio of a strong shock in a perfect gas. The factor $(T^* \mu_0 / T_0 \mu^*)$ in (473b) is approximated by unity. Since the model radius R_b is not specified in the code, $\tilde{\varepsilon} K^2$ is computed and printed for $R_b = 0.3048$ m (1 ft). The parameter value $\tilde{\varepsilon} K^2$ for any specific model can be obtained by multiplying the printed value by the model radius in feet.

8.1.6 Shock Standoff Distance

NATA computes the ratio Δ/R_b of the shock standoff distance to the body radius for each type of model. This ratio is of interest because it is an observable of model tests in wind tunnels. In general, it depends upon the shock strength as measured by the density ratio ϵ_ρ, the model geometry, and the gas equation of state. The equation of state dependence is weak and is neglected in NATA.

For hemispherical models, Δ/R_b is computed from the following curvefit to Van Dyke's results (ref. 71 and ref. 64, p. 462):

$$\frac{\Delta}{R_b} = \begin{cases} 0.78\, \epsilon_\rho & \text{for } \epsilon_\rho \leq 0.19 \\ 0.78\, \epsilon_\rho \left[1 + 3.5\, (\epsilon_\rho - 0.19)^{1.6}\right] & \text{for } \epsilon_\rho > 0.19 \end{cases} \tag{475}$$

Figure 35 compares Van Dyke's results with values obtained using the computer program documented in reference 63 and with Vinokur's results (refs. 65, 66) based on the constant-density approximation. The two sets of results from numerical inviscid flowfield solutions are in good agreement. Vinokur's results are too low by about 17 percent.

For flat-faced cylindrical models in axisymmetric flow, Δ/R_b is calculated using a fit to Vinokur's results (refs. 65, 66), multiplied by a correction factor of 1.17 based on the comparison for spherical models in figure 35. The corrected fit is

$$\frac{\Delta}{R_b} = 1.12\, \epsilon_\rho^{0.39} \tag{476}$$

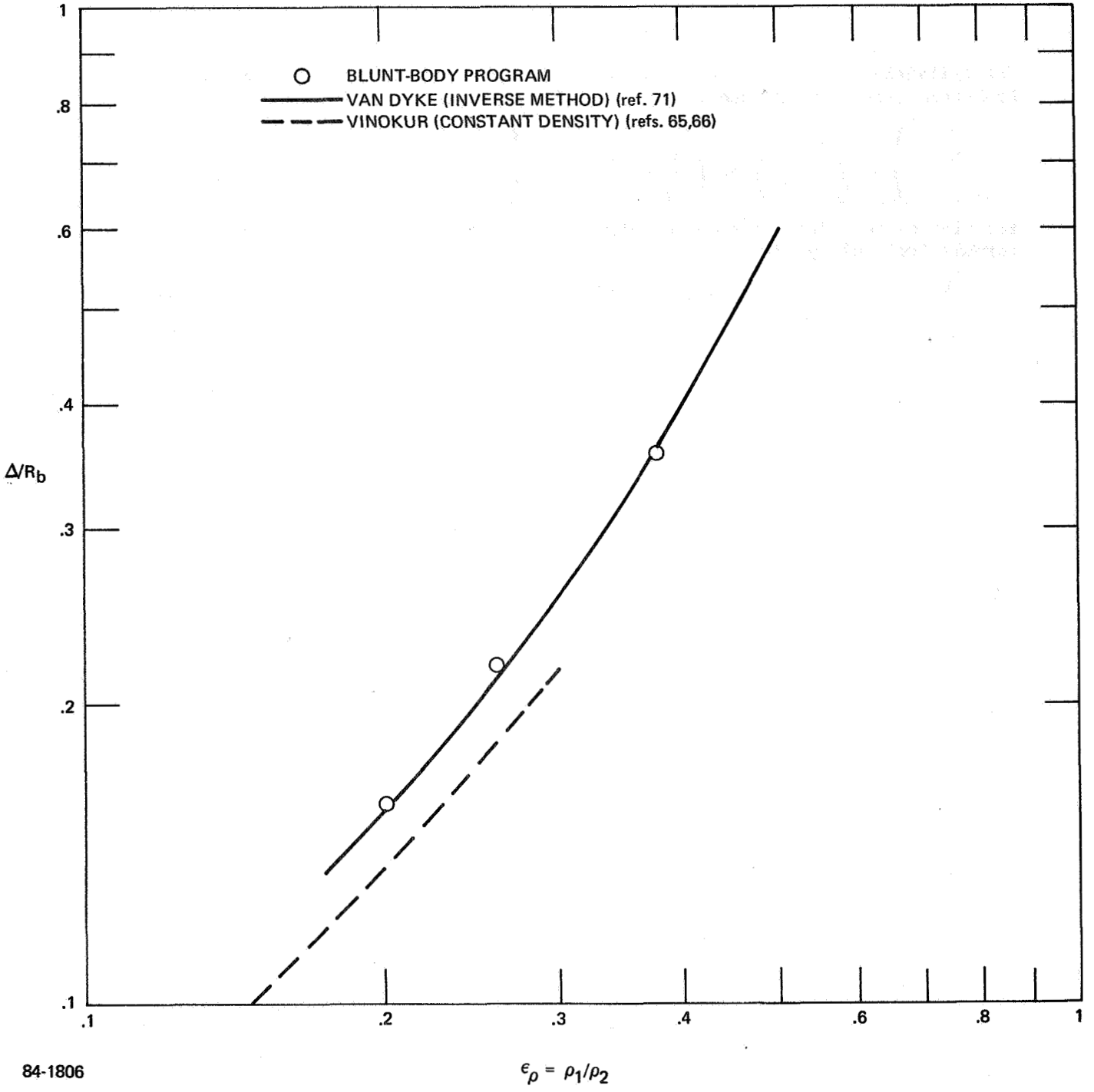

Figure 35 SHOCK STANDOFF DISTANCE ON A SPHERE

For cylindrical models in two-dimensional flow, equation (6.5.14) of Hayes and Probstein (ref. 64) is used*:

$$\frac{\Delta}{R_b} = \left\{ \frac{2}{\epsilon_\rho \left[\left(1 + \frac{1}{2}\epsilon_\rho\right) \ell n \left(\frac{4}{3\epsilon_\rho}\right) - \frac{1}{2}\epsilon_\rho \right]} - 1 \right\}^{-1} \tag{477}$$

For flat-faced models in two-dimensional flow, Δ/R_b is calculated from the formula (ref. 64, p. 310)

$$\frac{\Delta}{R_b} = -1.23 \sqrt{\epsilon_\rho}\, \ell n \left(0.79 \sqrt{\epsilon_\rho}\right) \tag{478}$$

8.1.7 Comparisons with Experimental Data

Scott (ref. 72) has measured pressure and heat transfer distributions over a 5.08-cm radius hemisphere in the NASA-Johnson Space Center 10 Mw arc tunnel. The test conditions are summarized in table I. The stagnation enthalpy was determined from careful energy balance and mass flow measurements. The models were positioned 2.5 cm downstream of the 0.508-m diameter nozzle exit. The 0.521-m effective test section diameter listed in table I was obtained by extrapolating the 15-degree expansion angle of the conical nozzle from the actual exit plane to the model station.

The free-stream conditions listed in the second part of table I are based upon runs with the current version of NATA and differ slightly from the conditions tabulated in reference 72. The initial conditions for the NATA solutions were the stagnation enthalpy and mass flow. Effects of the boundary layer displacement thickness upon the effective flow cross section at the throat were taken into account in the determination of the effective reservoir temperature and pressure from these data. The inviscid flow solution assumed chemical non-equilibrium. The boundary layer was included in the solution and had a major effect upon the effective area ratio at the test station.

Table II summarizes the measurements of model stagnation point conditions in reference 72, and presents NATA results for comparison. The conditions listed as NATA results are based on calculations for a chemically frozen shock layer and a frozen boundary layer. These assumptions concerning the chemical state of the flow around the model are justified by the low pressure.

The NATA predictions of stagnation pressure on the model are about 6 percent higher than the measurements in both cases. Since the stagnation pressure varies with the effective area ratio, this agreement is better than might have been expected in view of the uncertain accuracy of approximations used in the calculation of the displacement thickness for the boundary layer on the nozzle wall.

Scott (ref. 72) measured heat transfer to models coated with both nickel and Teflon in order to investigate catalytic effects. The catalytic efficiency

*Hayes and Probstein give the formula in terms of the shock radius, R_s. In (477), it has been re-expressed in terms of body radius R_b, assuming $R_s = R_b + \Delta$.

TABLE I

TEST CONDITIONS FOR STAGNATION CONDITION MEASUREMENTS

Case	1	2
Data		
Standard nozzle number	10	10
Stagnation enthalpy, MJ/kg	25.3	17.6
Total mass flow, g/sec	13.6	22.7
Test section diameter, m	0.521	0.521
Axial coordinate, m	0.950	0.950
NATA Results		
Mach number	10.1	9.3
Static temperature, ^{o}K	267	321
Static pressure, atm	3.65×10^{-5}	5.53×10^{-5}
Free-stream density, kg/m^3	3.05×10^{-5}	4.41×10^{-5}
Free-stream velocity, km/sec	4.35	4.07
Geometric area ratio	356	356
Effective area ratio	161	202
Free-stream mole fractions		
N_2	0.270	0.456
N	0.461	0.236
O	0.269	0.308
Other species	$< 3.2 \times 10^{-5}$	$< 1.1 \times 10^{-5}$

TABLE II

COMPARISON OF CALCULATED AND MEASURED STAGNATION CONDITIONS

Case	1	2
Measurements		
Pressure, atm	4.83×10^{-3}	6.26×10^{-3}
Heat flux (nickel), W/cm^2	56	55
Heat flux (Teflon), W/cm^2	36	35
Shock standoff, Δ/R_b	0.17	0.10
NATA Results		
Pressure, atm	5.17×10^{-3}	6.62×10^{-3}
Heat flux (non-catalytic), W/cm^2	35.0	35.1
Shock standoff, Δ/R_b	0.16	0.14
$h_D/(h_e - h_w)$	0.619	0.516
N_{Le}	0.824	0.961
Heat flux for $\Phi = 1$, W/cm^2	85.3	71.6
$\mathcal{E} K^2$	1.0	1.3
Re_F	130	220

of Teflon for atom recombination is much lower than that of nickel. The NATA calculations of stagnation point heat flux to a non-catalytic surface agree with the data for the Teflon-coated model to within about 3 percent. The higher heat transfer rates for nickel could be accounted for by assuming values for Φ less than unity in equation (466). Table II lists values of heat flux for $\Phi = 1$, calculated from the values for $\Phi = 0$ using (466) and the tabulated values of $h_D/(h_e - h_w)$ and N_{Le}.

The close agreement of the NATA stagnation point heat flux results with Scott's data for the Teflon-coated models has to be regarded as fortuitous. The low density parameter $\bar{\epsilon} K^2$, calculated from equations (473) and (474), is about unity in both cases. Thus, the flow around the model is on the boundary of the merged layer regime, and low-density effects upon the heat transfer are expected to be of substantial magnitude.

Table II includes values of Cheng's Reynolds number parameter Re_F, defined as

$$Re_F = \frac{\rho_1 u_1 R_b}{\mu_s} \cdot \frac{1}{\epsilon_\rho \sqrt{2}} = \frac{1 + \epsilon_\rho}{\epsilon_\rho^2 \sqrt{2}} \bar{\epsilon} K^2 \qquad (479)$$

Cheng has presented a correlation of stagnation point heat transfer as a function of this parameter (fig. 9 in ref. 73). For Re_F in the range from 100 to 200, the ratio q/q_{BL} of the actual heat transfer rate to its value based on boundary layer theory is about 1.0 ±0.1, within the scatter of the data. At somewhat higher values of Re_F in the vicinity of 500, q/q_{BL} peaks at about 1.1 ±0.2, before beginning its asymptotic approach toward unity as $Re_F \to \infty$.

Scott's calculations (ref. 72), based upon a two-dimensional viscous flow-field model, indicate that the heat flux to the Teflon-coated model is 20 to 30 percent higher than the flux to a completely non-catalytic surface. Thus, it appears likely that the NATA heat flux results are actually about 20 to 30 percent high under these low-density conditions.

Table II also gives experimental values of the ratio Δ/R_b of the shock stand-off distance to the model radius, based upon the luminous region of the shock layer in photographs reproduced in reference 72. The NATA predictions of Δ/R_b are roughly in agreement with the data.

8.2 Wedge-Model Calculations

NATA provides calculations of conditions on a blunt wedge with arbitrary leading edge radius and arbitrary (but not excessively large) inclination of the wedge surface to the flow. The principal quantities calculated are the heat flux, the surface pressure, the displacement thickness of the boundary layer on the wedge, and the shock ordinate, all as functions of distance from the leading edge. The positions on the wedge where these calculations are done are under input control. These positions can be specified in terms of an initial distance from the leading edge and a constant increment to generate a sequence of evenly spaced points, or by direct input of the positions. Both methods can be used together, if desired.

The locations in the wind tunnel at which wedge-condition calculations are performed are controlled by the same inputs as are used to specify locations for stagnation-point model condition calculations. The leading edge of the wedge is assumed to be positioned at each of the specified locations. The actual variation in free stream conditions with distance along the wedge is neglected; in each case, the wedge is assumed to be inserted into a uniform flow with the velocity, density, etc., prevailing at the location of the leading edge.

The control variables in NATA are preset such that wedge calculations are not normally performed. To invoke the wedge calculations, it is necessary to specify one or more model positions, and to input positive values for NANGLE (the number of specified angles of attack) and NRADLE (the number of leading edge radii). Normally, stagnation-point model condition calculations are done in addition to the wedge calculations. However, the stagnation-point calculations can be suppressed.

The analysis underlying the wedge condition calculations is explained in the remaining parts of this section. Section 8.2.1 summarizes the classical theory of high-density supersonic flow over wedges. Section 8.2.2 discusses the low density flow over wedges including bluntness and displacement effects, as formulated by Cheng, et al. (ref. 74) and Kemp (ref. 75). Section 8.2.3 presents an analytical representation of the solutions of the Cheng equation; and Section 8.2.4 explains certain modifications of the Cheng-Kemp results as used in NATA. Section 8.2.5 discusses limits to the validity of the calculations, and Section 8.2.6 presents a comparison of NATA wedge calculations with experimental data.

8.2.1 Classical Wedge Theory

Supersonic flow over a wedge is relatively easy to calculate if the leading edge is sharp and the gas density is high. For a sharp leading edge, the shock is attached to the body at the leading edge if the Mach number is high enough. If the density is high, the boundary layer thickness is small in comparison with the shock layer thickness (except in a small region near the leading edge); thus, the shock is essentially straight, the density and flow velocity behind it are constant, and the streamlines behind the shock are parallel to the wedge surface. Under these circumstances, the conditions between the shock and the surface can be determined using oblique shock theory (ref. 64, p. 217-221 or ref. 42, p. 85-89). The solution for the conditions behind the shock can be reduced to the solution of a cubic equation in the case of a perfect gas.

8.2.2 Low-Density Hypersonic Flow Over a Wedge

Wedge models to be tested in arc-heated wind tunnels must have blunt leading edges to avoid excessively high heat transfer and melting or ablation of the leading edge. Also, if the models are fairly large, they must be tested at stations where the nozzle area ratio is large, and thus where the Mach number is high and the free stream density low. Hypersonic low-density flow over a blunt wedge is dominated by effects which are neglected in the classical theory for sharp wedges.

The shock over a blunt leading edge is detached, and nearly normal in the region near the stagnation streamline. The gas which passes through this strong shock over the leading edge undergoes a much larger increase in entropy than that which flows through the highly oblique portion of the shock further to the rear. This shock-heated gas forms a low-density "entropy layer" between the outer edge of the boundary layer and the inner boundary of a conventional thin shock layer.

At low free-stream densities, the thickness of the boundary layer on the wedge is comparable with that of the inviscid shock layer. The thick boundary layer displaces the inviscid flow away from the body surface, by an amount which increases with distances from the leading edge. This displacement results in an induced pressure which is highest near the leading edge, because the shock is less oblique than it would be in the absence of the boundary layer.

Cheng et al. (ref. 74) formulated an analytical treatment of the combined effects of bluntness and boundary layer displacement on the hypersonic flow over a wedge. Their theory treated the boundary layer using local flat-plate similarity with the simplifying assumptions of Prandtl number unity, viscosity proportional to absolute temperature, and constant wall temperature. The Newton-Busemann pressure law (ref. 64) was applied to the outer thin shock layer. The continuity equation for the entropy layer was approximated using the assumption $\gamma - 1 \ll 1$, where γ denotes the specific heat ratio for the gas. The theory was found to predict the trend of experimental heat transfer data very well, but the predicted heat transfer was too low by about 40 percent.

Kemp (ref. 75) modified the Cheng theory to include the effects of $\gamma \neq 1$ to first order. This modification brought the theoretical predictions into good agreement with experimental data, not only for heat transfer but also for surface pressure and shock shape. The wedge calculations in NATA are based on Kemp's analysis, which will be referred to as the Cheng-Kemp theory.

The fundamental relation in the theory is the Cheng equation:

$$(z - \Gamma\zeta)\frac{d}{d\zeta}\left(z\frac{dz}{d\zeta}\right) - \left(z\frac{dz}{d\zeta}\right)^{1/2} = 1 \qquad (480)$$

Here z is a non-dimensional variable proportional to the shock ordinate, while ζ is a non-dimensional distance from the leading edge of the wedge, and the constant parameter Γ is proportional to the angle of attack. The definitions of these quantities in terms of physical variables differ a little between the original and modified versions of the theory. In Kemp's form of the theory, in the notation of Boger and Aiello (ref. 76),

$$z = \frac{A^4}{\gamma^2} \cdot 8\epsilon_\rho (rN)^4 Y_s/k^3 t \qquad (481a)$$

$$\zeta = \frac{A^7}{\gamma^3} \cdot \frac{16\epsilon_\rho^2 (rN)^6}{k^4} \cdot \frac{x}{t} \qquad (481b)$$

$$\Gamma = \frac{\gamma}{A^2} \cdot \frac{k\alpha}{2\epsilon_\rho (rN)^2} \qquad (481c)$$

where

$A = \frac{\gamma + 1}{2}$

$\epsilon_\rho = \frac{\gamma - 1}{\gamma + 1}$

$r = 0.664 + 1.73\, T_w/T_0$

$N = M\sqrt{C/N_{Re,\,t}}$

$N_{Re,\,t} = \rho_1 u_1 t/\mu_1$, Reynolds number based on leading-edge thickness

Y_s = ordinate of shock (figure 36)

k = drag coefficient of the leading edge (4/3 for a cylindrical leading edge, 2 for a flat-faced edge)

x = coordinate parallel to the free-stream velocity, zero at the leading edge (see figure 36)

α = angle of attack in radians (see figure 36)

$C = \frac{\mu(T^*)}{\mu(T_1)} \cdot \frac{T_1}{T^*}$

T^* = Cheng's reference temperature,

$T^* = T_0\,[1 + 3\,(T_w/T_0)]/6$

T_0 = stagnation temperature

T_w = wall temperature

γ = ratio of specific heats

M = free-stream Mach number

t = thickness of leading edge (see figure 36)

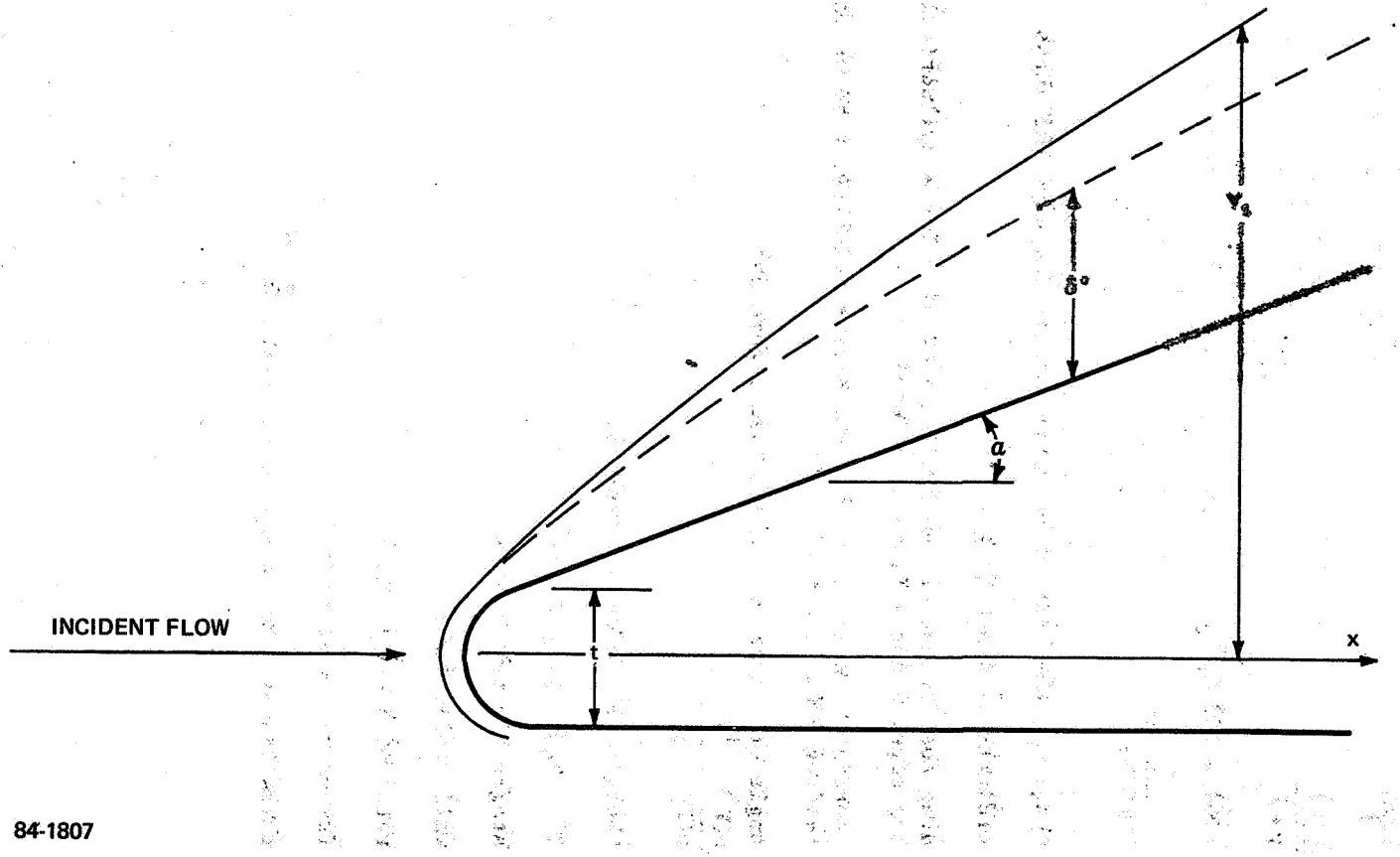

Figure 36 GEOMETRY OF FLOW OVER A BLUNT WEDGE

8.2.3 Analytical Curvefit to the Solution of the Cheng Equation

For zero angle of attack ($\Gamma = 0$), equation (480) has the analytical solution* (ref. 74):

$$z = 2\left[\frac{1}{3}\lambda^{3/2} - \frac{1}{2}\lambda + \sqrt{\lambda} - \ell n\,(1+\sqrt{\lambda})\right] \tag{482a}$$

$$\zeta = \frac{1}{3}(1+\sqrt{\lambda})^4 - \frac{22}{9}(1+\sqrt{\lambda})^3 + 9(1+\sqrt{\lambda})^2 - \frac{46}{3}(1+\sqrt{\lambda}) + \frac{10}{3}\ell n\,(1+\sqrt{\lambda}) - 4\sqrt{\lambda}\,\ell n\,(1+\sqrt{\lambda}) + 2\,[\ell n\,(1+\sqrt{\lambda})]^2 + \frac{76}{9} \tag{482b}$$

in terms of a parameter λ defined by

$$\lambda = z\frac{dz}{d\zeta} \tag{483}$$

For $\Gamma \neq 0$, the solution of (480) cannot be obtained in analytical form. However, the solution can be approximated by assuming that

$$(zz')' = [(zz')']_{\Gamma=0} + \Gamma^2 \tag{484}$$

where the prime denotes $d/d\zeta$ and $[(zz')']_{\Gamma=0}$ is evaluated as a function of ζ from the solution (482), (483) for zero angle of attack:

$$[(zz')']_{\Gamma=0} = \frac{1}{z}(1+\sqrt{\lambda}) \tag{485}$$

For given ζ, the parameter λ must be obtained by numerical solution of equation (482b) and z must then be computed from (482a). Figure 37 compares the approximation (484), represented by the curves, with exact numerical solutions** of equation (480) for various values of Γ. The approximation (484) is most accurate for small Γ. For example, with $\Gamma = 0.1$, the maximum error is about 6 percent. Even for large values of Γ, the error in (484) is less than about 10 percent except in the region where $(zz')'$ is leveling off and beginning to approach its asymptotic value of Γ^2 for large ζ. In this region, for large Γ, the exact solution undershoots the asymptotic value and approaches it in an oscillatory manner. For $\Gamma = 100$, the difference between (484) and the exact solution becomes as large as a factor of about 1.45 in this region.

However, Cheng et al. (ref. 74) suggest that the oscillations in the exact solution, which are responsible for these large differences, are unphysical artifacts of the system of approximations upon which the theory is based. If so, the approximate formula (484) might have higher physical accuracy than the exact solution. Comparisons with experimental data, presented below, support this conjecture.

---

*The equations in reference 74 corresponding to (482) contain minor errors. The correct forms were given by Cheng, H.K., et al (ref. 77)

**These numerical solutions were computed and provided by R. C. Boger, Avco Systems Division.

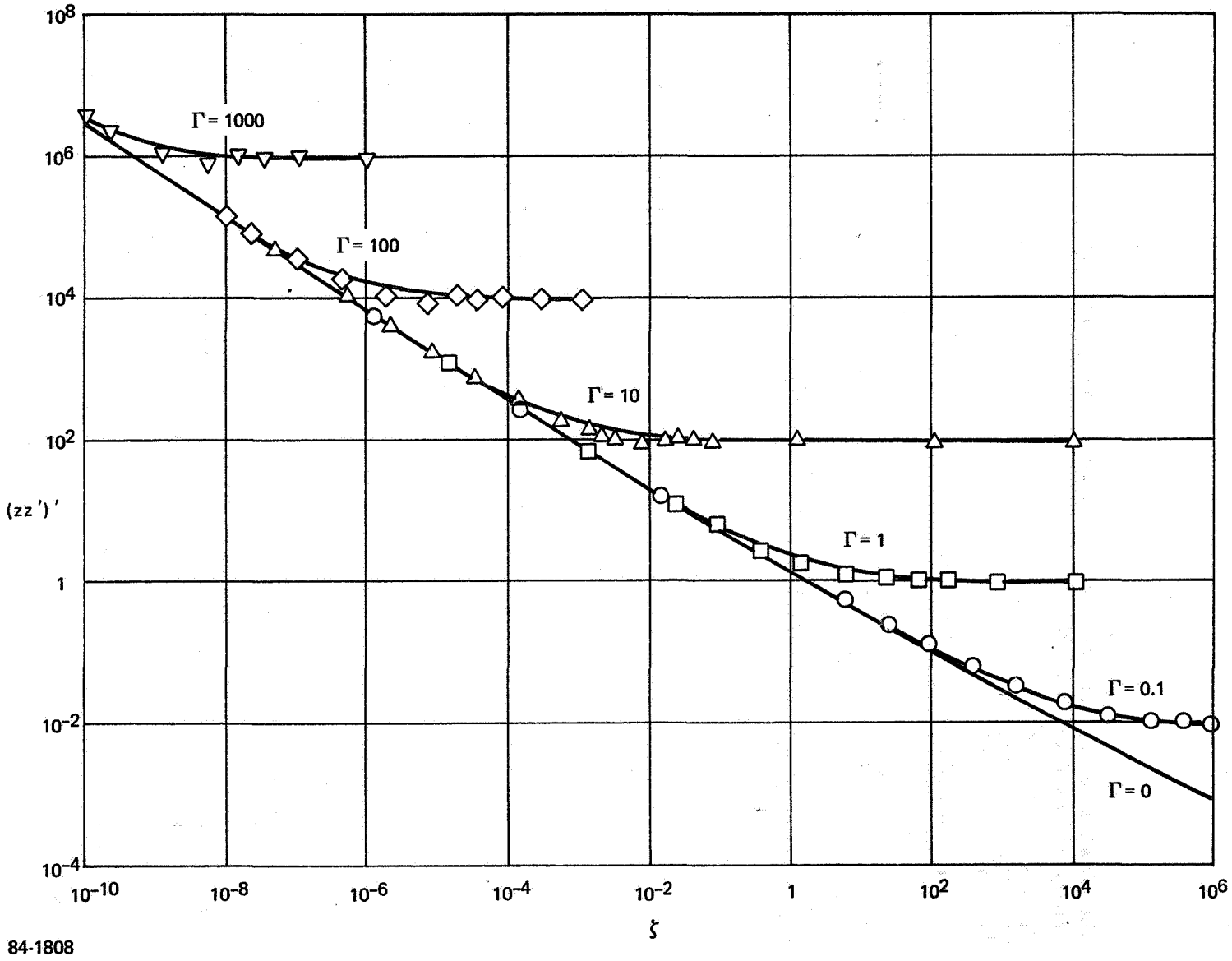

Figure 37 SOLUTIONS OF THE CHENG EQUATION FOR FLOW OVER A WEDGE (POINTS – EXACT NUMERICAL SOLUTIONS; CURVES – ANALYTICAL CURVEFIT)

The physical conditions at the surface of the wedge are given by the Cheng-Kemp theory in the form (ref. 76):

$$\frac{p_w}{p_1} = \frac{A^5}{\gamma^2} \cdot \frac{4\gamma\epsilon_\rho^2 M^2 (\tau N)^4}{k^2} \cdot (zz')' \tag{486}$$

$$C_H = \frac{A^6}{\gamma^{5/2}} \cdot \frac{2.656\,\gamma^{1/2}\epsilon_\rho^2 \tau^5 N^6}{k^3} \cdot \frac{(zz')'}{\sqrt{zz'}} \tag{487}$$

$$\delta^* = \frac{\gamma^2}{A^5} \cdot \frac{k^3 t}{8\epsilon_\rho (\tau N)^4} \cdot \frac{\sqrt{zz'}}{(zz')'} \tag{488}$$

Here p_w/p_1 is the ratio of the pressure on the wedge surface to the free-stream pressure, C_H is the surface heat transfer coefficient,

$$C_H = \frac{q_w}{\rho_1 u_1 (h_0 - h_w)} \tag{489}$$

and δ^* is the boundary layer displacement thickness. The shock ordinate Y_s may be obtained from (481a):

$$Y_s = \frac{\gamma^2 k^3 t}{8 A^4 \epsilon_\rho (\tau N)^4} \cdot z \tag{490}$$

The quantity $(zz')'$ appearing in (486) is given directly by the approximate solution (484) of the Cheng equation. The quantity zz' in (487) and (488) can be obtained from (484) and (483):

$$zz' = \int_0^\zeta [(zz')']_{\Gamma=0}\, d\zeta + \Gamma^2 \zeta$$

$$= [zz']_{\Gamma=0} + \Gamma^2 \zeta = \lambda + \Gamma^2 \zeta \tag{491}$$

The variable z in (490) is then given by a further integration:

$$\frac{1}{2} z^2 = \int_0^\zeta [zz']_{\Gamma=0}\, d\zeta + \frac{1}{2} \Gamma^2 \zeta^2$$

$$z^2 = [z^2]_{\Gamma=0} + \Gamma^2 \zeta^2 \tag{492}$$

where $[z^2]_{\Gamma=0}$ may be obtained by squaring equation (482a).

Figures 38 and 39 compare the approximate solution based on (484) with experimental data on the pressure and heat transfer distributions over the surface of a very blunt wedge in a hypersonic air stream. The experimental points are

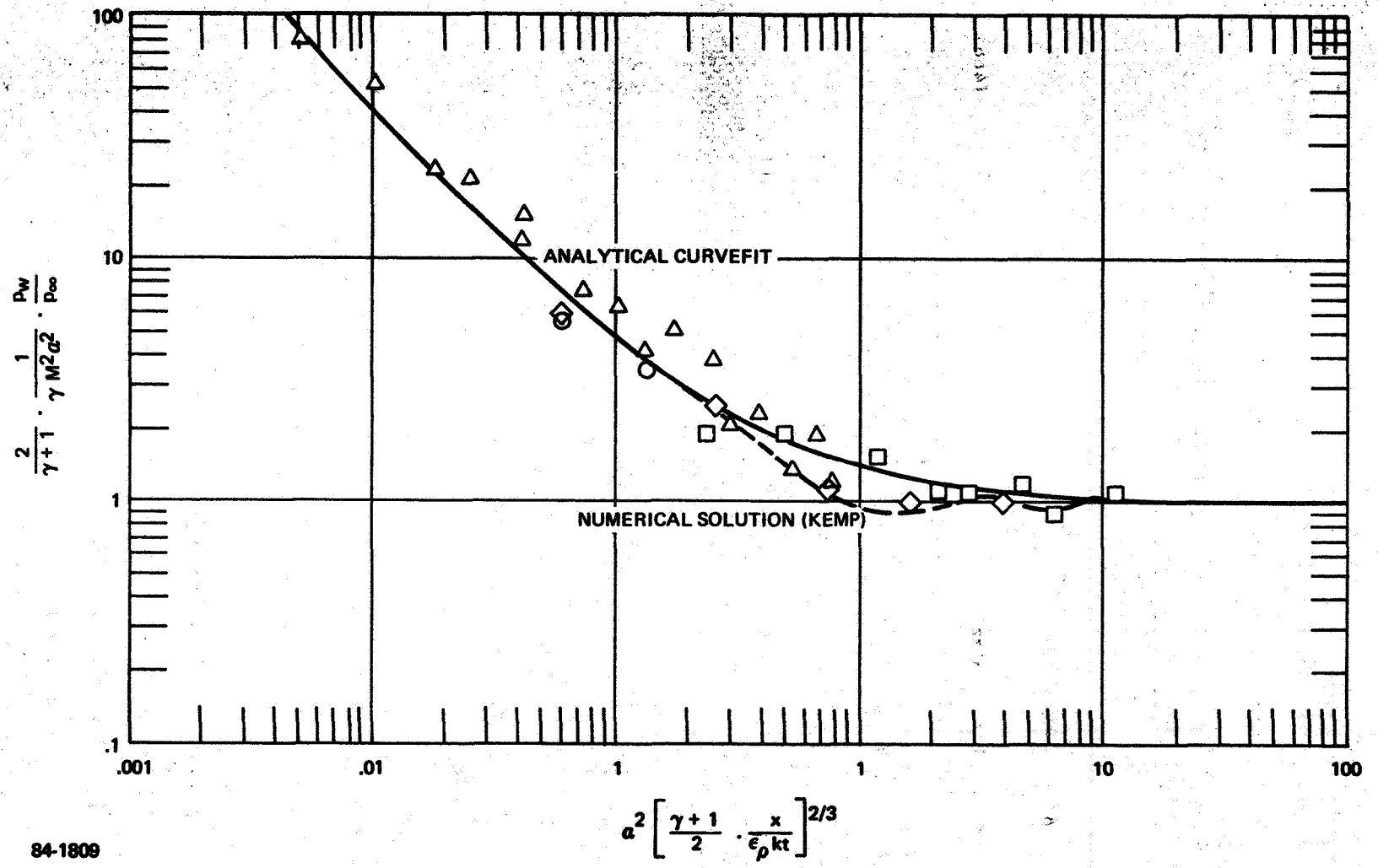

Figure 38 COMPARISON OF ANALYTICAL CURVEFIT TO THE CHENG EQUATION SOLUTION WITH EXPERIMENTAL PRESSURE DATA

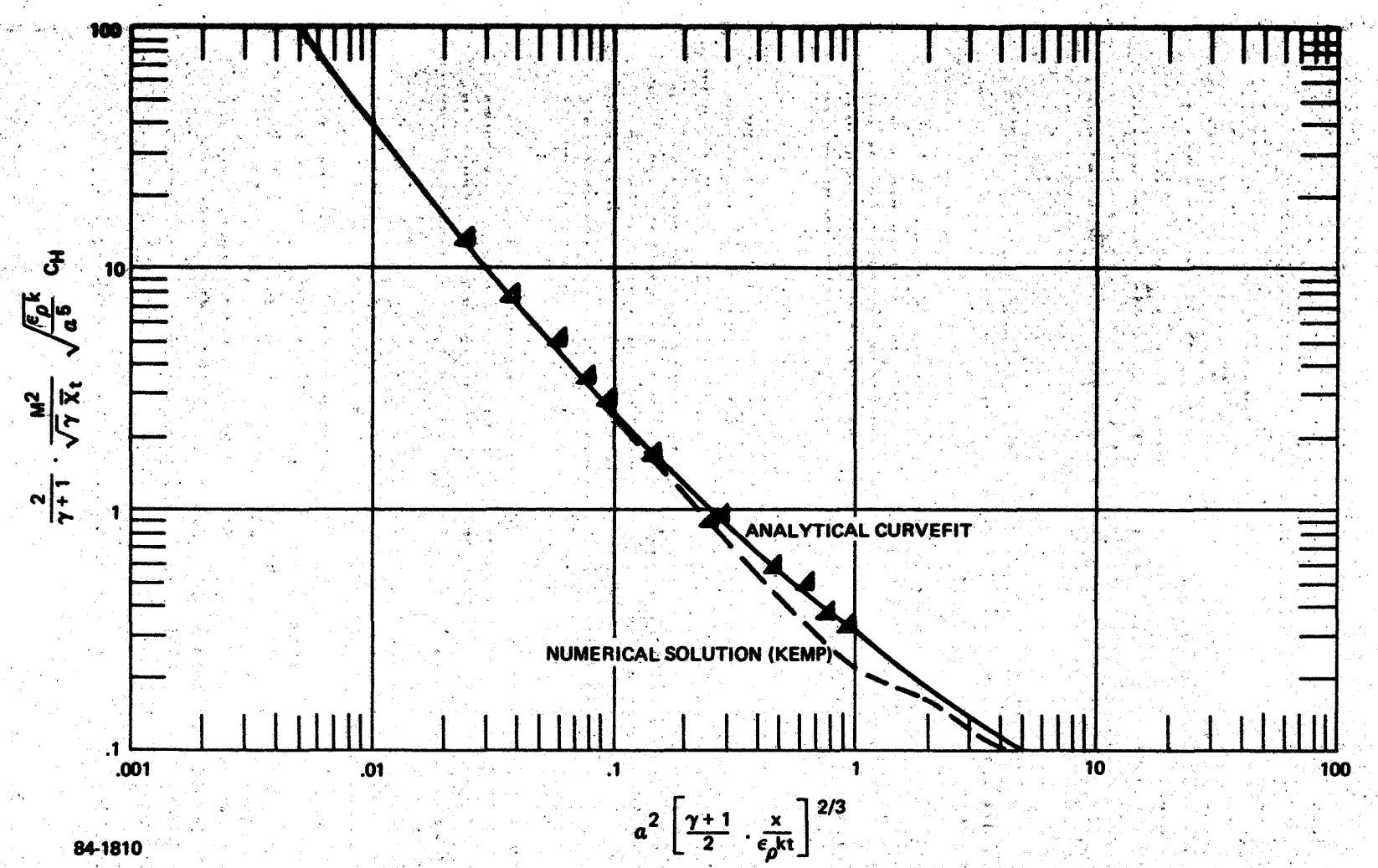

Figure 39 COMPARISON OF ANALYTICAL CURVEFIT TO THE CHENG EQUATION SOLUTION WITH EXPERIMENTAL HEAT TRANSFER DATA

from figure 10 of Kemp's paper (ref. 75). For a flow which is dominated by the effects of leading-edge bluntness, the non-dimensional coordinate ζ is small, and the left-hand side of the Cheng equation (480) is dominated by its first term. If the term $\sqrt{zz'}$ is neglected, the solution of the Cheng equation for $\Gamma = 0$ is found to be

$$z = (9/2)^{1/3}\, \zeta^{2/3} \tag{493}$$

Then (484) gives for general Γ

$$(zz')' = (2/9)^{1/3}\, \zeta^{-2/3} + \Gamma^2 \tag{494}$$

and

$$zz' = 6^{1/3}\, \zeta^{1/3} + \Gamma^2\, \zeta \tag{495}$$

If these expressions are substituted into (486) and (487), there results after some algebraic manipulation

$$\frac{2}{\gamma+1} \cdot \frac{1}{\gamma M^2 a^2} \cdot \frac{p_w}{p_1} = 1 + \frac{0.382}{\xi} \tag{496a}$$

$$\frac{2}{\gamma+1} \cdot \frac{1}{\sqrt{\gamma}} \cdot \frac{M^2}{\bar{X}_t} \sqrt{\frac{\epsilon_\rho k}{a^5}}\, C_H = \frac{0.332 \left(1 + \dfrac{0.382}{\xi}\right)}{\xi^{1/4} \sqrt{1.145 + \xi}} \tag{496b}$$

where

$$\xi \equiv a^2 \left(\frac{\gamma+1}{2} \cdot \frac{x}{\epsilon_\rho k t} \right)^{2/3} \tag{497a}$$

$$\bar{X}_t \equiv M^3 \sqrt{C/N_{Re,\,t}} \tag{497b}$$

The unbroken curves in figures 38 and 39 represent equations (496a) and (496b), respectively. The agreement with the experimental data is similar to that shown in Kemp's original figure 10. In the region $\xi \simeq 1$, where the pressure curve in figure 38 is levelling out, the agreement in both pressure and heat flux is better than is obtained with the exact solution of the Cheng equation (shown by the dashed curves in figures 38 and 39).

8.2.4 Modifications of the Cheng-Kemp Formulas

Since $(zz')'$ is proportional to the pressure and ζ is proportional to the distance from the leading edge, figure 37 may be regarded as a non-dimensional plot of the pressure distribution over the surface of the wedge. The parameter Γ corresponds to the angle of attack. For $\Gamma = 0$, the pressure falls as $\zeta^{-2/3}$ for very small ζ and as $\zeta^{-1/2}$ for very large ζ. For Γ non-zero and positive, the pressure levels off to an asymptotic value, corresponding physically to the

classical wedge pressure. From (484), (486), and (481c) the asymptotic pressure is given by

$$\left(\frac{p_w}{p_1}\right)_{x\to\infty} = A\gamma M^2 a^2 \tag{498}$$

For small angles of attack, classical oblique shock theory (ref. 64, p. 218-220) gives the pressure on the wedge as

$$\left(\frac{p_w}{p_1}\right)_{os} = 1 + \frac{\gamma M^2 a^2}{1-\epsilon_{\rho,os}} \tag{499}$$

where $\epsilon_{\rho,os}$ is the density ratio across the oblique shock wave.

Since $A = (\gamma+1)/2$, equations (498) and (499) agree under the following conditions:

$$\frac{\gamma M^2 a^2}{1-\epsilon_{\rho,os}} >> 1 \tag{500a}$$

$$\epsilon_{\rho,os} = \frac{\gamma-1}{\gamma+1} \tag{500b}$$

The second of these equations implies that the shock is strong even though oblique. For small wedge angles of a few degrees, these conditions are satisfied only for considerably higher Mach numbers than are likely to be encountered in the use of NATA to correlate arc tunnel data on wedges.

Possible modifications of the Cheng-Kemp results for the conditions on wedge models have been studied in an effort to obtain formulas with a wider region of applicability. For theoretical reasons it appears inadvisable to change Kemp's choice of the value $(\gamma+1)/2$ for the parameter A. An alternative and better way to obtain the correct asymptotic wedge pressure is to modify the definition of the parameter Γ. In place of equation (481c), Γ is now redefined as

$$\Gamma^2 = \Omega\left[\left(\frac{p_w}{p_1}\right)_{os} - 1\right] \tag{501}$$

where

$$\Omega \equiv \frac{\gamma k^2}{4 A^5 \epsilon_\rho^2 M^2 (\tau N)^4} \tag{502}$$

and $(p_w/p_1)_{os}$ is the surface pressure ratio based on oblique shock theory. In addition, the pressure formula (486) is modified to

$$\frac{p_w}{p_1} = \frac{(zz')'}{\Omega} + 1 \tag{503}$$

which is simply (486) with a term of unity added to the right-hand side. In the asymptotic constant-pressure region, where $(zz')'$ is equal to Γ^2, (501) and (503) give $p_w/p_1 = (p_w/p_1)_{os}$. Under conditions such that equations (500) are satisfied, (501) and (503) reduce approximately to the original Cheng-Kemp formulas.

In the Cheng-Kemp theory, the heat transfer coefficient and displacement thickness are calculated from formulas involving the surface pressure. In the notation of reference 76,

$$C_H = 0.332 \sqrt{\frac{C}{N_{Re,t}}} \frac{p/p_1}{\sqrt{\int_0^x \frac{p\,dx}{p_1 t}}} \tag{504a}$$

$$\frac{\delta^*}{t} = A \epsilon_\rho \tau M^2 \sqrt{\frac{C}{N_{Re,t}}} \frac{p_1}{p} \sqrt{\int_0^x \frac{p\,dx}{p_1 t}} \tag{504b}$$

Thus, consistency requires that the modification (503) in the pressure formula (486) be accompanied by corresponding modifications in the formulas for C_H and δ^*

Substitution of (503) and (481b) into (504) gives

$$C_H = \frac{2.656\, A^6 \epsilon_\rho^2 (\tau N)^5 N}{\gamma^2 k^3} \cdot \frac{(zz')' + \Omega}{\sqrt{zz' + \Omega \zeta}} \tag{505a}$$

$$\delta^* = \frac{\gamma^2 k^3 t}{8 A^5 \epsilon_\rho (\tau N)^4} \cdot \frac{\sqrt{zz' + \Omega \zeta}}{(zz')' + \Omega} \tag{505b}$$

According to the Cheng-Kemp theory, the shock ordinate is given by

$$Y_s = A \left[x \tan\alpha + \delta^* + \frac{\gamma \epsilon_\rho kt M^2}{2 p_w/p_1} \right] \tag{506}$$

In the original form of the theory, this relation is equivalent to the Cheng equation (480). If p_w/p_1 and δ^* are now assumed to be given by (503) and (505b) in place of (486) and (488), a new formula for Y_s is obtained:

$$Y_s = Ax \tan\alpha + \frac{\gamma^2 k^3 t}{8 A^4 \epsilon_\rho (\tau N)^4} \cdot \frac{1 + \sqrt{zz' + \Omega \zeta}}{(zz')' + \Omega} \tag{507}$$

The first term on the right can no longer be expressed in terms of Γ, because Γ as defined by (501) is not simply proportional to the wedge angle α. In spite of the modifications, (507) does not give the correct asymptotic shock angle at large distances from the leading edge of a sharp plate, because the coefficient A is related to the density ratio for an infinitely strong shock rather than that for the actual oblique shock, which can be rather weak. An ad hoc further modification could be made to force (507) to give the shock angle in the classical wedge limit correctly, but such a change would have an adverse effect on the accuracy in cases in which the bluntness and displacement effects are important. Accordingly, (507) is used as it stands.

The modified formulas (503), (505), and (507) are no longer consistent with the Cheng equation (480). Thus, these formulas do not represent a new form of the Cheng-Kemp theory, but only a set of ad hoc modifications of its results.

8.2.5 Limits of Validity

The original Cheng-Kemp theory is valid in the strong-interaction regime under conditions such that merging and slip effects are unimportant. Kemp (ref. 75) gives the following criteria:

$$\bar{\nu} \equiv M \sqrt{\frac{C}{N_{Re,\,x}}} < 0.15 \tag{508}$$

$$\chi_\epsilon \equiv \epsilon_\rho \tau M^3 \sqrt{\frac{C}{N_{Re,\,x}}} > 1 \tag{509}$$

If the condition (508) is violated, merging or slip effects become significant. If (509) is violated, the strong-interaction approximation breaks down. These criteria define lower and upper values of the distance from the leading edge, bracketing the region in which the original Cheng-Kemp theory is expected to be valid. The lower limit x_ℓ is determined by the onset of merging or slip effects; from (508),

$$x_\ell = \frac{44\, M^2 C}{Re/m} \text{ metres} \tag{510a}$$

where Re/m is the free-stream Reynolds number per metre. The upper limit x_u is the position at which the strong interaction approximation breaks down; from (509),

$$x_u = \frac{\epsilon_\rho^2 \tau^2 M^6 C}{Re/m} \text{ metres} \tag{510b}$$

If the free stream Mach number M is too low, these limits come together and the original Cheng-Kemp theory is not valid anywhere on the wedge. If x_ℓ is set equal to x_u, equations (510) give

$$M_{min} = \frac{2.6}{\sqrt{\epsilon_\rho \tau}} \sim 7 \tag{511}$$

The original Cheng-Kemp theory has no region of validity for Mach numbers lower than M_{min}. The modifications to the results of the Cheng-Kemp theory discussed in Section 8.2.4 were designed to extend the region of applicability of the results beyond the point at which strong interaction theory breaks down. To the extent that these modifications prove to be successful, the modified formulas are not limited by the criterion (509), but can be applied even for $x > x_u$.

No analogous approximation has been developed to extend the utility of the Cheng-Kemp theory into the region where merging and slip effects are important. However, according to Vidal and Bartz (refs. 78, 79), free-molecule flow theory gives an approximate upper limit to the heat transfer to the surface of a wedge.

A calculation of the free-molecule heat transfer coefficient is performed in NATA; if the resulting heat flux is lower than that predicted by the Cheng-Kemp theory, the free-molecule value is printed in place of the other. From Probstein (ref. 80), the free-molecule heat flux is

$$q_w = a_e P_1 \sqrt{\frac{R T_1}{2\pi W}} \left\{ \left[S^2 + \frac{\gamma}{\gamma - 1} - \frac{\gamma + 1}{2(\gamma - 1)} \cdot \frac{T_w}{T_1} \right] \left[e^{-(S \sin\alpha)^2} + \sqrt{\pi}\, S \sin\alpha \,(1 + \operatorname{erf}(S \sin\alpha)) \right] - \frac{1}{2} e^{-(S \sin\alpha)^2} \right\} \tag{512}$$

where W is the mean molecular weight,

$$S \equiv M \sqrt{\frac{\gamma}{2}} \tag{513}$$

and a_e is the thermal accommodation coefficient. In NATA, a_e is assumed equal to unity.

Unfortunately, the pressure predicted by free molecule theory is not an approximate upper limit to the actual pressure on the wedge (ref. 79). In some cases, the measured pressure is nearly an order of magnitude larger than the free molecule value. Thus, the latter does not provide a criterion for limiting the calculated pressures.

8.2.6 Comparison with Experimental Data

Scott (ref. 81) has measured the heat flux to a blunt wedge in the NASA Johnson Space Center 10 Mw Arc Tunnel Facility. The test conditions are summarized in Table III. The stagnation enthalpy of the flow was determined from careful energy balance and mass flow measurements. The leading edge of the wedge model was positioned 2.5 cm downstream of the 0.635-m diameter exit orifice of the nozzle. The effective test section diameter given in Table III was calculated by extrapolating the nozzle expansion to the position of the leading edge.

The reservoir conditions were determined in the NATA solution from mass flow and stagnation enthalpy inputs. The non-equilibrium flow solution included the boundary layer. Table IV compares the NATA predictions of conditions on the wedge with Scott's experimental measurements of the heat flux to the surface of the wedge. Measurements of surface pressure were not performed. In Table IV, x_w denotes the distance along the surface of the wedge from its leading edge. The values tabulated under "Cheng-Kemp Modified" are based on the modified Cheng-Kemp formulas (501), (502), (503) and (505). Those given under "Cheng-Kemp Unmodified" are based on the original Cheng-Kemp theory, equations (486)-(488). The heat flux calculated from the modified Cheng-Kemp formulas is about 20 percent low. The original Cheng-Kemp theory gives fluxes too low by 26 percent.

In this case, the condition (510b) for validity of the strong interaction approximation is satisfied for x_w up to 48 cm. Thus, the unmodified Cheng-Kemp theory is applicable over the entire region covered by the experimental data, so that the differences between the results from the modified and unmodified formulas are small. The condition (510a) predicts that merging effects become significant in this case for x_w less than 14 cm.

TABLE III

TEST CONDITIONS FOR WEDGE HEAT TRANSFER MEASUREMENTS

Data	
Standard nozzle number	10
Stagnation enthalpy, MJ/kg	13.9
Total mass flow, g/sec	90.7
Test section diameter, m	0.648
Axial coordinate, m	1.174
Pitot pressure, atm	1.43×10^{-2}
Wedge angle of attack, degrees	15
Wedge leading edge radius, cm	0.95
NATA Results	
Mach number	9.7
Static pressure, atm	1.09×10^{-4}
Pitot pressure, atm	1.40×10^{-2}
Free-stream density, kg/m^3	9.26×10^{-5}
Free-stream velocity, km/sec	4.07
Free-stream temperature, ^{o}K	329
Frozen specific heat ratio (γ)	1.471
Geometric area ratio	551
Effective area ratio	393
Free-stream mole fractions	
N_2	0.584
N	0.081
O	0.335
Other species	$< 1 \times 10^{-4}$

TABLE IV

CALCULATED AND MEASURED CONDITIONS ON A WEDGE MODEL

Quantity	Cheng-Kemp Modified	Cheng-Kemp Unmodified	Measured
Angle of attack parameter, Γ	11.6	11.2	-
Conditions at x_w = 18.8 cm			
p_w , atm	2.24×10^{-3}	2.03×10^{-3}	-
q_w , W/cm^2	8.21	7.66	10.44
δ^* , cm	1.05	1.12	-
Conditions at x_w = 26.4 cm			
p_w , atm	2.10×10^{-3}	1.89×10^{-3}	-
q_w , W/cm^2	6.88	6.40	8.62
δ^* , cm	1.25	1.34	-
Conditions at x_w = 34.1 cm			
p_w , atm	2.01×10^{-3}	1.80×10^{-3}	-
q_w , W/cm^2	6.05	5.62	7.49
δ^* , cm	1.42	1.53	-

REFERENCES

1. Lordi, J. A.; Mates, R. E.; and Moselle, J. R.: Computer Program for the Numerical Solution of Nonequilibrium Expansions of Reacting Gas Mixtures. NASA CR-472, May 1966.

2. Moelwyn-Hughes, E. A.: Physical Chemistry. Pergamon Press, 1957.

3. Herzberg, G.: Molecular Spectra and Molecular Structure I. Spectra of Diatomic Molecules. Van Nostrand, 1950.

4. Penner, S. S.: Chemistry Problems in Jet Propulsion. Pergamon Press, 1957.

5. Hirschfelder, J. O.; Curtiss, C. F.; and Bird, R. B.: Molecular Theory of Gases and Liquids. John Wiley & Sons, Inc., 1964.

6. Yos, J. M.: Transport Properties of Nitrogen, Hydrogen, Oxygen, and Air to 30,000° K. Rep. RAD-TM-63-7, Avco Research and Advanced Development Division, Mar. 1963.

7. Yos, J. M.: Approximate Equations for the Viscosity and Translational Thermal Conductivity of Gas Mixtures. Rep. AVSSD-0112-67-RM, Avco Missile Systems Division, Apr. 1967.

8. Hirschfelder, J. O.: Heat Conductivity in Polyatomic or Electronically Excited Gases. II. J. Chem. Phys., vol. 26, no. 2, Feb. 1957, pp. 282-285.

9. Spitzer, L.: Physics of Fully Ionized Gases. Second ed., Interscience Publishers, Inc., 1962.

10. Devoto, R. S.: Transport Coefficients of Partially Ionized Argon. Phys. Fluids, vol. 10, no. 2, Feb. 1957, pp. 354-364.

11. Devoto, R. S.; and Li, C. P.: Transport Coefficients of Partially Ionized Helium. J. Plasma Phys., vol. 2, pt. 1, Feb. 1968, pp. 17-32.

12. Meador, W. E., Jr.; and Staton, L. D.: Electrical and Thermal Properties of Plasmas. Phys. Fluids, vol. 8, no. 9, Sept. 1965, pp. 1694-1703.

13. Liboff, R. L.: Transport Coefficients Determined Using the Shielded Coulomb Potential. Phys. Fluids, vol. 2, no. 1, Jan.-Feb. 1959, pp. 40-46.

14. Hahn, H.-S.; Mason, E. A.; and Smith, F. J.: Quantum Transport Cross Sections for Ionized Gases. Phys. Fluids, vol. 14, no. 2, Feb. 1971, pp. 278-287.

15. Williams, R. H.; and DeWitt, H. E.: Quantum-Mechanical Plasma Transport Theory, Phys. Fluids, vol. 12, no. 11, Nov. 1969, pp. 2326-2342.

16. Spitzer, L.; and Harm, R.: Transport Phenomena in a Completely Ionized Gas. Phys. Rev., vol. 89, Mar. 1953, pp. 977-981.

17. Mason, E. A.; and Monchick, L.: Heat Conductivity of Polyatomic and Polar Gases. J. Chem. Phys., vol. 36, no. 6, Mar. 15, 1962, pp. 1622-1639.

18. Nyeland, C.; and Mason, E. A.: Adiabatic Excitation Transfer in Gases: Effects on Transport. Phys. Fluids, vol. 10, no. 5, May 1967, pp. 985-991.

19. Monchick, L.: Collision Integrals for the Exponential Repulsive Potential. Phys. Fluids, vol. 2, no. 6, Nov.-Dec. 1959, pp. 695-700.

20. Kihara, T.; Taylor, M. H.; and Hirschfelder, J. O.: Transport Properties for Gases Assuming Inverse Power Intermolecular Potentials. Phys. Fluids, vol. 3, no. 5, Sept.-Oct. 1960, pp. 715-720.

21. Schlichting, H.: Boundary Layer Theory. Sixth ed., McGraw-Hill Book Co., Inc., 1968.

22. Otis, J. H., Jr., et al: Strategic Reentry Technology Program (STREET-A) Final Report, Vol. II, Task 7.5 Nosetip Ablation Phenomena. Rep. SAMSO-TR-70-247, Vol. II, USAF Space and Missile Systems Organization, Nov. 1970, pp. 6-19.

23. Cohen, C. B.; and Reshotko, E.: The Compressible Laminar Boundary Layer with Heat Transfer and Arbitrary Pressure Gradient. NACA Rept. 1294, 1956.

24. Thwaites, B.: Approximate Calculation of the Laminar Boundary Layer. Aero. Quarterly, vol. 1, pt. 3, Nov. 1949, pp. 245-280.

25. Hayes, W. D.; and Probstein, R. F.: Hypersonic Flow Theory. Academic Press, 1959.

26. Dewey, C. F., Jr.; and Gross, J. F.: Exact Similar Solutions of the Laminar Boundary Layer Equations. Rep. RM-5089-ARPA, RAND Corp., 1967.

27. Howarth, L., ed.: Modern Developments in Fluid Dynamics - High Speed Flow, Vol. I. Clarendon Press (Oxford), 1953.

28. Stewartson, K.: Correlated Incompressible and Compressible Boundary Layers. Proc. Roy. Soc., ser. A, vol. 200, no. 1060, Dec. 1949, pp. 84-100.

29. Stewartson, K.: The Theory of Laminar Boundary Layers in Compressible Fluids. Clarendon Press (Oxford), 1964, pp. 61-65.

30. Burke, A. F.: Private communication.

31. Bray, K. N. C.: Chemical and Vibrational Nonequilibrium in Nozzle Flows. Vol. I, part II of Nonequilibrium Flows, ch. 3, P. P. Wegener, ed., Marcel Dekker (New York), 1970, pp. 59-157.

32. Hall, J. G.; and Treanor, C. E.: Nonequilibrium Effects in Supersonic Nozzle Flows. AGARDograph 124, 1967.

33. Chu, B. T.: Wave Propagation and the Method of Characteristics in Reacting Gas Mixtures with Applications to Hypersonic Flow. WADC TN-57-213, Brown University, 1957.

34. Dunn, M. G.; and Lordi, J. A.: Measurement of $N_2^+ + e^-$ Dissociative Recombination in Expanding Nitrogen Flows. AIAA J., vol. 8, no. 2, Feb. 1970, pp. 339-345.

35. Bray, K. N. C.: Electron-Ion Recombination in Argon Flowing Through a Supersonic Nozzle. High Temperature Aspects of Hypersonic Flow, ch. 4, W. Nelson, ed., Pergamon Press (New York) pp. 67-87.

36. Appleton, J. P.; and Bray, K. N. C.: The Conservation Equations for a Nonequilibrium Plasma. J. Fluid Mech., vol. 20, no. 4, Dec. 1964, pp. 659-672.

37. Bowen, S. W.; and Park, C.: Computer Study of Nonequilibrium Excitation in Recombining Nitrogen Plasma Nozzle Flows. AIAA J., vol. 9, no. 3, Mar. 1971, pp. 493-499.

38. Eschenroedèr, A. Q.; Boyer, D. W.; and Hall, J. G.: Nonequilibrium Expansions of Air with Coupled Chemical Reactions. Phys. Fluids, vol. 5, no. 5, May 1962, pp. 615-624.

39. Schreier, O.; and Sperner, E.: Introduction to Modern Algebra and Matrix Theory. Chelsea Publ. Co. (New York), 1951.

40. Pennington, R. H.: Introductory Computer Methods and Numerical Analysis. Macmillan Co., 1965.

41. Bray, K. N. C.: Atomic Recombination in a Hypersonic Wind Tunnel Nozzle. J. Fluid Mech., vol. 6, no. 1, Jan. 1959, pp. 1-32.

42. Liepmann, H. W.; and Roshko, A: Elements of Gasdynamics. John Wiley & Sons, 1957.

43. Carnahan, B.; Luther, H. A.; and Wilkes, J. O.: Applied Numerical Methods. John Wiley & Sons, 1969.

44. Treanor, C. E.: A Method for the Numerical Integration of Coupled First-Order Differential Equations with Greatly Different Time Constants. Math. of Computation, vol. 20, no. 93, 1966, pp. 39-45.

45. Lomax, H.; and Bailey, H. E.: A Critical Analysis of Various Numerical Integration Methods for Computing the Flow of a Gas in Chemical Nonequilibrium. NASA TN D-4109, Aug. 1967.

46. Wegener, P. P.: Experiments on the Departure from Chemical Equilibrium in a Supersonic Flow. ARS J., vol. 30, no. 4, April 1960, pp. 322-329.

47. Wegener, P. P.: Supersonic Nozzle Flow with a Reacting Gas Mixture. Phys. Fluids, vol. 2, no. 3, May-June 1959, pp. 264-275.

48. JANAF Thermochemical Tables. Dow Chemical Co., Midland, Mich.

49. Fay, J. A.: and Riddell, F. R.: Theory of Stagnation Point Heat Trensfer in Dissociated Air. J. Aero. Sci., vol. 25, no. 2, Feb. 1958, pp. 73-85.

50. Bade, W. L.: Stagnation-Point Heat Transfer in a High-Temperature Inert Gas. Phys. Fluids, vol. 5, no. 2, Feb. 1962, pp. 150-154.

51. Finson, M. L.; and Kemp. N. H.: Theory of Stagnation-Point Heat Transfer in Ionized Monatomic Gases. Phys. Fluids, vol. 8, no. 1, Jan. 1965, pp. 201-204.

52. Dorrance, W. H.: Viscous Hypersonic Flow. McGraw-Hill Book Co., 1962.

53. Rose, P. H.; and Stark, W. I.: Stagnation Point Heat Transfer Measurements in Dissociated Air. J. Aero. Sci., vol. 25, no. 2, Feb. 1958, pp. 86-97.

54. Yos, J. M.: Transport Properties of Nitrogen, Hydrogen, Oxygen, and Air to 30,000° K. Tech. Memo. RAD-TM-63-7, Avco Research and Advanced Development Division, Mar. 1963.

55. Goldstein, S., ed.: Modern Developments in Fluid Dynamics, Vol. II. Dover Publ. (New York), 1965, pp. 631-632.

56. Sibulkin, M.: Heat Transfer Near the Forward Stagnation Point of a Body of Revolution. J. Aero. Sci., vol. 19, no. 8, Aug. 1952, pp. 570-571.

57. Finson, M. L.: Theory of Stagnation Point Heat Transfer in Ionized Monatomic Gases. S. M. Thesis, Dept. of Mech. Engineering, Massachusetts Institute of Technology, June 1964.

58. DeRienzo, P.; and Pallone, A.J.: Convective Stagnation Point Heating for Re-entry Speeds Up to 70,000 fps Including Effects of Large Blowing Rates. AIAA J., vol. 5, no. 2, Feb. 1967, pp. 193-200.

59. Fay, J.A.; and Kemp, N.H.: Theory of Stagnation Point Heat Transfer in a Partially Ionized Diatomic Gas. AIAA J., vol. 1, no. 12, Dec. 1963, pp. 2741-2751.

60. Boison, J. C.; and Curtiss, H. A.: An Experimental Investigation of Blunt Body Stagnation Point Velocity Gradient. ARS J., vol. 29, no. 2, Feb. 1959, pp. 130-135.

61. Crawford, D. H.; and McCauley, W. D.: Investigation of the Laminar Aerodynamic Heat-Transfer Characteristics of a Hemisphere-Cylinder in the Langley 11-Inch Hypersonic Tunnel at a Mach Number of 6.8. NACA Rept. 1323, 1957.

62. Reinecke, W. G.: The Measurement and Comparison with Theory of Heat Transfer from Similar Laminar Boundary Layers to Aerodynamic Bodies in Supersonic and Hypersonic Gas Streams. Ph.D. Thesis, Princeton University, 1961.

63. Moretti, G.; and Bleich, G.: Three-Dimensional Inviscid Flow About Supersonic Blunt Cones at Angle of Attack. I: Numerical Technique for the Three-Dimensional Blunt-Body Problem. SC-CR-68-3728, Sandia Laboratories, Sept. 1968.

64. Hayes, W. D.; and Probstein, R. F.: Hypersonic Flow Theory. Second ed., Vol. I. Academic Press, 1966.

65. Vinokur, M.: Hypersonic Flow Around Bodies of Revolution Which are Generated by Conic Sections. LMSD-288139, General Research in Flight Sciences, January 1959 - January 1960, Vol. I, Part 1, Fluid Mechanics, Lockheed Missiles and Space Division, Jan. 1960.

66. Vinokur, M.; and Sanders, R. W.: Hypersonic Flow Around Blunt Bodies of Revolution Whose Shock Waves are Generated by Conic Sections. LMSD-288139, General Research in Flight Sciences, January 1959 - January 1960, Vol. I, Part 1, Fluid Mechanics, Lockheed Missiles and Space Division, Jan. 1960.

67. Cole, J. D.; and Brainerd, J. J.: Slender Wings at High Angles of Attack in Hypersonic Flows. Hypersonic Flow Research, F. Riddell ed., Academic Press, 1962, pp. 321-343.

68. Hiester, N. K.: Relative Operating Capabilities of Selected Electric-Arc Heated Re-Entry Environment Simulators. Stanford Research Institute, May 1964.

69. Jakob, M.: Heat Transfer. Vol. II. John Wiley and Sons, 1957.

70. Cheng, H. K.: The Blunt-Body Problem in Hypersonic Flow at Low Reynolds Number. IAS Paper 63-92, 1963.

71. Van Dyke, M. D.: The Supersonic Blunt Body Problem - Review and Extension. J. Aero/Space Sci., vol. 25, no. 8, Aug. 1958, pp. 485-496.

72. Scott, C. D.: An Experimental and Analytical Study of Slip and Catalytic Boundary Conditions Applied to Spheres in Low Reynolds Number Arc Jet Flows. Rarefied Gas Dynamics, Proc. of the Ninth International Symposium on Rarefied Gas Dynamics, M. Becker and M. Fiebig, eds., DFVLR Press (Porz-Wahn, Germany), 1974, pp. D. 14-1 to D. 14-12.

73. Cheng, H.K.: Viscous Hypersonic Blunt-Body Problems and the Newtonian Theory. Fundamental Phenomena in Hypersonic Flow, J. G. Hall, ed., Cornell University Press, 1966, pp. 90-131.

74. Cheng, H. K.; Hall, J. G.; Golian, T. C.; and Hertzberg, A.: Boundary-Layer Displacement and Leading-Edge Bluntness Effects in High-Temperature Hypersonic Flow. J. Aerospace Sci., vol. 28, no. 5, May 1961, pp. 353-381.

75. Kemp, J. H., Jr.: Hypersonic Viscous Interaction on Sharp and Blunt Inclined Plates. AIAA J., vol. 7, no. 7, July 1969, pp. 1280-1289.

76. Boger, R. C.; and Aiello, G. F.: Hypersonic Flow on Yawed Wedges with Leading-Edge Bluntness and Viscous Interaction. J. Spacecraft and Rockets, vol. 8, no. 7, July 1971, pp. 729-735.

77. Cheng, H. K.; Hall, J. G.; Golian, T. C.; and Hertzberg, A.: Errata - Boundary Layer Displacement and Leading-Edge Bluntness Effects in High-Temperature Hypersonic Flow. J. Aerospace Sci., vol. 29, no. 3, Mar. 1962, p. 355.

78. Vidal, R. J.; and Bartz, J.A.: Experimental Studies of Low-Density Effects in Hypersonic Wedge Flows. Rarefied Gas Dynamics, vol. I, J. H. de Leeuw, ed., Academic Press, 1965, pp. 467-486.

79. Vidal, R. J.; and Bartz, J. A.: Surface Measurements on Sharp Flat Plates and Wedges in Low-Density Hypersonic Flow. AIAA J., vol. 7, no. 6, June 1969, pp. 1099-1109.

80. Probstein, R. F.: Aerodynamics of Rarefied Gases. Rarefied Gas Dynamics, F. M. DeVienne, ed., Pergamon Press, 1960, pp. 258-275.

81. Scott, C. D.: Convective Heating to Rounded Edge Gaps in Arc Jet Flow. Test Rept., Structures and Mechanics Div., NASA Johnson Space Center, 1974.

*U.S. GOVERNMENT PRINTING OFFICE: 1975 - 635-052/86

NATIONAL AERONAUTICS AND SPACE ADMINISTRATION
WASHINGTON, D.C. 20546

OFFICIAL BUSINESS
PENALTY FOR PRIVATE USE $300

SPECIAL FOURTH-CLASS RATE
BOOK

POSTAGE AND FEES PAID
NATIONAL AERONAUTICS AND
SPACE ADMINISTRATION
451

U.S. MAIL

POSTMASTER: If Undeliverable (Section 158 Postal Manual) Do Not Return

"The aeronautical and space activities of the United States shall be conducted so as to contribute . . . to the expansion of human knowledge of phenomena in the atmosphere and space. The Administration shall provide for the widest practicable and appropriate dissemination of information concerning its activities and the results thereof."

—NATIONAL AERONAUTICS AND SPACE ACT OF 1958

NASA SCIENTIFIC AND TECHNICAL PUBLICATIONS

TECHNICAL REPORTS: Scientific and technical information considered important, complete, and a lasting contribution to existing knowledge.

TECHNICAL NOTES: Information less broad in scope but nevertheless of importance as a contribution to existing knowledge.

TECHNICAL MEMORANDUMS: Information receiving limited distribution because of preliminary data, security classification, or other reasons. Also includes conference proceedings with either limited or unlimited distribution.

CONTRACTOR REPORTS: Scientific and technical information generated under a NASA contract or grant and considered an important contribution to existing knowledge.

TECHNICAL TRANSLATIONS: Information published in a foreign language considered to merit NASA distribution in English.

SPECIAL PUBLICATIONS: Information derived from or of value to NASA activities. Publications include final reports of major projects, monographs, data compilations, handbooks, sourcebooks, and special bibliographies.

TECHNOLOGY UTILIZATION PUBLICATIONS: Information on technology used by NASA that may be of particular interest in commercial and other non-aerospace applications. Publications include Tech Briefs, Technology Utilization Reports and Technology Surveys.

Details on the availability of these publications may be obtained from:

SCIENTIFIC AND TECHNICAL INFORMATION OFFICE

NATIONAL AERONAUTICS AND SPACE ADMINISTRATION

Washington, D.C. 20546